Study of the mechanisms and species involved in the retention of uranium (VI) at trace concentration at the clay-solution interface

Shangyao Guo

UNIVERSITÉ DE STRASBOURG

ÉCOLE DOCTORALE 182 : PHYSIQUE & CHIMIE-PHYSIQUE

[INSTITUT PLURIDISCIPLINAIRE HUBERT CURIEN – UMR CNRS 7178]

THÈSE présentée par :

[SHANGYAO GUO]

Soutenue le : **08 Septembre 2023**

pour obtenir le grade de : **Docteur de l'université de Strasbourg**

Discipline/ Spécialité : Chimie Physique

Study of the mechanisms and species involved in the retention of uranium(VI) at trace concentration at the clay-solution interface

THÈSE dirigée par :

M. Rémi Barillon	Professeur, Université de Strasbourg
Mme Mirella Del Nero	CR CNRS, Institut Pluridisciplinaire Hubert Curien, Strasbourg

RAPPORTEURS :

M. Glaus Martin	Chercheur, Paul Scherrer Institut, Suisse
M. Grégory Lefèvre	DR CNRS, Chimie Paris Tech – Université Paris Sciences & Lettres

---

AUTRES MEMBRES DU JURY :

Mme Barbara Ernst	Professeur, Université de Strasbourg
M. Benoît Madé	IR, Agence nationale pour la gestion des déchets radioactifs
M. Romain Dagnélie	IR, Commissariat à l'Energie Atomique-Université Paris Saclay

À ma famille

致为我默默付出和支持的家人

Acknowledgements

This may be the most challenging chapter to write because there are so many people to whom I want to express my sincere acknowledgment. The invaluable help of all those people during my Ph.D. project made this work possible and gave me an unforgettable academic experience. I hope I will not forget anyone who has contributed in any way to support me during my Ph.D. project.

I greatly acknowledge my thesis director: Pr Rémi BARILLON, director of IPHC and Vice-president of the University of Strasbourg, for directing this thesis and allowing me to carry out my work in an excellent scientific and human environment. Although he has a busy schedule, whenever he has the opportunity, he always takes the time to come to the laboratory with good humor to discuss my work, encourage me, and care for me and my family.

I am deeply grateful to my supervisor and thesis co-director, Dr. Mirella DEL NERO, for supervising me during my Ph.D. project and helping me overcome this challenge. I greatly appreciate her invaluable daily guidance in all my research works (designing the experiences, analyzing, interpreting the data, discussing the result…), which allow me to have a very enriching experience. I greatly thank her for her effort, time, and understanding in helping me succeed in my Ph.D. study. This wouldn't have been possible without her help.

I would like to greatly acknowledge all the jury members: Dr. Glaus MARTIN, Dr. Grégory LEFÈVRE, Pr Barbara ERNST, Dr. Benoit MADÉ, Dr. Romain DAGNÉLIE, for their interest in my work, time to review my thesis and insightful comments.

The completion of this Ph.D. would not have been possible without the support of Dr. Olivier COURSON. I would like to express my sincere gratitude to him for all his invaluable help throughout my Ph.D. study.

I am grateful to Dr. Sylvia GEORG for her help in the preparation of materials, the use of ATR-FTIR equipment, the numerous sample analysis of ICP-MS…. Furthermore, I would like to thank her for inviting me several times to her home to enjoy delicious food (tarte flambée, raclette…etc.) and to spend convivial moments with our lab mates and your family.

My profound appreciation goes to Dr. Anne BOOS, Mrs Islah EL MASOUDI, and Mrs Pascale RONOT for providing us access to the ICP-MS and ICP-OES. There must be great thanks to M. Alexandre LECOINTRE for his help meeting our liquid nitrogen need for all the ATR FTIR measurements.

I would like to sincerely thank my friends, lab mates, and colleagues for the cherished time spent together in the lab and social settings, which made my studies and life in France a wonderful time.

Last but not least, I would like to express my sincere gratitude to my family. Without their tremendous understanding and encouragement, they have always given me; it would be impossible for me to complete my study.

Contents

Preface

This thesis funded by the European Joint Programme on Radioactive Waste Management (EJP EURAD) has been conducted in the Radiochemistry team of the Institut Pluridiscipliniare Hubert Curien (UMR 7178)-CNRS, Strasbourg. This work is carried out within the Work Package 5 FUTURE fundamental understanding of radionuclide retention under the context of deep geological disposal of radioactive waste. The purpose of this work is to gain inside into the sorption mechanism of uranium(VI) at the clay (e.g., Illite) - solution interface in the presence of ligands (e.g., phosphate ligand) and competitive cations (e.g., Fe(III)). The results obtained during the Ph.D. work have been presented as publications (published or in preparation) or oral/poster communications:

Publications:

Abstracts of international conferences:

1. **Guo S.**, Del Nero M., Meyer-Georg S., Courson O. and Barillon R. (2021). In situ ATR-FTIR study of uranyl sorption at illite-solution interface in the presence of phosphate ions. Goldschmidt conference, July 4-9, Lyon, France. DOI:10.7185/gold2021.7556.

2. **Guo S.**, Del Nero M., Meyer-Georg S., Courson O. and Barillon R. (2022). In situ ATR - FTIR study of uranyl sorption at illite - solution interface in the presence of phosphate ligands. 10th International conference on High Level Environmental Radiation Areas (ICHLERA), June 27-30, Strasbourg, France.

Articles in preparation:

1. **Shang Yao Guo**, Mirella Del Nero, Olivier Courson, Syvlia Meyer-Georg and Remi Barillon. Speciation studies at the Illite – solution interface: Part 1 – sorption of phosphate ions. Submit to Colloid and Interface A: Physicochemical and Engineering Aspects (undergoing).

2. **Shang Yao Guo**, Mirella Del Nero, Olivier Courson, Syvlia Meyer-Georg and Remi Barillon. Speciation studies at the Illite – solution interface: Part 2 – Co-sorption of uranyl and phosphate ions. Submit to Colloid and Interface A: Physicochemical and Engineering Aspects (undergoing).

International or national conferences:

1. **Guo S.** (2020) Mechanisms and species of uranyl sorption and desorption at the compacted clay-solution interface at low concentration of uranyl (μM). *Ph.D. Event, Annual Meeting of EJP-EURAD-Future, September 15*. Oral communication.

2. **Guo S.** (2021) In situ ATR - FTIR study of uranyl sorption at illite - solution interface in the presence of phosphate ligands. *Annual meeting of EJP-EURAD-Future programme*, *Jun 27-29.* Oral communication.

3. **Guo S.**, Del Nero M., Meyer-Georg S., Courson O. and Barillon R. (2021) In situ ATR - FTIR study of uranyl sorption at illite - solution interface in the presence of phosphate ions. *Goldschmidt conference, July 4-9, Lyon, France.* Oral communication.

4. **Guo S.**, Del Nero M., Meyer-Georg S., Courson O. and Barillon R. (2022). In situ ATR - FTIR study of uranyl sorption at illite - solution interface in the presence of phosphate ligands. *10th International conference on High Level Environmental Radiation Areas (ICHLERA), June 27-30*, *Strasbourg, France.* Oral communication.

5. **Guo S.**, Del Nero M., Meyer-Georg S., Courson O. and Barillon R. (2022) In situ ATR-FTIR study of uranyl ions sorption at the illite-solution interface in the presence of phosphate ions. *2es Rencontres Rayonnement Radio-Chimie, August 31 – September 2*, *Nice, France.* Poster presentation.

6. **Guo S.**, Del Nero M., Meyer-Georg S., Courson O. and Barillon R. (2022) Batch experiments and in situ ATR-FTIR spectroscopy study of uranyl ions (de)sorption at the illite-solution interface in the presence of phosphate and carbonate ligands and

competitive cations (Fe^{3+}). *Annual meeting of EJP-EURAD-Future programme*, *October 24-25, Duren, Germany.* Oral communication.

Introduction générale

Contexte de la thèse

Le stockage dans des formations géologiques profondes est une option considérée pour la gestion et le confinement à long terme des déchets radioactifs de haute activité (HA) ou de moyenne activité à vie longue (MA-VL) qui sont produits par l'industrie nucléaire en France. Les roches hôtes envisagées sont des formations argileuses (e.g. projet CIGEO piloté par l'ANDRA sur les argiles du Callovo-Oxfordien dans la Meuse) qui apparaissent stables, homogènes sur de grandes épaisseurs, et quasi-imperméables afin de limiter la migration potentielle depuis les sites de stockage de radionucléides (RN) mobilisés par les eaux naturelles e.g. [1]. Ces formations ont aussi des capacités fortes de rétention/ piégeage (noté ci-après « sorption ») des RN permettant de retarder la mobilisation des RN, e.g. [1–3]. Dans le cadre d'études de sûreté, des recherches ont été menées depuis ces dernières décennies pour comprendre les mécanismes de la sorption des RN sur les roches argileuses ,e.g., [3–7]. L'enjeu, scientifique et sociétal, est de développer in fine des modèles prédictifs fiables du transport réactif des RN dans ces roches, en conditions de champ proche ou lointain des stockages, et notamment en cas de perturbations chimiques des milieux.

Afin de répondre à cet enjeu lié au stockage des déchets radioactifs, le programme EURAD 2019-2024 (European Joint Programme on Radioactive Waste Management) de la Commission Européenne a fédéré des recherches et le partage de connaissances d'acteurs européens (agences, organismes de recherche, etc.). Cette thèse s'inscrit dans le Work Package 5 FUTURE «Fundamental UndersTanding of radionUclide REtention » de l'EJP EURAD coordonné par l'ANDRA. Les études menées dans FUTURE visent à obtenir des données opérationnelles et mécanistes nécessaires à une compréhension fine des processus contrôlant le transport de RN dans des systèmes eaux - roches, pour des conditions réalistes de stockage. Cela implique entre autres d'étudier la sorption des RN -et leur réversibilité- à la surface d'argiles au contact d'eaux naturelles. Cette thèse concerne l'étude de l'influence de ligands inorganiques et de cations

compétiteurs pertinents sur les mécanismes de la sorption / désorption de l'uranium hexavalent (U(VI)) à des concentrations à l'échelle des traces à l'interface roche argileuse - eau.

Objectifs de la thèse et démarche

La rétention et la mobilité de l'uranium(VI) dans les systèmes eau-roche dépendent de la distribution des ions uranyle qui s'opère entre les solutions et les surfaces minérales e.g., [8]. Cette distribution est contrôlée par la spéciation chimique de U(VI) qui dépend de l'affinité du métal pour des ligands en solution et/ou des ligands présents aux interfaces minéral-solution (tels que les groupes hydroxyle de surface), de la structure et la stabilité respective des espèces aqueuses et surfaciques formées, et des conditions physico-chimiques du système e.g., [8]. La compréhension du comportement de U(VI) dans ces systèmes nécessite donc une connaissance approfondie sur les interactions aux interfaces métal-ligand-minéral-solution et sur les mécanismes de sorption. L'étude de l'influence des ligands phosphate ou carbonate est pertinente du fait de leur capacité à complexer l'U(VI) et à s'adsorber (surtout pour les ions phosphate) à la surface des argiles et des oxy-hydroxydes de Fe ou d'Al, dont ils modifient la réactivité de surface, à pH acide /neutre et basique, respectivement. De plus, de nombreuses études ont montré que ces ligands participent à la formation de complexes ternaires surface-ligand-U(VI) ou surface-U(VI)-ligand -et/ou à la formation de précipités de surface de phosphate d'uranyle, selon les conditions-, sur des minéraux de type oxy-hydroxyde de Fe ou d'Al et contribuent ainsi à la rétention de l'uranium e.g., [9–13]. Or, si des informations macroscopiques et moléculaires sont disponibles sur la spéciation de U(VI) sur ces oxy-hydroxydes, l'identité des espèces uranyle formées à la surface des argiles reste peu explorée d'un point de vue moléculaire, en particulier en présence d'ions phosphate ou carbonate et pour U(VI) sorbé à des concentrations traces. Du fait de la complexité et de la diversité des structures et des propriétés de surface des argiles, la formation de complexes ternaires et/ou précipités de

surface phosphatés de l'ion uranyle lors de la sorption de l'U(VI) sur des argiles reste discutée dans la littérature. De plus, les effets compétiteurs et / ou synergiques de cations tel que Fe^{3+} sur la (co)sorption entre U(VI) et ligand sur les argiles sont à clarifier. Il est nécessaire d'acquérir des données mécanistes sur ces systèmes pour mieux comprendre et modéliser le devenir de U(VI) dans les systèmes roches argileuses - eaux.

Le but principal de cette étude est d'acquérir des connaissances mécanistes sur la sorption des ligands phosphate et carbonate sur une roche argileuse, et leur influence sur la sorption des ions uranyle et des ions ferriques. Il s'agit ensuite d'appliquer les connaissances acquises dans ces systèmes « modèles » à l'interprétation du comportement de U(VI) mesuré dans un système comprenant argile, ligand et cation compétiteur (envisagé ici dans le cas des ligands phosphate, uniquement). Un défi majeur à relever est d'obtenir de données de la spéciation de U(VI) in-situ, à l'interface argile-ligand-eau, et pour des concentrations en U à l'échelle de traces (< 10 µM).

Les objectifs spécifiques sont :

- De quantifier les processus de la (co)sorption des ligands et/ou de U(VI) et du Fe(III) sur l'argile en fonction de paramètres physico-chimiques clés, i.e., pH, temps de réaction, ratio argile/eau, concentrations des ligands et métaux, à partir de l'obtention données expérimentales et macroscopiques (mesures des quantités sorbées, de la charge de surface impartie à l'argile, de la réversibilité de la sorption),
- D'identifier finement les espèces phosphatées et/ou carbonatées formées à la surface de l'argile et les mécanismes mis en jeu au cours du processus de sorption (complexation vs. précipitation de surface, compétition entre métaux, etc.), par suivi spectroscopique in-situ de l'interface argile-ligand-solution par spectroscopie infrarouge à transformée de Fourrier à réflexion totale atténuée (IRTF-RTA).

La roche argileuse utilisée est l'Illite du Puy (noté ici IdP) qui a pour phase minérale principale l'illite, un minéral argileux non gonflant (formé d'un empilement de feuillets TOT, composés d'un tétraèdre de silice (T), un octaèdre d'alumine (O) et un tétraèdre de silice (T), avec essentiellement du potassium pour cation interfoliaire), qui est une argile commune à de nombreuses roches argileuses.

Matériel et méthodes

Dans un premier temps, des caractérisations physico-chimiques (compositions minéralogiques et chimiques, mesures de surface spécifiques, etc.) expériences de mises à l'équilibre de l'IdP avec des solutions aqueuses à différents pH et ratios argile/solution ($R_{S/L}$) ont été réalisées, afin de mesurer les quantités de ligands et cations métalliques mis en solution par dissolution de la roche, et ainsi évaluer leur pertinence pour une étude de la sorption de l'uranium. Suite à ces expériences, les ligands phosphate et carbonate, et les ions ferriques, ont été choisis pour une étude plus détaillée. L'IdP a été purifiée pour la rendre Na-homoionique (argile notée NaIdP) et éliminer les minéraux carbonatés et les oxy/hydroxydes de fer présents dans la roche initiale [14]. La purification permet d'aborder les mécanismes de la sorption de U(VI) sur l'illite, en présence de ligands et de cations compétiteurs, en contrôlant les conditions.

Des expériences en lot ont été réalisées afin d'obtenir des données macroscopiques. Les systèmes étudiés dans le cas des ligands phosphate sont les suivants : NaIdP-ligand-solution, NaIdP-ligand-ion uranyle-solution, NaIdP-ligand-Fe^{3+}-solution et NaIdP-ligand-ion uranyle-Fe^{3+}-solution, ainsi que des systèmes de référence (sans ligand ou sans argile). Pour étudier la sorption d'ions uranyle en présence de ligands carbonate, les expériences ont été réalisées sous conditions de p_{CO2} atmosphérique et p_{CO2} égal à 2.5 %. L'influence des paramètres clés sur la sorption étudiés sont le pH (3-9), les concentrations en U(VI) et/ou en Fe(III) (de 1 à 15µM) et en ligands (pour le phosphate : 10 à 250µM), le temps de réaction (2 heures à 4 jours) et le

rapport solide / liquide ($R_{S/L}$ de 0,5 à 6 g/L). Les analyses des solutions expérimentales finales ont été effectuées pour déterminer le pourcentage et les quantités de métal et/ou ligand sorbés. La mobilité électrophorétique (ME) des particules de NaIdP a également été mesuré afin d'analyser les modifications de la charge de surface de l'illite dues aux réactions de sorption et de contribuer à l'identification des espèces formées à la surface de l'argile.

Les identifications in-situ des espèces surfaciques à l'échelle moléculaire se sont basées sur l'analyses de spectres infrarouges mesurées in-situ, à l'interface argile-solution, dans une gamme caractéristique (900-1200 cm^{-1}) des vibrations d'élongation P-O e.g., [15,16] et/ou une gamme caractéristique des vibrations d'élongation C-O de 1000 à 1700 cm^{-1} e.g., [17]. L'objectif était d'analyser les environnements de coordination des ions phosphate / carbonate tels que modifiés par leur sorption sur l'argile, et par la co-sorption des ions uranyle et fer, pour documenter la formation et l'identité des espèces phosphatées et carbonatées formées à la surface de l'argile.

Plan de la thèse

Ce manuscrit de thèse inclut quatre chapitres. Le premier chapitre présente une revue bibliographique générale qui résume les processus de sorption à l'interface minéral-solution, les interactions entre les ions uranyle et phopshate, les processus de (co-)sorption des ions uranyle sur les oxy-hydroxydes et les argiles, et les contributions de la spectroscopie (*in-situ*) IRTF-RTA pour les études des mécanismes de la sorption à l'interface minéral-solution. Dans ce chapitre, la moitié du contenu est constituée de regroupements des introductions de deuxième et troisième chapitre qui sont sous forme de publication. Le deuxième chapitre présente les résultats de la sorption de ligands phosphate à l'interface illite – solution électrolyte. Dans ce chapitre nous présentons les résultats de la spectroscopie de surface IRTF-RTA mesurée *in-situ*, des expériences en lot et des analyses de mobilité électrophorétique qui contribuent tous à

l'étude les espèces phosphatées formées à l'interface. Cette étude préliminaire est importante avant d'étudier la co-sorption d'ions uranyle et phosphate, parce qu'elle permet de distinguer les espèces de phosphate et les espèces d'uranyle phosphaté. Dans le troisième chapitre, nous avons étudié les mécanismes de la co-sorption d'ions uranyle et phosphate à l'interface Illite – solution électrolyte en utilisant la même méthode que celle appliquée dans le deuxième chapitre. Dans le dernier chapitre nous avons d'abord étudier la co-sorption d'ions ferrique et phosphate à l'interface Illite – solution électrolyte ; ensuite nous avons étudié l'effet du fer(III) sur la sorption d'ions uranyle à l'interface en présence de ligands phosphate. Nous avons également appliqué la méthode utilisée dans les chapitres précédants.

Bien que des expériences de sorption d'ions uranyle en présence de ligands carbonate ou sous atmosphère contrôlée (P_{CO2} 2.5%) aient été réalisées, les résultats ne sont pas présentés dans ce manuscrit.

Chapter I. State of the ART

1. Sorption processes at the mineral-solution interface

The sorption of inorganic and organic ions is one of the most important processes controlling the fate of ions in the environment. The retention or release of a aqueous compound at the interface between the solid phase and water controls the mobility of substances in the environment and these processes have been described in terms of the sorption isotherm [18]. The term “sorption” has been proposed to describe any process taking place at the interface leading to a phase change of solute (e.g., from liquid to solid) or the transformation of a surface due to the presence of the solute or its environment [19]. Manceau et al. 2002 have identified nine basic processes at the interface (**Fig.I-1**) described as follows: physi- and chemisorption, attachment and detachment, absorption or inclusion (impurity ion whose size and charge is similar to those of one of the ions in the crystal), organo-mineral complexation, complexation to bacterial exopolymer and the cell outer membrane, and hetero-nucleation (epitaxial growth). Sorption mechanisms at the mineral-water interface can be described in detail as follows: (i) ionic exchange, (ii) surface complexation, (iii) surface precipitation, (vi) sorption process related to hydrophobic characteristics of the surface, (v) absorption i.e., incorporation of sorbate into sorbent, (vi) diffusion in the solid phase [19].

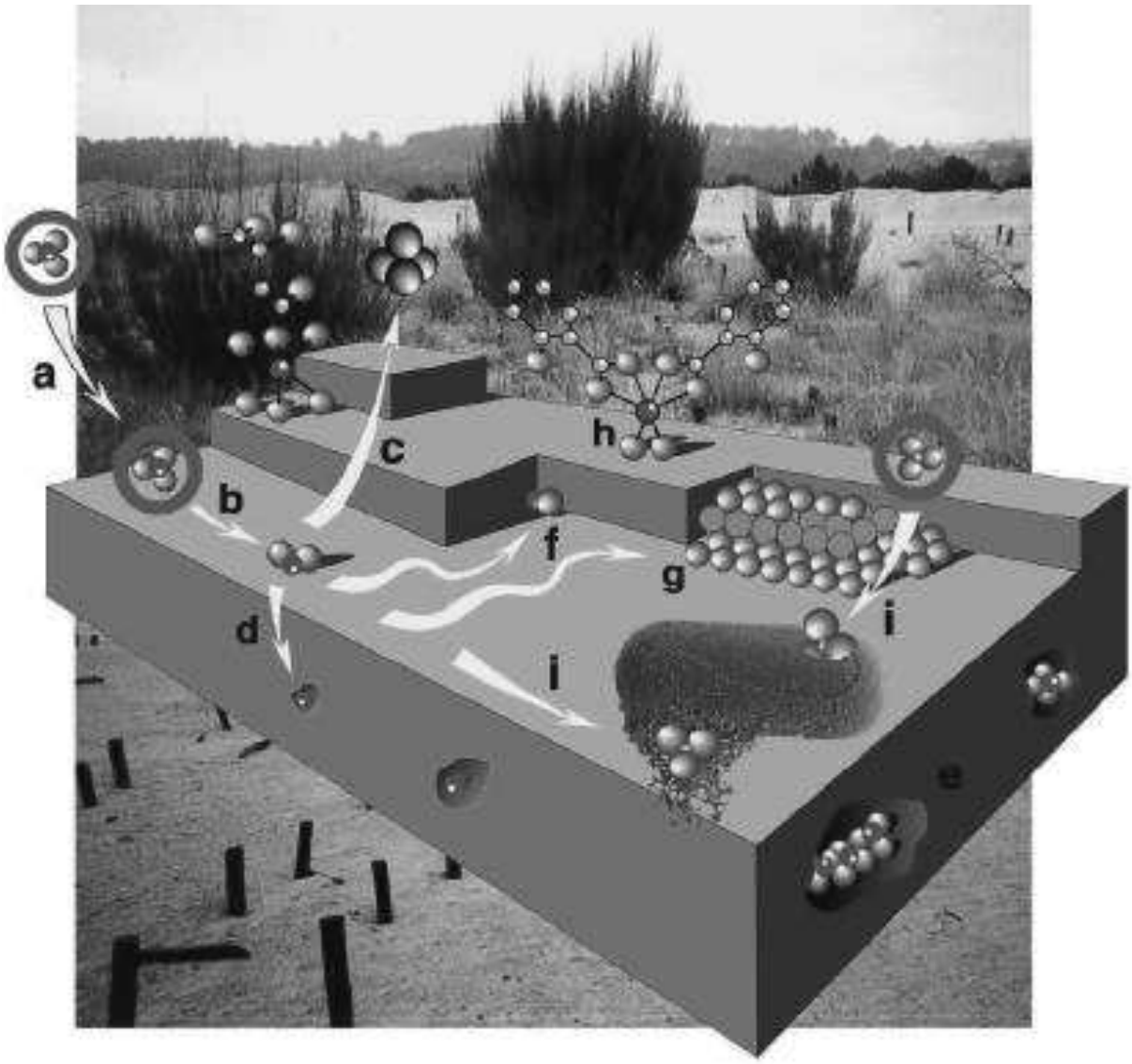

Fig.I-1. A molecular and atomic level schema illustration of basic processes at mineral-water interface: a) physisorption, b) chemisorption, c) detachment, d) absorption or inclusion, e) occlusion, f) attachment, e) hetero-nucleation (epitaxial growth), h) organo-mineral complexation, i) complexation to bacterial exopolymer and the cell outer membrane [20].

1.1. Physico-chemical reaction at the mineral-solution interface

In the formation of outer-sphere surface complexation (OSC) of sorbate at the mineral-solution interface, the driving forces involved in this mechanism could be the electrostatic forces including van der Waals attraction forces (**Fig.I-1**, a). These two forces are described as long-range forces by Stumm et al. 1992 [21]. The OSC could be also formed via hydrogen bonds

e.g., [17]. Ions involved in the outer-sphere surface complexation mechanism keep their hydration sphere and are held on a charged surface within the diffuse ion swarm by electrostatic forces [20]. In this case, the hydrated ions are separated from the sorbent surface typically by two oxygen layers at a distance larger than 4.5 Å between the solid surface and hydrated ions [20] i.e., there are no chemical bonds formed between the surface atom(s) of solid and sorbate species. OSC usually takes place at the mineral surface having a permanent negative (phyllosilicate mineral surface) or positive (layer double hydroxides) charge due to the aliovalent isomorphic lattice substitution [20], this permanent charge is independent of external conditions [20,22] such as pH, ionic strength and sorbate concentration. As the OSC species are bound loosely to the sorbent surface and can be easily exchanged by other ions, metal(loid) ions that are retained at exchangeable surface sites of sorbent are highly mobile and readily available to living organisms [20].

The mechanism of most surface-controlled processes depends on the coordinative environment at the solid-water interface [21]. Chemical reaction occurring at the mineral-solution interface involves the disassociation or establishment of chemical bonds at the surface of the mineral (i.e., formation of chemical bond(s) between the atom(s) of ions in the liquid phase and the atom(s) at the surface of solid phases such as inner-sphere surface complexation, or the disassociation of a chemical bond(s) between the surface atoms of solid phase such as dissolution of solid phases). Inner-sphere complexation (ISC) of sorbate at the surface of sorbent is one important chemical reaction involved in forming a chemical bond between the sorbate ions and the mineral surface. In the ISC process, cations or oxyanions coordinate to the surface by sharing one or several ligands (generally oxygens) with one or several cations from the sorbent [20]. The progressive incorporation of sorbed ions in the sorbent structure may occur during crystal growth [20], i.e., the formation from monolayer to multilayer of sorbed ions, especially when the surface loading of sorbate is high. The reversible release of the ions sorbed by the ISC to

the environment is more difficult than the ions sorbed in the ionic exchange mechanism [20] and could inhibit the dissolution of minerals such as the sorption of phosphate ions, humic acids and macro-molecules [21]. On the other hand, the formation of ISC (e.g., oxalate, dicarboxylates, and hydroxy-carboxylic) could facilitate the detachment of a central metal ion from a solid phase (sorbent) into the bulk liquid phase and therefore enhance the dissolution of the solid phase [21]. The protonation or deprotonation could also enhance the dissolution of minerals [21].

1.2. Surface complexation model

A concept of molecular-level representation of the surface complexation model is shown in **Fig.I-2**a-c. Structure of surface compounds could be divided into the following three categories: (i) inner-sphere versus outer-sphere surface complexes (i.e., chemical bond -short-range forces- versus electrostatic forces -long-range forces-), (ii) mononuclear versus binuclear (e.g., aqueous metal ion coordinate to one versus two surface ligands of mineral such as oxygens), (iii) monodentate versus bidentate (e.g., aqueous ligand coordinate to one versus two surface metal ions of mineral) [19,21]. **Fig.I-2**a shows some OSC models for hydrated ions (Cl^-, Na^+, and Fe^{2+}) via electrostatic forces [19] and hydrogen bonds e.g., sorption of carbonate at hematite surface [17]. Some ISC models (e.g., monodentate, bidentate, mononuclear and binuclear) are given in **Fig.I-2**b. The formation of a tridentate surface complex requires the participation of two crystallites of mineral [15]. This complex model is not considered in the present study and not shown in **Fig.I-2**. A surface complex species could simultaneously have the ISC and OSC model at the mineral-electrolyte solution interface, as shown in **Fig.I-2**c. Several authors have studied the sorption of phosphate ligand at the iron oxyhydroxide (e.g., ferrihydrite and hematite) -electrolyte solution interface, and they suggested that a mononuclear surface species of phosphate ligands may be coupled with a hydrogen bond with neighborhood hydroxyl functional site (**Fig.I-2**c) [16,23]. Arai et al. 2001 also suggested a binuclear surface species of

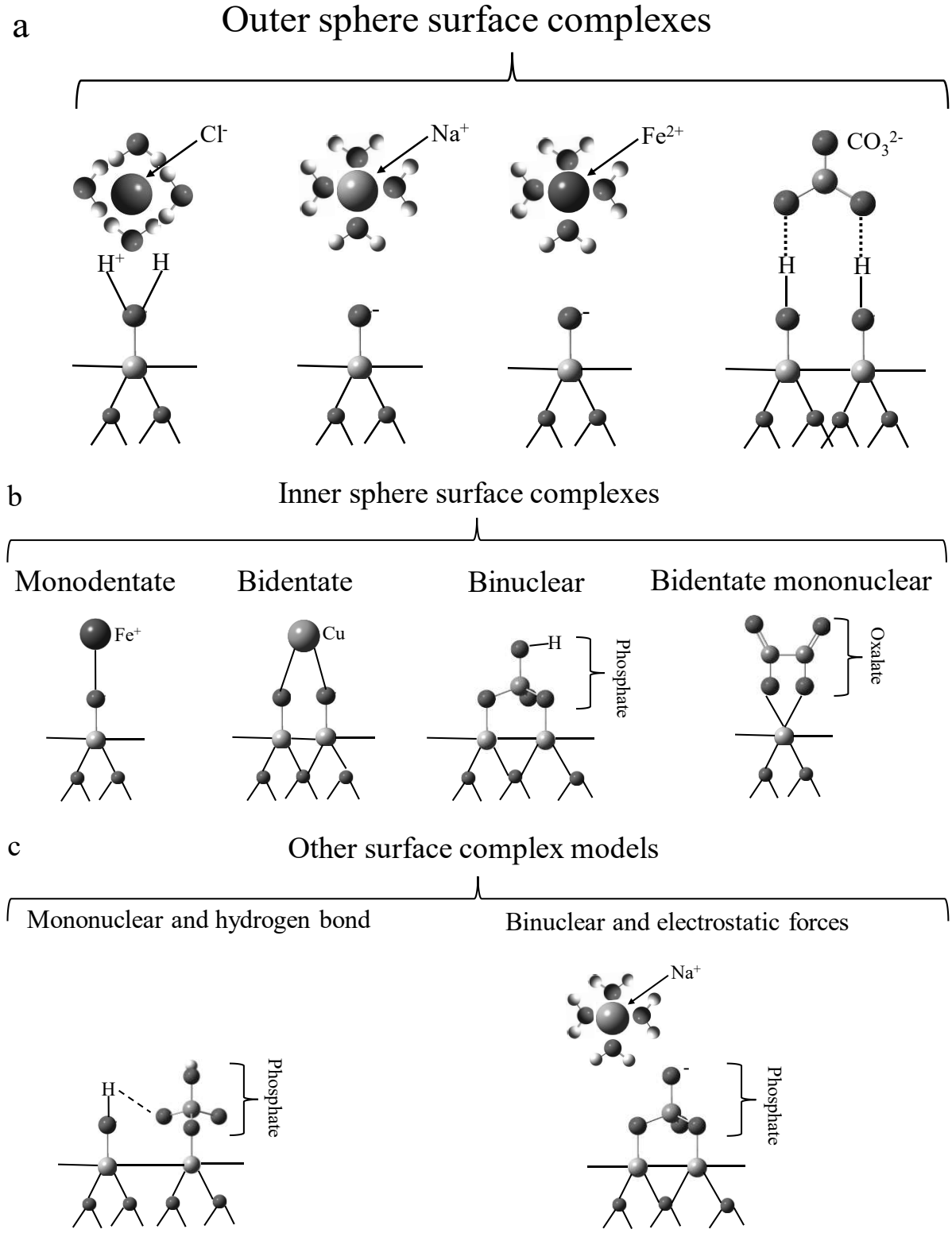

Fig.I-2a-c. Conceptual schema of different surface complex models at mineral surface. Fig.I-2a-b is adapted from Bargar et al. and Laura et al. [17,19]. Fig.I-2c is adapted and inspired from Arai and Sparks, [16]

phosphate ligand which could associate with sodium ions via electrostatic forces [16]. Surface precipitation of sorbate ions i.e., the formation of a tridimensional solid phase at the mineral surface, another important sorption mechanism, is not illustrated in **Fig.I-2**.

1.3. Mineral surface reactivity and surface charge

Mineral surface reactivity. Surface structure, in particular the structural identity of the surface species, controls the surface reactivity of minerals [24]. The surface reactivity of minerals influenced by adsorption reaction is described as follows, (i) the formation of the solid phase (nucleation, precipitation, crystal growth, biomineralization), (ii) dissolution (weathering) of minerals, (iii) surface-catalyzed redox processes (including heterogeneous photochemical processes) [21,24]. The application of these surface reactivity in geochemistry, soil science, and sediment chemistry is important [21].

Surface charge of mineral. There are three main ways to develop the surface charge of solid particles [21]. Firstly, chemical reactions at the surface of solid particles could develop the surface charge [21], such as protonation and deprotonation reactions, chemisorption of anions via ligand exchange, and chemisorption of cations. The surface charge of particles that contain ionizable functional groups: -OH, -COOH, $-OPO_3H_2$, -SH depends on the degree of ionization i.e., proton transfer capacity and therefore on the concentration of H^+ or OH^- in the medium i.e., pH [21]. Secondly, the development of surface charge at the phase boundary may arise from lattice imperfections at the solid surface and isomorphous substitution within the lattice [21]. Finally, the surface charge of solid particles may come from the adsorption of a hydrophobic species or a surfactant ion via so-called hydrophobic bonding, hydrogen bond, and Van der Waals interaction [21]. The net total surface charge (noted as σ_p) of the particle could express as follows [21]:

$$\sigma_p = \sigma_0 + \sigma_H + \sigma_{IS} + \sigma_{OS}$$

σ_0: permanent structural charge (general presence for a mineral) developed by aliovalent isomorphic substitution in minerals (such as in TOT type clay minerals);

σ_H: net proton charge i.e., charge developed by the protonation and deprotonation reaction at the surface;

σ_{IS}: inner-sphere complex charge;

σ_{OH}: outer-sphere complex charge.

The charge state of a solid surface depends on the spatial distribution of free (electric or ionic) charge in its neighborhood; this distribution is ideally considered as an electric double layer (EDL) (**Fig.I-3**) [21]. Based on the Gouy-chapman theory, the surface charge density σ_p is related to the potential ψ (volt) at the surface, which is used for the correction of surface complex formation constants in different surface complexation models [21]. The surface complexation models such as the constant capacitance model (CCM) [25], the diffuse double layer model [26], the triple-layer [27], and the various four layer model [28], are largely applied for the mineral-solution interface [29] i.e., for the surface charge density calculation and the surface potential calculation at the mineral-solution interface. These surface complexation models consider adsorption reactions as analogous to aqueous complexation reactions and assume that the local excess surface charge of mineral is balanced by electrolyte ions through forming a diffuse swarm of "counterions" near the surface [29] (**Fig.I-3**). In these models, the ions in the diffuse layer are retained only by electrostatic forces [29], i.e., no participation of hydrogen binding and van der Waals forces. These methods have different descriptions in electric double layer [30] and therefore have different model parameters [29].

While surface complexation modeling is not carried out in the present study using the previously mentioned methods, the diffuse double layer is presented here to show the relation between the surface charge and the surface potential. In this model, based on Gouy-chapman theory, the surface charge density (σ_p in C m^{-2}) is calculated as follows [21] :

$$\sigma_p = (8RT\varepsilon\varepsilon_0 c \times 10^3)^{1/2} \sinh\left(\frac{Z\psi F}{2RT}\right)$$

R: molar gas constant (8.314 J mol^{-1} K^{-1});

T: the absolute temperature (K);

Ɛ: the dielectric constant of water (Ɛ=78.5 at 25°C);

$Ɛ_0$: the permittivity of free space (8.854×10^{-12} $C^2J^{-1}m^{-1}$);

C: molar electrolyte concentration [M];

Z: ionic charge of electrolyte;

ψ: the surface potential (volt)

F: Faraday constant 96490 [Coulomb mol^{-1}]

At low potential, the above equation can be linearized as follows:

$$\sigma_p = \varepsilon\varepsilon_0\kappa\psi$$

K: double layer thickness K^{-1} (in meters) is defined as:

$$\kappa = ((2F^2 I \times 10^3)/\varepsilon\varepsilon_0 RT)^{1/2}$$

I: ionic strength [M]

As Ɛ=78.5 at 25°C, the charge density equation can be written as follows:

$$\sigma_p = 0.1174\, c^{1/2} \sinh(Z\psi \times 19.46)$$

With simplification, the surface charge could be expressed as a function of ionic strength and surface potential:

$$\sigma_p \cong 2.31\, I^{1/2}\psi$$

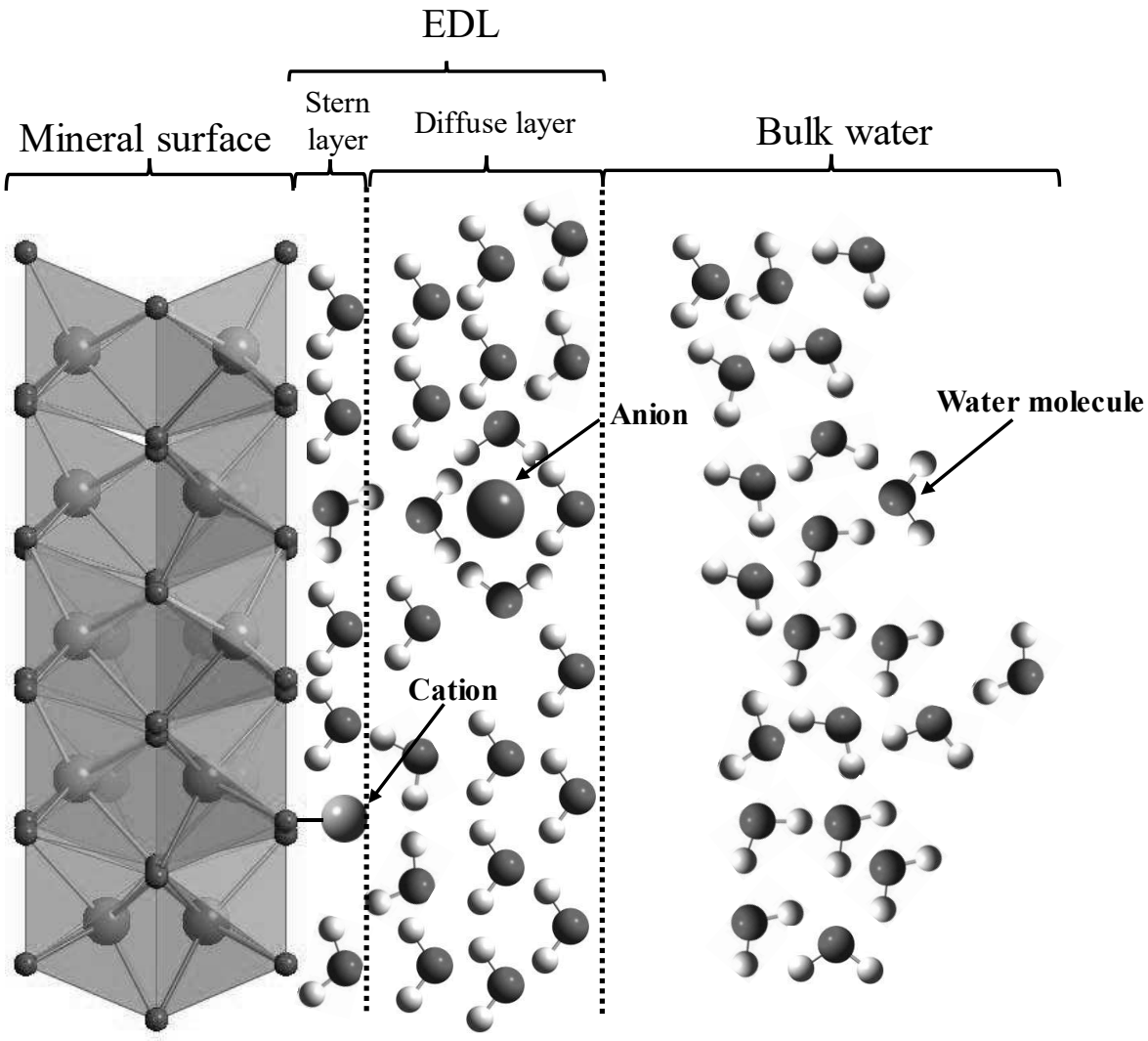

Fig.I-3. A conceptual schema of the electric double layer model at the molecular level. Adapted and inspired from Brown. [31].

1.3.1. Surface reactivity and charge of metal oxihydroxides

In the earth's crust, Si-, Al- and Fe- oxides are abundant components. These minerals represent a significant amount of the solid phases in natural waters, sediments, and soils [21]. In contact with water, these oxides' surface can progressively develop hydroxyl functional groups i.e., ≡S-OH, which have amphoteric properties, because these surface sites can behave as Lewis acids (as electron acceptors) or Lewis bases (as electron donors) [21]. Therefore, the amphoteric surface sites can react with aqueous cations and anions via different adsorption mechanisms,

influencing the surface reactivity of oxide minerals. As most oxide and hydroxide surfaces display amphoteric behavior (acid-base property of ≡S-OH) which can be used to explain their surface electric charge, the surface charge of (hydro)oxides significantly depends on pH [21]. Usually, the surface charge of oxide minerals is positive at low pH and negative at high pH [21].

1.3.2. Structure and surface reactivity and charge of clay minerals

Clay minerals are ubiquitous on our planet in geologic deposits, terrestrial weathering environments, and marine sediments [2,32]. They are layer-type aluminum phyllosilicate whose crystal particle size is at micrometer-level, giving these minerals an important surface reactivity that plays an essential role in natural and human activities e.g., biogeochemical cycling of metals and radioactive waste disposal [2]. Clay mineral structures are established by tetrahedral sheet (noted as T) and octahedral sheet (noted as O); based on the combination of different numbers of T and O sheets, they can be categorized first into layer types clay minerals such as kaolinite -TO type clay mineral-, illite and smectite -TOT type clay minerals- (**Fig.I-4**) [2]. According to the different types of octahedral site occupancy in the octahedral sheet by the metals, the clay minerals can further be recognized as dioctahedral clay minerals or trioctahedral clay minerals e.g., [2,22]. If all the octahedral sites are occupied by a divalent metal (Mg, Fe^{II}), the clay mineral is known as trioctahedral; if two-thirds of octahedral sites are occupied by a trivalent metal (Al, Fe^{III}), the clay mineral is known as dioctahedral e.g., [22]. Kaolinite, illite, and smectite are dioctahedral clay minerals with Al as the main octahedral cation e.g., [22].

A particular character of many TOT-type clay minerals is their high negative layer charge density [22] arising from the aliovalent isomorphic lattice substitution e.g., [2,20,22]. Two manners of aliovalent isomorphic replacement in clay minerals could be identified: in the tetrahedral or octahedral sheet e.g., [33]. In dioctahedral clay minerals, the substitution of Si^{IV} by Al^{III} in tetrahedral layers and the substitution of Al by Mg^{II}, Fe^{II}, and Fe^{III} in octahedral

layers are the most common e.g., [22]. In the former case, three oxygen atoms of the tetrahedron share the excess negative charge; these charges are localized and relatively strong inner-sphere surface complexes could be formed [33]. In the latter case, ten surface oxygen atoms of four silicon tetrahedra associated via their apexes with a single octahedron in the layer share the resulting negative charge; and outer-sphere surface complexes could be formed [33].

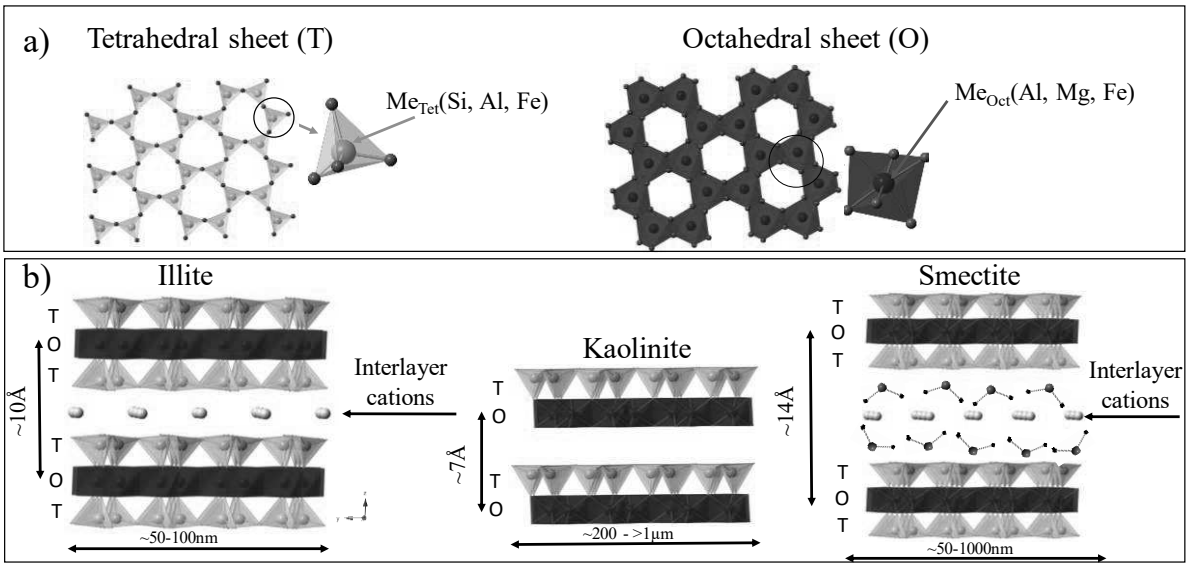

Fig.I-4. Structure of tetrahedral and octahedral sheet in clay minerals (a), and layer structure of kaolinite, illite, and smectite (b). Figures are adapted and modified from Tournassat et al. [22].

2. Uranium(VI) and phosphate ions interactions

2.1. Molecular structure of uranyl ions

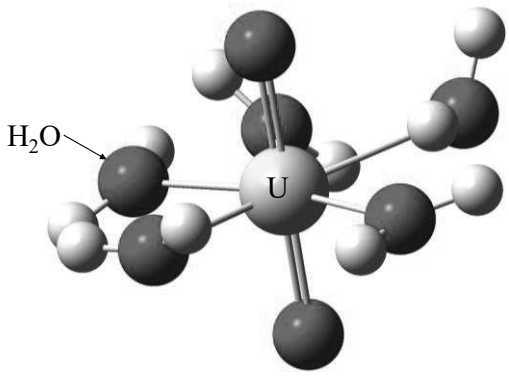

Fig.I-5. Molecular-level schema of hydrated uranyl ion, adapted from Jackson et al. [34].

The atomic number of uranium is 92, and its electronic structure is [Rn] $(5f)^3(6d)^1(7S)^2$. The electronic structure of Rn is $(1s)^2(2s)^2(2p)^6(3s)^2(3p)^6(4s)^2(3d)^{10}(4p)^6(5s)^2(4d)^{10}(5p)^6(4f)^{14}(5d)^{10}(6s)^2(6p)^6$. Uranium elements can display an oxidation state varying from +3 to +6 depending on oxy-reduction conditions. In most natural environments, uranium usually displays a hexavalent (VI) or tetravalent (IV) oxidation state. Under oxidizing conditions, uranium shows a stable hexavalent oxidation state and presents as hydrated UO_2^{2+} (uranyl ion) (usually coordinated with five water molecular [35] as shown in **Fig.I-5**). Under reducing conditions uranium is generally in a tetravalent oxidation state and, it can be oxidated to uranium(VI) if conditions become oxic [36]. In the molecular structure of uranyl ion, uranium is associated with two axial oxygen atoms via covalent bonds [35]. It can be coordinated by four, five (such as oxygen of water molecule **Fig.I-5**) and six equatorial ligands to form an overall coordination geometry of square, pentagonal, or hexagonal bipyramidal around the uranium center [35]. The average bond length of U^{VI}-O_{ax} is 1.793Å with a standard deviation of 0.0035Å and it is 2.368Å for the average of bond length of U^{VI}-O_{eq} with a standard deviation of 0.100Å [35]. U(VI) is considered a hard Lewis acid and prefers to bond to O and N functional groups and thus it could form a series of aqueous complexes and mineral phases in natural waters [37].

2.2. Speciation of uranyl ions in the presence of phosphate ions and carbonate ions

Uranium mainly exists in the oxidation states IV and VI in the environment. It has a higher solubility and a lower tendency to bind at functional groups existing at mineral surfaces in the latter than in the former case, which makes it potentially mobile in the hexavalent state, in the forms of uranyl (UO_2^{2+}) ions [38]. While U(IV) is largely controlled by poorly-soluble uraninite, U(VI) has a strong tendency to form, depending on pH, hydrolysis products and/or anionic carbonate species in natural waters, given its high solubility and its chemical affinity

for the dissolved ligands OH^- and CO_3^{2-} [39–42]. Uranyl ions may also participate to the formation of stable organic complexes with a variety of organic ligands in low pH waters, from simple di- tri-carboxylic acids to humic / fulvic acids [43,44]. They have moreover a high chemical affinity for phosphate ions, too [45,46]. Experimental studies have indeed shown that formation of uranyl phosphate complexes may increase the solubility of U(VI) in terrestrial waters depending on aqueous phosphate concentration and physicochemical conditions, i.e., at low pH (<6) and / or at low to moderate concentrations of other relevant (in)organic ligands like carbonate, fulvate, humate… [45].

2.3. Solubility of uranyl in the presence of phosphate ions and carbonate ions

It is well known that formation of secondary uranyl silicate and/or uranyl phosphate minerals, and sorption processes occurring at surfaces of relevant minerals in rocks and soils, e.g., Fe-/Al-oxihydydroxides and clays, may strongly retard the migration of U(VI) in oxic (ground)waters. Experiments have evidenced that precipitation processes of phosphate phases of the type chernikovite or (Ca-, Mg-, Na-)autunite may limit U(VI) solubility under certain conditions [45,47–51]. Experimental studies have also shown that, depending on physicochemical conditions, phosphate ions may either increase the solubility of REE/U due to formation of aqueous complexes [52] or limit it due to formation of sparingly soluble TME-phosphate (co)precipitates [52–59]. Field studies have moreover shown the presence of various (co)precipitates of U(VI)-phosphate phases in natural sites near U-ore deposits and in contaminated sites or sediments [47,60–69]. It has also been long suggested that processes of uranyl and phosphate (co)sorption are responsible for the long-term retention of U(VI) in some soils or subsurface media, where the trace metal is found in close association with phosphate

and with Fe(III)/Al(III) oxi-hydroxides or with clays [63,65,70–73], or with surface precipitates of Fe^{3+}-phosphate formed at surfaces of hematite [71,74,75].

2.4. Significance in the environment

Mechanistic knowledge of the sorption processes of phosphate ions (noted P, hereafter) onto minerals is of interest for several issues of ecosystem's functioning and health: the regulation of the mobility of P as potential contaminants of (ground)waters due to over-application of phosphate-containing fertilizers in agricultural soils, the long-term fate of rare earth elements (REE) and uranium (U) in soils near U ore deposits or former U mines [76,77], the stabilization / remediation of trace metal elements (TME) contaminations in soils by phosphate injections [78,79], and the scavenging properties of argillaceous formations as host rocks for disposal of high level radioactive wastes [2,3,7,80].

The environmental behavior of uranium (U) is a major issue of soil - sediment - water continuums due to the natural abundance of this metal in igneous or sedimentary rocks, its involvement in a variety of anthropogenic and industrial activities such as metal mining, water treatment, energy production, including nuclear plant development, which generate radioactive wastes or Technonogically-Enhanced Naturally Occurring Radioactive Materials, TE-NORM [81–84], its potential radiological and chemical toxicity [9], and the complexity of the biogeochemical processes that govern its fate in ecosystems [38,44]. Nuclear plants generate high amounts of spent nuclear fuel [85] and produce radioactive wastes whose main constituent is uranium (95%), with the remaining ones being fission products (4%) and plutonium (1%) [86]. Different strategies (such as vitrification, partitioning and transmutation, pyro-processing and deep geological repository) have been proposed to ensure a long-term management of the radioactive wastes [87]. In peculiar, storage of high-level radioactive wastes (HLW) in deep geological repositories in clay rock formations (such as Boom clay, Callovo-Oxfordian clay, Cox, and Opalinus clay, OPA) has been considered by several countries as an important strategy

since the mid-1980s [1]. Clay minerals are major constituents of argillaceous formations, e.g., 40-60 wt % for Cox [88] and 44-92% for OPA [89], and have remarkable physicochemical properties such as a low permeability, a high capacity of radionuclides (RN) retention and reducing properties, which make these formations prospective geological barriers for HLW repository [2,90,1,80,88]. In deep geological repositories, HLW would be isolated from contact with ground-waters by near field engineered multi-barrier systems (e.g., thick steel canisters, cementitious materials barrier and bentonite backfill) in order to prevent their dissolution and the subsequent migration of dissolved radionuclides [90] and RN-containing colloids to the human-accessible environment [88]. However, degradation in the long-term of the near-field multi-barrier system, such as corrosion of thick steel canisters and chemical cement degradation, could result in groundwater entering in contact with HLW [6,90]. The mechanisms and rates of the HLW dissolution, of the long-term diffusion/transport by ground-waters of RN in the host rock porosity, and of the immobilization of the RN by their sorption onto host rock minerals, are thus important safety issues [90,91].

3. (Co-)Sorption processes of uranyl ions onto metal oxihydroxides and clays

3.1. Sorption of phosphate and carbonate ions

Phosphate ions were long suggested to be predominantly sorbed as inner-sphere phosphate surface complexes (ISSC) via ligand exchange involving surface hydroxyl groups present at surfaces of Fe- and Al-hydroxides [92] or at edge surface sites of clays (e.g., [93]). Sorption of P onto these minerals was reported to diminish with pH, due to a progressive deprotonation of the surface hydroxyl groups [93] which is unfavorable to the electrostatic attraction of aqueous phosphate species existing in anionic forms, i.e., $H_2PO_4^-$, HPO_4^{2-} and PO_4^{3-}, in the range of pH (4-8) relevant to natural waters. In recent decades, an increasing number of mechanistic studies of model systems has made it possible to elucidate the speciation of phosphate sorbed, and phosphate and TME (co)sorbed, on the surfaces of Fe- or Al- (oxihydr)oxides. Molecular level

investigations using notably FTIR (Fourier Transform InfraRed spectroscopy) or EXAFS (extended X-Ray Absorption Fine Structure) spectroscopy have provided evidence of a strong chemical sorption of phosphate ions onto goethite [15,94–96], ferrihydrite [16] and hematite [23] due primarily to the formation of multiple ISSC of phosphate, whose nature depend on pH and/or P loading. Moreover, a transition was shown to occur onto Al-oxides, when increasing P loading and/or P sorption reaction time, between the formation of (multiple) phosphate ISSC and the subsequent formation of surface precipitates of Al-phosphates incorporating Al^{3+} ions released upon mineral dissolution [97–99].

Actually, basic mechanisms and species of the sorption of phosphate ions at surfaces of clay minerals have still to be clarified. Some papers have highlighted that an important parameter is the content of minor phases like metal-(oxihydr)oxides acting as strong sorbents of P in clay rocks and / or the presence of sorbed cations (e.g., Fe, Al and Ca) acting as bridging cations for P sorbed onto clays [100–102]. Borgnino et al. [100] have performed experiments of sorption of phosphate ions at the surface of a Fe-modified montmorillonite. They provided spectroscopic evidences for formation of multiple, pH-dependent phosphate surface complexes by performing in-situ ATR FTIR analyses of the montmorillonite–water interface. These authors suggested however that the phosphate surface species were formed on the surfaces of Fe-(hydr)oxides that pre-existed in the clay rock sample studied, rather than on the surface of montmorillonite itself. Phosphate ions sorbed onto a La-modified bentonite were shown to be immobilized as a rhabdophane phase ($LaPO_4 \cdot n\ HO_2$) by EXAFS and ^{31}P solid-state Nuclear Magnetic Resonance (NMR) analyses [103]. Van Emmerik et al. [104] conducted ^{31}P solid-state NMR investigations on the sorption of phosphate ions at the surface of kaolinite and found that P was sorbed via a combination of reactions of formation of phosphate ISSC, which involve singly-coordinated Al-OH sites at the clay edge, and surface precipitates of $AlPO_4$. A recent in-situ ATR FTIR study of P sorbed at the kaolinite–water interface confirmed the existence of multiple surface

species of phosphate in the pH range 4.5 - 7.5, with a predominant species involving aluminol surface sites of kaolinite [105]. EXAFS analyses of arsenate ions (as analogues of phosphate ions) sorbed at the kaolinite–water interface also indicated that a bidentate binuclear arsenate surface complex was formed in the pH range 4.5-6.8 by surface ligand exchange reactions involving aluminol sites present at the kaolinite edges [106]. The same type of surface complex was reported to form during the sorption of arsenate ions at the interface between a synthetic allophane and water at neutral pH [107]. Spectroscopic results therefore support an hypothesis that sorption reactions of phosphate ions onto pure clay minerals primarily relate to alumina-like layers of clays [101,102,108], especially for kaolinite that has a low cationic substitution in the T and O layers [109]. However, further work is needed to fully identify in-situ the (multiple) sorption species of phosphate formed onto clays having a more complex structure than kaolinite, e.g., TOT clays, and to clarify the effects of key parameters on prevailing sorption mechanism, e.g., surface complex vs. surface precipitate formation. This would provide useful information on the affinity of clayey fractions of soils and rocks towards TMEs as the P sorption is expected to influence the clay surface reactivity [110].

3.2. Sorption of uranyl ions

Numerous model system studies have been carried out over the last few decades to gain a comprehensive understanding of uranium(VI) sorption processes in natural systems and to obtain macroscopic and molecular data to increase the robustness of models that are used to predict the migration behavior of U(VI) in the environment. Experiments and/or surface complexation modeling studies have long suggested that a strong chemical sorption of uranyl ions prevails at surfaces of metal oxihydroxides [111–114] and clay minerals / rocks [88,90,115-118].

Molecular scale investigations have evidenced that U(VI) participates in the formation of inner-sphere surface complexes (ISSC) onto oxygen-based minerals, predominantly via bidentate

linkages to oxo surface groups. Several types of surface complexes were identified to form at surfaces of metal oxihydroxides and clays in the absence of phosphate ligands, whose nature depend on key physicochemical parameters of the system studied. Investigations by using Extended X-Ray Absorption Spectroscopy (EXAFS) and Attenuated Total Reflection Fourier Transform Infrared Spectroscopy (ATR FTIR) have revealed that surface-U(VI)-carbonato complexes may predominate the surface speciation of U(VI) sorbed onto hematite, -with the ternary complexes having an inner-sphere metal bridging structure-, under conditions relevant to aquifers and in a wide range of pH [119,120]. EXAFS analyses have also shown that bidendate edge-sharing and bidendate corner-sharing ISSC of uranyl were formed upon sorption of U(VI) onto goethite at pH 4-7 [12]. Speciation studies using EXAFS, X-Ray Photoelectron Spectroscopy, XPS, and Time Resolved Laser Induced Fluorescence Spectroscopy, TRLFS, have provided evidence that U(VI) was sorbed onto an Al-oxide in the forms of a bidentate ISSC of U(VI) and/or polynuclear uranyl surface species, depending on U surface coverage [121,122]. ATR FTIR analyses of U(VI) sorption onto alumina have revealed that three types of uranyl surface species were forming, in a wide range of pH, as a function of surface loading: a monomeric carbonate surface complex, an oligomeric surface complex, and a surface precipitate[123]. Further ATR-FTIR and TRLFS analyses have confirmed the formation of U(VI) carbonato surface species onto alumina, under conditions where aqueous uranyl tricarbonato species exist in solution [124]. Regarding clays, EXAFS analyses have provided evidence that uranyl ions are sorbed as exchangeable UO_2^{2+} in the interlayer space of clays at low pH, leaving the uranyl aquo-ion structure intact, and as additional ISSC of uranyl and / or U(VI) polynuclear surface species [90,125–127], and / or uranyl carbonato ISSC which form at edge sites of clay platelets when increasing pH [128]. Multiple uranyl surface species were also identified by ATR FTIR to co-exist at the surface of montmorillonite in contact with a solution at near-neutral pH and at a low concentration of U (20µM) [129].

3.3. Co-sorption processes

Co-sorption processes of phosphate and TME at surfaces of metal (Fe, Al) (oxihydr)oxides have been well studied, too. Co-sorption of P and U was suggested to imply the formation onto a Fe-oxide surface of surface precipitates of Fe^{3+}-phosphates on which uranyl ions are subsequently sorbed [130]. Tang and Reeder, [9] have studied the uranyl sorption species formed onto alumina in the presence of arsenate ions, which can be taken as chemical analogues for phosphate ions, and have provided evidence for the existence of uranyl arsenate surface precipitates by using EXAFS. Evidence was also given for formation of pH-dependent ternary uranyl phosphato surface complexes and additional surface precipitates of U(VI) phosphates (at high P loadings and long reaction times) along the co-sorption process of P and U onto α-Al_2O_3, by recording *in-situ* using ATR FTIR (Attenuated Total Reflection FTIR) spectroscopy the P-O stretching vibration modes of P (co)sorbed at mineral-solution interface, and by analysing fluorescence emission characteristics of the uranyl ions (co)sorbed [11,131].

Sediments and soils with a high content of clay minerals have also been reported to have a substantial phosphate-binding capacity [108], -even if clays have a lower P adsorption capacity than metal oxihydroxides [101,108,132]-. However, comparatively to metal (oxihydr)oxides, fewer mechanistic studies have been devoted to the sorption of phosphate ions and their co-sorption with U/REE onto clay minerals. Gladys-Plaska et al. [133] have evidenced by FTIR spectroscopy analysis the formation of U(VI)-phosphate surface complexes forming at edge sorption sites of red clays during the simultaneous sorption of U(VI) and phosphate ions. Troyer et al. [5] have investigated by EXAFS the effect of phosphate ions on U(VI) uptake at montmorillonite surface and found a transition between formation of uranyl phosphato ternary surface species and surface precipitates of U(VI) phosphate when increasing phosphate and/or uranyl concentration. They highlighted that ternary surface complexation occurred without a

macroscopic signature of P sorption, which was attributed to low binding of phosphate ions in the absence of U(VI).

Experiments have also shown that the presence of phosphate ligands promotes the sorption of U at the surface of silica[134] and metal (Al, Fe) oxihydroxides [11,111,112,135], which may nucleate precipitation of U(VI) phosphates. Several spectroscopic studies have aimed at elucidating the processes of (co)sorption of uranyl and phosphate ligands -or arsenate ligands as possible chemical analogues- onto metal (Fe, Al) (oxihydr)oxides [9,11-12,114,124,135] and onto clays [136,137], too. Based on EXAFS spectroscopic analysis, Singh et al. suggested a monodentate complexation between uranyl and phosphate for ternary surface complexes sorbed at low concentrations of U (≤10µM) and in the presence of phosphate ligands (100-130µM) onto goethite, at acidic-to-neutral pH. It has also been inferred from ATR FTIR and TRFLS analyses that uranyl ions are sorbed at acidic pH via formation of uranyl phosphato ISSC at low U coverage of Al-oxides, with a progressive transition occurring between the formation of the ternary surface complexes and the surface precipitation of U(VI)-phosphate when increasing P loading [11]. A trögerite-like surface precipitate of uranyl-arsenate has been shown to exist onto alumina by EXAFS analyses, under conditions of high total concentrations (> 50 µM) of U and arsenate ions and at acidic pH [9]. Regarding clays, Gładys-Plaska et al. [133] have shown from XPS and ATR-FTIR analyses the formation of U(VI)-phosphate surface complexes at edge sites of red clays during the simultaneous sorption of U(VI) and phosphate ions. Troyer et al. have investigated by EXAFS and TRLFS the effect of increasing concentrations of phosphate ions and uranyl ions (0.025-100µM) on the uptake of U(VI) by montmorillonite at pH 4-6 and have evidenced a transition between formation of uranyl phosphate surface complexes at low coverage of the clay by U and P, and surface precipitates of U(VI)-phosphates at high surface coverages. These authors have also identified the existence of a U(VI) carbonate ternary surface complex forming at pH 8. Therefore, it is interesting to continue studying the co-sorption of

uranyl and phosphate ions on the surface of other clays and to provide data from *in situ* spectroscopic monitoring of the clay – solution interface during the sorption process and/or as a function of a key parameter, e.g. pH, reaction time and surface coverage of sorbate. In particular, investigations of the surface speciation of uranyl and phosphate ions onto illite is needed to gain better knowledge on the mechanisms of uptake of U(VI) on illitic-rich clays such as those envisioned as far-field host rocks in HLW repository.

4. ATR FTIR spectroscopic technique to study the mineral–solution interface

4.1. Principles

Attenuated total reflection (ATR) spectroscopy is internal reflection spectroscopy. The latter technique is based on the fact that: when light is introduced into an optically denser medium with a high refraction index which is in contact with an optically rarer medium with a lower refraction index, the evanescent wave will be produced in the first few micrometers of the rarer medium [138,139]. As the energy of evanescent wave (E) decreases exponentially in the rarer medium (**Fig.I-6**), only the first micrometers of the medium are probed (e.g., Hug and Sulzberger, 1994). The energy of an evanescent wave is calculated as follows (e.g., Mirabella, 1993):

$$E = E_0 \exp\left[-\frac{2\pi}{\lambda_1}\left(sin^2\theta - n_{21}^2\right)^{\frac{1}{2}}Z\right] = E_0 \exp\left(-\gamma Z\right)$$

Where:

$\lambda_1 = \lambda/n_1$ and $n_{21} = n_2/n_1$

λ: wavelength in free space

λ_1: wavelength of the radiation on the denser medium

θ: angle of incidence relative to the normal

n_1: refractive index of the denser medium

n_2: refractive index of the rarer medium

Z: distance from the surface

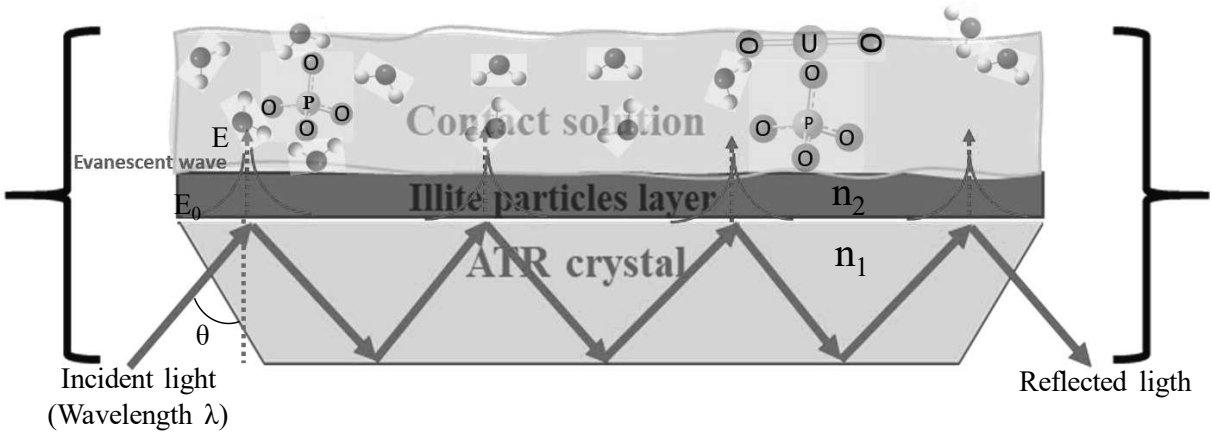

Fig.I-6. Scheme of an ATR crystal cell with a particle layer in contact with a solution. The critical parameters relating to the evanescent wave are shown in the scheme. Adapted and modified from Lefèvre et al. [139].

When the radiation is absorbed by the sample layer, the reflected wave becomes attenuated. For N reflections, the reflectance (R) can be calculated as follows:

$$R^N = (1 - \alpha d_e)^N$$

d_e: effective path length, defined as the thickness required to obtain the absorption in transmission measure

α: absorption activity of layer

The depth of penetration (d_p) probed by the evanescent wave in a rarer medium is calculated as follows (Lefèvre, 2004 and reference therein):

$$d_p = \frac{\lambda_1}{2\pi}(sin^2\theta - n_{21}^2)^{-1/2}$$

By converting the wavelength of radiation to its frequency (ν), the above equation can be written as follows:

$$d_p = \frac{1000}{2\pi\nu n_1}(sin^2\theta - n_{21}^2)^{-1/2}$$

As suggested by Hua and Sulzberger et al. [140], n_2 could be volume-weighted when the particle layer contacts with water, n_2 is expressed as follows:

$$n_2 = F_v \times n_{par} + (1 - F_v) \times n_{water}$$

F_v: volume fraction of solid

n_{par}: refractive index of pure solid phase

n_{water} (equal to 1.34): refractive index of water

4.2. In situ ATR-FTIR

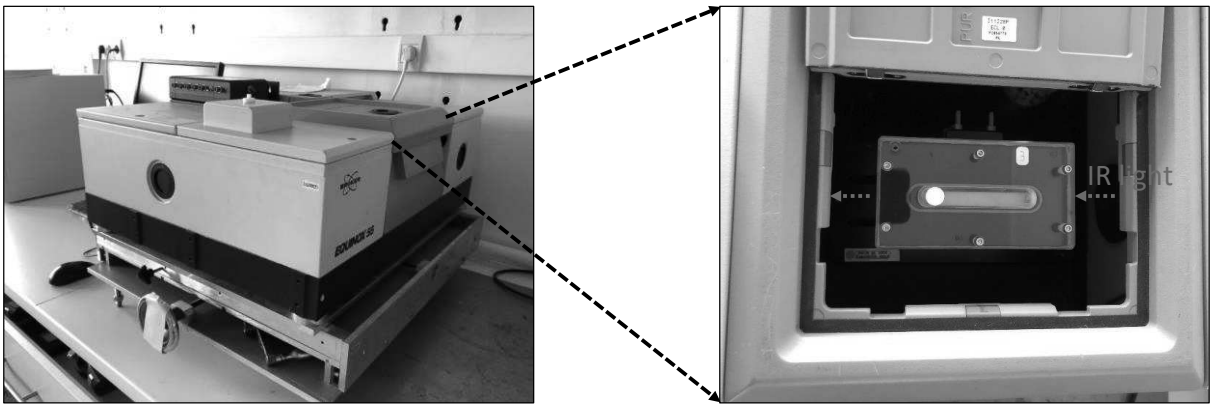

Fig.I-7. Schema of FTIR spectrometry (Equinox 55, Bruker) coupled with an ATR cell.

In situ ATR-FTIR spectroscopy apparatus is shown in **Fig.I-7**. The spectrometer is equipped with an ATR cell containing a ZnSe horizontal crystal (with an angle of incidence of 45°, a crystal size of 7.2×1.0×0.7cm^3 and 5 internal reflections) and with a MCT (Mercury Cadmium Telluride) detector that was cooled down by liquid nitrogen during FTIR spectra acquisition. This technique has several advantages: *(i)* it has an increased sensitivity for sorbed species [141] and is adapted to monitor processes taking place at mineral-solution interface (sorption, desorption, dissolution / precipitation …), *(ii)* it is powerful to study the surface speciation of oxyanions sorbed at the interface [139]; *(iii)* and it allows in-situ monitoring of multiple surface species [11,97].

4.3. Molecular symmetry of uranyl and phosphate ions

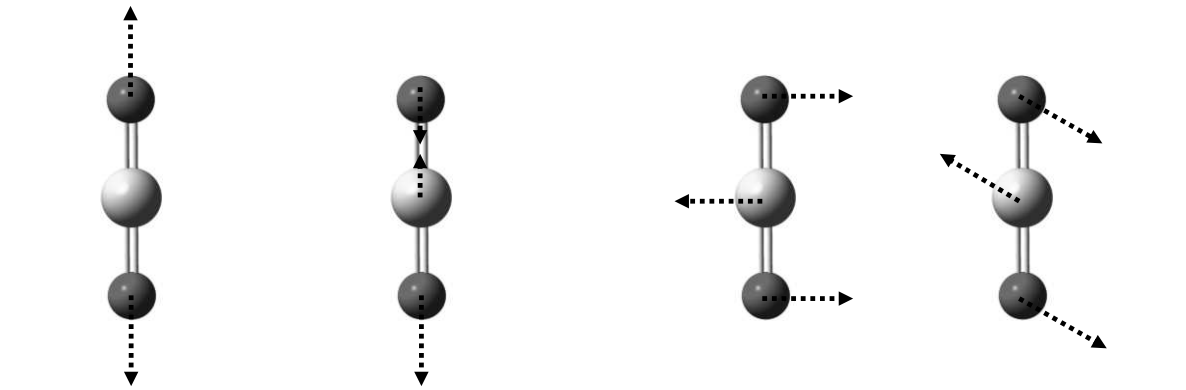

Fig.I-8. Schematic illustration of the vibrational modes of UO_2 unit, from left to right: symmetric stretching (υ_1), symmetric stretching (υ_3), in-plane bending (υ_2), out-plane bending (υ_3). Adapted from Nakamoto et al. and Lu et al. [142,143]

Fig.I-8 shows four vibrational modes of UO_2 unit: symmetric stretching (υ_1), symmetric stretching (υ_3), in-plane bending (υ_2), out-plane bending (υ_3). There are two characteristic vibration bands of the UO_2 unit, i.e., the antisymmetric band υ_3 (IR active) and the symmetric bending band υ_1 (Raman active), which were widely used in molecular-scale studies of the coordination environment of UO_2 unit in aqueous solution and in solid state [143]. Free (hydrated) uranyl ion shows a υ_3 band at 962cm^{-1} and a υ_1 band at 870cm^{-1} [144]. Replacement of the equatorial water molecules of uranyl ions during their complexation by ligands leads to a weakening of the U=O_{ax} axial bonds, and, consequently, the bonds' lengths are increased and the position of υ_3 and υ_1 bands are decreased (i.e., υ_3 < 962cm^{-1} and υ_1 < 870cm^{-1}) [144].

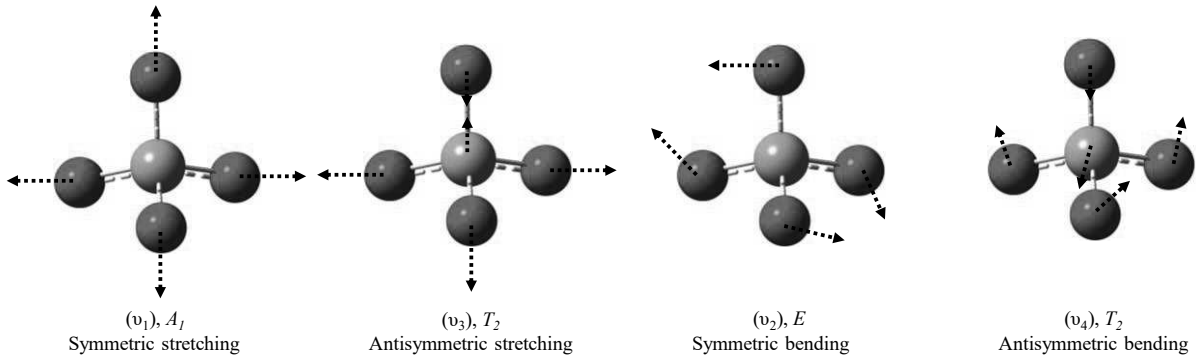

Fig.I-9. Schematic illustration of the vibrational modes of PO_4 unit, from left to right: symmetric stretching (υ_1) A_1, antisymmetric stretching (υ_3) T_2, symmetric bending (υ_2) E, antisymmetric bending (υ_4) T_2. Adapted from Nakamoto et al. [142].

FTIR data analysis of phosphate species is based on the number of resolved bands and their maxima position, i.e., number and position of IR-active υ_3 and υ_1 bands which reflect the possible molecular symmetry of the phosphate ions [16,23]. Tejedor-Tejedor and Anderson [15] have systematically studied the possible molecular configuration of phosphate ions in aqueous solution or sorbed at the goethite–H_2O (or D_2O) interface. All considerations on the molecular configurations and the evolution of molecular symmetry, i.e., reduction or increase of molecular symmetry, are based on changes of the coordination environment of the PO_4 unit due to, for example, formation of inner-sphere complex of phosphate ions in solution (protonation and/or complexation with metals) and at the solid–solution interface (complex of phosphate ions with cation(s) at basal plane / edge of particle clay surface).

The uncoordinated PO_4 unit possesses a tetrahedral geometry and the molecular symmetry of this tetragonal penta-atomic molecule belongs to the point group T_d [16,145], which has an important molecular symmetry (24 symmetry elements).

The unprotonated trivalent phosphate ion (PO_4^{3-}), which is the dominant aqueous species at pH>12, has four vibration bands related to asymmetric bending at 567cm^{-1} (T_2, υ_4), asymmetrical stretching at 1006cm^{-1} (T_2, υ_3), symmetric bending at 420cm^{-1} (E, υ_2) and

symmetrical stretching at 938cm^{-1} (A_1, υ_1) (**Fig.I-9**) [145]. All four vibrations are Raman-active but only the υ_3 and υ_4 are IR-active [145]. Only the υ_3 can be observed in our wavenumbers range, and the number of vibration bands of υ_3 and υ_1 is equal to two.

The unprotonated phosphate ion is progressively protonated with decreasing solution pH, i.e., from monoprotonated (HPO_4^{2-}) to triply protonated (H_3PO_4). The monoprotonated divalent phosphate ion is the main P species in the pH range 8-12. This ion has one coordinated hydrogen which reduces the molecular symmetry from the point group of T_d to C_{3v}, the later having 6 symmetry elements and the number of vibration bands of PO_4 unit increasing from 4 to 6 [146]. Another consequence of the reduction of molecular symmetry is that the υ_3 band splits into two υ_3 bands at 1077cm^{-1} (E) and 989cm^{-1} (A_1) and the υ_1 becomes IR-active and shifts to 850cm^{-1}, the frequency of others vibrational bands of PO_4 unit being under 800cm^{-1}. When a metal cation, in aqueous solution or sorbed at a mineral surface, is coordinated to PO_4^{3-}, the molecular configuration of phosphate ion may be unprotonated monodentate mononuclear. The molecular symmetry of this configuration should be the same as the monoprotonated phosphate, i.e., $C_{3v,}$ and two υ_3 (E, A_1) and one υ_1 would then be present.

Another phosphate species that has a molecular symmetry of C_{3v} is the fully protonated (or triprotonated) uncharged phosphate acid (H_3PO_4), which is the dominant aqueous species at pH<2.0. This molecule has the same number of P-O(H) vibration bands as HPO_4^{2-}, i.e., 6 vibration bands in which it has two υ_3 at 1174-1179cm^{-1}, 1006cm^{-1} and one υ_1 at 888-890cm^{-1} [15,16,146].

Further protonation of HPO_4^{2-} leads to formation of the diprotonated monovalent phosphate ion, $H_2PO_4^-$, which is the dominant specie at pH between 2 and 7. The presence of two coordinated hydrogens to PO_4 unit leads to a lower molecular symmetry than that of one coordinated hydrogen, i.e., the molecular symmetry is reduced from C_{3v} to $C_{2v,}$ and the number of molecular symmetry elements decreases from 6 to 4. As a result of molecular symmetry

reduction, υ_3 (*E*) splits in two υ_3 bands (B_1 and B_2) and the number of vibrational bands of PO_4 unit increases from 6 to 9 with three υ_3 vibration bands at 1160cm^{-1} (A_1), 1074cm^{-1} (B_1), 940cm^{-1} (B_2) and one υ_1 band at 874 cm^{-1} (A_1). The molecular symmetry may be similar to that of $H_2PO_4^-$ (i.e., C_{2v}) when PO_4^{3-} is coordinated by two equivalent aqueous cations or surface metal cations at mineral particle surface (i.e., two identical surface sites). In this case, the molecular configuration of PO_4 unit is unprotonated bridging bidentate mononuclear. In addition to the latter case, there are two other molecular configurations of PO_4 unit which have C_{2v} symmetry, i.e., unprotonated bidentate mononuclear complex and diprotonated bridging bidentate mononuclear complex.

4.4. ATR-FTIR contributions to understanding sorption mechanisms at molecule-level

As infrared absorption spectroscopy can probe chemical bonds [139] and it can provide in detail molecular vibration information on the structure of molecules e.g., [147], this technique has been used in studies of sorption mechanisms at the molecule level for years [139]. ATR-FTIR spectroscopy may be the most established setup of infrared absorption spectroscopy for studying the solid-to-liquid interface [147]. The application of this technique was first realized for the sorption of organic molecules onto suspensions in relation with the flotation process [138]; however, the quantification analysis in suspension is complicated by several factors, such as the impact of surface charge on dispersitivity with changing different solution parameters such as pH, adsorbate concentration, ionic strength [139]. Nevertheless, this technique has obtained advantages in studying inorganic ions sorbed onto oxides using the procedures developed by Hug and Sulzberger et al. [140]. A colloidal layer of oxides has been coated at the surface of ATR crystal by these authors in their study of oxalate sorption onto TiO_2, making possible a quantitative spectral analysis [139]. Many studies of sorption mechanisms of inorganic and organic ions onto (oxihydr)oxides have been carried out by using (in-situ) ATR-

FTIR spectroscopy (i.e., to study the identity of sorbates at the surface of mineral at the molecular level) such as the sorption of oxyanions (phosphate, carbonate, sulfate, selenate, selenite ions etc.) at the (oxihydr)oxides (e.g., Ti-, Fe-, Al-)–solution interface e.g., [16,17,23,97,98,148–151,151–153]; the sorption of organic ions at the (oxihydr)oxides–solution interface e.g., [140,141,154–156]. In-situ ATR-FTIR technique has also been applied in studies of the co-sorption mechanisms of metal and oxyanion ions at the (oxihydr)oxides–solution interface e.g., [119,120,157–162]. To our best knowledge, the contribution of in-situ ATR-FTIR spectroscopy to the molecular understanding of the sorption mechanism of sorbates, especially phosphate ion, uranyl ion, at the clay-to-electrolyte solution interface is not widely documented e.g., [105,137,163]. By using in-situ ATR FTIR technique (coupled with traditional batch sorption experiment and electrophoretic mobility analysis), the present studies contribute to a refined understanding of sorption mechanisms and surface speciation of uranium(VI) ions at the clay (e.g., illite)–electrolyte solution interface under different investigative conditions such as the effect of phosphate ligand and the effect of competitive cations e.g., Fe^{III} ions.

Chapter II. Speciation studies at the Illite - solution interface: Part 1 - Sorption of phosphate ions

Speciation studies at the Illite - solution interface: Part 1 - Sorption of phosphate ions

Shang Yao Guo, Mirella Del Nero*, Olivier Courson, Sylvia Meyer-Georg, Remi Barillon

Article submitted at Colloid and Surface A

1. Introduction

Mechanistic knowledge of the sorption processes of phosphate ions (noted P, hereafter) onto minerals is of interest for several issues of ecosystem's functioning and health: the regulation of the mobility of P as potential contaminants of (ground)waters due to over-application of phosphate-containing fertilizers in agricultural soils, the long-term fate of rare earth elements (REE) and uranium (U) in soils near U ore deposits or former U mines [76,77], the stabilization / remediation of trace metal elements (TME) contaminations in soils by phosphate injections [78,79], and the scavenging properties of argillaceous formations as host rocks for disposal of high level radioactive wastes [2,3,7,80]. It has long been known that phosphate ions have a high chemical affinity for trace metal elements like REE [164] and U, including uranium in its hexavalent state that is potentially mobile in the environment [52,165–167], as well as for the surfaces of Fe- or Al-(hydr)oxides and clays that are common minerals of soils and rocks [93,108,168,169]. Experimental studies have shown that, depending on physicochemical conditions, phosphate ions may either increase the solubility of REE/U due to formation of aqueous complexes [52] or limit it due to formation of sparingly soluble TME-phosphate (co)precipitates [52–59]. Field occurrence of such co-precipitates near U-ore deposits or sites/sediments contaminated by REE/U is well documented, too [59,170–179]. Field observations have suggested moreover that processes of (co)sorption of U/REE and phosphate ions at surfaces of iron (oxihydr)oxides and aluminum (oxihydr)oxides [8,173,180–185] and clays [8,181,185] are effective for the long-term retention of these TME in soils and (sub)surface media. Consistently, experimental studies have reported that the sorption of P

promotes the retention of REE/U onto these mineral surfaces, at acidic to neutral pH [130]. Phosphate ions were long suggested to be predominantly sorbed as inner-sphere surface complexes (ISSC) of phosphate, via ligand exchange involving surface hydroxyl groups present at surfaces of Fe- and Al-hydroxides [92] or at edge surface sites of clays [93]. Sorption of P onto these minerals was reported to diminish with pH, due to a progressive deprotonation of the surface hydroxyl groups [93] which is unfavorable to the electrostatic attraction of aqueous phosphate species existing in anionic forms, i.e., $H_2PO_4^-$, HPO_4^{2-} and PO_4^{3-}, in the range of pH (4-8) relevant to natural waters. In recent decades, an increasing number of mechanistic studies of model systems has made it possible to elucidate the speciation of phosphate sorbed, and phosphate and TME co-sorbed, on the surfaces of Fe- or Al- (oxihydr)oxides. Comparatively, fewer mechanistic studies have been devoted to the sorption of phosphate ions -and their co-sorption with U/REE- onto clay minerals.

Regarding Fe- or Al- (oxihydr)oxides, molecular level investigations using notably FTIR (Fourier Transform InfraRed spectroscopy) or EXAFS (extended X-Ray Absorption Fine Structure) spectroscopy have provided evidence of a strong chemical sorption of phosphate ions onto goethite [15,94–96], ferrihydrite [16] and hematite [23] by formation of multiple ISSC of phosphate, whose nature is strongly dependent on pH and/or P loading. A transition was shown to occur onto Al-oxides between formation of (multiple) ISSC of phosphate and subsequent formation of surface precipitates of Al-phosphates incorporating Al^{3+} ions released by mineral dissolution [97–99], when increasing P loading and/or P sorption reaction time in experiments. Co-sorption of phosphate ions and U(VI) at surface of a Fe-oxide was suggested to imply the formation of surface precipitates of Fe^{3+}-phosphates on which uranyl ions are subsequently sorbed [130]. In contrast, Tang and Reeder [9] have provided evidence for the formation of uranyl arsenate surface precipitates by performing EXAFS analyses of uranyl sorbed onto alumina in the presence of arsenate ions (which can be taken as chemical analogues for

phosphate ions). Finally, studies reporting *in-situ* monitoring by ATR FTIR (Attenuated Total Reflection FTIR) spectroscopy of the P-O stretching vibration modes of P (co)sorbed with uranyl ions at the α-Al_2O_3-solution interface, and analyses of fluorescence emission characteristics of U (co)sorbed [11,131], have shown that a transition exists between formation of ternary uranyl phosphato surface complexes and surface precipitates of U(VI) phosphates. Like for experiments of sorption of phosphate ions alone, this transition occurs when increasing values of P loading and/or reaction time in the experiments of co-sorption of P and U.

Regarding clay minerals, it has been widely reported that sediments and soils with a high content of clays have a substantial phosphate-binding capacity [108], -even if clays have a lower P adsorption capacity than metal oxihydroxides [101,108,132]-. Gladys-Plaska et al. [133] have shown by FTIR analysis the existence, at edge sorption sites of red clays, of uranyl phosphate surface complexes formed during the co-sorption of U(VI) and phosphate ions. Troyer et al. [5] have investigated by EXAFS the effect of phosphate ions on U(VI) uptake by montmorillonite. They found a transition existing between formation of uranyl phosphato ternary surface species and surface precipitates of U(VI) phosphates, when increasing phosphate and/or uranyl concentration in experiments. These authors highlighted that ternary surface complexation occurred without a macroscopic signature of P sorption, which was attributed to a low binding of phosphate ions in the absence of U(VI). However, basic mechanisms and species of the sorption of phosphate ions at surfaces of clay minerals have still to be clarified. Some papers have highlighted that an important parameter is the content of minor phases like metal-(oxihydr)oxides acting as strong sorbents of P in clay rocks, and / or the presence of sorbed cations (e.g., Fe, Al and Ca) bridging P sorbed to the clay surfaces [100–102]. Borgnino et al. [100] have performed sorption experiments of phosphate ions at the surface of a Fe-modified montmorillonite. These authors evidenced by using in-situ ATR FTIR the formation of multiple, pH-dependent phosphate surface complexes at mineral–water interfaces but suggested that the

sorption took place onto Fe-(hydr)oxides pre-existing in the clay sample studied, rather than on the surface of montmorillonite itself. Phosphate ions sorbed onto a La-modified bentonite were shown to be immobilized as a rhabdophane phase ($LaPO_4 \cdot n\ HO_2$) by EXAFS and ^{31}P solid-state Nuclear Magnetic Resonance (NMR) analyses [103]. Van Emmerik et al. [104] conducted ^{31}P solid-state NMR investigations on the sorption of phosphate ions at the surface of kaolinite. They found that P was sorbed via a combination of reactions of formation of phosphate ISSC, which involve singly-coordinated Al-OH sites at the clay edge, and surface precipitates of $AlPO_4$. A recent in-situ ATR FTIR study of P sorbed at the kaolinite–water interface confirmed the existence of multiple surface species of phosphate in the pH range 4.5 - 7.5, with a predominant species involving aluminol surface sites of kaolinite [105]. EXAFS analyses of arsenate ions (as analogues of phosphate ions) sorbed at the kaolinite–water interface also indicated that a bidentate binuclear arsenate surface complex was formed in the pH range 4.5 - 6.8 by surface ligand exchange reactions involving aluminol sites present at the kaolinite edges [106]. The same type of surface complex was reported to form during the sorption of arsenate ions at the interface between a synthetic allophane and water at neutral pH [107]. Spectroscopic results thus support an hypothesis that sorption reactions of phosphate ions onto pure clay minerals primarily relate to alumina-like layers of clays [101,102,108], especially for kaolinite that has a low cationic substitution in the T and O layers [109]. Further work is however needed to identify in-situ the (multiple) sorption species of phosphate formed onto clays having a more complex structure than kaolinite, e.g., TOT clays, and to investigate the effects of key parameters on prevailing sorption mechanism. This would provide useful information on the affinity of clayey fractions of soils and rocks towards TMEs, as P sorption is expected to influence the clay surface reactivity [110].

In the present study, we addressed the effects of phosphate concentration and reaction time on the sorption mechanisms of phosphate ions onto Illite. This clay mineral was considered in this

study (as a purified homonionic Na-Illite) because of its abundance in soils, sediments and deep geological clay rock formations. For example, Illite is a major clay phase in some rocks expected to be used as hosts of high-level radioactive waste repositories (e.g., Callovo-oxfordian clay and Opalinous clay). The objective was to identify the phosphate surface species formed in-situ at Illite-solution interface along the P sorption process, with paying a particular attention to a possible transition between formation of ternary surface complex of phosphate and Al-phosphate surface precipitates, when increasing reaction time or P loading. To this end, we combined macroscopic sorption experiments, electrophoretic mobility measurements, and in-situ ATR FTIR spectroscopy monitoring of Illite-P-solution interface along the sorption process of P. Batch sorption experiments were carried out to characterize the effects of solid-to-liquid ratio ($R_{S/L}$), pH and total concentration of phosphate ions ($[P]_{I,aq}$) on the macroscopic sorption of P. Complementary electrophoretic mobility (EM) measurements of the clay suspensions were made in order to provide indirect information on surface charges imparted to clay surface by reactions of sorption of phosphate species. *In situ* ATR FTIR spectroscopy experiments were performed to record *in-situ* the P-O stretching vibration modes of phosphate sorbed at Illite-solution interface. This technique has several advantages: *(i)* it has an increased sensitivity for sorbed species [141] and is adapted to monitor processes taking place at mineral-solution interface (sorption, desorption, dissolution / precipitation …), *(ii)* it is powerful to study the speciation of oxyanions sorbed at the interface [139]; *(iii)* and it allows in-situ monitoring of multiple surface species [11,97]. Data presented here contribute to a refined understanding of sorption mechanisms and surface speciation of phosphate ions at the Illite–water interface.

1. Materials and methods

1.1. Source materials

All the solutions used in experiments were prepared by using ultrapure Milli-Q water (purity > 18 MΩ.cm) and reagent grade chemicals. Source material used in this study was an argillaceous

clay (called “Illite du Puy”), which collected in the region of Le Puy-en-Velay in the Massif Central Mountains in France and was provided by the company “Argile Verte du Velay”. Two clay stock samples were used. The first one, noted here as “IdP”, corresponds to the particle size fraction lower than 77 μm of the Illite du Puy source material and it was used in the experiments as received. The second stock sample noted here as “NaIdP” was obtained by purification of a subsample of IdP in order to convert the initial Illite into a Na-homoionic Illite. The subsample was conditioned by acid washing and subsequent exchange of the exchangeable cations against Na^+ by using the method detailed by Glaus et al. [14]. The treatment is also expected to remove hydrolyzed products -such as hydroxy-aluminum compounds-, phosphate impurities and soluble minerals like calcite [14,80]. Briefly, a multistep conditioning procedure was carried out as follows. An IdP subsample (50 g) was brought in contact with a known volume (1 L) of a 1M NaCl/0.1M formate buffer (FB) solution (with FB being a 0.05 M Na-formate - 0.05 M formic acid solution at pH 3.5, and the solid-to-liquid ratio, being equal to 50 $g.L^{-1}$). After a 4-hours equilibration of the clay suspension by gentle stirring, the particles were left to settle overnight by sedimentation. The supernatant solution was then removed and the particles were re-suspended by addition (to 1 L) of a 1 M NaCl / 0.1 M FB solution (ratio: 50 $g.L^{-1}$). The procedure described above was repeated six times in order to largely remove acid-soluble Ca^{2+}-mineral phases, too. Remaining solid was then washed three times by 0.1 M NaCl in order to remove format buffer, exchanged cations and solubilized impurities. It was filled into dialysis bags (Visking® dialysis tubing, MWCO: 12-14 kDa, Pore diameter: ca. 25 Å, SERVA, Heidelberg, Germany) and dialyzed with a "clay water" prepared as follows. A subsample of 1g of IdP was brought in contact with 10mL of Milli-Q® water in a dialysis bag. The dialysis bag was then equilibrated with 3 L of Milli-Q® water during 24 h and the concentration of Na^+ in the external solution was measured. The external solution was removed and refilled with Milli-Q® water until the concentration of Na^+ in the external solution dropped

to < 1 mM. This external dialyzed solution was named "clay water". Final solid sample was dried at 40°C and then powdered in an agate mortar and sieved. The size fraction < 75 µm was selected and taken as the final NaIdP stock sample, which was stored in a desiccator until its use in experiment.

1.2. Characterization of Illite du Puy

1.2.1. Mineralogical and chemical analyses

The mineralogical compositions of IdP and NaIdP were obtained from X-ray diffraction (XRD) sample analyses conducted with a Bruker diffractometer (D8 Advance Eco) at the ITES Institute (Institut Terre et Environnement de Strasbourg, Strasbourg University, France). The measurements were performed on both the whole-rock samples and the clay size (< 2 µm) fractions. The latter's were isolated by settling, and oriented on glass slides and XRD analyses were performed: a) without any treatment, b) after sample saturation overnight in ethylene-glycol (EG), c) after sample heating at 490°C for 4 h, and d) after sample saturation overnight in hydrazine [186]. Clay minerals constitutive of the < 2 µm fraction of samples were then identified by values of their layer and interlayer spacing deduced from diffractograms [187]. A semi-quantitative estimation of the percentage of each clay mineral was made by using the software DIFFRAC.EVA version 4.3, with an error in reproducibility of the measurements of less than 5 % for each mineral. Chemical analyses of the IdP and NaIdP samples, and their respective clay size fraction (< 2 µm), were conducted at SARM-CRPG (Service d'Analyse des Roches et Minéraux, Centre de Recherches Pétrographiques et Géochimiques, Nancy, France). Major element and trace element analysis were made by using a Thermo Fischer ICap 6500 inductively coupled plasma optical emission spectrometer (ICP-OES) and a Thermo Elemental X7 inductively coupled plasma mass spectrometer (ICP-MS), respectively. The analytical precision, which depends on the element concentration, was determined to be lower than 0.1 %

(weight % oxides) and in the range 5-20 % for ICP-OES and ICP-MS measurements, respectively (< 10 % for U in the range of concentrations > 10 $\mu g.g^{-1}$).

1.2.2. Specific surface area

Specific surface areas of IdP and NaIdP samples were determined by N_2-BET measurements using an ASAP2420 surface area and porosity analyzer. Subsamples were degassed for 4 h at 150°C before measurements. Values of specific surface areas were found to be equal to 92 and 107 $m^2.g^{-1}$ for IdP and NaIdP, respectively. These values are in good agreement with the value (97 $m^2.g^{-1}$) obtained by Bradbury and Baeyens [188].

1.2.3. Preliminary experiments of (Na)IdP-solution interactions

Preliminary experiments were conducted in order to determine the chemical evolution of a solution brought in contact with IdP or NaIdP, respectively, as function of key physicochemical parameters. Batch experiments were performed under atmospheric conditions and at a given ionic strength value (0.005 M NaCl), for varying values of solid-to-solution ratio (from 0.5 to 6 $g.L^{-1}$ and 0.5 to 3$g.L^{-1}$ for IdP and NaIdP, respectively), reaction time (24 hours - 7 days), and pH (3-7). Suspensions of (Na)IdP were prepared in individual (50mL) polypropylene tubes at desired values of solid-to-solution ratios ($R_{S/L}$) and initial pH (2.3 to 3.8 for IdP and 2.7 to 6.2 for Na-IdP). The suspensions were then equilibrated by gently shaking end-over-end during a desired reaction time (from 2 hours to 4 days). Final pH was measured (uncertainty: 0.05 pH unit). After the equilibration step, the suspensions were centrifuged at 9000 rpm for 3 hours for a solid–solution separation (cut-off: 16 nm for Illite). A defined volume of supernatant solution was taken from each individual tube and was acidified at pH < 1 by adding a small amount of 67% HNO_3 for analysis of major and trace elements by ICP-OES (Varian 720es) and ICP-MS (Agilent 7700x), respectively (uncertainty ranges of 2-20 % and 5-20 %, respectively). The analyses were performed at the Department of Analytical Sciences of IPHC, Strasbourg, France.

1.3. Macroscopic sorption of phosphate ions

1.3.1. Experimental procedure

Batch sorption experiments were carried out at 25°C under atmospheric conditions to evaluate the effect of pH, total concentration of phosphate ions (noted $[P]_{I,aq}$), and solid-to-solution ratio ($R_{S/L}$) on the retention of phosphate ions at the NaIdP–solution interface. Batch experiments (performed in 0.005 M NaCl electrolyte solution) were carried out to obtain: (i) phosphate sorption edges (in the range of final pH, pH_F, of 3-8) at various $R_{S/L}$ ($R_{S/L}$: 1, 2 or 3 $g.L^{-1}$, $[P]_{I,aq}$: 20 µM), (ii) sorption edges at two phosphate concentrations (20 µM and 100 µM, $R_{S/L}$: $3g.L^{-1}$) and (iii) phosphate sorption isotherms at pH4 ($[P]_{I,aq}$ in the range 20-200 µM, $R_{S/L}$: $3g.L^{-1}$). The experiments were conducted as follows. Suspensions of NaIdP in 0.005 M NaCl electrolyte solutions were pre-equilibrated for 3 days in 15 mL polypropylene centrifuge tubes, at desired values of $R_{S/L}$ and pH. If necessary, solution pH was adjusted during pre-equilibration by adding very small volumes of a 0.1 M HCl or 0.1 M NaOH solution. After 3 days of pre-equilibration, an aliquot of a stock phosphate solution of 0.05 M was added in the tubes to achieve the desired $[P]_{I,aq}$ value and the tubes were gently shaken end-over-end for 4 days. Final pH were measured after a 4-days contact time of sorbate(s)–suspension. Separation between solid and solution phases was carried out by centrifugation of the suspensions for 3 hours at 9000 rpm (cutoff: ca.16 nm for Illite). The supernatants were then removed from the tubes after centrifugation. An aliquot was taken for electrophoretic mobility (noted as EM) measurements. Another aliquot was taken for chemical analyses after acidification at pH < 1 by addition of 2% HNO_3. Each experiment was performed in duplicate. Blank experiments without solid were also conducted in a similar manner than those with solid.

1.3.2. Analysis of experimental solutions of sorption experiments

Measurements of EM of suspended particles present in supernatant aliquots collected at the end of the sorption experiments were made by using a Zetasizer Nano equipment (Malvern). Each sample was measured three times and standard error was then calculated. Quantitative analysis of final aqueous phosphate concentrations ($[P]_{F,aq}$) in supernatant aliquots (re-filtered at 0.20 µm) were made by ion chromatography (Eco IC, Metrohm, uncertainties of 1 – 10%). An aliquot of each supernatant was also acidified to pH < 1 by adding a small amount of 67% HNO_3 and it was stored at 4°C prior to further chemical analyses. Percentages of P sorbed, and amount of P sorbed (in µmol.g^{-1} clay), were calculated as follows:

$$\%\ P\ sorbed = \frac{[P]_{I,aq} - [P]_{F,aq}}{[P]_{I,aq}} \times 100$$

$$Amount\ P\ sorbed\ (\mu mol/g) = ([P]_{I,aq} - [P]_{F,aq}) \times \frac{V}{M}$$

With $[P]_{I,aq.}$: initial aqueous concentration of sorbate (µmol.L^{-1}), $[P]_{F,aq}$: final aqueous concentration of sorbate (µmol.L^{-1}), *V*: volume of liquid (L) and *M*: mass of solid phase (g). Uncertainties on sorption percentage and surface coverage were estimated to be lower than 10%.

1.4. In-situ ATR FTIR experiments

1.4.1. Procedures of clay deposition on the ATR crystal

Acquisition of IR spectra at the mineral-solution interface was carried out by using a Bruker Equinox IFS 55 infrared spectrometer equipped with an ATR cell containing a ZnSe horizontal crystal (with an angle of incidence of 45°, a crystal size of 7.2×1.0×0.7 cm^3 and 5 internal reflections) and with a MCT detector (system cutoff: ca. 900 cm^{-1}) that was cooled down by liquid nitrogen during FTIR spectra acquisition. Prior to experiment, the ZnSe crystal was either coated with a thin and stable film of IdP or NaIdP brought subsequently in contact with a 0.005 M NaCl electrolyte, or it was directly brought in contact with a previously pre-equilibrated

NaIdP suspension from which the clay particles are left to settle and cover the crystal. Both methods have the advantage of allowing an in-situ monitoring of the solid–solution interface along a process of sorbate sorption.

The former method was shown to be powerful to monitor sorbate sorption at aluminum oxide–solution interface, with a good reproducibility of the FTIR sorption experiments and an increased sensitivity of the technique for surface species [11,97]. It was used in this study to monitor the dissolution of IdP and NaIdP along interactions with an electrolyte solution, and to gain thereby IR reference data on the (surface) structures of the clay samples studied. It was conducted using a multistep procedure as follows : (i) an IdP or NaIdP suspension was prepared (contact time : 0.5 h, $R_{S/L}$=5 $g.L^{-1}$, pH 6.2) and particles were left to settle by sedimentation during 1 hour, (ii) ca. 2mL of the supernatant were then pipetted, deposited uniformly onto the ZnSe crystal surface, and let to dry overnight at ambient temperature (25°C) for settling of particles, (iii) the crystal was dried at 40°C for 3 hours, and (iv) the coating obtained after drying was gently rinsed with an electrolyte at a pH similar to that of the initial suspension and was dried slowly under a N_2 gas flow. The whole procedure described above was repeated for four times. This procedure was found to be repeatable and it allowed to deposit a thin film of ca.3 mg of solid onto the crystal.

The latter method, i.e., covering of the ATR crystal with an equilibrated two-layers NaIdP–electrolyte solution system, was used to monitor the sorption of phosphate ions at the clay-solution interface, for near-equilibrated systems (in order to avoid IR signals due to solid dissolution). It was conducted as follows: (i) a NaIdP suspension was prepared (contact time of 3 days, $R_{S/L}$= 3 $g.L^{-1}$, pH 4), (ii) 10mL of the suspension were then pipetted and added into the ATR cell, (iii) the suspension was left to settle for 3 days and (iv) an ATR FTIR spectrum was taken as a reference baseline prior to sorbate addition.

1.4.2. Monitoring of the clay-solution interface

In-situ ATR FTIR spectroscopy experiments were performed to monitor the clay–solution interface during interaction of (Na)IdP with a 0.005 M NaCl electrolyte solution, and to gain insights into IR vibrations due to mineral's structure and or to structural reorganization of the interface with time. After coating of the ATR crystal with a dried thin film of IdP or NaIdP (cf. §2.3.1), the film was brought in contact with a volume of 10mL of a 0.005 M NaCl electrolyte solution in the ATR cell, in order to perform FTIR measurements of the (Na)IdP–solution interface (pH 6.2 for IdP and pH 4 for NaIdP). A FTIR spectrum was immediately recorded as a reference baseline after electrolyte addition. The (Na)IdP-solution interaction process was then monitored during 3 hours. Each IR spectrum was recorded during 20min with an average of 2000 scans/spectrum at a resolution of 4 cm^{-1}.

1.4.3. Monitoring of the clay–solution interface along sorption of phosphate ions

Experiments were performed to monitor in-situ the sorption of phosphate ions at the interface between NaIdP and a near-equilibrated electrolyte solution, and to gain insights into IR vibration bands of surface species. Two types of ATR FTIR experiments of sorption of phosphate ions were performed. The first one was devoted to monitor the NaIdP-phosphate-solution interface as a function of reaction time, for a $[P]_{I,aq}$ value of 100µM and a pH value of 4. It was conducted as follows. After covering of the ATR crystal with the two-layers NaIdP-electrolyte solution system and recording of a FTIR spectrum as a reference baseline (cf. §1.4.1), a defined amount of a stock phosphate solution was added in the ATR cell in order to achieve a $[P]_{I,aq}$ value of 50 µM. IR spectra of the interface were then recorded during 1 hour (one spectrum per 20min.). Total concentration of aqueous P added was increased to 100µM by introduction of an appropriate amount of the stock phosphate solution in the cell. The IR spectra of the interface were then collected as a function of time (t_R up to 3 days). The second ATR FTIR experiment aimed at investigating the NaIdP-solution interface during a continuous

increasing of $[P]_{I,aq}$ value from 100 µM to 300 µM. The experiment was performed as described above up to the collection of IR spectra at $[P]_{I,aq}$ of 100 µM, for a t_R value equal to 17 h, which was previously shown to allow appearance of IR signals of sorbed ISSC of phosphate (based on FTIR results of above mentioned first-type experiment). The total concentration of phosphate was then raised from 100 to 300 µM by successive additions every hour of 50 µM of phosphate ions. IR spectra were collected after each increase in aqueous phosphate concentration and then every twenty minutes.

1.4.4. Blank solution experiments

Blank experiments (without clay) were performed by using electrolyte solutions at various total concentrations of phosphate ions, in order to: (i) get values of detection limits of the ATR FTIR technique for aqueous phosphate solution species, (ii) record IR spectra of aqueous phosphate species taken as "references" for sorption species, and (iii) identify a possible formation of phosphate precipitates, depending on experimental conditions. For these blank experiments, a defined volume of a 0.005 M NaCl electrolyte solution was brought at a desired pH value and was added in the ATR cell crystal. A spectrum of reference was taken. Then, a defined volume of the phosphate stock solution was added to the electrolyte solution in the ATR cell in order to attain a defined $[P]_{I,aq}$ value. Total concentration of aqueous P added was then increased by successive additions of defined volumes of the stock phosphate solution. Phosphate aqueous species, and their detection limits, were studied in the range of $[P]_{I,aq}$ values of 20–450 µM (45–225 µM at pH 4, 50–150 µM at pH 4.9, 30–450 µM at pH 6.2, 20–150 µM at pH 7.0). After each addition, one or several spectra were recorded.

1.4.5. Analysis of FTIR spectra

Analyses of FTIR spectra were focused on the mid-infrared region from 900–1200 cm^{-1} where bands associated with various P-O(H) stretching vibrations of phosphate unit, i.e., where υ_3

triply degenerated asymmetric stretching and υ_1 non degenerated symmetric stretching vibration bands, are found [15,16,23,146]. There is also a broad band in IR spectra of $H_2PO_4^-$ and H_3PO_4 aqueous species that has been attributed to the δ(P-OH) bending vibration located at ca. 1220–1240cm^{-1} [23,189]. The software OriginPro version 9.1 was used for correction of baseline of the FTIR interface spectra. A linear baseline was fitted between 1200 and 900 cm^{-1} in the raw spectra, and was brought to a zero value. The software was also used for the decomposition of the baseline-corrected spectra in order to resolve IR bands with Gaussian lines, and the least-square fitting was applied. No constraints were applied on adjustable parameters (band position, band intensity and band width) during spectral decompositions. The band maxima position was adjusted only for a very few spectra showing low absorbance.

1.4.6. Short overview of published IR data on aqueous phosphate species

FTIR data analysis is based on the number of resolved bands and their maxima position, i.e., number and position of IR-active υ_3 and υ_1 bands which reflect the possible molecular symmetry of the phosphate ions [16,23]. Tejedor-Tejedor and Anderson [15] have systematically studied the possible molecular configuration of phosphate ions in aqueous solution or sorbed at the goethite–H_2O (or D_2O) interface. All considerations on the molecular configurations and the evolution of molecular symmetry, i.e., reduction or increase of molecular symmetry, are based on changes of the coordination environment of the PO_4 unit due to, for example, formation of inner-sphere complex of phosphate ions in solution (protonation and/or complexation with metals) and at the solid–solution interface (complex of phosphate ions with cation(s) at basal plane / edge of particle clay surface). The uncoordinated PO_4 unit possesses a tetrahedral geometry and the molecular symmetry of this tetragonal penta-atomic molecule belongs to the point group T_d [16,145], which has an important molecular symmetry (24 symmetry elements). Fig. A1 in Supplementary Information shows the calculated speciation diagram of phosphate ion. Equilibrium constants used in calculations are given in Table A1.

The unprotonated trivalent phosphate ion (PO_4^{3-}), which is the dominant aqueous species at pH > 12, has four vibration bands related to asymmetric bending at 567 cm^{-1} (T_2, υ_4), asymmetrical stretching at 1006 cm^{-1} (T_2, υ_3), symmetric bending at 420 cm^{-1} (E, υ_2) and symmetrical stretching at 938 cm^{-1} (A_1, υ_1) [145]. All four vibrations are Raman-active but only the υ_3 and υ_4 are IR-active [145]. Only the υ_3 can be observed in our wavenumbers range, and the number of vibration bands of υ_3 and υ_1 is equal to two.

The unprotonated phosphate ion is progressively protonated with decreasing solution pH, i.e., from monoprotonated (HPO_4^{2-}) to triply protonated (H_3PO_4). The monoprotonated divalent phosphate ion is the main P species in the pH range 8-12. This ion has one coordinated hydrogen which reduces the molecular symmetry from the point group of T_d to C_{3v}, the later having 6 symmetry elements and the number of vibration bands of PO_4 unit increasing from 4 to 6 [146]. Another consequence of the reduction of molecular symmetry is that the υ_3 band splits into two υ_3 bands at 1077 cm^{-1} (E) and 989 cm^{-1} (A_1) and the υ_1 becomes IR-active and shifts to 850 cm^{-1}, the frequency of others vibrational bands of PO_4 unit being under 800 cm^{-1}. When a metal cation, in aqueous solution or sorbed at a mineral surface, is coordinated to PO_4^{3-}, the molecular configuration of phosphate ion may be unprotonated monodentate mononuclear. The molecular symmetry of this configuration should be the same as the monoprotonated phosphate, i.e., C_{3v}, and two υ_3 (E, A_1) and one υ_1 would then be present.

Another phosphate species that has a molecular symmetry of C_{3v} is the fully protonated (or triprotonated) uncharged phosphate acid (H_3PO_4), which is the dominant aqueous species at pH < 2.0. This molecule has the same number of P-O(H) vibration bands as HPO_4^{2-}, i.e., 6 vibration bands in which it has two υ_3 at 1174-1179 cm^{-1}, 1006 cm^{-1} and one υ_1 at 888-890 cm^{-1} [15,16,146].

Further protonation of HPO_4^{2-} leads to formation of the diprotonated monovalent phosphate ion, $H_2PO_4^-$, which is the dominant specie at pH between 2 and 7. The presence of two coordinated

hydrogens to PO_4 unit leads to a lower molecular symmetry than that of one coordinated hydrogen, i.e., the molecular symmetry is reduced from C_{3v} to $C_{2v,}$ and the number of molecular symmetry elements decreases from 6 to 4. As a result of molecular symmetry reduction, υ_3 (*E*) splits in two υ_3 bands (B_1 and B_2) and the number of vibrational bands of PO_4 unit increases from 6 to 9 with three υ_3 vibration bands at 1160 cm^{-1} (A_1), 1074 cm^{-1} (B_1), 940 cm^{-1} (B_2) and one υ_1 band at 874 cm^{-1} (A_1). The molecular symmetry may be similar to that of $H_2PO_4^-$ (i.e., C_{2v}) when PO_4^{3-} is coordinated by two equivalent aqueous cations or surface metal cations at mineral particle surface (i.e., two identical surface sites). In this case, the molecular configuration of PO_4 unit is unprotonated bridging bidentate mononuclear. In addition to the latter case, there are two other molecular configurations of PO_4 unit which have C_{2v} symmetry, i.e., unprotonated bidentate mononuclear complex and diprotonated bridging bidentate mononuclear complex.

2. Results

2.1. Chemical and mineralogical compositions of Illite du Puy

The mineralogical compositions of the IdP and NaIdP samples, and of their clay-size fraction (< 2µm), are given in Table 1. Calcite is the major mineral constitutive of IdP, followed by feldspars (mainly potassic) and clays, i.e., Illite and kaolinite. Quartz and siderite are present in the sample as minor minerals, and hematite as an accessory mineral. The clay fraction has a quite simple composition dominated by Illite, then kaolinite. A striking feature is the disappearance of the main mineral, i.e., calcite, after Na-homonionic conditioning of Illite du Puy. NaIdP is composed mainly by Illite and feldspars -and small amounts of kaolinite and quartz-, while no carbonates (calcite, siderite) nor hematite were detected by XRD analysis.

Table II-1. Mineralogical composition (semi-quantitative estimation in %) of IdP and NaIdP samples and their clay fractions (< 2 µm).

	Clay		Carbonate		Feldspar			Iron Oxide	
	Illite	*Kaolinite*	*Calcite*	*Siderite*	*Microcline*	*Orthoclase*	*Albite*	*Hematite*	*Quartz*
IdP	18.5	5.4	32.8	3.3	18.2	11.6	6.3	0.4	3.5
NaIdP	30.2	7.2	*<5%*		20.6	20.5	16.6	*<5%*	4.9
IdP$_{(<2\mu m)}$	79	21	*<5%*			*Traces*		*<5%*	
NaIdP$_{(<2\mu m)}$	76	24	*<5%*			*Traces*		*<5%*	

The major element compositions of IdP and NaIdP are given in Table 2 and are consistent with those of silicate rocks whose mineralogy is dominated by K-feldspars, carbonates and clays. Fe_2O_3 represents a significant percentage (< 5%) of compositions of the two rocks studied, although siderite and hematite cannot be detected in NaIdP by XRD analysis. Iron minerals may therefore represent less than 5% of NaIdP minerals and / or Fe is incorporated in the clay's structure, as proposed by Poinssot et al. [190] for conditioned Na-Illite. Removal of carbonate minerals upon homoionic conditioning is highly marked in the rock compositions by a sharp decrease of the percentage of CaO from IdP to NaIdP. The treatment also led to removal of traces of phosphate minerals. Chemical composition of NaIdP is consistent with that given for Na-Illite by Bradbury and Baeyens [188], whose Na-homoionic conditioning procedure for Illite du Puy has been used in the present study.

Table II-2. Major element composition of IdP and NaIdP samples (in wt/wt percent oxide).

	SiO_2	Al_2O_3	Fe_2O_3	K_2O	CaO	MgO	TiO_2	P_2O_5	Na_2O	MnO	Loss of ignition
IdP	44.64	19.68	6.64	5.82	5.42	3.16	0.65	0.26	0.15	0.057	12.94
NaIdP	51.20	22.30	7.52	6.58	0.09	3.34	0.75	<0.1%	0.6	0.050	8.90

Trace metal compositions of IdP and NaIdP are given in Supplementary Information (Table A2). For both rocks, the order of concentrations is as follows: Rb, Ba, Zn (> 150 $\mu g.g^{-1}$) > Cr, Cs (80-100 $\mu g.g^{-1}$) > Pb, As, La, Cu, Ga, Ni (50-20 $\mu g.g^{-1}$) > other TME including U (ca. 3$\mu g.g^{-1}$). It is to be noticed that concentrations are lower in NaIdP than in IdP for Sr (180 vs. 70

$\mu g.g^{-1}$), As and Ln, due to removal of carbonate and/or phosphate minerals after rock conditioning.

2.2. Illite du Puy – solution interactions

Batch experiments were performed to gain insights into the evolution of the chemical composition of a solution in contact with Illite du Puy, for different values of clay-to-solution ratio ($R_{S/L}$). Supplementary Information (Tables A3-4) shows values of pH, and concentrations of cations and anions (noted as $[]_{F,aq}$), of the final experimental solutions after a 5-days contact with IdP. Experimental solutions at initial pH of 2.29 ± 0.05 remain acidic for low $R_{S/L}$ (1-2 $g.L^{-1}$) and reach a near-neutral to slightly basic pH value for higher $R_{S/L}$ (3-6 $g.L^{-1}$). The slight and sharp increase of pH during experiments was likely due to fast reactions of protonation of functional groups existing at IdP surface (hydroxyl groups) and/or to mineral dissolution. Final concentrations of cations are in the order: $[Ca]_{F,aq}$ (1-2.5 mM) > $[K]_{F,aq}$ (230-300 µM) > $[Mg]_{F,aq}$ (50-120 µM). Silica concentration increases with final pH ($[Si]_{F,aq}$: 140-230 µM) whereas Al sharply decreases ($[Al]_{F,aq}$: 110-10 µM). Major anions are phosphate ions that reach an almost constant concentration for a range of $R_{S/L}$ studied ($[PO_4^{3-}]_{F,aq}$: ~ 4 µM for $R_{S/L} \geq 2 g.L^{-1}$, **Fig.II-1**b), and fluoride ions, while sulfates and nitrates show much lower concentration values (<10 µM). Concentrations of uranium, nickel and lanthanides remain in the ppb level. Results of speciation calculations performed by using the Visual MINTEQ (Ver 3.1) code and the database used are reported in Supplementary Information (Tables A5-6). Phosphate ions are expected to be major ligands that influence the speciation of trace metals in the pH range 4–7, as well as carbonate ions for pH > 6.8, for solutions at equilibrium with atmospheric CO_2. Calculations also show that solutions at near-neutral pH ($R_{S/L} > 2 g.L^{-1}$) are oversaturated with respect to secondary phosphate minerals such as $AlPO_4 \cdot 1.5H_2O_{(S)}$ and $MnHPO_{4(S)}$, which suggests that precipitation of secondary phosphate phases may possibly affect metal behavior in IdP-solution systems. An interesting feature is that, whatever pH and $R_{S/L}$ values, $[Fe]_{F,aq}$ displays an almost

constant value (ca. 3 µM) in the final solutions. At near-neutral pH, its value decreases with an increase of the filtration threshold (**Fig.II-1**a). This evidences the formation of colloidal phases containing Fe, which is consistent with speciation calculations indicating that the experimental solutions at near-neutral pH are oversaturated with respect to Fe(III) - (oxihydr)oxides. Results of experiments for the NaIdP-solution systems are given in Supplementary Information (Tables A3-4 and Figs. A2-3). It was observed that the Illite sample conditioning drastically decreased the values of $[Ca]_{F,aq}$ and $[anions]_{F,aq}$ of final experimental solutions, including for phosphate ions (Table A3). In contrast, $[Fe]_{F,aq}$ values remain of the same order of magnitude and the formation of colloidal phases containing Fe is likely regardless of the Illite sample studied. For the NaIdP - solution systems, values of $[Si]_{F,aq}$ and $[Al]_{F,aq}$ of final experimental solutions sharply decrease with pH, suggesting a control by dissolution and/or precipitation of a same mineral phase, such as clay.

These data support the need for macroscopic and spectroscopic work to elucidate the speciation of phosphate ions on the clay surface, as they are major ligands of IdP-solution systems and can therefore strongly affect the sorption behavior of trace metals onto Illite du Puy.

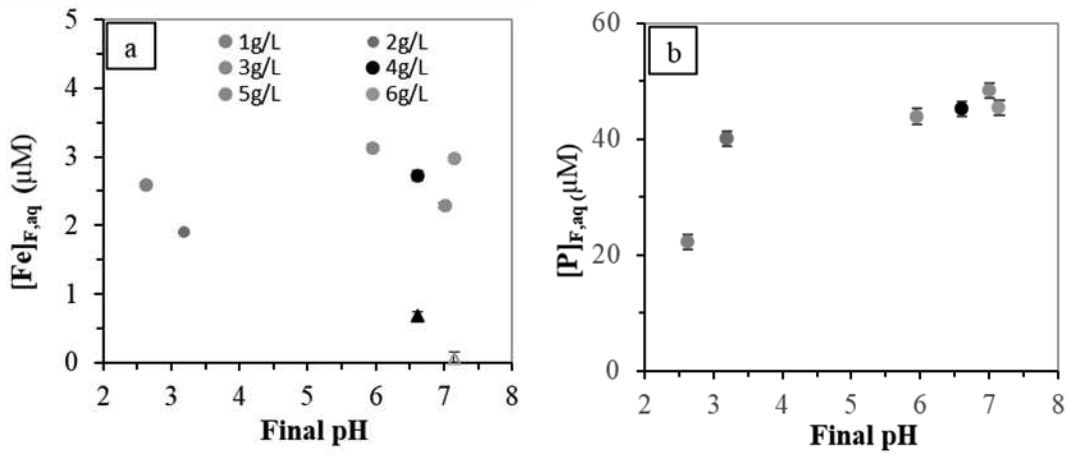

Fig.II-1. Final experimental concentrations of (a) Fe ions and (b) phosphate ions vs. final pH of solutions contacted with Illite du Puy (IdP) at various IdP - solution ratios ($R_{S/L}$:1-6 $g.L^{-1}$).

Experimental conditions: initial pH 2.3, 0.005M NaCl electrolyte, 5 days contact time. Cercle and triangle symbols are for solutions centrifuged and filtered at 3 kDa, respectively.

2.3. Macroscopic sorption behavior of phosphate ions

2.3.1. Sorption edge of phosphate ions

Fig.II-2 shows a plot of the sorption edges of phosphate ions in NaIdP - 0.005 M NaCl electrolyte solution, at different values of total phosphate concentration ($[P]_{I,aq}$: 20 µM and 100 µM) and clay-to-solution ratio ($R_{S/L}$ = 1, 2 and 3 $g.L^{-1}$). The percentage of P sorbed is quite constant in the pH range 3-6, within our experimental uncertainties, and it decreases for pH values higher than 6. Several hypothesis may account for this pH dependence. First, a progressive deprotonation of the amphoteric silanol sites present at clay surfaces is expected when increasing pH to values higher than 6, consistently with the pK_a constant values reported in literature (Table. A7, Supporting Information). Second, a pH value of 6 coincides with the appearance of the aqueous species HPO_4^{2-}, whose relative contribution to aqueous phosphate speciation becomes equal to that of $H_2PO_4^-$ at pH ca. 7.1 (Fig. A1, Supporting Information). All these features contribute to an increasing of electrostatic repulsion between clay surface and aqueous phosphate at near-neutral to neutral pH, which is unfavorable to phosphate adsorption [93]. **Fig.II-2**b shows that the pH-dependence of surface coverage of NaIdP by phosphate ions (in $\mu mol.g^{-1}$) does not depend on the clay-to-solution ratio, at low $[P]_{I,aq}$ (20 µM) under experimental conditions investigated ($R_{S/L}$ in the range 1-3 $g.L^{-1}$). This suggests that similar sorption sites and/or sorption species are involved whatever the $R_{S/L}$ value. In contrast, an increasing of the $[P]_{I,aq}$ value (from 20 to 100 µM) results in a strong decrease of the percentage of P sorbed, throughout the pH range investigated. A concomitant (non-linear) increase of surface coverage, is observable, too, and it is more marked at acidic pH than at pH higher than

6. This illustrates the existence of different types of phosphate sorption species with increasing surface coverage of NaIdP by phosphate ions. Goldberg and Sposito [33] proposed a value of density of surface sites onto soil minerals of 1.25-2.5 sites.nm^{-2} in their modeling study of phosphate adsorption onto a soil. A value of surface site density of 2.31 sites.nm^{-2} was proposed by Davis and Kent [30] for sites at Illite platelet edges. Bradbury and Baeyens [188] used a value of 80 µmol.g^{-1} (which would correspond to ca. 0.4 sites.nm^{-2}) for surface site capacity of Illite du Puy platelet edges (40 µmol.g^{-1} for aluminol sites and 40 µmol.g^{-1} for silanol sites) in their modeling study of experimental data on macroscopic sorption of TME. These authors also considered a small amount (ca. 2 µmol.g^{-1} or 0.01 sites.nm^{-2}) of high affinity sites present at edge clay platelets in order to successfully fit the TME sorption isotherms. Based on surface site density values of Bradbury and Baeyens [188], it can be inferred that the sorption edges of phosphate ions reported in the present study would reflect P retention mechanisms that involve mainly the high-affinity sites existing at NaIdP particle edges, where strong interactions with adsorbate can occur, and that low-affinity edge surface sites have a limited contribution. At the highest P surface coverage studied (for $[P]_{I,\,aq}$ = 100 µM), multiple surface sites and/or phosphate sorption species are likely involved in the retention of P onto NaIdP.

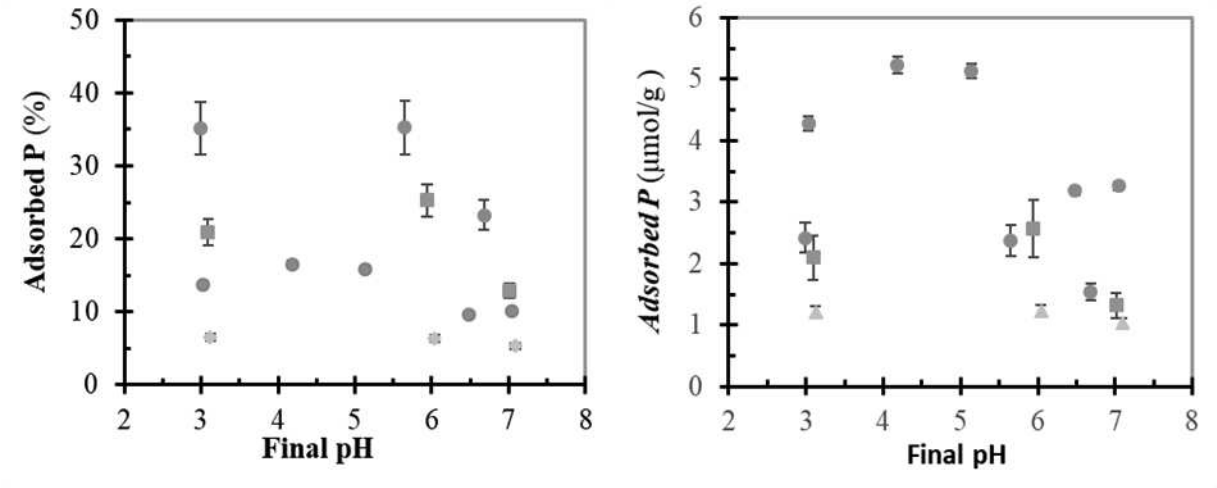

Fig.II-2. Sorption edges of phosphate ions onto NaIdP obtained at different clay-to-solution ratios - $R_{S/L}$ (♦: 1g.L^{-1}, ■: 2g.L^{-1} or ●●: 3g.L^{-1}) and total P concentrations - $[P]_{I,aq}$ (▲■●:

20µM or ●: 100µM). Experimental conditions: 0.005 M NaCl electrolyte solutions, reaction time (t_R) of 4 day, NaIdP-electrolyte solution system pre-equilibration of 3 days (t_{pre-eq}).

2.3.2. Sorption isotherm of phosphate ions

Fig.II-3 shows the sorption isotherm of phosphate ions onto NaIdP at acidic pH (pH_F: 4±0.05; $[P]_{I,aq}$: 20-200 µM; $R_{S/L}$: 3 $g.L^{-1}$, t_{pre-eq}: 3 days, t_R: 4 days). At this pH value, main phosphate species are $H_2PO_4^-$. There was observed a decrease in the percentage of P sorption with increasing $[P]_{I,aq}$, which suggests the successive formation of several phosphate species at the NaIdP–solution interface and/or a progressive saturation of different sorption sites present at the clay edges. In contrast, surface coverage by phosphate (in $\mu mol.g^{-1}$ clay) increases when increasing $[P]_{I,aq}$ up to a value of ca. 50-60 µM. Such a behavior is typical of the successive formation of various surface complexes of distinct stability and / or successive implications of high-affinity and low-affinity surface sites for phosphate surface species formation, as already mentioned for the P sorption edge recorded at a $[P]_{I, aq}$ value of 100µM (cf § 3.3.1). A plateau in amount of phosphate ions sorbed (at 5-6 $\mu mol.g^{-1}$ of phosphate sorbed) is observable in **Fig.II-3** (insert) at $[P]_{I, aq}$ values higher than ≈ 60 µM. This result suggests a saturation of total sorption sites available for phosphate retention. It also indicates no significant involvement of secondary processes like (surface) precipitation of phosphate phases, under the conditions investigated.

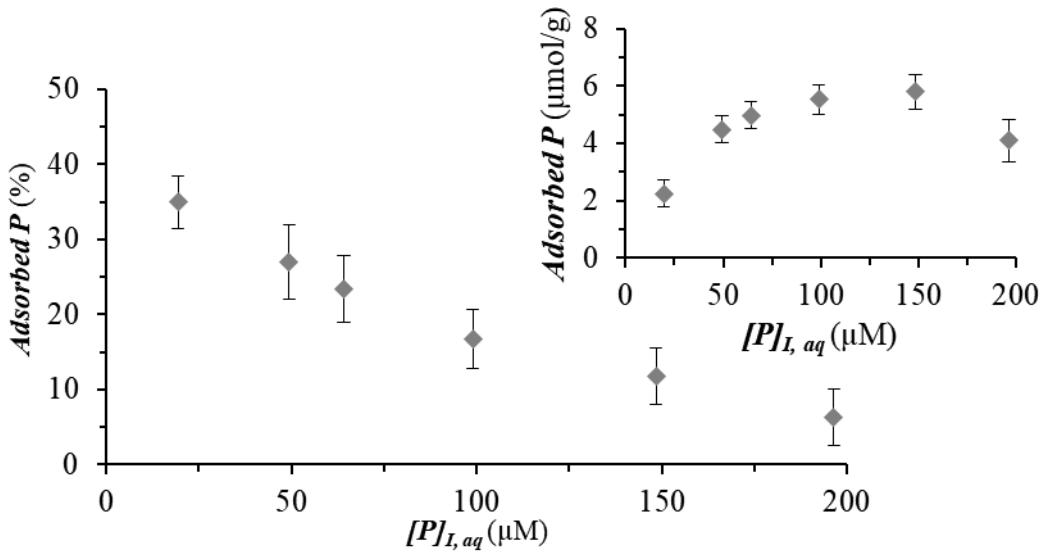

Fig.II-3. Sorption isotherms of phosphate ions (results in % of adsorbed P; insert: P surface coverage in µmol.g^{-1}) onto NaIdP, at pH 4 and at $[P]_{I,aq}$ in the range 20-200 µM. Experimental conditions: 0.005 M NaCl electrolyte solutions, $R_{S/L}$ = 3 g.L^{-1}, t_R = 4 days, $t_{pre\text{-}eq}$ = 3 days.

2.3.3. Electrophoretic mobility

Fig.II-4 shows pH dependency of electrophoretic mobility (EM) for NaIdP-0.005 M NaCl solution suspensions at different $[P]_{I,aq}$ values. In the absence of any potential-determining ion other than OH^-/H^+, NaIdP particles display a low value of isoelectric point (IEP ≈ 3), *i.e.*, of pH at which EM and surface potential are equal to zero. This is consistent with previous studies reporting a low value of isoelectric point (IEP) for illitic minerals [191,192]. A sharp decrease of EM with pH is also observable in **Fig.II-4**. These EM results reflect both a structural negative charge of Illite and successive (de)protonations with pH of amphoteric surface functional groups (like silanol then aluminol/ferrinol sites) present at clay surface edges in NaIdP (cf. Table A7 in Supporting Information for values of 1st and 2nd protonation constant of surface hydroxyl groups onto clay minerals). **Fig.II-4** also reveals that, in the acidic pH range, EM of NaIdP in the suspensions is diminished and the point-of-zero charge (PZC) shifts towards a lower pH (< 3) at high phosphate concentration ($[P]_{I,aq}$ = 100 µM). This feature evidences a

mechanism of strong sorption of phosphate ions that adds negative charges to the clay surface, such like a mechanism of formation of ISSC of phosphate by exchange of surface ligands.

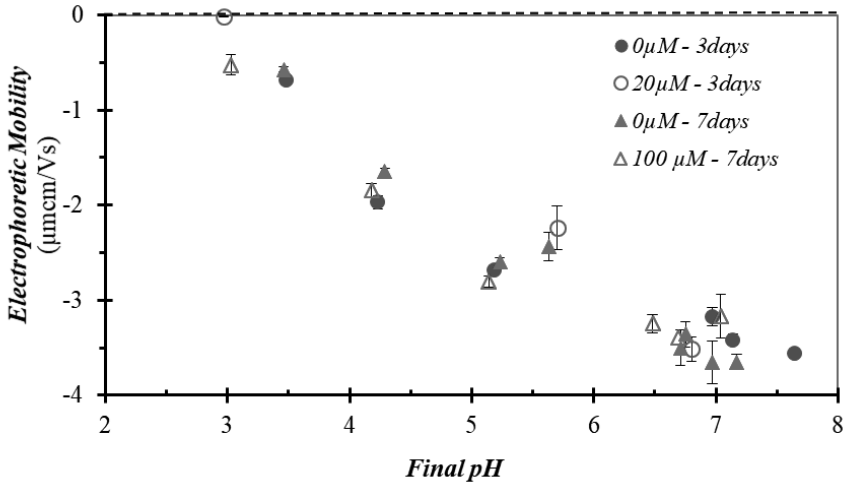

Fig.II-4. pH dependence of electrophoretic mobility of NaIdP particles in final experimental solutions at different phosphate concentrations ($[P]_{I,aq}$=0, 20 or 100 µM). Corresponding data on P sorption are given in **Fig.II-2**. Experimental conditions: 0.005 M NaCl electrolyte solutions, $R_{S/L}$ = 3 g.L^{-1}, t_R = 4 days and t_{pre-eq} = 3 days for P sorption experiments, for the "blank" experiments ($[P]_{I,aq}$ = 0 µM, t_R = 3 and 7 days).

2.4. ATR FTIR studies

2.4.1. Clay – solution interactions

ATR FTIR experiments were performed to monitor the evolution of the clay–solution interface with time, along the processes of dissolution and surface reorganization (cf. § 1.4.1/1.4.2). In these experiments, a thin layer of IdP or NaIdP was coated on the ATR crystal surface and brought in contact with a 0.005 M NaCl solution at pH 6 and 4, respectively. The aim is to identify positions of vibration bands of the IdP structure/surface, *e.g.*, Si-O and/or Si-OH vibration bands, which may actually interfere with ν(P-O) signals in the 900-1200 cm^{-1} range. **Fig.II- 5**a shows the evolution of *in-situ* IR spectra collected at the IdP–solution interface as a

function of time. There was observed the appearance of a strong "negative" absorbance in the spectral region 800-1200 cm^{-1} since the first hour of IdP-solution contact, whose growing rate decreases with time. Six band maxima of the negative absorbance were observed. Decomposition of the spectra provided values of six vibrations band maxima at 835, 873, 912, 979, 1040 and 1110 cm^{-1}. Table A8 in Supporting Information provides a succinct literature data on the OH deformation and SiO stretching vibrational bands of clay minerals. The bands at 835, 873 and 912 cm^{-1} can be attributed to OH bending vibrational mode of Al-Mg-OH, Al-Fe-OH and Al-Al-OH, respectively, in the structure of clay minerals [193,194]. The band at 979 [194], 1040 and 1110 cm^{-1} correspond to SiO stretching vibrational mode [194–196]. The main band at 980 cm^{-1} is reported to be characteristics for Si-O stretching vibration of Si-O-H groups which is attributed to asymmetric vibration of Si-OH, and it may reflect the presence of OH groups at surface of polymerized silica [196]. Hence, the "negative" absorbance provide evidence for processes of dissolution and surface reorganization of the clay sample with time. **Fig.II- 5**b shows the evolution of *in-situ* IR spectra collected at the NaIdP–solution interface as a function of time. As previously, there was observed the appearance of a "negative" absorbance in the range 800-1200 cm^{-1} (which almost stabilizes after ca 3 hours), showing upon spectra decomposition three band maxima at 917, 966, and 1008 cm^{-1} as a main band. The latter is characteristics of the Si-O stretching band in the micas group, like Illite [197].

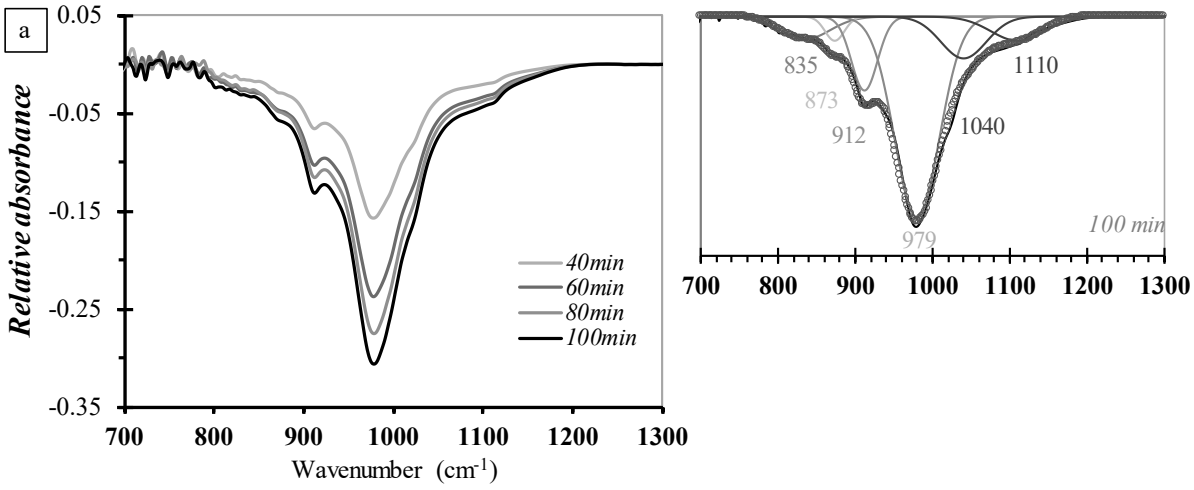

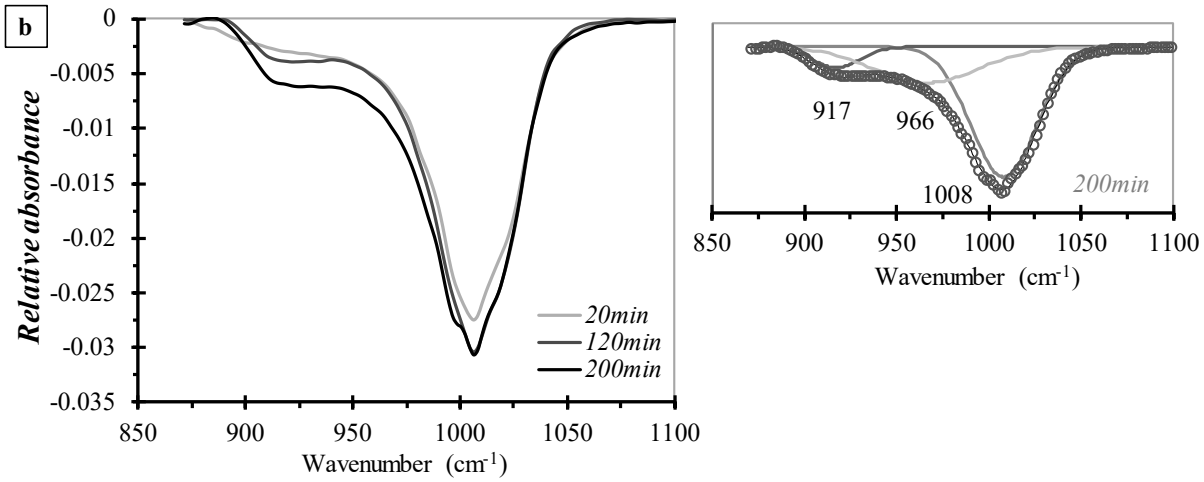

Fig.II- 5. Evolution of in situ ATR FTIR spectra recorded at: (a) IdP–solution and (b) NaIdP–solution interface, as a function of time, and results of spectra decomposition (insert). Experimental conditions: 0.005 M NaCl electrolyte solution at pH (a) 6.2 and (b) 4.0 added to a thin film of clay coated on the ATR crystal.

2.4.2. IR spectra of phosphate solutions

IR spectra of phosphate species sorbed at the NaIdP–solution interface are compared to references such as IR spectra of phosphate species in aqueous solution (at pH 4-7, in an 0.005 M NaCl electrolyte solution) in order to: (i) detect a possible contribution of solution P species to IR signals of Illite–phosphate-solution interface, and (ii) to distinguish outer-sphere surface complexes of phosphate (OSSC) from ISSC of phosphate formed at the interface. Figs. 6a-d show the IR spectra collected for solutions at pH 4, 4.9, 6.2 and 7.0, respectively, in which the phosphate concentration was increased. Diprotonated phosphate ion ($H_2PO_4^-$, C_{2v}) is the predominant aqueous phosphate species at pH between 4 and 6.2 (Fig. A1, Supporting Information) and presents fours bands at 1160, 1075, 940 cm^{-1} and 870 cm^{-1} ascribed to υ_3(P-O), υ_3(P-O), υ_3(P-OH) and υ_1(P-OH) vibrations, with the first three bands corresponding to υ_3 assignment and the last one to υ_1 assignment [16,145]. These four bands could be observed in

IR spectra recorded at high aqueous phosphate concentration ($[P]_{I,aq}$>1mM). In the range of $[P]_{I,aq}$ values investigated in this study, only the υ_3(P-O) bands at 1160 and 1075 cm^{-1} were observable, and the relative IR absorption band intensities increased with increasing $[P]_{I,aq}$. There was observed that peak's shape and absorption maxima of these two υ_3 bands became better defined when increasing phosphate concentration. The detection limit for this aqueous species is thus estimated to be approximately of 45 µM in the pH range 4-6.2, a concentration at which IR band intensities are very close to background noise level. **Fig.II- 6**d shows the IR spectra collected as function of $[P]_{I,aq}$ at pH 7, a value close to the constant of deprotonation of $H_2PO_4^-$ (to HPO_4^{2-}). At this pH value, a mixture of di- and mono- protonated phosphate ions is expected to be present in the solution. Due to the low phosphate concentration used in this study, only the υ_3(P-O) bands of HPO_4^{2-} at 1077 is observable. It seems that the overlapping of υ_3(P-O) bands of $H_2PO_4^-$ and HPO_4^{2-} at 1077 cm-^{1} decreases the detection limit to ca. 20 µM.

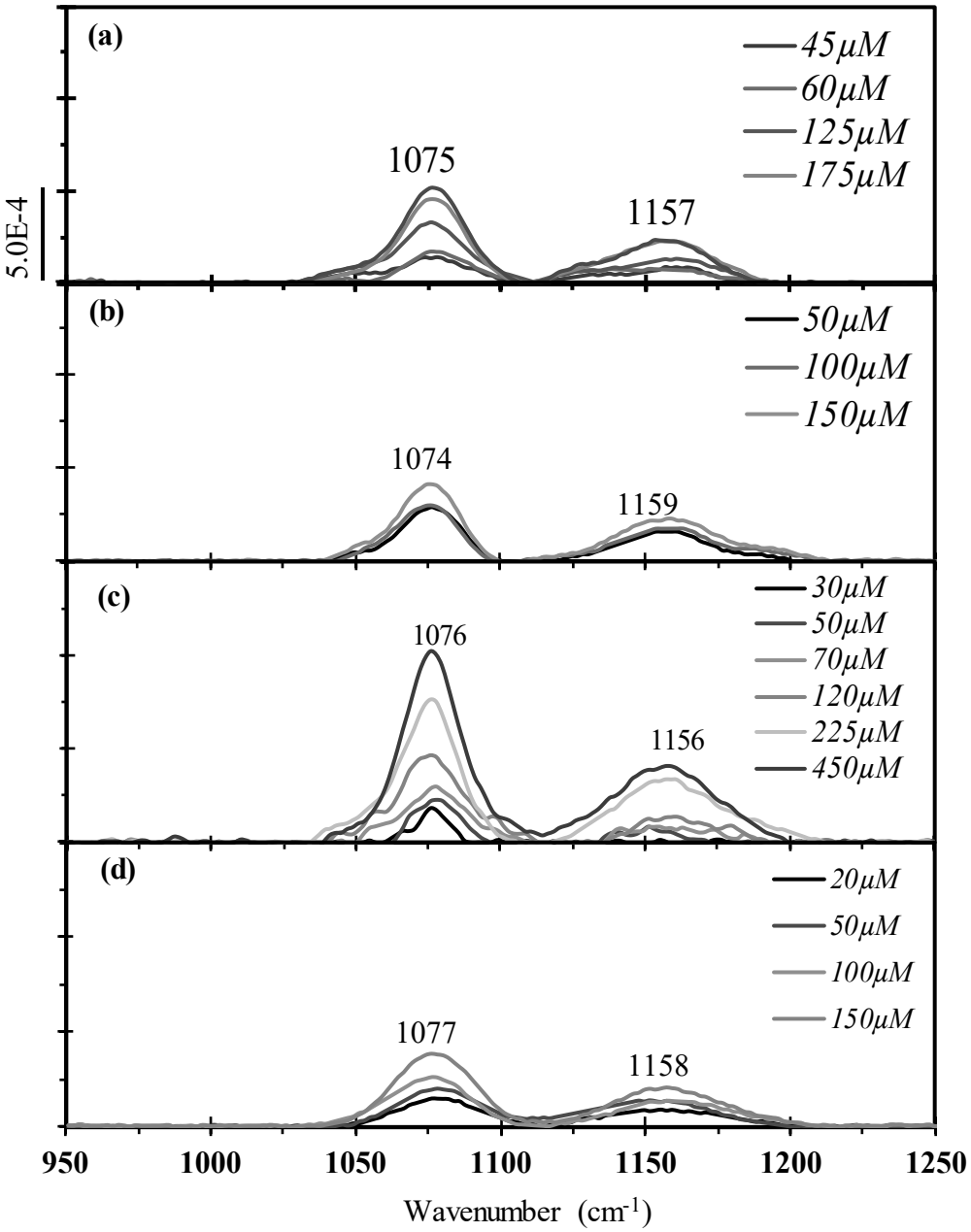

Fig.II- 6. ATR FTIR spectra of phosphate solutions at increasing $[P]_{I,aq}$ values and at pH of: (a) 4.0, (b) 4.9, (c) pH 6.22, and, (d) pH 7. Background electrolyte: 0.005 M NaCl.

2.4.3. IR spectra of aqueous solutions containing PO_4^{3-} and Fe^{3+} ions

Although the concentration of Fe^{3+} ions released in aqueous solution was found to be low (<4µM) in our experiments of (Na)IdP-solution interactions (cf. §3.2), ATR FTIR analyses were made to determine the IR band positions of aqueous iron(III)–phosphate species. The

analysis was expected to be helpful to detect the potential contribution of OSSC and ISSC of iron–phosphate (surface) species to IR signals of the NaIdP-phosphate-solution interface. **Fig.II- 7** shows that four IR absorption bands at 1041, 1085, 1124 and 1149 cm^{-1} were resolved upon decomposition of IR spectra of an aqueous solution containing Fe^{3+} and PO_4^{3-} ions. Based on the FTIR data given by Tejedor-Tejedor and Anderson [15], the bands at 1041, 1089 and 1149 cm^{-1} could be attributed to $FeHPO_4^{+}$ aqueous complex, the main species dominating the speciation of Fe under the conditions investigated (and to additional contribution of $FeH_2PO_4^{2+}$, a minor species). The bands at 1043 and 1125 cm^{-1} could relate to the $Fe_2PO_4^{3+}$ species [15]. $Fe_2(OH)PO_3^{2+}$ aqueous species is reported to display a set of bands at 1041,1085 and 1124 cm^{-1} but it is not significantly formed at pH 4, according to speciation calculations.

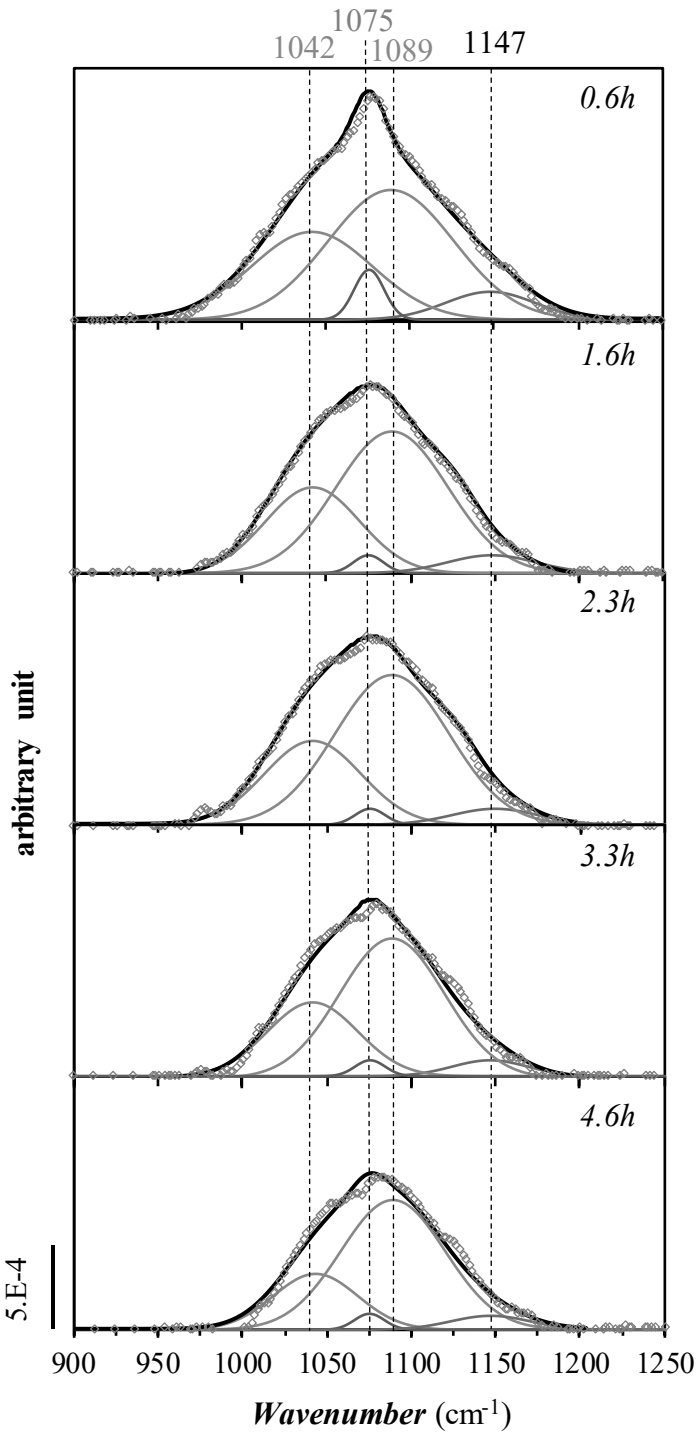

Fig.II- 7. ATR FTIR spectra of a solution at $[P]_{I,aq}$ of 100 µM and $[Fe]_{I,aq}$ of 10 µM and pH 4. Background electrolyte: 0.005 M NaCl, t_R: up to 4.6 hours. Circles: experimental curve; lines: results of spectrum decomposition.

2.4.4. ATR FTIR monitoring of phosphate sorption at clay – solution interface

Effect of reaction time. **Fig.II- 8**a shows the ATR FTIR spectra recorded by *in-situ* monitoring of the sorption of phosphate ions at NaIdP–solution interface at pH 4 (two successive additions, at t_R = 0 and 1 hour, respectively, of 50µM of aqueous P to a two-layers NaIdP–solution system, cf. §2.3.1 and 2.3.3). There was observed the appearance of a weak absorbance in the whole region 1050-1250 cm^{-1} after addition of 50 µM of P, which slightly increases with an increasing of total phosphate concentration to a value of 100 µM (cf. spectra at $[P]_{I,aq}$ = 50µM / t_R = 20min and $[P]_{I,aq}$ = 100 µM / t_R = 1h20min, respectively). From short to intermediate reaction time (t_R of ca. 19h), there was observed the appearance and the progressive increase of a broad absorbance at lower wavenumbers, which increases dramatically up to a reaction time of 3 days and shifts the IR absorption signals towards the region 1000-1100 cm^{-1}.

At short reaction time (t_R < 8 hours), the absorbance observed on the IR spectra of the interface is weak, which makes it somewhat difficult to decompose the signals. However, it can be inferred from spectra decomposition (**Fig.II- 8**b) that the very short-term spectra (t_R < 1h20min) were dominated by two broad bands centered at 1075 and 1160 cm^{-1} with a small shoulder centered at 1035 cm^{-1}. Peak maxima position of the two broad bands were similar to those recorded for the phosphate–water system under similar conditions (**Fig.II- 6**a) but their intensity is higher. This suggests that at least a fraction of aqueous phosphate ions was involved in the formation of a phosphate surface species onto NaIdP (noted here: species A). Decomposition of spectra reveals that the intensity of the two bands of species A show a progressive decrease with time (for t_R > 2 hours), until disappearance (**Fig.II- 8**b). In contrast, a band centered at 1035cm^{-1} (which occurred as a broad shoulder on the short-term spectra) increases slightly with time (t_R < 8h). A poorly-defined band centered at ca. 1132 cm^{-1} could be also identified. It seems that the latter band is independent of the concentration of phosphate ions and reaction times. At an intermediate reaction time (t_R = 19h) the band positioned at 1035

cm^{-1} is well resolved and its intensity shows a further dramatic increase with time (t_R = 3 days). A shoulder at a lower wavenumber (at 1003 cm^{-1}) and a band positioned at 1095cm^{-1} are also present in the IR interface spectra collected at intermediate and long reaction times. We assign the bands at 1003, 1035, 1095 and 1132 cm^{-1} to υ_3 (P-O), as the IR active υ_1 (P-OM, M: metal or hydrogen atom) bands are located at wavenumbers lower than 900 cm^{-1} [23]. The maxima positions of the three υ_3 (P-O) bands are different from those of aqueous $H_2PO_4^-$ species and phosphate surface species A, which evidences that at least another phosphate surface species is formed at the interface. Based on band maxima positions from short to long reaction times, we interpret the evolution of the IR signals by the formation of a P surface species at the interface (noted here: species B), whose contribution grows with time. Further addition of phosphate ions (100 µM) to the 3-days aged system induced no significant change in band's intensity, which rather suggests that no additional surface complex / precipitate of phosphate is forming onto NaIdP under the investigated conditions, in good agreement with the results of macroscopic sorption experiments (cf. § 3.3.2). The increase of absorbance of the band at 1035 cm^{-1} and the decrease of that at 1075 cm^{-1} with time may reflect the kinetics of a conversion from outer sphere to inner sphere surface complex of phosphate.

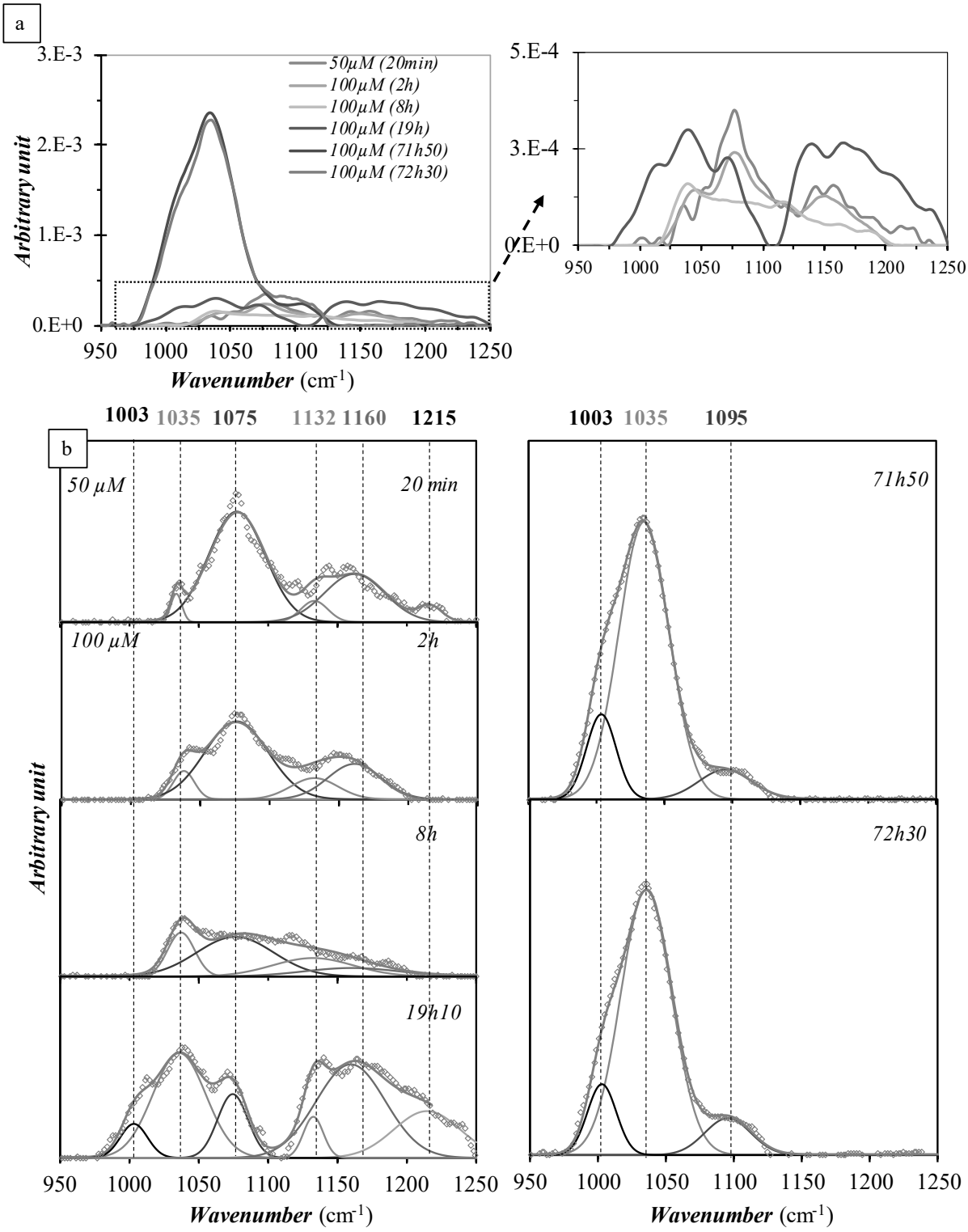

Fig.II- 8. (a) Evolution of in situ ATR FTIR spectra recorded at NaIdP–phosphate-solution interface, as a function of time, and (b) results of spectra decomposition. Experimental conditions: 0.005 M NaCl electrolyte solution at pH 4, $[P]_{I,aq}$ of 50 µM (20min), 100 µM (t_R: 2

hours up to 3 days). Aqueous P was added to a two-layers solution-clay deposited on the ATR crystal.

Effect of phosphate ion concentration - **Fig.II- 9** shows the ATR FTIR spectra recorded by *in-situ* monitoring of the sorption of phosphate ions at NaIdP–solution interface as a function of total phosphate concentration ($[P]_{I,aq}$: 50-300 µM), at pH 4 and a reaction time < 24 hours. at pH4 (successive additions of aqueous P to a two-layers NaIdP–solution system, cf. § 2.3.1 and 2.3.3). There was observed an increase of IR absorbance with increasing phosphate concentration (**Fig.II- 9**a). At low phosphate concentration (50 µM), a well-defined band at 1075 cm^{-1} and a broad band were present in the region 1000-1250 cm^{-1}. Results of spectra decomposition (**Fig.II- 9**b) indicates that the broad band maxima is located at 1160 cm^{-1}, with two shoulders at 1215cm^{-1} and at 1132 cm^{-1}. These bands (i.e., 1075, 1132, 1160 and 1215 cm^{-1}) are present in the range of phosphate concentration 50-250 µM. At a $[P]_{I,aq}$ value of 100 µM and after an intermediate reaction time (t_R=17 hours, spectrum 2 in **Fig.II- 9**a), a shoulder of weak absorbance appears at a wavenumber lower than that of the band at 1075 cm^{-1}. This evolution is similar to that reported for the previous experiment (cf. §3.3.4). An increasing of absorbance was observable with increasing total concentration of phosphate, which appeared to be due to the growing of a well-defined P-O stretching band with a maxima at 1035 cm^{-1} (**Fig.II- 9**b). At $[P]_{I,aq}$ values higher than 150 µM, another small shoulder centered at 1005 cm^{-1} appeared and increased with increasing phosphate concentration. These bands are similar to those identified at long reaction time in the previously-described ATR FTIR experiment for surface phosphate species B (cf. §3.3.4). The band at 1095 cm^{-1} (of species B) could however not be observed (at $[P]_{I,aq}$ < 250 µM) possibly due to overlapping of the band at 1075 cm^{-1} which exhibited a strong absorbance.

Hence, seven absorption bands (at 1003, 1037, 1075, 1095, 1132, 1160 and 1215cm^{-1}) were identified on the ATR FTIR spectra recorded during monitoring of the NaIdP – phosphate –

solution interface along an increasing of phosphate ion concentration. These bands are assigned to the same surface species as those described previously for the ATR FTIR experiments on the effect of reaction time. The bands at 1075, 1160 and 1215 cm^{-1} correspond to the species A. The bands at 1003, 1037, 1095 -and possibly 1132 cm^{-1}- relate to species B. Note that the band at 1132 cm^{-1} of low absorbance is independent on phosphate concentration ($[P]_{I,aq} < 250$ μM) and reaction time (for $t_R < 19$ hours).

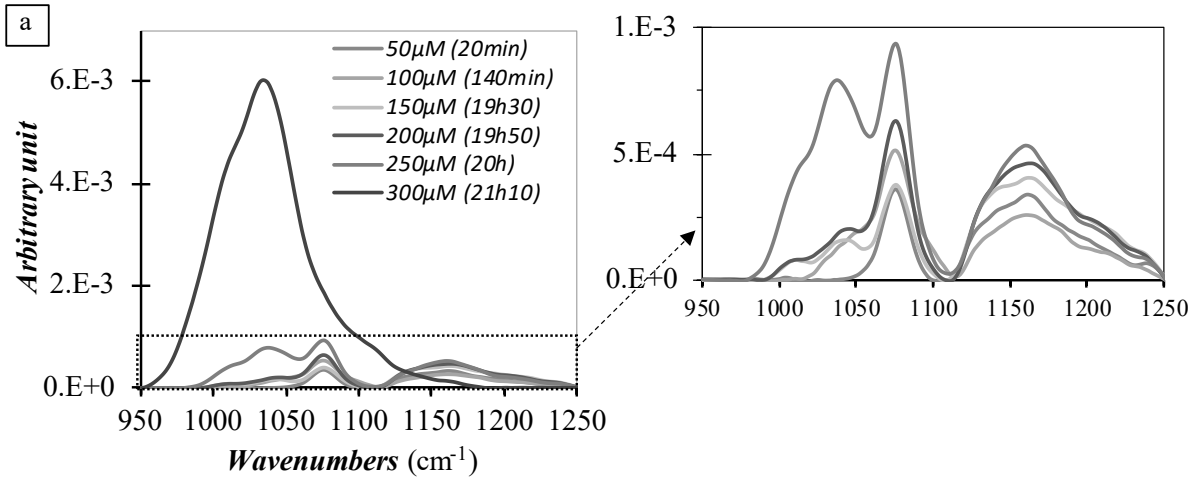
a
50µM (20min)
100µM (140min)
150µM (19h30)
200µM (19h50)
250µM (20h)
300µM (21h10)
Arbitrary unit
6.E-3
4.E-3
2.E-3
0.E+0
950 1000 1050 1100 1150 1200 1250
Wavenumbers (cm-1)
1.E-3
5.E-4
0.E+0
950 1000 1050 1100 1150 1200 1250

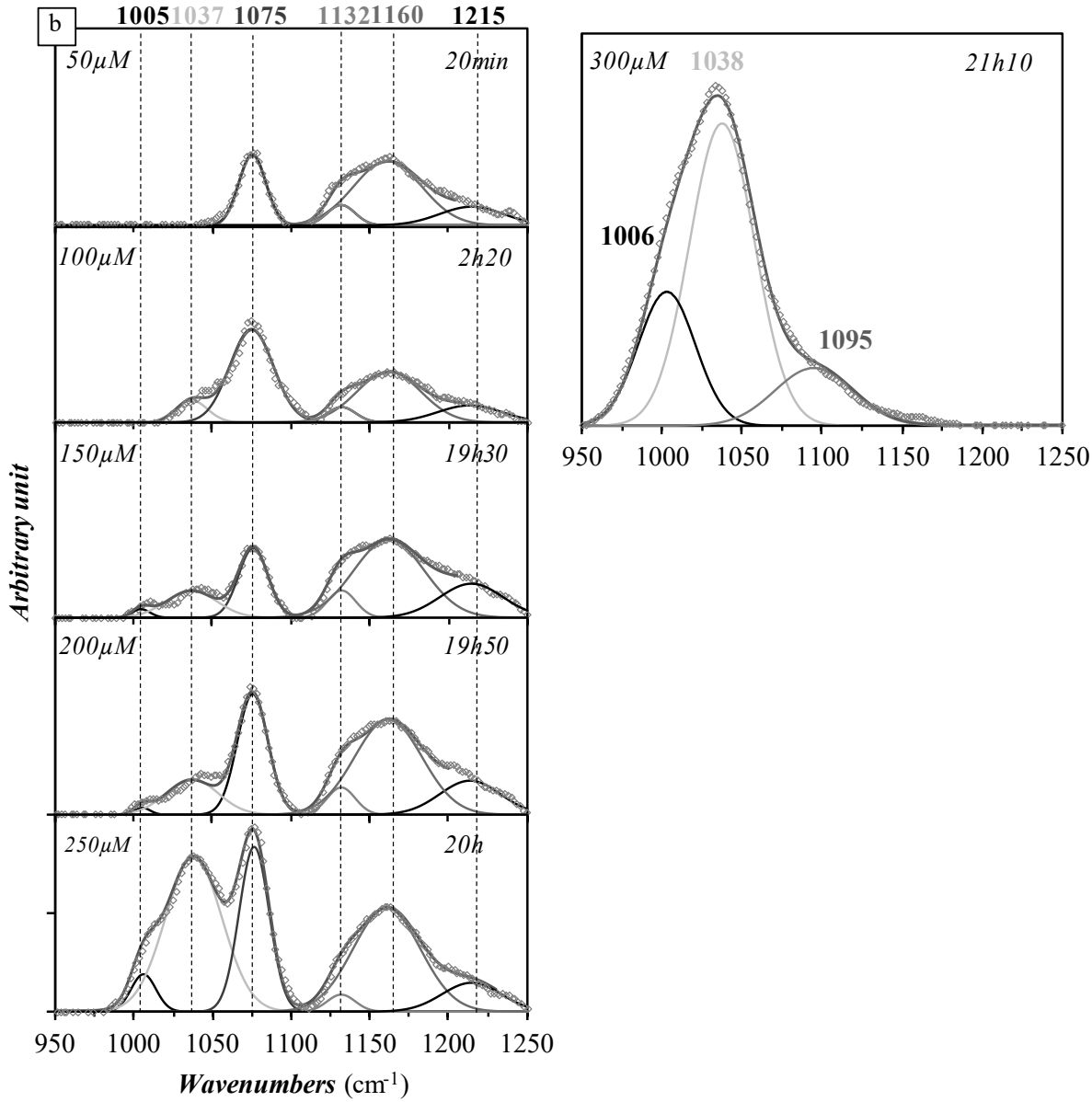
b
1005 1037 1075 1132 1160 1215
50µM 20min
100µM 2h20
150µM 19h30
200µM 19h50
250µM 20h
Arbitrary unit
950 1000 1050 1100 1150 1200 1250
Wavenumbers (cm-1)
300µM 1038 21h10
1006
1095
950 1000 1050 1100 1150 1200 1250

Fig.II- 9. (a) In situ ATR FTIR spectra results of the sorption of phosphate at NaIdP–solution interface as a function of phosphate concentration ($[P]_{I,aq}$: 50-300 µM) and (b) results of spectra decomposition. Experimental conditions: 0.005 M NaCl electrolyte solution at pH4, t_R up to 19 hours. Aqueous P was added to a two-layers solution-clay deposited on the ATR crystal.

3. Discussion and conclusion

3.1. Macroscopic sorption of phosphate ions at Illite–electrolyte solution interface

Sorption edges of phosphate ion sorption onto NaIdP presented here for low [P]I,aq values (lower than 100 µM) show that the highest percentage of phosphate sorption was found at acidic pH (3-6), with this percentage decreasing with increasing pH. This findings are consistent with previous studies of phosphate ion sorption onto aluminum-oxide, Illite, and kaolinite [97,101,104]. Del Nero et al. [97] showed a maximal and quite constant sorption of phosphate ions onto alumina at pH 3-6, and a decrease in sorption at higher pH. The authors proposed that two sorption mechanisms, i.e., formation of ISSC/OSSC and surface precipitation of Al-phosphates, were involved in the retention of phosphate ion at the alumina-electrolyte solution interface with increasing P loading at acidic pH. At low surface coverage, P sorption was shown to be controlled by reactions of surface complexation *i.e.*, by surface ligand exchange reactions implying high affinity aluminol edge sites, and by formation of an outer-sphere phosphate surface complex at protonated aluminol surface sites (e.g., $\equiv AlOH_2^+$). Edzwald et al. [101] examined the macroscopic uptake of P by (not conditioned) clay minerals like Illite, kaolinite and montmorillonite. They observed that the sorption of phosphate ions was maximal at pH4-5 and further decreased at higher pH, which is a similar pH-dependence than that observed in the present study for NaIdP. The authors concluded that the aluminol surface groups of clays, which have an isoelectric point at high pH, are more important in sorption of phosphate ions than silanol surface groups (which have a negative charge down to a pH of 2). Edzwald et al. [101] also emphasized that the adsorbed metals (e.g., iron) as bridging cations present at the

surface of clay and/or of metal (e.g., Fe- and Al-) oxides contained in the clay sample, controlles the retention of phosphate ions. Van Emmerik et al. [104] studied the sorption of phosphate ions onto a pretreated kaolinite (at different concentrations of phosphate ions in the range 1-10 mM). Their data also showed that the percentage of phosphate ion sorption was maximal and constant in the range of pH3-5 and decreased with pH, at low and high surface loadings. They reported that formation of ISSC and/or surface precipitates of phosphate at edge sites of the alumina-like layer of kaolinite was predominant over the studied pH range, depending on surface loading of phosphate ions. The sorption edge and sorption isotherms of phosphate ions presented in this study for NaIdP are consistent with the above-mentioned studies suggesting a predominant role on phosphate ion sorption of the aluminol and/or ferrinol surface sites present at edges of Illite. Our macroscopic data suggested successive formation, with increasing $[P]_{I,aq}$ (< 200 µM) or with decreasing $R_{S/L,}$ of surface complexes of distinct stability. Alternately, high-affinity and low-affinity surface sites may be successively implicated in formation of phosphate surface species onto NaIdP, up to a surface coverage of ca. 5-6 µmol.g^{-1} for which no clay surface sites are available anymore for the P sorption (see § 3.3.1, §3.3.2). Such a limiting surface coverage is consistent with values of surface concentrations of low affinity and high affinity aluminol sites expected to exist at NaIdP clay platelets [188]. It is unlikely that significant amounts of Al-phosphate surface precipitates are involved in phosphate ion sorption at acidic pH onto NaIdP under our experimental conditions ($[P]_{I,aq} \leq 200\mu M$), as P surface coverage reaches a plateau. Therefore, it is likely that the aluminol surface sites at NaIdP edges mostly participate to the formation of ISSC of phosphate under our investigated conditions, which may be favored at acidic pH by a first step of electrostatic attraction between the positively charged clay surface (due to existence of protonated aluminol sites as $\equiv SOH_2^+$) and the negatively charged aqueous phosphate ions (HPO_4^{2-} and $H_2PO_4^-$) approaching the surface (formation of OSSC of phosphate). EM measurements are useful to determine the isoelectric

point (IEP) of colloidal materials as well as to distinguish ISSC from OSSC formation [16,198]. Later surface species are reported to influence the value of EM but they do not produce changes in IEP, whereas ISSC formation may lead to surface charge reversals and shifts in IEP [16,97,198]. EM data showing charge reversal and IEP shifts to lower pH value with increasing phosphate loading onto minerals were reported in the literature as indirect evidences of formation of ISSC of phosphate ions at the interface between solution and kaolinite or iron / aluminum (hydro)oxides [15,16,97,99,168,199]. As long as the edge aluminol (and/or ferrinol) sites are responsible for phosphate sorption onto clay, sorption reactions of phosphate ions at such sites would play a role on surface charge evolution of clay. The EM data presented here show charge reversals and a shift in IEP to a lower value of pH as a consequence of phosphate ion sorption onto NaIdP. These findings clearly support the existence of a strong sorption of phosphate ions onto Illite, i.e., formation of ISSC of phosphate at aluminol sites that impart negative charges to the surface of NaIdP.

3.2. ATR FTIR spectroscopic study of P sorption at Illite–solution interface at pH 4

Phosphate surface species A (1075, 1160 and 1215 cm^{-1}).

Phosphate surface species A has two υ_3 bands at 1075, 1160 cm^{-1} and a broad band centered at 1215 cm^{-1}. The position of these bands are very similar to those of the dissolved phosphate species ($H_2PO_4^-$, C_{2v}), as reported by [15]. The latter also have a band at 1215 cm^{-1} assigned to the δ(P-OH) bending mode of dissolved phosphate species (e.g., $H_2PO_4^-$, C_{2v}) [15,16,23,146]. In the present study, a broad and weak band at 1215 cm^{-1} is present in IR interface spectra recorded at short reaction time during the sorption process of phosphate ions at the interface (while it was not observed in IR analyses of the phosphate – electrolyte solution system). That the band at 1215 cm^{-1} of the δ(P-OH) bending mode was observed during the P sorption process suggested the formation of OSSC species of phosphate. Accumulation of negatively charged

phosphate ions by electrostatic attraction as counter-ions to balance positively charged edge sites created at the clay-solution interface, i.e., $\equiv SOH_2^+$ sites, and/or by weak hydrogen bonding to surface water or surface hydroxyl sites, might increase their absorbance. Molecular symmetry of sorbed phosphate ions is expected to be similar to that of dissolved phosphate species (C_{2v}) if the phosphate ions is weakly sorbed. The numbers of P-OH bands of the weakly sorbed phosphate should be the same as for the corresponding aqueous P species, and the peak position should be close, too [16]. The maximal number of υ_3 vibrational bands of PO_4 unit for a C_{2v} or lower molecular symmetry is three [23] because the υ_3 vibrational bands is triply degenerated when PO_4 units have a T_d molecular symmetry mode [145]. Theoretically, the third υ_3 band located at 940 cm^{-1} should be present in IR signals for an OSSC species of phosphate. The band was however not observable in our IR interface spectra possibly due to: (i) the strong IR absorbance of NaIdP–solution system below 1000 cm^{-1} as observed by Borgnino at al. [100] for an iron modified montmorillonite, and (ii) cutoff of detector at ~ 900 cm^{-1}. We thus conclude that the phosphate surface species A with IR bands at 1075, 1160 and 1215 cm^{-1} is an OSSC of diprotonated phosphate ions (as: $\equiv SOH_2^+ \cdots H_2PO_4^-$) formed at NaIdP–solution interface, which predominates the phosphate surface speciation at short reactions times and / or at low phosphate concentrations.

Phosphate surface species B (1005, 1037, 1095 and 1132 cm^{-1}).

Phosphate surface species B has four υ_3 bands at 1005, 1037, 1095 and 1132 cm^{-1} whose band intensity increases with reaction time -except the poorly-defined band at 1132 cm^{-1}. This species exhibits a vibration band at 1035 cm^{-1} that predominates at a long reaction time (> 24 hours). Borgnino et al. [100] have shown in an ATR FTIR study of phosphate sorption at the Fe-modified montmorillonite–solution interface that, at a low pH value, two ISSC of phosphate were formed at the surface of iron(III) (hydr)oxides present in the clay. The first one was shown to be an unprotonated bidentate surface complex, $\equiv (FeO)_2PO_2$, with υ_3 bands at 1088, 1049

and 941 cm^{-1}. The authors suggested a C_{2v} or lower molecular symmetry for this ISSC, whose band maxima positions resulted from shifts of υ_3 bands of $H_2PO_4^-$ (at 1160, 1076 and 940 cm^{-1}). The second one was proposed to be a monoprotonated bidentate surface complex, e.g., $\equiv (FeO)_2(OH)PO$, whose bands' positions were at 1128, 1011 and 978 cm^{-1}, with a C_1 molecular symmetry. Dolui et al. [105] investigated by using *in situ* ATR FTIR the mechanisms of phosphate sorption ($[P]_{I,aq}$ = 100 μM) at acidic pH at the kaolinite–solution interface and they identified five υ_3 bands (1138, 1108, 1086, 1074 and 1061 cm^{-1}). They reported the formation of multiple surface species of phosphate ions at the surface of kaolinite with a predominant surface species (ISSC or surface precipitate) formed at edge aluminol sites whose band position was at 1138 cm^{-1}. Li et al. [98] studied surface speciation of phosphate ions at the α-Al_2O_3–electrolyte solution interface from pH 5 to 9 by using ^{31}P solid state NMR coupled with ATR FTIR and DFT calculation. Five IR bands (at 1130-1131, 1092-1096, 1053-1060, 1020-1025 and 1005-1010 cm^{-1}) were identified. The authors concluded on the co-existence of two surface complexes species of phosphate ions as predominating surface species at pH 5: a monoprotonated bidentate binuclear surface complex, as $\equiv (AlO)_2(OH)PO$, and an unprotonated bidentate binuclear surface complex, as $\equiv (AlO)_2PO_2$. The authors observed at high pH a decrease in intensity of bands at 1130 and 1010 cm^{-1}, which relate thus to the protonated species (and bands at 1096, 1060 and 1020 cm^{-1} may relate to unprotonated species). Del Nero et al. [97] investigated the sorption mechanisms of phosphate at acidic pH onto α-Al_2O_3 by *in situ* ATR FTIR and zeta potential measurements. They reported formation at low surface coverage of an ISSC of phosphate that decreased surface charge of alumina and had possibly IR bands at 1084 and 1033 cm^{-1}. The main phosphate surface species was shown to become progressively a surface precipitate of Al-phosphate incorporating Al^{3+} ions released by mineral dissolution, with a band at 1137 cm^{-1} and a constant surface charge, when increasing surface coverage by phosphate ions. Based on bands' positions, molecular symmetry

considerations, and above-mentioned literature data, we assign the three υ_3 bands positioned at 1005, 1037 and 1095 cm^{-1} for species B identified in the present study to a monodentate binuclear surface complex species formed at edge surface sites of clay, i.e., $\equiv (SO)_2PO_2$ (S: Al and / or Fe). The symmetry of the phosphate unit for species B is C_{2v} or lower. The small υ_3 bands at 1132 cm^{-1} can be tentatively assigned to limited formation of a monoprotonated monodentate binuclear surface complex $\equiv (SO)_2(OH)PO$ (S: Al and / or Fe), as similar band position were reported for ISSC of phosphate of the type $\equiv (AlO)_2(OH)PO$ (Li et al. [98]) and $\equiv (FeO)_2(OH)PO$ (Borgnino et al. [100]) formed onto Al- and Fe-oxides, respectively, and / or to low amounts of Al-phosphate surface precipitates.

3.3. Conclusions

This study provides valuable information on the mechanisms of phosphate ion sorption at the Illite – solution interface, for a range of aqueous phosphate concentrations (20-200 µM) and clay-to-solution ratios investigated that led to low to moderate coverage of the clay surface by P (2-6 $\mu mol.g^{-1}$). It was found that the percentage of P sorption is dependent on pH and phosphate concentration. Macroscopic and EM data suggested moreover mechanisms of strong phosphate ion sorption, which added negative charges to the clay surface and could involve multiple sorption species and/or surface sites present on the clay edges (high affinity sites and low amounts of low affinity sites, respectively). Data acquired by *in situ* monitoring of the Illite-solution interface by ATR FTIR spectroscopy provided evidence that phosphate ions were primarily sorbed at acidic pH via the increasing formation, with time and aqueous phosphate concentration, of inner-sphere phosphate surface complexes, probably monodentate binuclear surface complexes, i.e., $\equiv (SO)_2PO_2$ (S: Al and / or Fe), involving hydroxyl surface sites on the clay edges. These surface species were characterized by υ_{as}(P-O) bands positioned at 1003, 1035 and 1095 cm^{-1}, and were formed by transformation over time of an outer-sphere phosphate surface complex that dominates phosphate surface speciation at low reaction times and low P

concentration. The information on phosphate surface speciation provided by the present study is useful for better understanding the surface reactivity of clays in soils and natural subsurface systems. The data also help provide background knowledge for further studies of complex ternary systems of TME/radionuclide-phosphate-clay-solution, which are of major interest, for example, in assessing the safety of high-level radioactive waste disposal in clay rocks.

Acknowledgments

We thank for analyses of clay samples: ITES (Institut Terre et Environnement de Strasbourg, Strasbourg University, France) for mineralogical analyses, SARM-CRPG (Service d'Analyse des Roches et Minéraux, Centre de Recherches Pétrographiques et Géochimiques, Nancy, France) for major element and trace element analysis, and ECPM (École de Chimie des Polymères et Matériaux, Strasbourg, France) for BET measurements. We are grateful to the A. Boos for giving us access to the ICP-OES and ICP-MS equipments of the "Plateforme des Inorganiques" of IPHC for our solution analyses.

Funding

This research work was funded by the European Joint Programme on Radioactive Waste Management EURAD of the European Commission (contract number CNRS 198255) and took place in the frame of the WP FUTURE of EURAD.

Appendix A. Supporting information

Chapter III. Speciation studies at the Illite - solution interface: Part 2 – Co-sorption of uranyl and phosphate ions

Speciation studies at the Illite - solution interface: Part 2 – Co-sorption of uranyl and phosphate ions

Shang Yao Guo, Mirella Del Nero, Olivier Courson, Sylvia Meyer-Georg, Remi Barillon

Article submitted at Colloid and Surface A

1. Introduction

The environmental behavior of uranium (U) is a major issue of soil - sediment - water continuums due to the natural abundance of this metal in igneous or sedimentary rocks, its involvement in a variety of anthropogenic and industrial activities such as metal mining, water treatment, energy production, including nuclear plant development, which generate radioactive wastes or Technonogically-Enhanced Naturally Occurring Radioactive Materials, TE-NORM [81–84], its potential radiological and chemical toxicity [9], and the complexity of the biogeochemical processes that govern its fate in ecosystems [38,44]. Nuclear plants generate high amounts of spent nuclear fuel [85] and produce radioactive wastes whose main constituent is uranium (95%), with the remaining ones being fission products (4%) and plutonium (1%) [86]. Different strategies (such as vitrification, partitioning and transmutation, pyro-processing and deep geological repository) have been proposed to ensure a long-term management of the radioactive wastes [87]. In peculiar, storage of high-level radioactive wastes (HLW) in deep geological repositories in clay rock formations (such as Boom clay, Callovo-Oxfordian clay, Cox, and Opalinus clay, OPA) has been considered by several countries as an important strategy since the mid-1980s [1]. Clay minerals are major constituents of argillaceous formations, e.g., 40-60 wt % for Cox [88] and 44-92% for OPA [89], and have remarkable physicochemical properties such as a low permeability and a high capacity of radionuclides (RN) retention, which make these formations prospective geological barriers for HLW repository

[2,90,1,80,88]. In deep geological repositories, HLW would be isolated from contact with ground-waters by near field engineered multi-barrier systems (e.g., thick steel canisters, cementitious materials barrier and bentonite backfill) in order to prevent their dissolution and the subsequent migration of dissolved radionuclides [90] and RN-containing colloids to the human-accessible environment [88]. However, degradation in the long-term of the near-field multi-barrier system, such as corrosion of thick steel canisters and chemical cement degradation, could result in groundwater entering in contact with HLW [6,90]. The mechanisms and rates of the HLW dissolution, of the long-term diffusion/transport by ground-waters of RN in the host rock porosity, and of the immobilization of the RN by their sorption onto host rock minerals, are thus important safety issues [90,91].

Uranium mainly exists in the oxidation states IV and VI in the environment. It has a higher solubility and a lower tendency to bind at functional groups existing at mineral surfaces in the latter than in the former case, which makes it potentially mobile in the hexavalent state, in the forms of uranyl (UO_2^{2+}) ions [38]. While U(IV) is largely controlled by poorly-soluble uraninite, U(VI) has a strong tendency to form, depending on pH, hydrolysis products and/or anionic carbonate species in natural waters, given its high solubility and its chemical affinity for the dissolved ligands OH^- and CO_3^{2-} [39–42]. Uranyl ions may also participate to the formation of stable organic complexes with a variety of organic ligands in low pH waters, from simple di-tri-carboxylic acids to humic / fulvic acids [43,44]. They have moreover a high chemical affinity for phosphate ions, too [45,46]. Experimental studies have indeed shown that formation of uranyl phosphate complexes may increase the solubility of U(VI) in terrestrial waters depending on aqueous phosphate concentration and physicochemical conditions, i.e., at low pH (<6) and / or at low to moderate concentrations of other relevant (in)organic ligands like carbonate, fulvate, humate, etc [45].

It is well known that formation of secondary uranyl silicate and/or uranyl phosphate minerals, and sorption processes occurring at surfaces of relevant minerals in rocks and soils, e.g., Fe-/Al-oxihydydroxides and clays, may strongly retard the migration of U(VI) in oxic (ground)waters. Experiments have evidenced that precipitation processes of phosphate phases of the type chernikovite or (Ca-, Mg-, Na-)autunite may limit U(VI) solubility under certain conditions [45,47–51]. Field studies have moreover shown the presence of various (co)precipitates of U(VI)-phosphate phases in natural sites near U-ore deposits and in contaminated sites or sediments [47,60–69]. It has also been long suggested that processes of uranyl and phosphate (co)sorption are responsible for the long-term retention of U(VI) in some soils or subsurface media, where the trace metal is found in close association with phosphate and with iron(III)/Al(III) oxi-hydroxides or with clays[63,65,70–73], or with surface precipitates of Fe^{3+}-phosphate formed at surfaces of hematite [71,74,75].

Numerous model system studies have been carried out over the last few decades to gain a comprehensive understanding of uranium(VI) sorption processes in natural systems and to obtain macroscopic and molecular data to increase the robustness of models that are used to predict the migration behavior of U(VI) in the environment. Experiments and/or surface complexation modeling studies have long suggested that a strong chemical sorption of uranyl ions prevails at surfaces of metal oxihydroxides [111–114] and clay minerals or rocks [115,116,90,117,118,6,88]. Experiments have also shown that the presence of phosphate ligands promotes the sorption of U at the surface of silica[134] and metal (Al, Fe) oxihydroxides [11,111,112,135], which may nucleate precipitation of U(VI) phosphates.

Further molecular scale work has evidenced that U(VI) participates in the formation of inner-sphere surface complexes (ISSC) onto oxygen based minerals, predominantly via bidentate linkages to oxo surface groups. Investigations by using Extended X-Ray Absorption Spectroscopy (EXAFS) and Attenuated Total Reflection Fourier Transform Infrared

Spectroscopy (ATR FTIR) have revealed that surface-U(VI)-carbonato complexes may predominate the surface speciation of U(VI) sorbed onto hematite, -with the ternary complexes having an inner-sphere metal bridging structure-, under conditions relevant to aquifers and in a wide range of pH [119,120]. EXAFS analyses have also shown that bidendate edge-sharing and bidendate corner-sharing ISSC of uranyl were formed upon sorption of U(VI) onto goethite at pH 4-7 [12]. Speciation studies using EXAFS, X-Ray Photoelectron Spectroscopy, XPS, and Time Resolved Laser Induced Fluorescence Spectroscopy, TRLFS, have provided evidence that U(VI) was sorbed onto an Al-oxide in the forms of a bidentate ISSC of U(VI) and/or polynuclear uranyl surface species, depending on U surface coverage [121,122]. ATR FTIR analyses of U(VI) sorption onto alumina have revealed that three types of uranyl surface species were forming, in a wide range of pH, as a function of U surface loading: a monomeric carbonate surface complex, an oligomeric surface complex, and a surface precipitate[123]. Further ATR-FTIR and TRLFS analyses have confirmed the formation of U(VI) carbonato surface species onto alumina, under conditions where aqueous uranyl tricarbonato species exist in solution [124]. Regarding clays, EXAFS analyses have provided evidence that uranyl ions are sorbed as exchangeable UO_2^{2+} in the interlayer space of clays at low pH, leaving the uranyl aquo-ion structure intact, and as additional ISSC of uranyl and / or U(VI) polynuclear surface species [90,125–127], and / or uranyl carbonato ISSC which form at edge sites of clay platelets when increasing pH [128]. Multiple uranyl surface species were also identified by ATR FTIR to co-exist at the surface of montmorillonite in contact with a solution at near-neutral pH and at a low concentration of U (20 μM) [129]. This short review illustrates that U(VI) is sorbed at surfaces of Al- / Fe-oxihydroxides and clays in a variety of chemical forms, with the U surface speciation being primarily controlled by key physicochemical parameters of the system studied, such as pH, presence of carbonate ligands, and mineral surface properties governing U surface coverage.

Several spectroscopic studies have aimed at elucidating the processes of (co)sorption of uranyl and phosphate ligands -or arsenate ligands as possible chemical analogues- onto metal (Fe, Al) (oxihydr)oxides [9,11,135,12,114,124] and onto clays [136,137], too. Based on EXAFS spectroscopic analysis, Singh et al. [60] have suggested a monodentate complexation between uranyl and phosphate ions to form ternary surface complexes onto goethite, at acidic-to-neutral pH and at low concentrations of U (≤10µM), in the presence of phosphate ligands (100-130µM). It has also been inferred from ATR FTIR and TRFLS analyses that uranyl ions are sorbed at acidic pH via formation of uranyl phosphato ISSC at low U coverage of Al-oxides, with a progressive transition occurring between the formation of the ternary surface complexes and the surface precipitation of U(VI)-phosphates when increasing P loading [11]. EXAFS analyses have also provided evidence for formation at acidic pH of a trögerite-like surface precipitate of uranyl-arsenate onto alumina, under conditions of high total concentrations (> 50 µM) of U and arsenate ions [9]. Hence, there appears that the prevalent mechanism controlling the co-sorption of U(VI) and phosphate ions on metal (oxihydr-)oxides is highly dependent on a key parameter, which is the mineral surface coverage by U and P.

To our best knowledge, two spectroscopic studies have so far been devoted to co-sorption of uranyl and phosphate ions onto surfaces of clays. Gładys-Plaska et al.[137] have shown by XPS and ATR FTIR analyses that U(VI)-phosphate surface complexes form at the edge sites of red clays during the simultaneous sorption of U(VI) and phosphate ions. Troyer et al.[136] have investigated by EXAFS and TRLFS the effect of increasing concentrations of phosphate ions and uranyl ions (0.025-100µM) on the uptake of U(VI) by montmorillonite at pH 4-6. The authors have evidenced a transition between formation of uranyl phosphate surface complexes and surface precipitates of U(VI)-phosphates with increasing clay surface coverages by sorbates. They have also identified the existence of a uranyl carbonate ternary surface complex forming at pH 8. A complete understanding of the mechanisms of co-sorption of uranyl and phosphate

ions on clays requires additional spectroscopic work to acquire data on the speciation of U and P sorbed on clays with various surface properties. The latter are expected to control, among others, the clay surface coverages by U and P which are main parameters influencing sorption mechanisms. Moreover, investigations of the surface speciation of uranyl and phosphate ions onto Illite is mandatory to gain better knowledge on the mechanisms of uptake of U(VI) on illitic-rich clays such as those envisioned as far-field host rocks in HLW repository. To this end, providing data from *in situ* spectroscopic monitoring of the clay – solution interface during the sorption process as a function of a key parameter, e.g. pH, reaction time and surface coverages, is needed.

The aim of this study was to determine the mechanisms of sorption of low level concentrations of U(VI) onto a homo-ionic Na-Illite in the presence of phosphate ligands and to identify the (multiple) uranyl phosphato surface species formed at the clay–solution interface. First, batch sorption experiments were carried out to quantify the macroscopic sorption of U and P. Sorption edges were recorded in a wide pH range (3-8), at various clay-to-solution ratio ($R_{S/L}$: 1-3 $g.L^{-1}$). Sorption isotherms were obtained at acidic pH, for a range of concentrations of U ($[U]_{I,aq}$: 1 – 25 µM) and P ($[P]_{I,aq}$: 20 – 200 µM). Measurements of electrophoretic mobility (EM) of suspended clay particles, and its variation with key parameters studied, were performed to determine the charges imparted by sorption reactions to the clay surface and to gain information on surface species formed. Second, experiments of *in situ* monitoring of clay - U(VI) - phosphate – solution interface by ATR FTIR spectroscopy were conducted in order to investigate the surface speciation of U-P sorbed at acidic pH, as a function of time and total concentration of uranyl ($[U]_{I,aq}$: 2-10 µM) or phosphate ($[P]_{I,aq}$: 50-200 µM) ions. The sorption species were identified by (changes in) coordination environments of sorbed phosphate units that were deduced from changes in FTIR spectra of Illite-aqueous solution interface recorded in the region 900-1200 cm^{-1} (characteristics of P-O stretching vibrations). Spectroscopic data

and macroscopic data presented here provide useful information on the surface speciation of uranyl ions sorbed onto Illite in the presence of phosphate ligands, which could serve modelling of migration behavior U(VI) in argillaceous formations.

2. Materials and methods

Analytical grade chemical products and ultrapure Milli-Q water (purity >18 MΩ.cm) were used in all experiments.

2.1. The clay sample used

The clay sample used in the experiments is a homoionic Na-Illite (noted as NaIdP) obtained by conditioning of a size fraction (< 77 μm) of an Illite du Puy (noted as IdP) purchased at a company (Argile Verte du Velay of Lissieu) and collected in the region "Le Puy-en-Velay" in the Massif Central Mountains in France. The conditioning procedure is given in [14] and is expected to remove hydrolyzed products such as hydroxy-aluminium compounds, phosphate impurities and soluble minerals like calcite [14,80]. Methods used and results obtained on the mineralogical and chemical characteristics of the samples are described in details in Part I. of our work (Guo et al., [200]) and are summarized hereafter. Specific surface areas of IdP and NaIdP were found to be equal to 92 and 107 $m^2.g^{-1}$, respectively, in agreement with a previously published value of 97 $m^2. g^{-1}$ obtained by M.H. Bradbury [116]. Mineralogical compositions of whole rocks and their clay size fractions (< 2 μm), as obtained by X-ray diffraction analyses, considerations of layer and interlayer spacings of clays (e.g. Brindley and Brown [187]) and semi-quantitative estimates by using the DIFFRAC.EVA software (4.3 version, error <5%) are described as follows. IdP is mainly composed by calcite (38%), feldspars (36%) like microcline, orthoclase and albite, and Illite (19%) and low amounts of kaolinite, quartz, siderite, and hematite. Carbonate minerals and iron minerals were efficiently removed by homo-ionic conditioning. Main minerals of NaIdP are Na-Illite (30%) and feldspars (58%) and accessory

minerals are quartz and kaolinite. Clay fraction of both samples only contains Illite (> 75%) and kaolinite. Major element composition of NaIdP obtained by Inductively Coupled Plasma Optical Emission Spectrometry analysis (ICP-OES, analytical error <0.1%) is consistent with that of a K-rich silicate rock and with removal of carbonate minerals and phosphate minerals during clay conditioning (CaO < 1% in wt/wt % oxide and P_2O_5 under detection limit). It is to be noted that Fe concentration remains significant (Fe_2O_3: 8% in wt/wt % oxide) and indicates either presence of accessory Fe-minerals (< 5%) and/or an incorporation of Fe in clay structures. Trace metal element (TME) compositions obtained by ICP Mass spectrometry (ICP-MS, analytical error: 5-20 %) indicate that concentrations of Sr, As and Lanthanides are lower in NaIdP than IdP, likely due to removal of carbonate and/or phosphate minerals during clay conditioning. Concentrations of other TMEs are similar in both clay samples (> 150ppm for Rb, Ba, Zn, Cr and Cs; < 50 ppm for other TMEs; ca. 3 ppm for U).

2.2. Batch sorption experiments

Preliminary experiments carried out in the Part I of this work (Guo et al., *submitted*) have provided insights into the chemical evolution of a 0.005 M NaCl electrolyte solution brought in contact with the clay samples. The results have indicated that phosphate ions are main inorganic ligands released in solution during IdP-solution equilibration, which could therefore strongly affect the behavior of uranium (VI) at trace level onto Illite du Puy. Unlike for IdP, no significant amounts of phosphate ions and uranium(VI) were detected in final experimental solutions equilibrated with NaIdP. This sample was chosen to study the co-sorption processes of uranyl and/or phosphate ions onto clay, under well-controlled laboratory conditions.

2.2.1. Uranyl sorption

Batch experiments were carried out under atmospheric conditions and at 298K to evaluate the effect of pH, of total concentration of uranyl ions ($[U]_{I,aq}$) and clay-to-solution ratio ($R_{S/L}$) on

the macroscopic uptake of uranyl ions by NaIdP. Sorption edges were obtained in the pH range 3-8, at different values of $[U]_{I,aq}$ (1 and 12 µM) and $R_{S/L}$ (1, 2 and 3 $g.L^{-1}$). Sorption isotherms ($[U]_{I,aq}$ varying from 1 to 10 µM) were also obtained at pH 3, 3.5 and 4, respectively, and at $R_{S/L}$ equal to 3 $g.L^{-1}$. The individual experiments were conducted at defined values of $R_{S/L}$ and pH as described below. Given amounts of NaIdP subsamples were introduced in individual 15 mL polypropylene tubes and brought in contact with 10 mL of an electrolyte solution (0.005 M NaCl), at defined initial values of pH. The suspensions were pre-equilibrated for a duration (t_{pre-eq}) of 3 days. When necessary, the pH value was re-adjusted by adding very small volumes of a 0.1M HCl or 0.1M NaOH solution in the tubes. After pre-equilibration time, a given volume of a U(VI) stock solution (with $[U] = 4.61\times10^{-3}$ M, solution acidified at pH 1 by HCl) was introduced in the individual tubes to achieve defined $[U]_{I,aq}$ values. The tubes were then gently rotated end-over-end and shaken during 4 days. After this contact time (t_R), the final pH of the suspensions was measured. Separation between solid and solution phases was achieved by a 3 hours centrifugation at 9000 rpm of the individual tubes containing the suspensions (Illite cutoff: ca.16 nm). The supernatants were then removed from the individual tubes. Foe each supernatant, a given volume was taken for electrophoretic mobility (EM) measurement and another one was acidified by a 2% HNO_3 solution for analysis of final aqueous concentration of U(VI) (noted here as $[U]_{F,aq}$). Each experiment was carried out in duplicate. Blank experiments without solid were also performed in a similar way than described above.

2.2.2. Uranyl and phosphate ions (co)sorption and desorption

Co-sorption experiments were conducted to investigate the effect of the presence of phosphate ligands on the uptake of uranyl ions in NaIdP–electrolyte solution (0.005 M NaCl) systems, at different values of pH and $[U]_{I,aq}$, and for a given clay-to-solution ratio ($R_{S/L}$ = 3 $g.L^{-1}$). First, the pH dependence of the (co)sorption of uranyl ions and phosphate ions was investigated in

the pH range 3-8, at two different U concentrations ($[U]_{I,aq}$ = 1 and 12 µM, respectively) and a moderate concentration of total P ($[P]_{I,aq}$ = 100 µM). Second, sorption isotherms of uranyl ions (for $[U]_{I,aq}$ varying in the range 1-12 µM) were obtained at pH 4 and at two concentrations of phosphate ions ($[P]_{I,aq}$: 20 and 100 µM, respectively). Experiments were conducted as described in paragraph 2.2 except that known volumes of stock solutions of phosphate ions and uranyl ions, respectively, were added simultaneously to the individual tubes in order to achieve desired $[P]_{I,aq}$ and $[U]_{I,aq}$ values in experiments. Two of the co-sorption experiments (at pH_F equal to 5.2 and 4.1, respectively) were moreover used for studying the kinetics of desorption of U(VI) and provide information on the reversibility of the (co)sorption processes. After the step of equilibration of the two above-mentioned sorption experiments, the pH of the suspensions were brought to a value of 3.2 in the individual tubes. The tubes were then gently rotated end-over-end and shaken during ca. 15 days. Aliquots of the suspensions were regularly taken for solid-solution separation. Supernatants were prepared and used for chemical analysis of final aqueous U concentration.

2.3. Sample analyses

At the end of each experiment, the supernatant of the centrifuged sample was taken for EM measurements (Zetasizer Nano equipment Malvern, three measurements per sample) and an aliquot was also diluted with 2% HNO_3 prior to its analysis by ICP-MS to determine final aqueous concentration of uranium (cf. Guo et al., *submitted*). Each supernatant was also analyzed by ion chromatography to determine final concentration of phosphate ions (Eco IC, Metrohm, analytical uncertainties: 1–10%). Percentage (%) and amount (µmol. g^{-1}) of sorbates sorbed were calculated as follows:

$$\%\ sorbed = \frac{C_i - C_{eq}}{C_i} \times 100\ \%$$

$$Amount\ sorbed = (C_i - C_{eq}) \times \frac{V}{M}$$

$C_{init.}$ and C_{eq} are the aqueous concentration of sorbate (µmol.L^{-1}) in initial and final experimental solution, respectively, *V* the volume of solution (in L) and *M* the mass of solid sample (in g). Uncertainties on the percentage of sorption and surface coverage were estimated to be lower than 10% for both uranium and phosphate.

2.4. In-situ ATR FTIR spectroscopy experiments

Methods used and results obtained during ATR FTIR experiments of the sorption of 20-250 µM phosphate ions onto NaIdP are reported elsewhere (Guo et al.[200]), as well as for "blank" experiments designed to acquire reference data on IR vibrations of (Na)IdP structures or aqueous phosphate species. In the present study, experiments were performed to monitor by ATR FTIR spectroscopy the *in situ* evolution of the (Na)IdP - solution interface during (co)sorption of phosphate ions and uranyl ions. The (co)sorption processes were investigated for trace levels of U ($[U]_{I,aq}$: 2-10 µM). Complementary "blank" experiments were also designed to get reference data on IR vibrations of aqueous uranyl phosphate species and/or on possible U(VI)-phosphate precipitates formed directly from solutions. Each IR spectrum (an average of 2000 scans/spectrum, resolution of 4 cm^{-1}) was collected during 20 minutes.

2.4.1. Monitoring of the clay–solution interface along (co)sorption

The method used to cover the ATR crystal with a two-layers NaIdP–solution system was described in details elsewhere (Guo et al.[200]). Briefly, the method consisted in equilibrating a clay-solution system in a polyethylene tube gently shaken during 3 days (at pH 4 and $R_{S/L}$ = 3 g.L^{-1}), and introducing then the suspension in the ATR cell and letting the clay particles sediment onto the ZnSe crystal during 3 days. Sorption experiment was started after recording a reference baseline. Two experiments were performed to gain insights into the effects of two key parameters on the mechanisms and species involved: uranyl concentration and reaction

time, respectively. The first experiment was carried out to monitor changes in coordination environments of sorbed P along an increasing of [U]I,aq (2-10 µM) as follows. In a first step, 100 µM of aqueous P was added to a two-layers NaIdP–solution system prepared in the ATR cell (two successive additions of a small volume of a stock phosphate solution to reach a $[P]_{I,aq}$ value of 50 µM and, after twenty minutes, of 100 µM), and the FTIR interface spectra were recorded during 2 hours. In a second step, the concentration of U in the ATR cell was progressively increased by stepwise additions of small volumes of a stock solution of U to increase $[U]_{I,aq}$ by 2 µM per hour. After each addition, FTIR interface spectra were recorded. The second experiment aimed at monitoring the NaIdP-solution interface as a function of reaction time (t_R = 3 days) along the process of (co)sorption of phosphate ions and uranyl ions (simultaneous additions in the ATR cell of small volumes of the P stock solution and U stock solution to reach values of $[U]_{I,aq}$ of 8 µM and $[P]_{I,aq}$ of 100 µM, and recording of FTIR interface spectra during 3 days).

2.4.2. Blank ATR FTIR experiments

ATR FTIR spectroscopy analyses of solutions were made (in the absence of clay) in order: (i) to obtain IR spectra of reference for aqueous complexes formed between uranyl ions and phosphate ligands and/or to identify U(VI)-phosphate precipitates likely to form under certain conditions, and (ii) to determine detection limits for the U(VI) phosphato species / precipitates. Uranyl phosphate solution species were studied at pH 4, for a given aqueous phosphate concentration ($[P]_{I,aq}$ = 100 µM) and an increasing of $[U]_{I,aq}$ (from 2 to 8 µM) that were similar to those investigated in the first ATR FTIR sorption experiment (cf. paragraph 2.4.2). Desired volumes of stock solutions of P and U(VI) were added simultaneously to a 0.005 M NaCl electrolyte solution in the ATR cell and the IR spectra were recorded (t_R < 4 hours).

2.4.3. Analysis of the FTIR spectra

Analysis of the FTIR spectra recorded was focused on the mid-infrared region 900–1200 cm^{-1} which is characterized by the presence of the υ_3 P-O(M) antisymmetric stretching and / or υ_1 P-O(M) symmetric stretching (M: hydrogen or metal atom) vibration bands [15,146]. The OriginPro version 9.1 software was applied for baseline correction and decomposition of IR spectra to identify IR peaks (Gaussian lines and least-square fitting). Adjustable parameters (such as position, intensity, and width of bands) were kept free during spectra decomposition. Only in few spectra showing very low absorbance, the band position was adjusted. In previously published studies of phosphate sorption onto Fe- and Al- (hydro)oxides, band's number and position in the region 900–1200 cm^{-1} were widely used in consideration of phosphate molecular symmetry [15,16,146,201,202]. In addition, δ(P-OH) bending band may be present as a broad band at 1220–1240 cm^{-1} in IR spectra of aqueous species as $H_2PO_4^-$ and $H_3PO_4^0$ [189,201] and / or outer sphere phosphate surface species formed at mineral minerals. Previously published studies of uranyl coordination environments by using vibrational spectroscopy were mainly focused on the infrared-active U-O antisymmetric stretching band (υ_3) observable at 900–980 cm^{-1} and on the Raman-active U-O symmetric stretching band (υ_1) at 800–880 cm^{-1} [203,204]. For complexes of uranyl ions formed in solution or at mineral surface, the υ_3 of the uranyl unit was found to be in the range 890–954 cm^{-1} and the υ_1 in the range 834–870 cm^{-1} [11,204,205]. The υ_3 band of uranyl unit was expected to be not easily observable in IR spectra of NaIdP–solution systems, due to a high IR absorption of clays at ~950 cm^{-1} (e.g., [206]) and to our system cutoff at ~900 cm^{-1}.

2.4.4. Short overview of published IR data on uranyl and phosphate species

Phosphate ions. A short summary of the molecular symmetry analysis of PO_4 unit in phosphate ions is given here, based on previously published papers [15,16,145,146]. Aqueous phosphate speciation in 0.005 M NaCl electrolyte solution is dominated at pH > 12 by PO_4^{3-} ions, which

have a T_d molecular symmetry. These unprotonated phosphate ions have two IR-active IR bands corresponding to antisymmetric bending at 567 cm^{-1} (T_2, υ_4) and antisymmetric stretching at 1006 cm^{-1} (T_2, υ_3) [145]. The monoprotonated $HPO_4^{2-}{}_{(aq)}$ and triply protonated $H_3PO_{4(aq)}$ ions are main species at pH 8-12 and at pH < 2, respectively, and have a C_{3v} molecular symmetry. The former has three IR-active bands: two υ_3 bands at 1077 (E) and 989 cm^{-1} (A_1) and one υ_1 band at 850 cm^{-1} (A_1). The latter has two υ_3 at 1174 and 1006 cm^{-1} and one υ_1 at 890 cm^{-1} [15,16,146]. In the pH range 2-7, $H_2PO_4^-$ ions are predominant phosphate species and display a C_{2v} molecular symmetry. They have three υ_3 vibration bands at 1160 (A_1), 1074 (B_1), 940 (B_2) cm^{-1} and one υ_1 band at 874 cm^{-1} (A_1) [16,145]. The number and bands' position of IR-active bands υ_3 and υ_1 of aqueous phosphate ions are references to be used in the analysis of molecular symmetry of PO_4 unit in phosphate species sorbed at mineral–solution interfaces (e.g., Elzinga and Sparks [201]) or participating in aqueous complexes(e.g., Tejedor-Tejedor and Anderson [15]).

Uranyl ions. Two vibration bands characteristics of the UO_2 unit, i.e., the antisymmetric band υ_3 (IR active) and symmetric band υ_1 (Raman active), were widely used in molecular-scale studies of the coordination environment of UO_2 in aqueous solution or in solid state [143]. Free (hydrated) uranyl ion shows a υ_3 band at 962 cm^{-1} and a υ_1 band at 870 cm^{-1} [144]. Replacement of equatorial water molecules of uranyl ions during their complexation by ligands leads to a weakening of the $U{=}O_{ax}$ axial bonds, and consequently, bonds' lengths are increased and positions of υ_3 and υ_1 bands are decreased (i.e., υ_3 < 962 cm^{-1} and υ_1 < 870 cm^{-1}) [144]. The IR-active band (υ_3, 962cm^{-1}) was studied here in blank ATR FTIR experiments.

Uranyl-phosphate aqueous species and/or precipitates. To our best knowledge, few studies have been devoted to acquire IR spectra of aqueous uranyl phosphate complexes by using ATR FTIR spectroscopy. Nguyen Trun al [203] have investigated, by using Raman spectroscopy, aqueous uranyl complexes formed with different ligands such as F^-, Cl^-, Br^-, SO_4^{2-}, HSO_4^-, NO_3^-,

ClO_4^-, $CH_3CO_2^-$ and $C_2O_4^{2-}$. The authors studied shifts in υ_1 band of UO_2 (Raman active, symmetry stretching of U=O) when varying solution parameters like pH, ionic strength and ligand-to-uranyl ratios. Comarmond et al [134] have investigated aqueous uranyl phosphate species at pH 4 (at $[U]_{I,aq} = [P]_{I,aq} = 20$ µM). These authors have indicated that low solubility of U(VI)-phosphate aqueous complexes made it difficult to get vibrational data. Nevertheless, they could observe that the IR spectra of a freshly prepared uranyl phosphate solution was almost identical to that of a U(VI) phosphate precipitate (acquired after ultracentrifugation of an aged U-P-solution system). They identified IR bands at 1125, 994 and 919 cm^{-1} and suggested to attribute the latter to the υ_3 band of UO_2 and the formers to υ_3 bands of PO_4 units (having a C_{3v} molecular symmetry when coordinated to uranyl ions, likely in a monodentate complexation mode). Comarmond et al [134] have moreover identified by using TRLFS spectroscopy the precipitates formed from their studied solutions as being $(UO_2)_3(PO_4)_{2(s)}$. Čejka et al. [207] also observed similar IR spectral features for several U(VI) phosphates, for which the υ_3 bands of UO_2 unit and PO_4 unit were found at 880-920 cm^{-1} and at 995-1000 and 1115-1123 cm^{-1}, respectively (e.g., at 915, 1000 and 1120 cm^{-1} and 919, 995 and 1123 cm^{-1} for meta-autunite, $Ca(UO_2)_2(PO_4)_2 \cdot 6\text{-}8H_2O$, and sabugalite, $HAl(UO_2)_4(PO_4)_4$ $6\text{-}8H_2O$, respectively).

3. Results and discussion

3.1. Macroscopic sorption behavior of uranyl ions

3.1.1. Uranyl sorption edges and isotherms

Fig.III- 1. shows the effects of pH on macroscopic (co)sorption of U(VI) at two total concentrations ($[U]_{I,aq}$: 1 and 12 µM) and phosphate ions ($[P]_{I,aq}$=0 or 100 µM), and on particle EM in NaIdP - solution systems ($R_{S/L}$: 3 $g.L^{-1}$, electrolyte: 0.005 M NaCl). There were observed S-shaped uranyl sorption edges (**Fig.III- 1**a) whose values of pH_{50} (the pH at which the

percentage of U sorption is equal to 50%) are in the acidic pH domain. In the absence of P, a ten-fold increase in $[U]_{I,aq}$ induces a small shift in the pH_{50} value (from ca. 3.9 to 4.1 for $[U]_{I,aq}$ varying from 1 µM to 12 µM) and U(VI) uptake is almost complete in the pH range 6-8. This suggests that multiple sorption species and/or clay surface sites are involved in the uptake of U at pH < 5 and in the range of studied U surface coverage (< 3.8 µmol.g^{-1}, **Fig.III- 1**a). A limited change in the respective contributions of high and low affinity surface sites at clay edge platelets are likely. If considering a simple hypothesis, which is that each uranyl ion sorbed is bound to a single sorption site at the surface of clay, the calculated value of surface site occupancy by U is found to be very low (ca. 0.02 sites. nm^{-2}). This value is much lower than published values reported in literature, for example, for density of total sites at edges of Illite platelets (e.g., 2.31 sites.nm^{-2} given by Davis and Kent [30], 0.4 sites.nm^{-2} by Bradbury and Baeyens [116,208], or for density of low-affinity sites on clay basal planes (e.g., 13-16 sites. nm^{-2} given by Jeon and Nam [209]). However, Bradbury and Baeyens [116,208] considered in their modeling studies of the sorption of uranyl ions and other TME onto Illite du Puy that a small amount (ca. 0.01 sites.nm^{-2} or 2µmol.g^{-1}) of very high affinity sites were present at the clay platelet edges, whose total surface site capacity was higher (40µmol.g^{-1} for aluminol sites and 40µmol.g^{-1} for silanol sites). Based on the work by these authors, it is expected that a small amount of high affinity surface sites present at NaIdP particle edges can be involved in very strong interactions with sorbates, and can control the sorption of U(VI) at the lowest concentration of U studied (*i.e.*, at $[U]_{I,aq}$=1 µM and $R_{S/L}$ = 3 g.L^{-1}, **Fig.III- 1**a). A limited fraction of lower-affinity edge surface sites may contribute to U sorption at a ten-fold higher U concentration, which would be consistent with the decrease in the percent of U sorption observable when increasing $[U]_{I,aq}$ in experiment, at a given acidic pH (*i.e.*, at $[U]_{I,aq}$ = 12 µM, **Fig.III- 1**a). Complementary sorption isotherms acquired at pH 3, 3.5 and 4.1 in an extended U concentration range ($[U]_{I,aq}$: 1-25 µM) are given in Supplementary Information (Figs. B1-B2). There was observed a slight increase in

the percent of U sorption at the highest U concentrations investigated (at pH 4), as well as a non-linear increase in amount sorbed, which indicates the formation of additional uranyl sorption species at high U surface coverage, including possibly U(VI) (surface) precipitates. Results obtained on the effect of a decrease of $R_{S/L}$ (from 3 to 1g.L^{-1}) on the U(VI) sorption edges further confirm that a small amount of very high affinity sites is available for U sorption at NaIdP edges, as shown by Bradbury and Baeyens [116,208] (Figs. B3-S4 in Supplementary Information). At low concentration of U ($[U]_{I,aq}$=1μM), a decrease of $R_{S/L}$ had no or slight effects on U sorption edges and on values of clay surface coverage by U. High affinity surface sites may thus mainly be responsible for sorption of trace level of U at the clay edge platelets under these conditions. In contrast, a decrease of $R_{S/L}$ for a ten-fold concentration of U in experiments ($[U]_{I,aq}$=12μM) induced a significant shift in the position of the U sorption edge (from 4.1 to 4.8) and a non-linear increase in U surface coverages (at pH>5). Sorption of uranyl ions, at high U concentration and low $R_{S/L}$, may thus lead to a saturation of the high affinity sites and may involve multiple types of surface sites and/or uranyl sorption species.

3.1.2. Effect of uranyl sorption on electrophoretic mobility

EM measurements of NaIdP in suspension in 0.005 M NaCl (pH: 3-8, $R_{S/L}$: 3 g.L^{-1}) have been detailed in our previous study (Guo et al. [200]). The isoelectric point (IEP) of NaIdP, *i.e.*, the pH at which EM and surface potential are equal to zero, was found to be at a low value (pH_{IEP}~3). EM was shown to further diminish with pH due to deprotonation of amphoteric hydroxyl (silanol, aluminol or ferrinol) surface sites. Results obtained herein on the effect of U(VI) sorption (and co-sorption of uranyl and phosphate ions) on EM values are given in **Fig.III- 1**c, where they are compared to EM values acquired previously in the absence of phosphate and / or uranyl ions. There was observed that sorption of 1-12 μM of uranyl ions at acidic pH values has no significant effect on EM values, within our experimental uncertainties. An effect is visible at near-neutral pH (~7) where the quantitative sorption of U induces an increase of EM

(for $[U]_{I,aq}$ = 12 µM), which suggests the formation of U sorption species imparting positive charges to the clay surface.

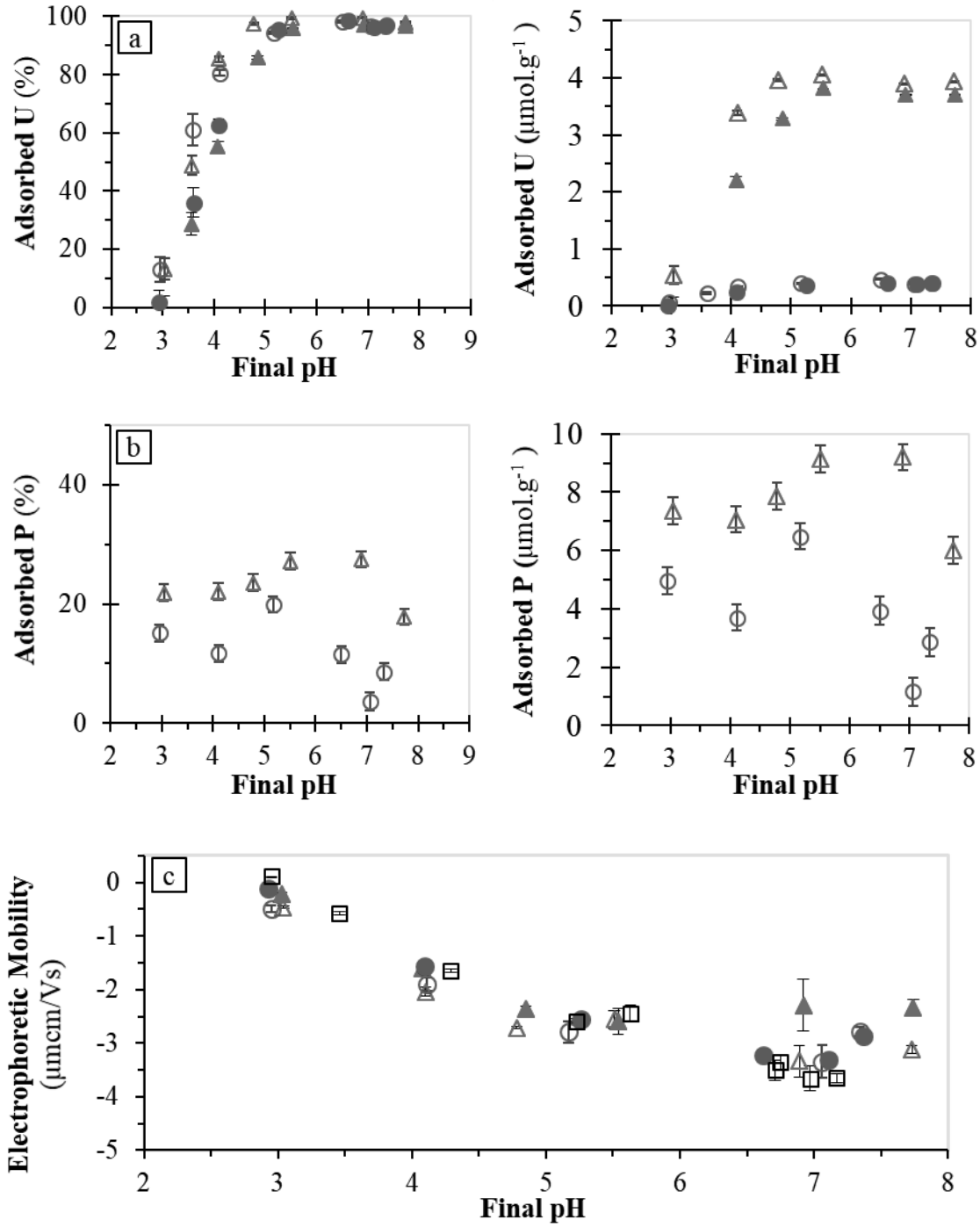

Fig.III- 1. Sorption of uranyl ions (a) and phosphate ions (b), and on electrophoretic mobility (c), as a function of final pH for 3 $g.L^{-1}$ NaIdP contacted (t_R= 4 days) with 0.005 M NaCl electrolyte solutions at different total concentrations of U(VI) ($[U]_{I,aq}$ = 0, 1 or 12 µM), in the absence and in the presence of phosphate ions ($[P]_{I,aq}$ = 0 or 100 µM). NaIdP-electrolyte systems

were pre-equilibrated (t_{pre-eq} = 3days) prior to sorbate addition. EM data of blank experiments (without U and P - × plot) are taken from Guo et al. [200] (○: $[U]_{I,aq}$ = 1µM and $[P]_{I,aq}$ = 100 µM - △: $[U]_{I,aq}$ = 12 µM and $[P]_{I,aq}$ = 100 µM - ▲,● without P - □: Blank).

3.1.3. Effect of phosphate ligand on the macroscopic sorption of U

Fig.III- 1a shows that the presence of phosphate ions ($[P]_{I,aq}$ = 100 µM) led to a significant shift of the U(VI) sorption edges towards lower pH values, for the U concentrations studied ($[U]_{I,aq}$=1 and 12 µM). At acidic pH, significant increases in surface coverages of the clay by U were observed, too (1-2 and 3-4 µmol $U.g^{-1}$ at pH 3-4 and 4-5, respectively, at $[U]_{I,aq}$ = 12 µM). Hence, at acidic pH, the presence of P promotes the sorption of U(VI) onto NaIdP. There was also observed an increase of the percentage of phosphate sorbed with an increase of U concentration in experiment, in the pH range investigated (**Fig.III- 1**b and Fig. B5 in Supplementary Information). Clay surface coverage by P was increased, too (of ca. 2 and 6 µmol $P.g^{-1}$ at acidic and near-neutral pH, respectively). Thus, the increase in U sorption observed upon addition of phosphate ligands in the NaIdP-solution systems was likely due to the formation of (multiple) ternary uranyl phosphate surface complexes and/or U(VI) phosphate surface precipitates. **Fig.III- 1**c indicates that the presence of phosphate ligands slightly decreased the EM values of the clay particles in the pH range studied, *i.e.*, it conferred negative charges on the mineral surfaces, suggesting the involvement of phosphate anions in the surface complexes formed. Furthermore, based on the values published by Bradbury and Baeyens for the surface sites of the conditioned Illite du Puy (about 2 µmol.g^{-1} or 0.01 sites.nm^{-2}), we can hypothesize that uranyl phosphate surface complexes formed on NaIdP involve high-affinity and low-affinity hydroxyl (amphoteric) sites present on the clay rim platelets, in the case of experiments performed $[U]_{I,aq}$ and $[P]_{I,aq}$ values. Complementary U sorption isotherms acquired for a wide range of U concentrations (Figs. B1 and B2, Supplementary Information) show, that at acidic pH, the promotion of uranyl ion sorption upon addition of phosphate ions is higher at

high U concentrations ($[U]_{I,aq} \geq 12$ µM) than at the lowest concentration studied, suggesting that multiple uranyl phosphate species are successively formed in NaIdP-phosphate-solution systems when $[U]_{I,aq}$ increases. Since limited formation of uranyl phosphate colloidal phases was observed in the absence of NaIdP (5-10% of total U, for $[U]_{I,aq}$=1-10 µM and $[P]_{I,aq}$=100 µM, see Fig. B7 in Supplementary Information), the contribution of a U(VI) phosphate precipitation mechanism from supersaturated solutions cannot be excluded to explain the increased retention of U observed in NaIdP - phosphate - solution systems at the highest value of $[U]_{I,aq}$ studied (25 µM).

3.1.4. Reversibility of the sorption of U in the presence of phosphate ligands

The results of the desorption experiments of uranyl ions ($[U]_{I,aq}$ = 12 µM) previously sorbed at pH values of ~4 and ~5, respectively, and in the presence of phosphate ligands ($[P]_{I,aq}$ = 100 µM), are presented in **Fig.III- 2**. There was observed a sharp decrease of the percentage of U sorption when bringing the experimental pH from its initial value to a value of 3.2. There was found that the U(VI) desorption is fast and almost complete within a few hours. Actually, the percentage of total U retained at pH 3 onto clay surface after a few-hours desorption was found to be around 20% (which is slightly higher than the percentage of U sorption at pH 3 under similar conditions of U and P concentrations, see **Fig.III- 1**a). These features provide evidence that the U-P co-sorption process is mostly reversible under the conditions investigated, and that the uranyl phosphate surface species formed onto NaIdP at acidic pH are most likely U-P surface complexes, at low concentrations of U (≤ 10 µM).

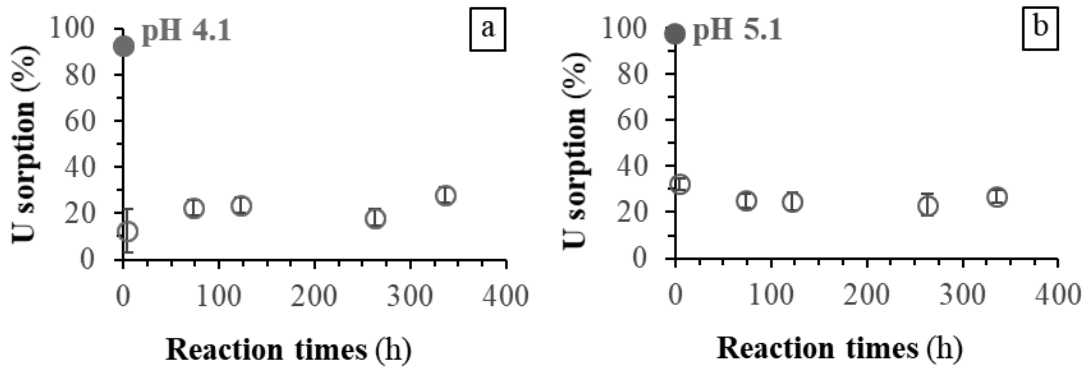

Fig.III- 2. Results on the kinetics of desorption of U(VI) previously sorbed in the presence of phosphate ions onto NaIdP at (a) a pH of 5.1 and (b) a pH of 4.1 (full circles), after a decrease of experimental pH to a value of 3.2 (empty circles). Conditions: $[P]_{I,aq}$ = 100µM, $[U]_{I,aq}$=12.5µM, $R_{S/L}$ = 3g.L^{-1}, 0.005M NaCl electrolyte solution.

3.2. In situ ATR FTIR study of uranyl-phosphate surface species

3.2.1. Reference IR spectra of uranyl phosphato solution species

Aqueous speciation of U(VI) in the presence of phosphate ligands ($[U]_{I,aq}$ = 2 µM and 10 µM; $[P]_{I,aq}$ = 100 µM), calculated by using the Visual MINTEQ code and data bases, are reported in Supplementary Information (Figs. B8-S9 and Table B1). In the pH range 4-8, the major aqueous species are: UO_2^{2+} (pH<4), $UO_2HPO_{4(aq)}$ (4<pH <6), $UO_2PO_4^-$ (6<pH<7) and $(UO_2)_2CO_3(OH)_3^-$ (7<pH<8). **Fig.III- 3**a reports ATR FTIR spectra (in wavenumber region 900-1200cm^{-1}) collected during 3 hours for uranyl phosphate solutions at pH 4 ($[U]_{I,aq}$ = 8 µM, $[P]_{I,aq}$ = 100 µM). The spectra show the appearance of IR absorption bands whose intensities were increasing during the first two hours. Three bands were observable, with the most intense one being positioned at 996 cm^{-1} and the others at 1122 and 924 cm^{-1}. It is to note that the absorbance of these bands is at least two orders of magnitude higher than that of vibrational bands recorded for the aqueous phosphate species $H_2PO_4^-$ (pH 4, $[P]_{I,aq}$: 100 µM, no U added, 0.005 M NaCl electrolyte solution). FTIR spectra of aqueous uranyl phosphate complexes and/or precipitate(s) forming at pH 4 and at a higher concentration of U ($[U]_{I,aq}$ = 8 µM) are shown in the **Fig.III-**

3b. There was observed an increase in intensity of IR absorption bands during the first 2 hours. In addition to the three above-mentioned IR bands (at 996, 1122 and 924 cm^{-1}), two other weak vibrational bands were observable. Weak intensities of these bands made it difficult to determine precisely the position of their maxima (at ca. 1055 and 1170 cm^{-1}, respectively). These bands could possibly be ascribed to an aqueous U-P species whose υ_3(P-O) bands are shifted compared to those reported (at 1160 and 1075 cm^{-1}) for the diprotonated phosphate ion ($H_2PO_4^-$, C_{2v}), which is the dominant aqueous phosphate species at pH 4. Maxima positions and relative intensities of the main bands (at 996 cm^{-1}, 1122 and 924 cm^{-1}) are consistent with previously published IR data by Čejka et al. [207] and Comarmond et al. [134] for uranyl phosphate complexes and/or of U(VI) phosphate minerals, which display almost similar IR features (cf. §2.4.4). Formation of a U(VI)-phosphate phase is in agreement with calculations indicating that solution used in experiment (at $[U]_{I,aq}$ = 8 µM and $[P]_{I,aq}$ = 100 µM) was highly over-saturated with regard to a U(VI) phosphate mineral, namely $(UO_2)_3(PO_4)_{2(s)}$, and slightly oversaturated with respect to Na-autunite (Supporting Information, Table B2). Moreover, batch experiments conducted in the absence of clay indicated the formation of uranyl phosphate colloids (Supplementary Information, Fig. B7) at pH 4, which would represent ca. 5% of total U. Concerning IR spectra of aqueous uranyl ions in the absence of phosphate, no absorption bands were observable for $[U]_{I,aq}$ < 10 µM (data not shown).

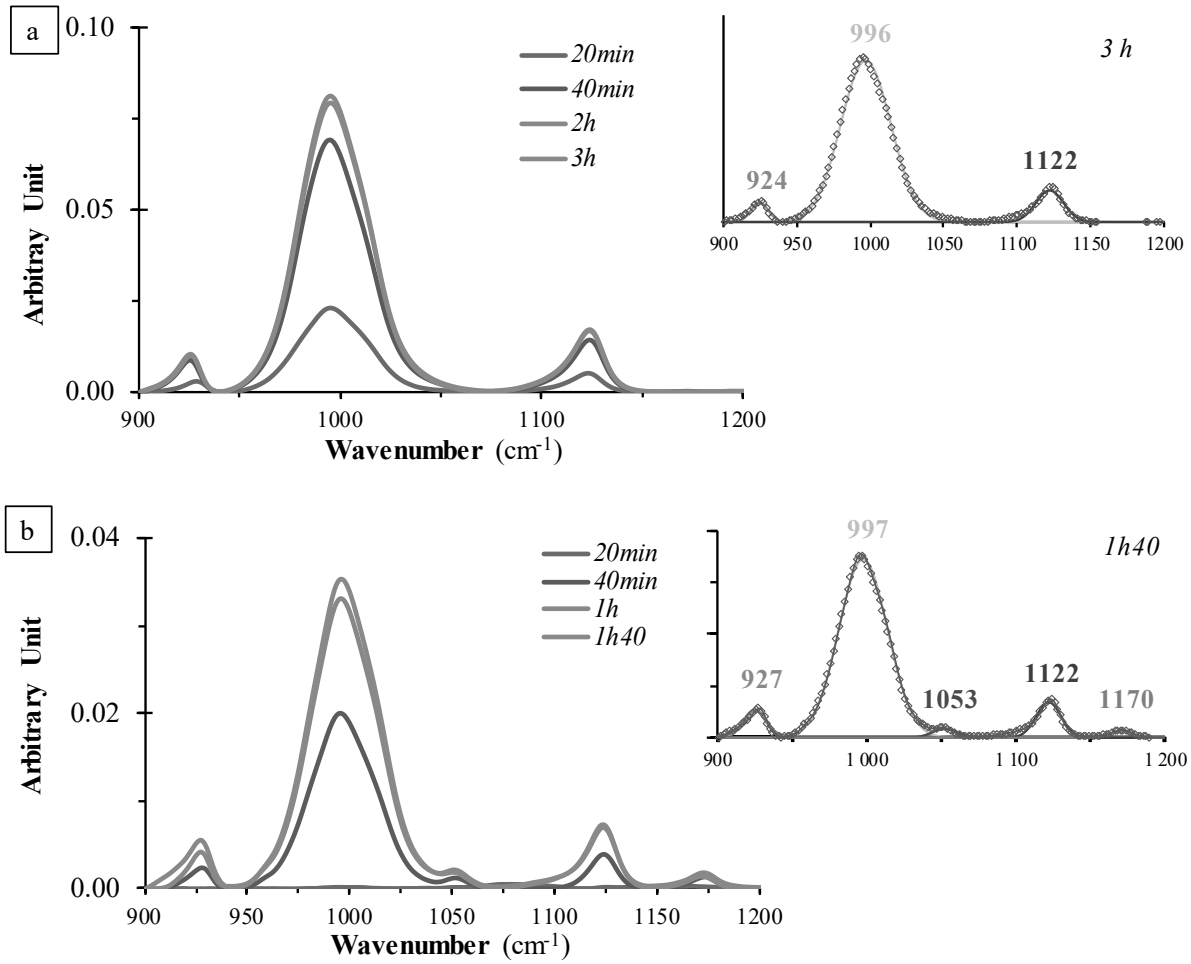

Fig.III- 3. ATR FTIR spectra of uranyl—phosphate solution species at different reaction time (t_R) in a 0.005 M NaCl electrolyte solution at pH 4, at $[P]_{I,aq}$ = 100 µM and (a) $[U]_{I,aq}$ = 2 µM or (b) $[U]_{I,aq}$ = 8 µM (inserted : decomposition of IR spectra).

3.2.2. *In situ* ATR FTIR experiments of (co)sorption of uranyl and phosphate ions

Effects of uranyl concentration. The NaIdP-phosphate-solution interface was monitored along an increase of total concentration of U(VI) (from 0 to 8 µM). After two successive additions of 50µM of phosphate ions in the two - layers NaIdP - solution system in the ATR cell, spectral data were recorded during a short reaction time of 2 hours (spectra 1 and 2, **Fig.III- 4**a). There was observed a well-defined band with a peak maximum at 1075 cm^{-1} and a broad band between 1100 and 1250 cm^{-1}, whose intensity increased with time. Based on spectra decomposition

shown in **Fig.III- 4**b, five IR absorption bands' maxima were identified (at 1037, 1075, 1132, 1157 and 1215 cm^{-1}). These data were consistent with our previous study on ATR FTIR experiments of sorption of phosphate ions onto NaIdP at acidic pH (Guo et al.[200]). Briefly, these bands were attributed to formation of an outer sphere surface complex (OSSC) of phosphate formed at low reaction time and/or low phosphate concentration, with bands at positions similar to those of aqueous $H_2PO_4^-$ species (species referred to as "P-species A", with IR bands at 1075, 1157 and 1215 cm^{-1}). This OSSC was found to convert into inner-sphere surface complexes (ISSC) of phosphate forming at high affinity sites present of clay edge platelets (a main surface complex referred to "P-species B" having υ_3 P-O bands at 1003, 1035 cm^{-1}, and another one with a υ_3 P-O band at 1132 cm^{-1},). The P-species B were shown to dominate the surface speciation of phosphate at high values of $[P]_{I,aq}$ and t_R in the absence of U(VI). The IR interface spectra recorded herein during a stepwise increase of uranyl ion concentration (by 2 µM per hour,) in a NaIdP-phosphate-solution system are given in **Fig.III-4**a (spectra 3 to 7, duration of experiment: 7 h). With first addition of U (t_R = 2 h), there was observed the appearance of a shoulder (with a maxima at 1050 cm^{-1}) on the left-hand side of the band at 1075 cm^{-1} and the disappearance of the bands of P-species B (at 1037 and 1132 cm^{-1}). Such a disappearance of ISSC of phosphate provides strong evidence of a change in the coordination environment of sorbed PO_4 units upon addition of U. Intensity of the band at ca. 1050 cm^{-1} increased with an increase of U(VI) concentration, although the absorbance remained quite low and spectra rather noisy -which made it difficult to decompose the IR signals and increased uncertainties on bands position-. Nevertheless, the existence and the growth of the IR band at ca. 1050 cm^{-1} evidenced the formation of uranyl-phosphate surface species onto Illite surface. This band was actually not observed on IR interface spectra recorded in NaIdP – phosphate - solution systems, neither at short reaction times (spectra 1-2 in **Fig.III- 4**a) or at long reaction times (Guo et al.[200]). This band cannot be attributed to a change in the

configuration of surface hydroxyl groups during sorption of uranyl ions, either, because it was not detected on the IR interface spectra recorded during "blank" experiments of U(VI) sorption onto NaIdP (at $[P]_{I,aq} = 0$, data not shown). Spectra decomposition results (**Fig.III- 4**b) show a small band centered at ~1126 cm^{-1}, too, which could be also assigned to the υ_3 P-O vibration mode and whose weak absorbance was independent of uranyl concentration. Possibly, this band corresponds to a uranyl phosphate surface species ("U-P species A") formed in limited amount and at low U concentration. In contrast, the bands at 1075 and 1157 cm^{-1} of P-species A showed a small decrease in intensity with increasing $[U]_{I,aq}$, concomitantly to the increase of the band at 1050 cm^{-1}. These results provide evidence of increasing formation with $[U]_{I,aq}$ of a uranyl phosphate surface species that has a main IR band at 1050 cm^{-1} (referred to as "U-P species B"). In summary, the IR data recorded during (co)sorption of U and P at the NaIdP–solution interface, as a function of uranyl ion concentration and for a short reaction time (t_R <7h), show : (1) the fast formation of an OSSC of phosphate (P-species A having IR bands at 1075 and 1160 cm^{-1}) before U addition and of an ISSC of phosphate (P-species B having IR bands at 1075 and 1160 cm^{-1}), (2) the fast formation of a uranyl phosphato surface species formed in limited amounts (U-P species A with a band at 1125 cm^{-1}) and of another uranyl phosphato surface species (U-P species B displaying a band at 1050 cm^{-1}), which occurs concomitantly to the disappearance of P-species B (at t_R < 3h), and, (3) the growth of U-P species B with an increasing of U concentration.

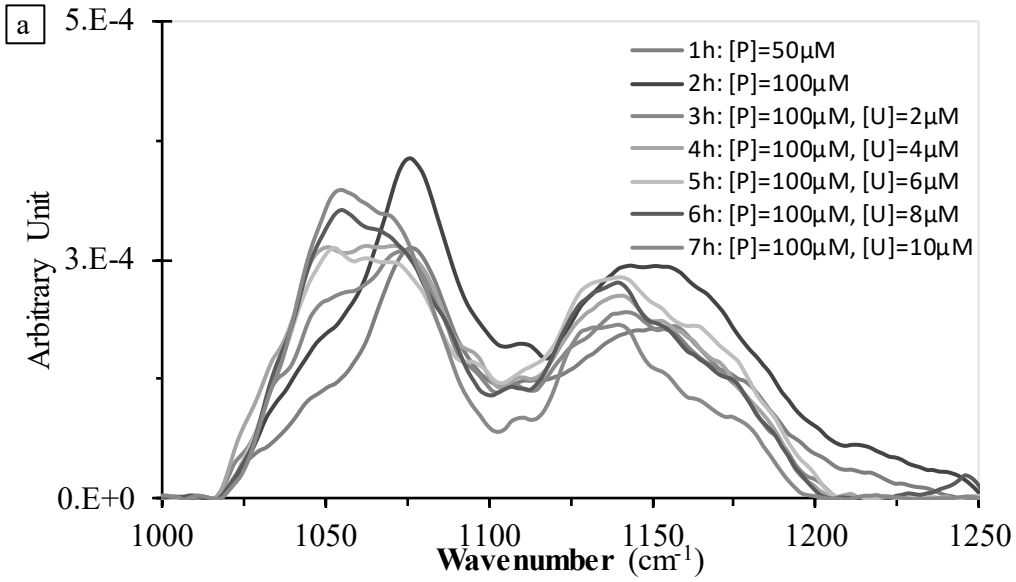
a
5.E-4
3.E-4
0.E+0
Arbitrary Unit
1h: [P]=50µM
2h: [P]=100µM
3h: [P]=100µM, [U]=2µM
4h: [P]=100µM, [U]=4µM
5h: [P]=100µM, [U]=6µM
6h: [P]=100µM, [U]=8µM
7h: [P]=100µM, [U]=10µM
1000
1050
1100
1150
1200
1250
Wavenumber (cm-1)

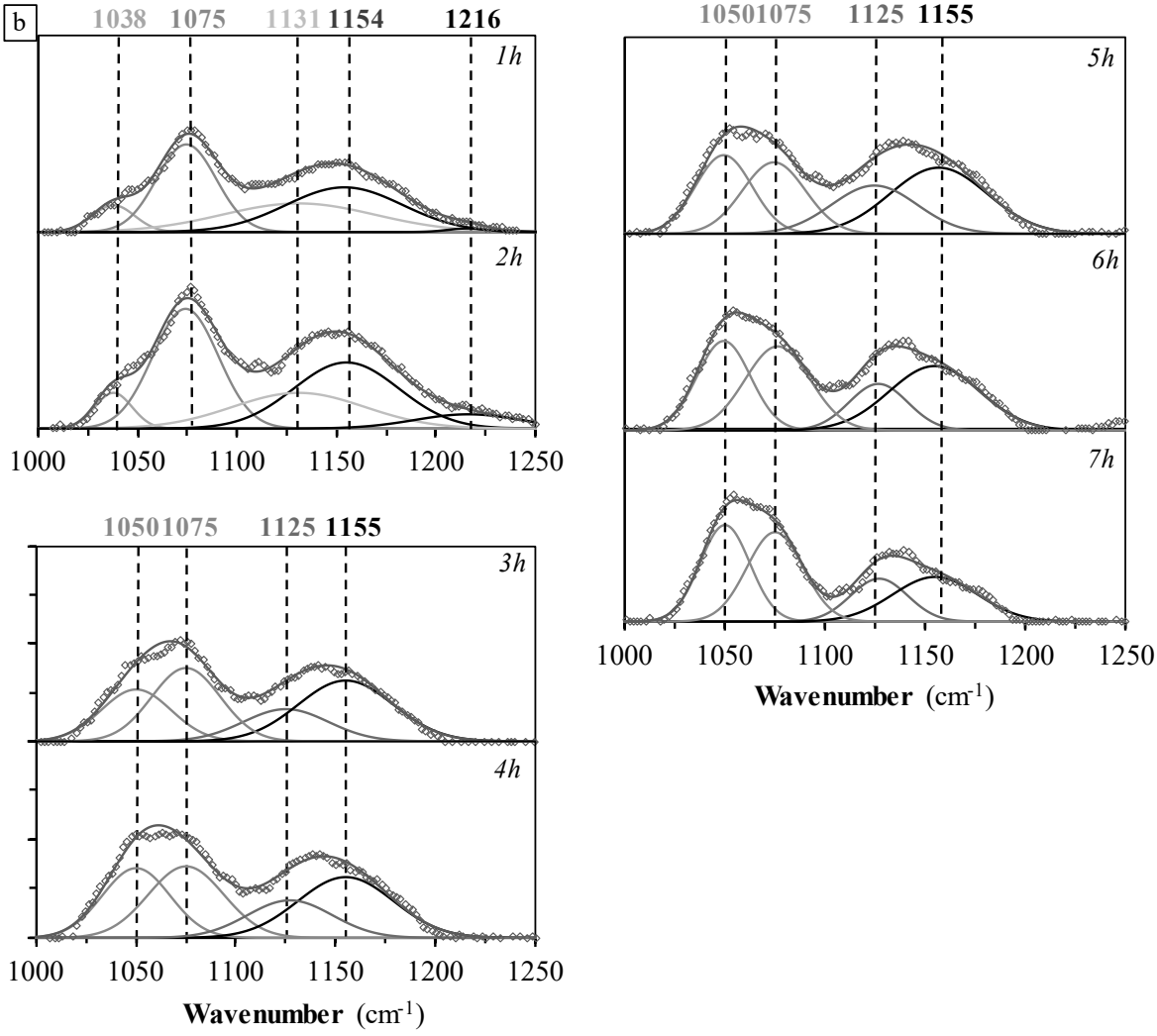
b
1038 1075 1131 1154 1216
1h
2h
3h
4h
10501075 1125 1155
5h
6h
7h
1000
1050
1100
1150
1200
1250
Wavenumber (cm-1)

Fig.III- 4. Results of in situ ATR-FTIR experiments of the (co)sorption of phosphate and uranyl ions at NaIdP–solution interface with increasing U(VI) concentration (conditions: pH 4, $[U]_{I,aq}$ in the range 0–10µM, $[P]_{I,aq}$=50-100 µM, , $R_{S/L}$ =3g.L^{-1}, t_R=1-7h, 0.005M NaCl electrolyte): (a) FTIR interface spectra and (b) spectra decomposition. See main text and paragraph 2.4.3 for experimental procedure.

Effect of reaction time (t_R). I*n situ* ATR FTIR monitoring as a function of time (t_R = 3 days) of the (co)sorption of uranyl and phosphate ions added simultaneously in NaIdP–solution system is illustrated in **Fig.III- 5**. A broad band with a low absorbance was observable in the range of wavenumbers 1025 – 1125 cm^{-1} for spectra recorded within a reaction time of 20 hours. The small band at 1123 cm^{-1} of "U-P species A" was observable only in the very short term. After a t_R of 20 hours, there was observed a broad band exhibiting two maxima and extending throughout the region of wavenumbers 950-1125cm^{-1}, with its absorbance increasing with time until stabilization at t_R = 3 days (**Fig.III- 5**a). For t_R < 20 hours, spectra were decomposed in five bands of weak absorbance and divided in two sets with maxima positions at 1075 and 1160 cm^{-1}, and 1053, 1081, 1114 cm^{-1}, respectively (**Fig.III- 5**b). All these bands can be assigned to υ_3 (P-O) vibration bands, based on the comparison with IR spectra of aqueous phosphate species [16,201]. As described previously, the former set of bands is assigned to an OSSC of phosphate (P-species A) and / or to $H_2PO_4^-$ species in solution, because the bands' position of these two types of phosphate species are expected to be similar. These bands displayed a decrease in intensity with t_R and were not observable anymore at t_R > 7 hours, while the other bands (at 1053 and 1081 cm^{-1} and the small one at 1114 cm^{-1}) showed an increase in intensity with t_R. Band at ~1055 cm^{-1} remained constant after 7 h and it was assigned to the U-P species B: as shown in the previous experiment, its appearance coincided with the introduction of uranyl ions in the NaIdP – phosphate - solution system and its intensity was growing with U concentration (but stabilized after one day). The well-defined band at 992 cm^{-}

[1] in **Fig.III- 5**was observable at t_R > 20 hours and its intensity increased concomitantly with that of the band at 1081 cm^{-1} along the sorption process, i.e., up to t_R~3 days. These two bands, and the small band at 1114 cm^{-1}, are tentatively gathered and attributed to P-O vibrations of a single uranyl phosphate surface species formed at a long reaction time (referred to as "U-P species C"), due to their similar evolution during sorption. In summary, the IR data recorded during (co)sorption of uranyl and phosphate ions at the NaIdP–solution interface as a function of time (3 days) show : (1) the presence at a short reaction time of an OSSC phosphate species that disappears rapidly (t_R < 5h) (P-species A with IR bands at 1075 and 1160 cm^{-1}), (2) the formation at a short reaction time of a uranyl phosphato surface species formed in limited amounts (the U-P species A with a band at 1125 cm^{-1}), (3) the formation of a uranyl phosphate surface species (U-P species B with a main band at 1052 cm^{-1}) whose growth stabilizes after t_R = 1 day, (3) the late appearance (at t_R = 1 day) and growth with time of an uranyl phosphate surface species that becomes dominant at t_R = 3 days (U-P species C with IR bands at 992, 1081 and 1114 cm^{-1}).

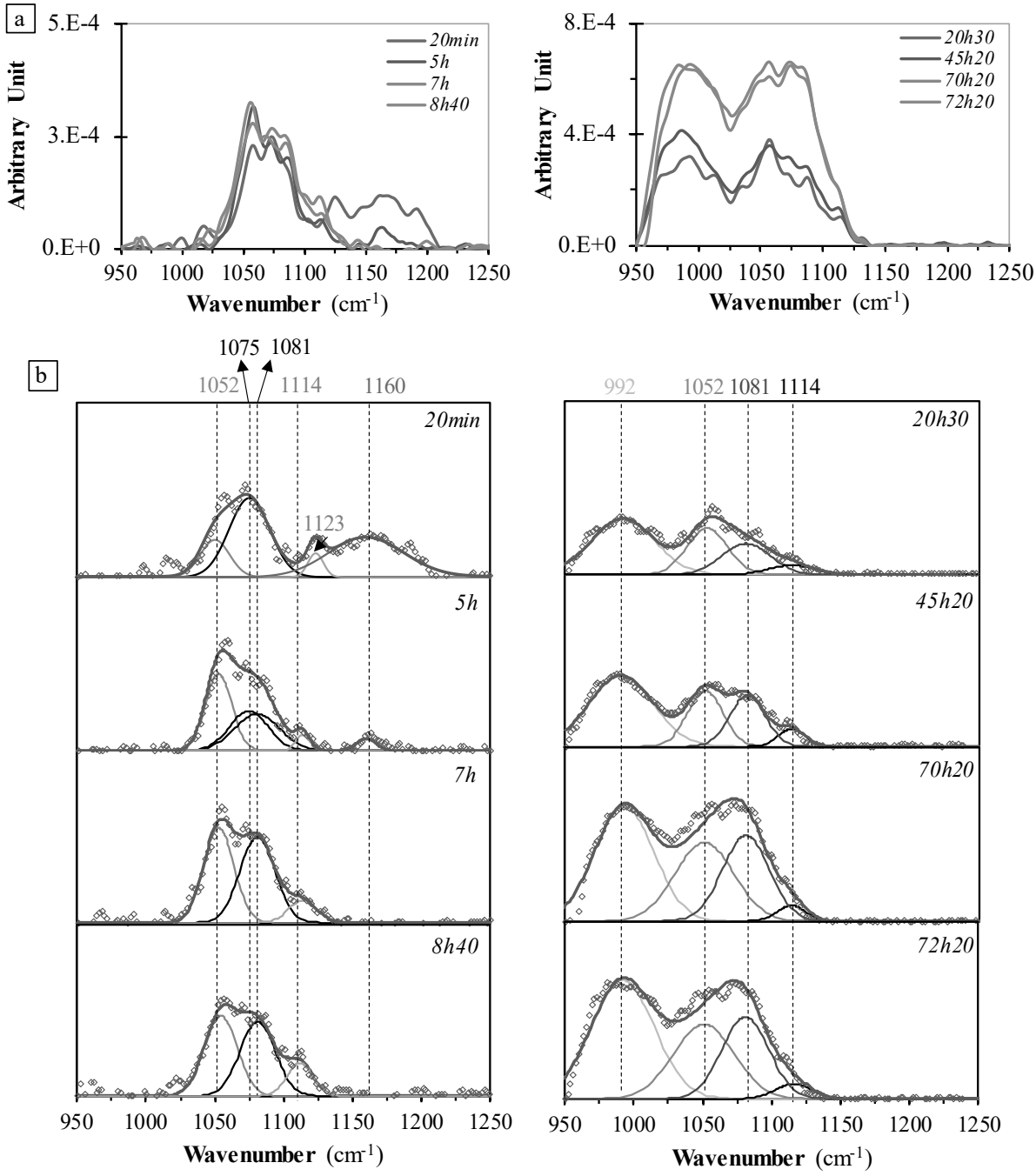

Fig.III- 5. Results of in situ ATR FTIR experiments of the (co)sorption of phosphate and uranyl ions at NaIdP–solution interface with increasing reaction time (conditions: pH 4, $[U]_{I,aq}$ = 8 µM, $[P]_{I,aq}$ = 100 µM, , $R_{S/L}$ = 3 g.L^{-1}, 0.005 M NaCl electrolyte): (a) FTIR interface spectra (8 points- Savistzky-Golay algoritm smoothed) and (b) spectra decomposition. See main text and paragraph 2.4.3 for experimental procedure.

4. Discussion and conclusions

4.1. Aqueous uranyl phosphate speciation

FTIR bands characteristics were reported in the present study for aqueous uranyl phosphate species formed at pH 4, at low (VI) concentrations and in the presence of phosphate ligands ($[U]_{I,aq}$: 2µM and 10µM, $[P]_{I,aq}$: 100µM), which were calculated to be predominantly in the form of $UO_2HPO_{4(aq)}$ species by using the MINTEQ code and database. The strong band at 996cm^{-1} and two small bands at 924 and 1122 cm^{-1} observable on the FTIR spectra are consistent with those reported by Comarmond et al. [134] for U-P solution species (formed at pH 4 and at values of $[U]_{I,aq}$ and $[P]_{I,aq}$ of 20 µM). These authors suggested the formation in their experiments of an aqueous uranyl phosphate complex, with a monodentate complexation mode between uranyl and phosphate ions based on the evidence of a C_{3v} molecular symmetry of PO_4 unit (two υ_3 P-O) and on band positions (at 1122 and 996 cm^{-1}). However, the high (baseline corrected) IR absorbance that we observed in our study suggested the precipitation of a U(VI)-phosphate phase (as the IR absorbance is at least two orders of magnitude larger than that of the uranyl phosphate surface species formed onto NaIdP, under similar conditions). Hence, experimental solutions studied (in the absence of NaIdP) might be instable and (pseudo)colloids of uranyl phosphates formed directly from the solutions might undergo a sedimentation onto the ATR FTIR crystal. This hypothesis is consistent with batch experiments results indicating formation of small amounts (ca. 5% of total U) of uranyl phosphate colloidal phases at pH 4, in the absence of NaIdP. It is also in agreement with calculations of saturation indexes of our experimental solutions containing uranyl (10µM) and phosphate ions (100µM), which indicated that an over-saturation with respect to a U(VI) phosphate mineral, namely $(UO_2)_3(PO_4)_{2(s)}$, and slight oversaturation with respect to Na-autunite. Former mineral phase was identified by Comarmond et al. [134] to form in their experiments. The IR bands identified in the present study show similar positions of υ_3 P-O bands at 1122 and 993 cm^{-1} and of υ_3 U=O

band at 940cm^{-1} than those reported in the literature for $(UO_2)_3(PO_4)_2 \cdot 4H_2O_{(s)}$ (Pekárek et al. [210]). However, the contribution of an aqueous uranyl phosphate complex to the IR spectra of our U-P solutions cannot be excluded. Actually, almost identical IR spectral features were reported by Comarmond et al. [134] for an aqueous uranyl phosphate species and U(VI) phosphate precipitates forming at acidic pH. According to these authors, binding between U(VI) and PO_4 unit of phosphate ions may occur in a monodentate mode for the aqueous uranyl phosphate complex formed in their experiments, which corresponds to a C_{3v} molecular symmetry. The main aqueous uranyl phosphate species expected in our experimental solutions at pH 4 is $UO_2HPO_{4(aq)}$, in which the molecular symmetry of PO_4 unit is C_1 (with three υ_3 P-O bands observable in IR spectra). Only two υ_3 bands were however observed in the IR spectra of the U-P solutions studied. DFT calculations carried out for different modes of uranyl-phosphate complexation have been reported in the literature by Jackson et al. [34]. These authors have indicated that hydrated UO_2HPO_4 species containing 4 structural water molecules (e.g., $UO_2HPO_4\ (H_2O)_4$) have a υ_3 band of U=O at 940cm^{-1}, which is close to the value reported by Comarmond et al. [134] and in the present work. Interestingly, the DFT calculation carried out by Jackson et al. [34] for a cluster of $UO_2HPO_4\ (H_2O)_4$ has shown the transfer of a proton from water equatorially-coordinated to the uranyl ion to an oxygen atom of the phosphate ion. This proton transfer was reported to lead to a diprotonated phosphate ion, i.e., $UO_2H_2PO_4(H_2O)_3OH$, with the PO_4 unit having a C_{3v} molecular symmetry. Based on the above discussion, it is likely that an aqueous uranyl phosphate complex with a molecular structure like $UO_2HPO_4(H_2O)_4$ (having an equivalent structure as $UO_2H_2PO_4(H_2O)_3OH$) contributed to IR signals of the U-P solutions studied here. There was also observed on our IR spectra two large υ_3 P-O bands at 1055 and 1170cm^{-1}. These bands may be attributed to formation of an additional aqueous uranyl phosphate complex, -as it was reported that solid phases have rather small band's width [134,146]-. Such additional complex possibly has a C_{2v}-like symmetry (as its υ_3 bands at 1052

and 1170cm^{-1} may result from a shift of the υ_3 bands at 1075 and 1160 cm^{-1} of $H_2PO_4^-$ aqueous species). A third υ_3 band of small intensity would be expected at a low wavenumber (around 940 cm^{-1}) but the strong band observable at 997 cm^{-1} in our IR spectra may overlap with it. The additional species is possibly $UO_2H_2PO_4^{+}{}_{(aq)}$ which is expected to exist as a minor uranyl phosphate aqueous species according to speciation calculations. If this species has a C_{2v}-like symmetry, the phosphate ion should be coordinated to the uranyl ion in a bidentate mode and the hydrated form of $UO_2H_2PO_4^+$ may be $UO_2H_2PO_4^+ \cdot 3H_2O$. Further spectroscopy studies using complementary techniques like TRLFS and EXAFS may be helpful to confirm this hypothesis.

4.2. Surface speciation of uranyl ions at the NaIdP-solution interface

A recent study carried out by Stockmann et al. [129] has shown the presence of two υ_3 U=O bands at 910 and 900 cm^{-1} on ATR FTIR spectra acquired during the sorption of uranyl ions (at $[U]_{I,aq}$: 20 µM) at near-neutral pH (6.8) onto montmorillonite. These authors have suggested that the strong sorption of aqueous $UO_2(OH)_2$ ions onto the clay surface had led to a shift in the wavenumber of υ_3 U=O band of more than 10 cm^{-1}. In the present study, the υ_3 IR bands of uranyl ions (< 960 cm^{-1}) could not be studied. However, our U(VI) macroscopic sorption results indicated that several sorption mechanisms / species can contribute to the uptake of uranyl ions by NaIdP, depending on key parameters such as pH, U concentration and clay-to-solution ratio. Data presented here show a decrease in the percent sorption of U, at a given acidic pH, when increasing U concentration in a certain range (1-10µM) or when decreasing the clay-to-solution ratio (from 3 to 1 g.L^{-1}). These trends strongly suggest that a very low amount of high affinity sorption sites (< 0.02 sites. nm^{-2}) at NaIdP edge platelets, which interact strongly with U, become progressively saturated while low affinity surface sites are increasingly involved on the U sorption, under above mentioned conditions. It has long been reported that TOT clay minerals display different types of surface sites having distinct concentrations and affinity towards H^+

and other aqueous ions [211], including silanol, aluminol and ferrinol sites at clay edges. Bradbury and Baeyens [116,208] have provided modelling of the sorption of trace metals and actinides onto Na-Illite by using a non-electrostatic model, which included two-sites protolysis non-electrostatic surface complexation and cation exchange. These authors could fit successfully the macroscopic data on the sorption of uranyl ions (at a concentration of ~0.1µM) by considering a mechanism of cation exchange implying UO_2^{2+} in clay interlayer space (and dominating in the pH range 2.5-3.5) and the strong sorption of U by formation of uranyl surface complexes of the types $\equiv SO^sUO_2^+$, $\equiv SO^sUO_2OH$ and $\equiv SO^sUO_2OH_2^-$ that involve high affinity sites (noted $\equiv SO^s$) present in low amounts (ca. 0.01 sites. nm^{-2}) at clay edges. Several EXAFS analyses have moreover provided evidence that uranyl ions are sorbed, at low pH, as exchangeable UO_2^{2+} in the interlayer space of smectitic clays, and at moderately acidic pH, as additional inner-sphere uranyl surface complex and / or U(VI) polynuclear surface species, depending on surface coverage [90,125–127]. Uranyl carbonato inner sphere surface complex were also shown to form at edge sites of smectite platelets when increasing pH[128]. Based on spectroscopic results, Troyer et al. [136] could fit their sorption isotherms of uranyl ions (in the range 1-10µM) on montmorillonite by using in surface complexation modeling three types of species, namely, cation-exchanged UO_2^{2+} (noted UO_2X_2), a cationic surface complex ($\equiv SOUO_2^+$) and a ternary uranyl carbonate surface complex ($\equiv SOUO_2CO_3^-$), which dominated at pH 4, 6 and 8, respectively. Our results are consistent with those reported in the above-mentioned modeling or spectroscopic studies. They suggest a variable contribution of both high affinity and low affinity surface sites to the sorption of uranyl ions onto NaIdP edges, at acidic pH, via formation of inner sphere surface complexes of U(VI), in most of the conditions investigated. Unlike for the montmorillonite studied by Troyer et al. [136], the relative contribution of cation-exchanged UO_2^{2+} is not observable for NaIdP, due to the difference in permanent structural charge between these two types of clay. As no significant effect of U(VI)

sorption on EM is observable at pH < 5 in our experiments, even at the highest U concentrations investigated, it is possible that the sorption mechanisms of U(VI) onto NaIdP included the deprotonation of the protonated hydroxyl sites (ferrinol / aluminol) followed by the formation of $\equiv SO^sUO_2^+$ surface complexes, and / or the formation of $\equiv SO^sUO_2OH$ surface complexes on neutral hydroxyl surface sites. Dahn et al. [212] have investigated by EXAFS the coordination environment of uranyl ions adsorbed onto NaIdP at pH 5 (in 0.1 M $NaClO_4$ electrolyte solution) and at low surface loading of U (4 $\mu mol.g^{-1}$) and have suggested a preferential binding of uranyl ions to the iron octahedral surface sites over the aluminum octahedral surface sites of the clay. No evidence on the contribution to U sorption of each type of surface hydroxyl (silanol, ferrinol, aluminol) on Na-Illite edges can be provided by the present study. At the highest U concentration values studied in our experiments (ca. 25 μM), we observed an increase in the percent of U sorption (and a nonlinear increase of the amount of U sorbed) which is attributable to the contribution of an additional sorption mechanism, likely the (surface) precipitation of a uranyl hydroxide phase. Such a later mechanism is possible as the sorption on low affinity edge sites of a high concentration of U (> 10 μM) may be less efficient to compete against the direct precipitation of a uranyl hydroxide from solution. We can alternately propose the formation of surface precipitates of uranyl (hydr)oxides and / or polynuclear uranyl surface species similar to those described by Sylwester et al. [125], which may nucleate on clay surface, even before all weak sorption sites available for U surface complexation become saturated.

4.3. Surface speciation of uranyl ions at the NaIdP–phosphate-solution interface

Uranyl sorption edges and isotherms presented here show that the presence of phosphate ligands (at 100 μM) led to a promotion of U(VI) sorption at acidic pH onto NaIdP, particularly at a high concentration of U (10 μM). The sorption of phosphate ions is enhanced by an increase of U concentration in experiment, too. These results suggest that (part of) uranyl ions were sorbed at the NaIdP – phosphate – solution interface via formation of ternary uranyl phosphato surface

complex(es) and/or U(VI) phosphate surface precipitates. Experimental results, such as the non-linear increase of U and P surface coverages when increasing U concentration (from 1 to 10µM), highlighted moreover the formation of multiple uranyl phosphate sorption species and/or the implications of several types of surface sites. Desorption experiments provided strong evidence that the sorption of U at acidic pH has occurred in the presence of phosphate ions mainly via a reversible process, i.e., via uranyl (phosphate) surface complex formation. Formation of such surface complexes were shown to impart negative charges to the clay surface throughout the pH range investigated, which is an indication of participation of phosphate anions to the surface complexes formed. Based on values of high-affinity sites given by Bradbury and Baeyens [116] for the conditioned Illite du Puy (ca. 2 µmol.g^{-1} or 0.01 sites.nm^{-2}), it is likely that formation of uranyl phosphato surface complexes formed in our experiments at high U and concentrations (12 µM and 100 µM, respectively) would involve both high- and low-affinity (amphoteric) sites at the clay edge platelets. It is to note that the contribution of a mechanism of uranyl phosphate precipitation from oversaturated solutions is not to be ruled out at the highest U concentration studied, in the presence of phosphate ligands ($[U]_{I,aq}$ = 25 µM, $R_{S/L}$ = 3 g.L^{-1} NaIdP).

Our *in situ* ATR FTIR experiments of the U – P (co)sorption onto NaIdP conducted at varying U concentration or as a function of reaction time provided valuable information on surface speciation. It was found that several species contributed to the phosphate surface speciation during U-P co-sorption, with three types of uranyl phosphate surface species being identified. At short reaction times (< 7 h), two uranyl phosphate species were identified onto NaIdP, with the first one (U-P species A) being formed at low U concentration and the second one (U-P species B) growing with an increase in U concentration. It is to note that, when phosphate ions were added before U in experiment, the formation of these two U-P species affected the IR signals of previously-formed phosphate surface species (with no U), i.e., it led to disappearance of IR bands of preexisting inner-sphere surface complex of phosphate and in a decrease in bands'

intensity of an OSSC of phosphate. Thus, pre-existing phosphate surface species formed onto NaIdP were desorbed and / or converted rapidly upon the addition of uranyl ions in the system and the subsequent rapid formation of U-P surface species. The latter are interpreted as being inner sphere uranyl phosphate surface species formed at edge sites of the clay platelets, which compete successfully against formation of ISSC of phosphate. The U-P species A has a (weak) IR band at ~1125 cm^{-1}, which is independent of the concentration of uranyl ions (2–10 μM). This suggests that its formation took place at high-affinity sites existing in limited amounts onto clay edges. Whether this species represents a surface precipitate (e.g., $(UO_2)_3(PO_4)_2 \cdot 4H_2O_{(s)}$) and / or an outer sphere surface complex (i.e., UO_2HPO_4 $(H_2O)_4$) having a band at 1122 cm^{-1}, can be ruled out. In such cases, its absorbance would increase with U concentration [97]. Conversely, U-P species B displays an IR band at ~1050 cm^{-1} whose intensity increases with U concentration in the range 2-8 μM, and it dominates phosphate speciation at low reaction times (7 hours). This species is likely a uranyl phosphato ISSC forming at low affinity sites onto clay edges. Actually, the band at 1050cm^{-1} can hardly be attributed to an OSSC of uranyl phosphate (having IR bands at positions close to those of aqueous $UO_2H_2PO_4^{+}{}_{(aq)}$ species), because an OSSC complex would display two bands at 1052 and 1170c m^{-1} of similar intensities (cf. discussion in 4.1). A reduction of molecular symmetry of PO_4 unit from C_{2v} to C_1 is expected if the aqueous uranyl phosphate species is involved in formation of the ternary surface complex. It is to note that formation, at a short reaction time during our ATR FTIR (co)sorption experiments, of two types of U-P inner sphere surface complexes has prevented the formation of (VI)-phosphate colloids, which were observed in the absence of clay and under similar solution conditions (see discussion 4.1). Formation of uranyl-phosphate ISSC surface complexes onto NaIdP is in good agreement with previously published spectroscopic studies of the (co)sorption, under conditions close to those used in the present study, of uranyl and phosphate ions at surfaces of aluminum / iron (hydr)oxide, SiO_2 and clays [11,12,134,136].

At a long reaction time (3 days) and high U concentration, two uranyl phosphate species were identified to exist onto NaIdP, namely, the rapidly-formed U-P species B (which remained stable in the long term) and another species (U-P species C) whose intensity was increasing with reaction time. The latter uranyl-phosphate surface species has three υ_3 P-O antisymmetric stretching band at 1114, 1080 and 992 cm^{-1}, which indicates a C_{2V} or lower molecular symmetry (likely C_1) of PO_4 unit. The band at 992 cm^{-1} was not observed at short reaction time (t_R=7h), possibly due to some interferences of IR absorption from clay structure at wavenumbers lower than 1000 cm^{-1}. The bands' positions of U-P species C are quite different than those observed on IR spectra of uranyl phosphate solutions, ruling out formation of uranyl phosphate OSSC and / or U(VI) phosphate colloids formed directly from solution. These positions are shifted significantly with respect to those reported in the literature for the group of autunite minerals but they compare well with them (1118, 1074 and 985cm^{-1} for autunite, and 1118, 1048 and 985cm^{-1} for meta-autunite [213]). Hence, we hypothesize that U-P species C is an autunite-like surface species. Troyer et al. [136] have investigated by EXAFS and TRLFS the effect of increasing concentrations of phosphate and uranyl ions (0.025-100 μM) on the uptake of U(VI) by montmorillonite at pH 4-6. These authors have evidenced a transition between formation of uranyl phosphate surface complexes at low coverage of the clay, and surface precipitates of U(VI)-phosphates at high surface coverage. If the U-P species C represented a U(VI) phosphate precipitate formed on NaIdP, this would imply that its formation occurred in very limited amounts under our experimental conditions (despite the dominance of its signal on the IR spectra), because our desorption data indicate primarily reversible co-sorption mechanisms. Therefore, we believe that the U-P species C is rather an autunite-like uranyl phosphate surface complex (e.g., as a polynuclear complex) that forms on NaIdP at a high reaction time.

4.4. Conclusions

To our best knowledge, the present study is the first one combining macroscopic experiments and in situ ATR FTIR study to investigate the (co)sorption mechanisms of phosphate ions and trace levels of uranyl ions at the illite–electrolyte solution interface.

All the macroscopic data reported here pointed at several sorption mechanisms / surface sites contributing to the uptake of uranyl ions by NaIdP and depending on key parameters such as pH, U concentration, clay-to-solution ratio and phosphate ligand concentration. In peculiar, data indicated that a low amount of high affinity sorption sites (<0.02 sites.nm-2) existing at the NaIdP edge platelets can strongly interact with U and become progressively saturated, while low affinity surface sites are increasingly involved in U sorption, when increasing U concentration (1-10µM) or decreasing clay-to-solution ratio (1-3 g.L-1) in experiment. It was also shown that presence of phosphate ligands enhances the sorption of U(VI) at acidic pH onto NaIdP and, conversely, the uptake of phosphate ions by the clay surface is promoted by an increase of the U concentration in sorption experiment. Macroscopic and EM data highlighted the formation of several types of uranyl phosphate species imparting negative charges to the clay surface and / or several types of sorption sites, with the mechanisms of U-P co-sorption remaining highly reversible. Data acquired by in situ monitoring of the illite-solution interface by ATR FTIR spectroscopy provided evidence that uranyl ions and phosphate ions were (co)sorbed at acidic pH mainly via the formation of three types of inner-sphere uranyl phosphate surface complexes: a surface complex forming rapidly at high affinity surface sites and displaying a (weak) υ3(P-O) band at ~1125cm-1, an additional complex forming at low affinity sites in increasing amounts with U concentration and displaying a band at ~1050cm-1, -with these two complexes competing successfully against formation of inner sphere phosphate surface complexes-, and, finally, an “autunite-like” uranyl phosphate surface complex (e.g.,

such as a polynuclear complex) having υ3(P-O) bands at 1114, 1080 and 992cm-1 and appearing at a long reaction time (>1 day) and at high U concentration (10µM).

Because illite is an important constituent of argillaceous formations envisaged for deep HLW repositories and phosphate ligands are omnipresent in argillaceous rocks and ground/ surface waters, the macroscopic and IR spectroscopic data acquired in the present study may serve in safety assessment of the repositories and may be useful for better understanding U(VI) migration / retention in the environment.

Acknowledgments

We thank for analyses of clay samples: ITES (Institut Terre et Environnement de Strasbourg, Strasbourg University, France) for mineralogical analyses, SARM-CRPG (Service d'Analyse des Roches et Minéraux, Centre de Recherches Pétrographiques et Géochimiques, Nancy, France) for major element and trace element analysis, and ECPM (École de Chimie des Polymères et Matériaux, Strasbourg, France) for BET measurements. We are grateful to the A. Boos for giving us access to the ICP-OES and ICP-MS equipments of the "Plateforme des Inorganiques" of IPHC for our solution analyses.

Funding

This research work was funded by the European Joint Programme on Radioactive Waste Management EURAD of the European Commission (contract number CNRS 198255) and took place in the frame of the WP FUTURE of EURAD.

Appendix B. Supporting information

Chapter IV. Effect of dissolved Fe(III) on the sorption of uranyl ions at the illite–solution interface in the presence of phosphate ligands

1. Introduction

Studying the migration behavior of radionuclides in the near and far field of high-level radioactive waste repositories is an important step in assessing the safety of disposal [85], which many countries are planning to carry out in geological barriers such as clay rocks due to the outstanding retention capacities of clays against radionuclides [1]. As uranium is a main radionuclide in spent fuel [86], many laboratory and field studies have so far been carried out to understand the retention mechanism of uranium by oxi-hydroxides e.g., [10,111–113] and clay minerals e.g., [3,6,7,116,214,215]. However, the effect of dissolved iron(III) ions on the sorption of uranium(VI) ions onto clay minerals in the presence of phosphate ligand is less documented. In deep geological repository environments, a release of Fe ions could potentially originate from several processes such as the followings: (i) corrosion of the steel canister (induced by host rock porewater and/or groundwater), in which radioactive wastes are stored [3,6,216,217], and corrosion of the steel lining the horizontal boreholes in the host rock -such as the COx clay in the case of underground storage in France- [217]; (ii) the dissolution of Fe (and Fe bearing) minerals in the host rock (e.g., pyrite, siderite and ilmenite in COx [218]), (iii) Fe ions initially present in pore water of host rock (e.g., aqueous Fe concentration varying from 0.002 to 0.21mmol.L^{-1} for COx-water systems [219]). As mentioned in Chapter 3, another repository safety issue related to the long-term degradation of near-field multi-barrier system is the release of radionuclides by the dissolution of radioactive waste. Therefore, the migration / retention behavior of radionuclides transported from repository environments to (sub)surface environments may be strongly affected by dissolved metals present in pore waters of host rock and/or (ground)waters, such as Fe^{3+} ions. First, clay mineral properties may be affected by the presence of Fe(III). D e Combarieu et al. [217] pointed out that the cation exchange capacity (CEC), the swelling capacity, and the mechanical and transport properties could be modified due to the presence of dissolved Fe ions. Some papers have highlighted, for example, that an

important parameter influencing P sorption mechanisms onto clays is the presence of cations like Fe^{3+} ions able to bridge P sorbed to the clay surfaces and / or to form minor phases like metal-(oxihydr)oxides acting as strong sorbents in clay rocks [100–102]. Second, Fe^{3+} may also potentially compete UO_2^{2+} ions for coordination at the clay surface. Further spectroscopic work is needed to get insight into the effect of dissolved metal ions on the mechanisms of sorption of uranium(VI) onto clay minerals, in the presence of inorganic ligands like phosphate ligands.

In the present study, we studied at the macroscopic and molecular levels the competitive and/or synergetic effects of Fe(III) ions on the (co)sorption of uranyl ions and phosphate ligands onto illite clay mineral by combining traditional batch sorption experiments and *in-situ* ATR-FTIR spectroscopic experiments. We investigated the illite – Fe(III) – phosphate solution system prior to the studies of the illite – U(VI) – Fe(III) – phosphate solution system. First, batch sorption experiments of Fe^{3+} ions were conducted at the illite–solution interface in the absence and presence of phosphate ligands as a function of pH (4-7), aqueous concentrations of Fe^{3+} ions (2-15µM), and times of reaction (4 hours – 4 days). The effect of Fe^{3+} ions on the sorption of U(VI) onto illite was carried out, in the presence of phosphate ligands (100µM), as a function of pH (3-8) at a given concentration of U(VI) (12µM) and Fe^{3+} (10µM). Second, *In-situ* ATR FTIR measurements of the co-sorption of Fe^{3+} and phosphate ions and the effect of Fe^{3+} ions on the co-sorption of U(VI) and phosphate ions onto illite were performed at pH 4 and reaction times of 24 hours and 4 days, respectively.

2. Material and methods

The clay sample used in the batch sorption experiments and the *in-situ* ATR-FTIR spectroscopy experiments performed in the presence of Fe^{3+} ions is NaIdP (size fraction <75µm of Na-homoionic illite du Puy). Ultrapure Milli-Q® water (>18 MΩ.cm) and analytical grade chemicals were used for preparing all the experimental solutions used. The experiments were performed under atmospheric conditions (25°C and atmospheric p_{CO2}) at a clay-to-solution ratio of $3 g.L^{-1}$ ($R_{S/L}$) and with a 0.005M NaCl background electrolyte.

2.1. Batch sorption experiments

Sorption of Fe(III) onto NaIdP and effect of phosphate ligands. Traditional batch sorption experiments were performed in order to obtain sorption edge and sorption isotherm of Fe^{3+} ions onto NaIdP. The key parameters studied in the batch experiments were the pH, the aqueous concentration of Fe(III) ions and / or phosphate ligands and the reaction time (sorption kinetics). Sorption kinetics of Fe(III) was studied for reaction times ranging from 4 hours to 4 days in the pH range 3-7, in the presence of phosphate ions ($[P]_{I,aq}$= 100µM). Sorption edges of Fe^{3+} ions and phosphate ligands (co)sorbed onto NaIdP were obtained ($[Fe]_{I,aq}$=10µM and $[P]_{I,aq}$=100µM). Sorption isotherms were acquired at pH=4 ($[Fe]_{I,aq}$=2-15µM), in the absence or in the presence of phosphate ligand ($[P]_{I,aq}$=0 or 100µM). The experiments were performed as follows: (i) clay suspensions brought at a value of $R_{S/L}$ of $3 g.L^{-1}$ were pre-equilibrated for 3 days, at defined pH values, in 15mL polypropylene centrifuge tubes, (ii) after the pre-equilibration period, desired volumes of a stock phosphate solution and/or a $FeCl_3$ stock solution were added (simultaneously) into the tubes to achieve desired initial aqueous concentrations of Fe(III) and phosphate ions, (iii) the tubes were gently shaken end-over-end for 4 days. After the sorption period, the final pH was measured and the solid – liquid separation was carried out by centrifugation of the suspension at 9000rpm during 3 hours (size cutoff:

16nm for illite). An aliquot of the supernatant was taken for measurement of electrophoresis mobility (EM). Supernatant was acidified at pH<1 by 2% HNO_3 for chemical analyses. Final concentration of Fe(III) was measured by ICP-OES or ionic chromatography (CI). ICP-MS was used to measure the final concentration of U(VI). The same method, as described in chapter 2, was applied for the calculations of the percentage and amount (in $\mu mol.g^{-1}$ clay) of sorption of uranium, iron and phosphate ions. Analytical uncertainties on the sorption percentage and surface coverage of iron were estimated to be lower than 2.5%.

Effect of Fe(III) ions on the sorption U(VI) onto illite, in the presence of phosphate ligands. The effect of Fe(III) ions on the sorption of U(VI) onto illite, in the presence of phosphate ligands, was studied as a function of a key parameter, namely pH. studied for pH. The experiments were conducted as described in the previous paragraph, excepted that known volumes of stock solutions of U(VI), Fe(III) and phosphate ions were added simultaneously to the centrifuge tubes in order to achieve the desired aqueous concentration of sorbates ($[U]_{I,aq}$=12µM, $[Fe]_{I,aq}$=10µM and $[P]_{I,aq}$=100µM, respectively), (ii) the centrifuge tubes containing preequilibrated suspension and adsorbates were gently shaken end-over-end for 4 days.

2.2. In-situ ATR-FTIR experiments

In-situ ATR-FTIR spectroscopy measurements were carried out with a Bruker Equinox IFS 55 infrared spectrometer equipped with a MCT detector (system cutoff: ca. $900cm^{-1}$). The detector was cooling down by liquid nitrogen during FTIR spectra acquisition. An ATR cell containing a manufactured ZnSe horizontal crystal (angle of incidence: 45°, crystal size: $7.2\times1.0\times0.7cm^3$ and 5 internal reflections) was used for all the spectroscopic experiments.

2.2.1. Blank solution experiments

FTIR spectra of aqueous species of Fe(III) and phosphate ions formed at pH 4. A "blank" experiment was carried out in order to obtain reference IR spectra for aqueous Fe-phosphate species formed in solution (under conditions similar to those used in experiments o co-sorption of Fe(III) and phosphate ions onto illite). This is mandatory to distinguish between OSSC and ISSC formed onto illite during co-sorption experiments. IR analysis was conducted for a 0.005M solution introduced in the ATR cell, in which desired volumes of stock solutions of Fe(III) and phosphate ions were added simultaneously to achieve target concentrations of Fe(III) and phosphate ions ($[Fe]_{I,aq}$=10µM and $[P]_{I,aq}$=100µM).

FTIR spectra of aqueous species of U(VI), Fe(III) and/or phosphate ions formed at pH 4. The purposes of this blank experiment were to record reference IR spectra for electrolyte solutions at pH 4 containing simultaneously U(VI), Fe(III) and phosphate ions and to identify the aqueous complexes and/or precipitates formed in U(VI) - Fe(III) – phosphate - solution systems. No U-phosphate-Fe ternary aqueous complexes can be formed according to speciation calculations (**Fig.IV- 3**). The IR analyses were carried out as described in the previous paragraph. The U(VI), Fe(III) and phosphate ions were added simultaneously in an electrolyte solution previously introduced in the ATR cell. The spectra were recorded during ~26 hours. As high IR absorption were observed due to the formation of $(UO_2)_3(PO_4)_2 \cdot 4H_2O_{(s)}$ colloids in solution, the IR signals of aqueous species could be invisible. An aliquot of the solution was then ultra-filtered at 1kDa (cutoff: ~1nm) in order to remove colloids suspended in solution, and the filtered solution was added to the ATR cell for recording of FTIR spectra during one hour.

2.2.2. Monitoring of the illite-solution interface along Fe(III)-U(VI)-phosphate (co)sorption

Performing a preliminary ATR FTIR experiment of the co-sorption of Fe(III) and phosphate ions at the NaIdP-electrolytic solution interface (at pH 4) was mandatory prior to study the

competing effect of Fe(III) ions on the co-sorption of U(VI) and phosphate ions onto illite. An experiment was thus conducted to identify Fe-phosphate species forming at illite-solution interface (for t_R < 24 hours). The experiment was carried out as described in the "Materials and Methods" section of chapter 2, except Fe(III) and phosphate ions were introduced simultaneously to the NaIdP-solution system pre-equilibrated in the ATR cell, by adding desired volumes of stock solutions to achieve the desired concentrations of Fe(III) and P ($[Fe]_{I,aq}$=10µM and $[P]_{I,aq}$=100µM). IR spectra of the Fe(III)-phosphate (co)sorption were recorded during 24 hours. The experiment of ATR FTIR monitoring of the competitive and/or synergetic effect of Fe(III) ions on the (co-)sorption of U(VI) and phosphate ions at the NaIdP-electrolytic solution interface was conducted in conditions similar to those described above. U(VI), Fe(III) and phosphate ions ($[Fe]_{I,aq}$=10µM, $[U]_{I,aq}$=10µM and $[P]_{I,aq}$=100µM) were introduced at the same time in a pre-equilibrated NaIdP – electrolyte solution system in the ATR cell and the spectra were recorded for ~3 days.

3. Results

3.1. Calculated aqueous speciation of Fe^{3+} and UO_2^{2+} ions

Calculations were made to acquire speciation diagrams of Fe^{3+} and UO_2^{2+} ions, for the initial solutions used in the experiments of the competitive sorption of U(VI) and Fe(III) onto NaIdP, in the presence of phosphate ligands. **Fig.IV- 1** gives the calculated speciation diagram of 10µM of Fe^{3+} ions in 0.005 M NaCl electrolyte solutions, in the pH range 2.5 – 8.5 (ionic strength: 0.005M), in the absence of phosphate ligands and in the presence of atmospheric CO_2. At pH 4, the two predominant species are the first and second hydrolysis products, $FeOH^{2+}$ and $Fe(OH)_2^+$ (representing 40% and 60 %, respectively, of total Fe concentration, $[Fe]_{I,aq}$). $Fe(OH)_2^+$ is the main aqueous species of iron(III) at pH>5.5. Fe^{3+} ions represent a significant contribution at pH<4, only.

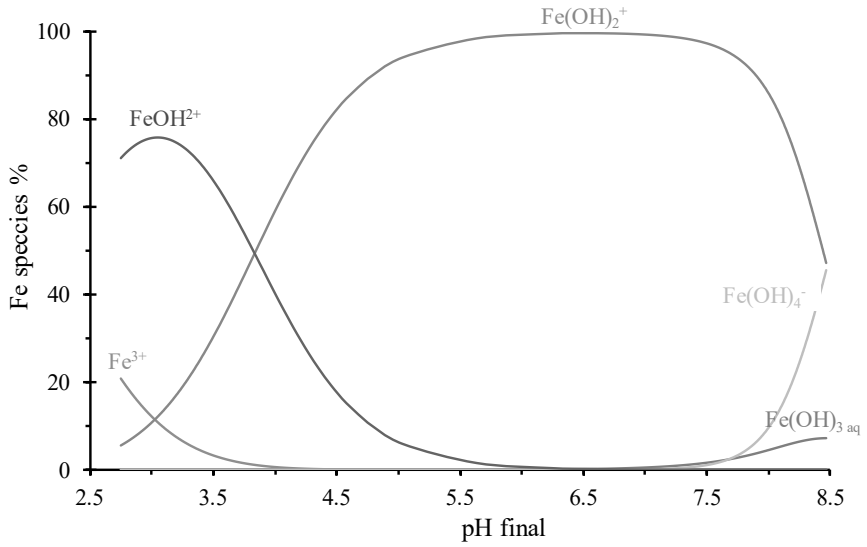

Fig.IV- 1. Speciation diagram of dissolved Fe(III) in 0.005M NaCl electrolyte solutions (solutions at $[Fe]_{I,aq}$ =10µM, ionic strength=0.005M). Calculations performed with Visual MINTEQ code and database.

Fig.IV- 2a,b give the speciation diagrams of dissolved Fe(III) in the presence of phosphate ligands, and of the corresponding dissolved ligand speciation, respectively, in 0.005M NaCl

electrolyte (solutions at: $[Fe]_{I,aq}$=10µM, $[P]_{I,aq}$=100µM, ionic strength: 0.005M), in the presence of atmospheric CO_2. Several phosphate complexes and hydrolysis products of iron(III) co-exist in aqueous solution in the pH range 4-8, together with protonated phosphate species. Fe(III) aqueous speciation (**Fig.IV- 2**a) is dominated in the pH range 2.5-4.5 by a Fe^{3+}-phosphate complex, $FeHPO_4^+$ (which represents more than 60% of $[Fe]_{I,aq}$ at pH 4 and diminishes with

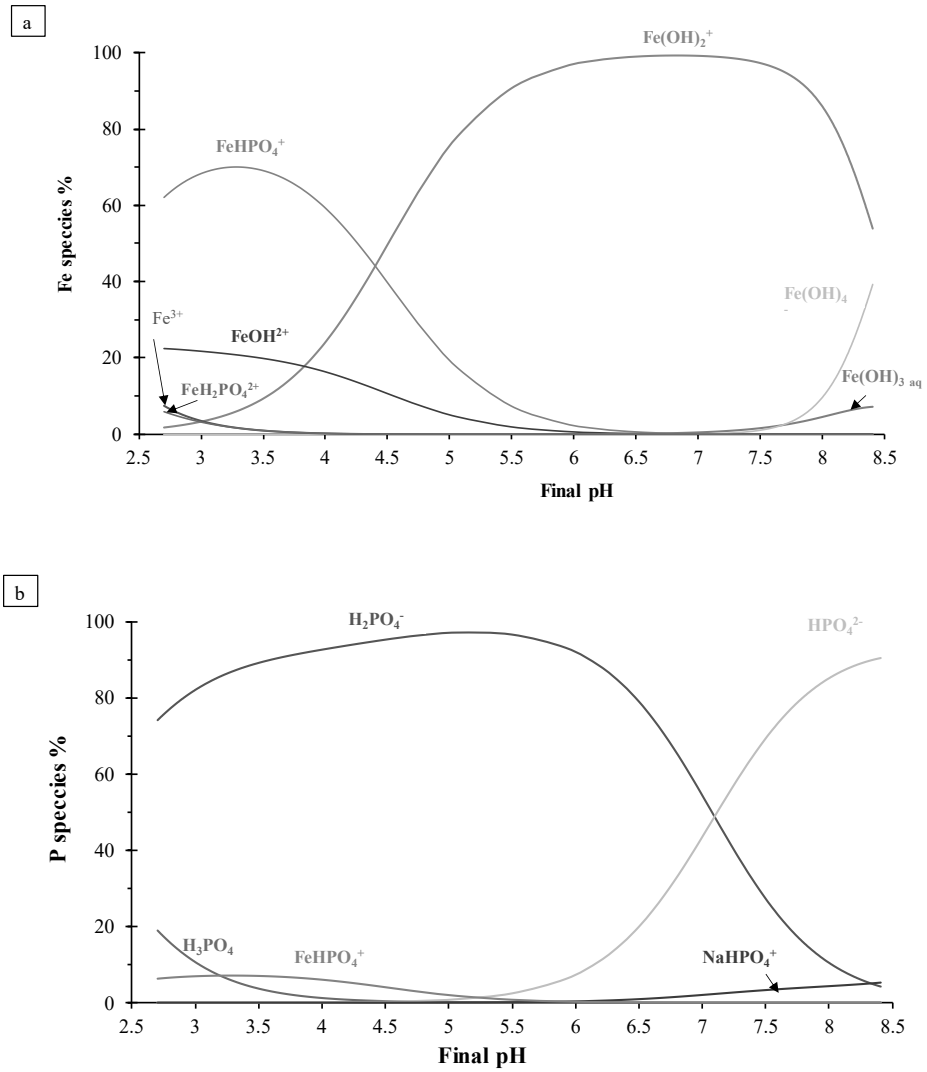

Fig.IV- 2. Speciation diagram of dissolved Fe(III) in 0.005M NaCl electrolyte solutions in the presence of phosphate ions (solutions at $[Fe]_{I,aq}$ =10µM, ionic strength=0.005M and $[P]_{I,aq}$ = 100µM). Calculations performed with Visual MINTEQ code and database.

pH to become negligible at pH 6.5). At pH 4, the two hydrolysis products, i.e., $FeOH^{2+}$ and $Fe(OH)_2^+$, display thus a much lower contribution to aqueous Fe species (ca. 15% and 25 %, respectively) than in the absence of phosphate ions. The latter Fe species ($Fe(OH)_2^+$) becomes the predominant iron(III) aqueous species at pH higher than 5.5. Fe^{3+} and $FeH_2PO_4^{2+}$ ions are present at pH <3, only. As regards to the aqueous speciation of phosphate ions (**Fig.IV- 2**b), there appears that the main Fe(III) phosphate complex, $FeHPO_4^+$, represents less than 10% of total phosphate ions ($[P]_{I,aq}$). Between pH 4 and 7, the phosphate speciation is dominated by $H_2PO_4^-$, with the contribution of HPO_4^{2-} increasing with pH.

Fig.IV- 3 give the speciation diagrams of dissolved U(VI) and Fe(III) ions present together in solutions containing phosphate ligands, and the corresponding dissolved ligand speciation ($[U]_{I,aq}$=10µM, $[Fe]_{I,aq}$=10µM, $[P]_{I,aq}$=100µM, 0.005M NaCl electrolyte solutions equilibrated with atmospheric CO_2). Regarding U (**Fig.IV- 3**a), at pH values lower than 4, the main uranyl aqueous species are UO_2^{2+} and UO_2HPO_4 and minor species are UO_2OH^+ and $UO_2H_2PO_4^+$. In the pH range 4-8, uranyl phosphate aqueous species dominate, with the main species varying from UO_2HPO_4 to $UO_2PO_4^-$ with increasing pH. Mixed hydroxide carbonate complex of uranyl ion, e.g., $(UO_2)_2CO_3(OH)_3^-$, and the uranyl carbonate complexes, become successively dominant at pH higher than 7 and 8, respectively. Speciation of Fe(III) is almost similar to that described previously for phosphate solutions (in the absence of U), with $FeHPO_4^+$ predominating at pH lower than 4 (**Fig.IV- 3**b) and hydrolysis products at higher pH. As regard the speciation of phosphate ions, **Fig.IV- 3**c shows that the diprotonated (at pH 3-7) and monoprotonated phosphate ions (at pH 7-8.5) are two main aqueous phosphate species (>80%), as described previously. The ferric phosphate complex, $FeHPO_4^+$, and the uranyl phosphate complex UO_2HPO_4, represent less than 10% of total phosphate ions at pH < 5 and in the pH

range 3-6, respectively. At pH 4, amount of aqueous phosphate species formed are in the following decreasing order: $H_2PO_4^-$ (~88%) > $FeHPO_4^+$ (~6%) > UO_2HPO_4 (~4%).

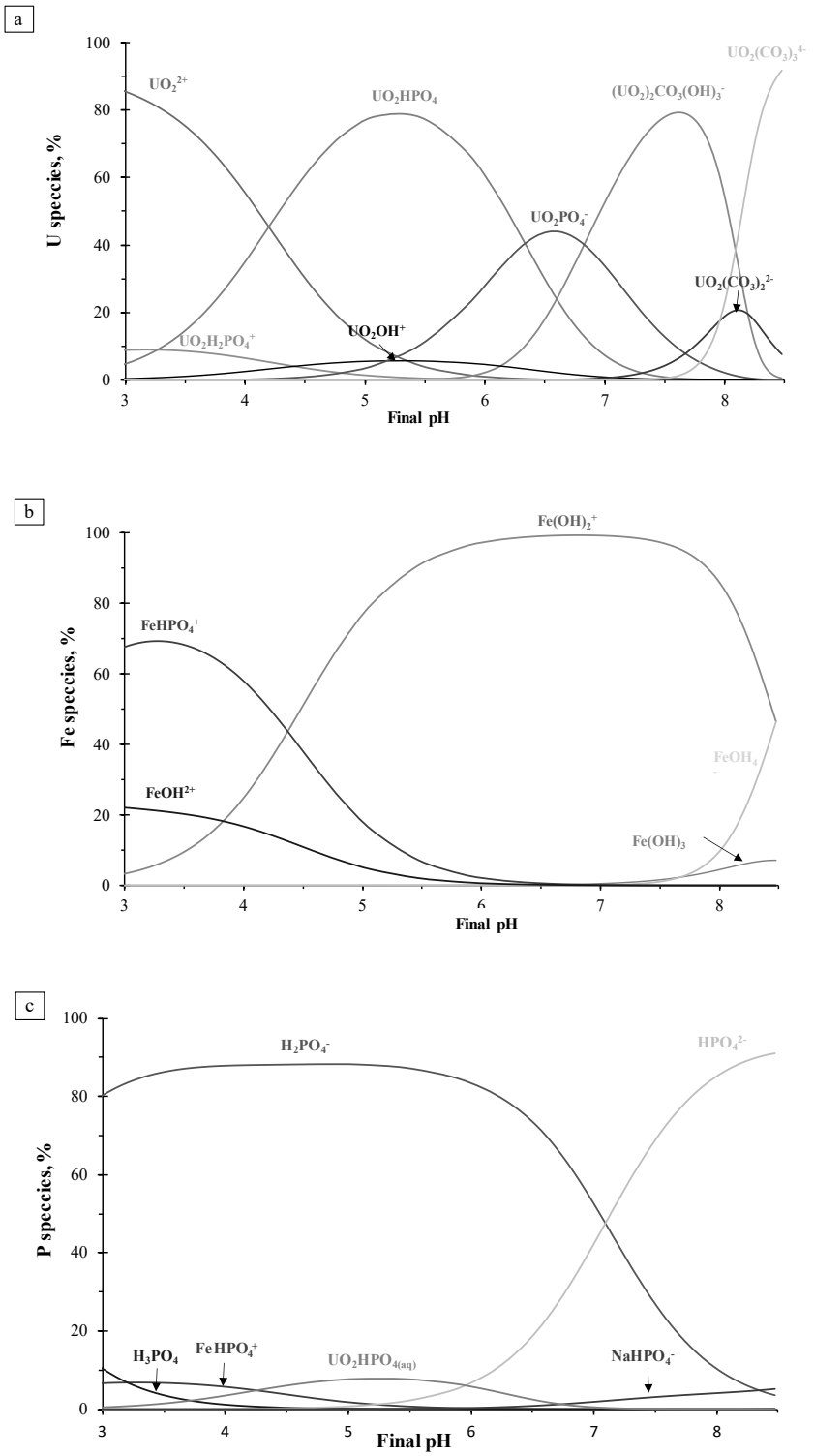

Fig.IV- 3. Speciation diagrams of dissolved (a) U(VI) and (b) Fe(III) in the presence of phosphate ligand and (c) of phosphate ligand, in 0.005 M NaCl electrolyte (solutions at

$[U]_{I,aq}$=10 µM, $[Fe]_{I,aq}$ =10 µM and $[P]_{I,aq}$ =100 µM). Calculations performed with Visual MINTEQ code and database.

3.2. Sorption of Fe^{3+} onto NaIdP and Effect of phosphate ligands

3.2.1. Effect of pH on macroscopic sorption of Fe^{3+} ions and EM

Fig.IV- 4 gives experimental results on the kinetics of sorption of Fe(III) ions onto NaIdP, in the presence of phosphate ligands and as a function of pH (for a ratio clay-to-solution of $3g.L^{-1}$ in 0.005M NaCl electrolyte solution). There was observed a two-steps kinetics of sorption. The percentage of Fe sorbed reaches values of ca 70-60% (depending on pH) within a reaction time t_R of 4 hours. After this step of rapid sorption, the rate of sorption diminishes. Percent sorption reaches values of ca. to 90% at t_R of 1 day, in the pH range from 5-7. Sorption was almost complete (ca. 95%) after 4 days and showed no dependence on pH, within the studied range. Other sorption experiments were thus conducted with a reaction time of 4 days.

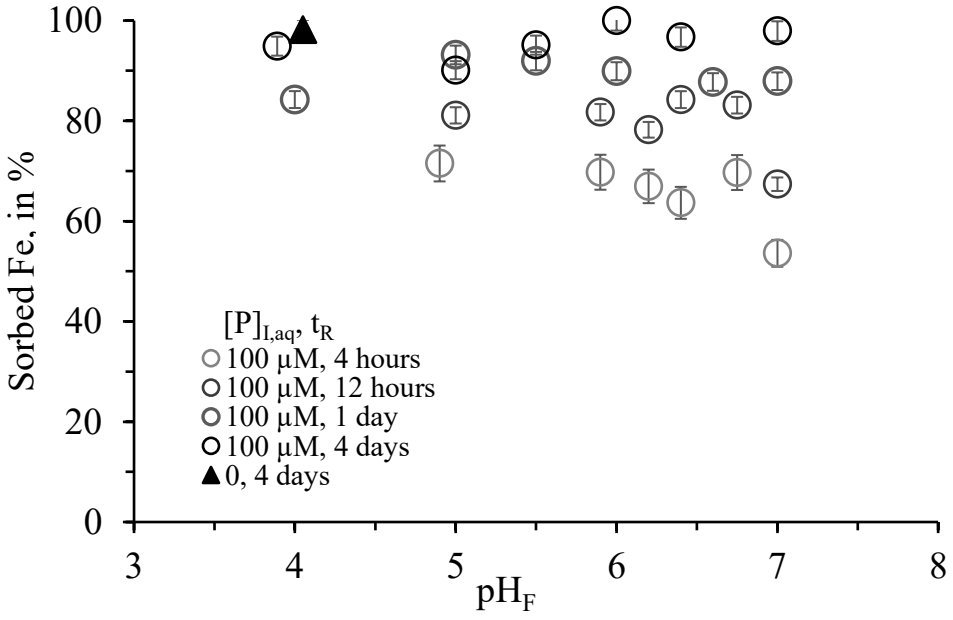

Fig.IV- 4. Percentage of Fe^{3+} ions sorbed ($[Fe]_{I,aq}$=10µM) onto NaIdP as a function of final pH (pH_F) at different reaction times (t_R), in the absence (at pH 4 only) or in the presence of

phosphate ligands ($[P]_{I,aq}$). Conditions: 0.005M NaCl electrolyte solution, clay-to-solution ratio ($R_{S/L}$): 3g.L^{-1}, pre-equilibration time of NaIdP suspensions (t_{pre-eq}): 3 days.

Fig.IV- 5 gives the pH dependence of EM values recorded for above described NaIdP – Fe(III) – phosphate solution systems. Complementary EM data acquired for NaIdP – solution systems studied in chapter 2 in the absence of dissolved Fe and/or phosphate ligands are reported, too. EM decreases as a function of pH, either in the absence or in the presence of dissolved Fe(III) and/or phosphate, which is mainly due to the deprotonation of the amphoteric hydroxyl groups existing at the clay edge platelets (cf. chapter 2). Electrophoretic mobility of NaIdP at a final pH of 4 shows values decreasing slightly in the order corresponding to experiments of: sorption of Fe ions only > co-sorption of Fe and P ions > sorption of P ions only (for t_R=4 days, $R_{S/L}$=3g.L^{-1} in 0.005M NaCl electrolyte, $[Fe]_{I,aq}$=0 or 10µM, $[P]_{I,aq}$=0 or 100µM). NaIdP in phosphate solutions at acidic pH display thus a slightly less negatively-charged surface in the presence than in the absence of iron(III), which suggests formation of Fe(III) surface species and / or Fe(III)-phosphate species imparting positive charges to the clay surface. For pH > 4, there was observed that the presence of Fe ions did not modify significantly an EM value for a NaIdP – phosphate solution system at a given pH (for $[P]_{I,aq}$=100µM). The hypotheses are: (i) formation of a neutral, Fe(III) phosphato surface complex and / or of Fe(III)-phosphate surface precipitates, or (ii) formation of Fe-colloids directly from the near neutral solutions, which are over-saturated with respect to Fe(III)-oxihydroxides.

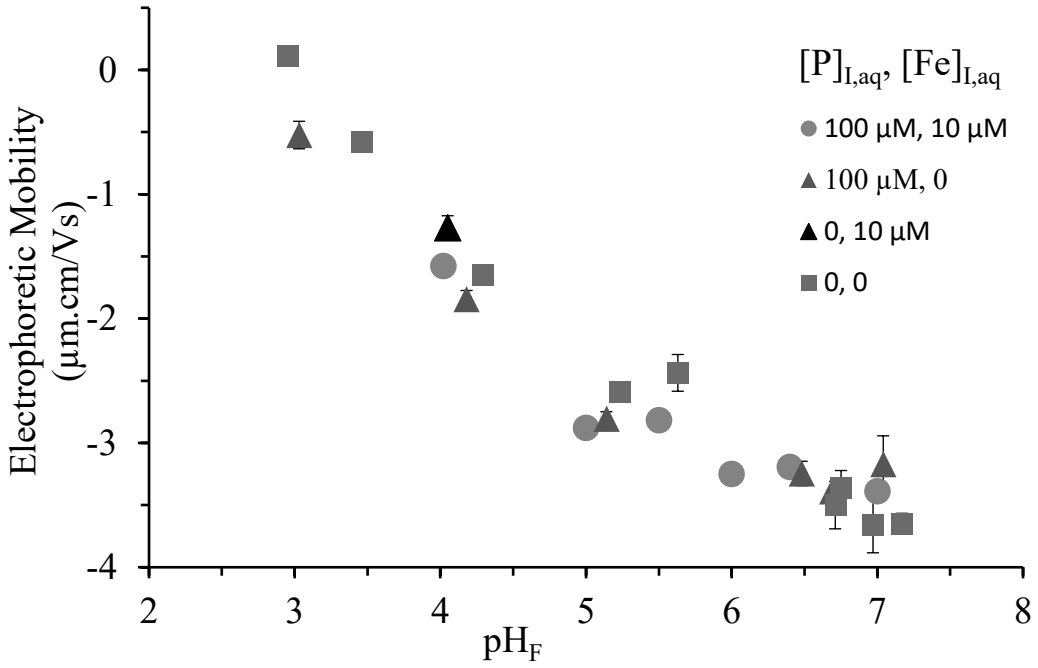

Fig.IV- 5. Electrophoretic mobility of NaIdP for experiments on the sorption of Fe^{3+} ions ($[Fe]_{I,aq}$, in µM), in the presence and in the absence of phosphate ligands ($[P]_{I,aq}$ in µM) described in **Fig.IV- 4**. EM data of chapter 2 on P sorption in the absence of Fe(III) and EM of NaIdP without sorbates are reported, too. Conditions: $R_{S/L}$=3g.L^{-1}, t_R=4 days. Electrolyte: 0.005 M NaCl.

3.2.2. Effect of Fe concentration on macroscopic sorption of Fe^{3+} ions and EM

To elucidate the effect of Fe^{3+} ions on the mechanisms of co-sorption of Fe and P, experiments were made at increasing total concentration of Fe ($[Fe]_{I,aq}$=2-15µM), in the absence and in the presence of phosphate ions. A focus was made on Fe (and P) sorption at acidic pH (**Fig.IV- 6**). Sorption isotherms show that sorption of Fe^{3+} ions is almost complete in the Fe concentration range studied, either in the presence or in the absence of phosphate ligands, except at low concentration ($[Fe]_{Iaq}$=2 µM). In the latter case, the effect of phosphate ions was observable and led to an increase of the percentage of Fe sorption (from ca. 90 to 100%, **Fig.IV- 6**a). Assuming that Fe^{3+} ions were sorbed at NaIdP surface would thus lead to values of Fe surface coverage

varying from ca. 0.6 to ca. 5µmol.g^{-1} (for $[Fe^{3+}]_{I,aq}$ increasing from 2 to 15 µM). These results suggest either that NaIdP and phosphate ions have no significant effects on the uptake of Fe – possibly due to formation of iron(III)-oxihydroxides directly from solution-, and / or they have no signature on the macroscopic Fe sorption in the range of concentrations studied (except at $[Fe^{3+}]_{I,aq}$=2µM). The former hypothesis is unlikely as the speciation of dissolved Fe(III) in the presence of phosphate ligands at pH 4 is dominated by a Fe-phosphate complex (**Fig.IV- 2**). Moreover, the experiments of Fe sorption showed that EM of NaIdP at pH 4 (**Fig.IV- 6**c): (i) is higher in the presence of Fe^{3+} ions (2-15µM) than in their absence, and (ii) is lowered in the presence of phosphate ions, for a given value of $[Fe]_{I,aq}$ in experiment or a given Fe surface coverage. It is to note that adding a low concentration of dissolved Fe(III) in experiment increases slightly EM of NaIdP contacted with phosphate solutions ($[P]_{I,aq}$=100µM), while increasing further the Fe concentration ($[Fe]_{I,aq}$: 4-15µM) has no significant additional effect. Fe sorption impart thus positive charges to NaIdP surface, even if solution pH and sorbed phosphate ions (at ($[P]_{I,aq}$=100µM) are main parameters determining the EM value.

In the absence of phosphate ligands, at least two types of Fe surface species are expected to be sorbed at the NaIdP surface, as a function of Fe concentration. At low concentration ($[Fe]_{I,aq}$ = 2 µM), they clearly impart a positive charge to the clay surface and they are likely inner-sphere surface complexes of Fe(III) formed at high affinity sites onto clay edges (≡S^{s}OH sites present in limited amounts, possibly at concentrations lower than 2 µmol.g^{-1}, cf. chapters 2-3). In contrast, at higher Fe concentrations, additional species formed tend to slightly decrease and/or to impart no significant charges to the surface. These species would likely correspond to neutral Fe surface complexes and/or to surface precipitates of Fe-oxihydroxides. Formation of colloids of Fe-oxihydroxides directly from solutions cannot be ruled out at the highest Fe concentrations investigated here.

In the presence of phosphate ligands, two main domains of sorption are observable in **Fig.IV-6**. First, a striking feature (**Fig.IV- 6**b) is that addition of low concentrations of dissolved Fe ($[Fe]_{I,aq}$ =2-4µM) to NaIdP-solution systems led to a decrease in percentage of P sorption and in clay surface coverage by phosphate (from ca. 6 to 1µmol.g^{-1}, for $[P]_{I,aq}$=100µM). In contrast, sorption of Fe^{3+} ions (**Fig.IV- 6**a) appears to be slightly promoted by the presence of the phosphate ligands, and the EM value is slightly increased (**Fig.IV- 6**c) -when compared to results obtained in the absence of P-. These findings evidence that: (i) Fe^{3+} ions at low aqueous concentrations successfully compete against phosphate ions for their sorption at high affinity surface sites –and at low affinity sites-, which are present at edges of NaIdP platelets, and (ii) Fe-phosphate surface species are formed onto NaIdP. Second, further increases in concentration of Fe^{3+} ions in experiments led to increases in amount of phosphate sorbed. The latter increased not linearly with Fe surface coverage so that the successive formation of at least two Fe-phosphato (surface) species (based on slopes of the P sorbed -vs-Fe sorbed curve at $[Fe]_{I,aq}\geq$4µM, **Fig.IV- 6**b) having no significant effect on EM, e.g., like a neutrally-charged Fe(III)-phosphate surface complex and/or surface precipitates, is hypothesized.

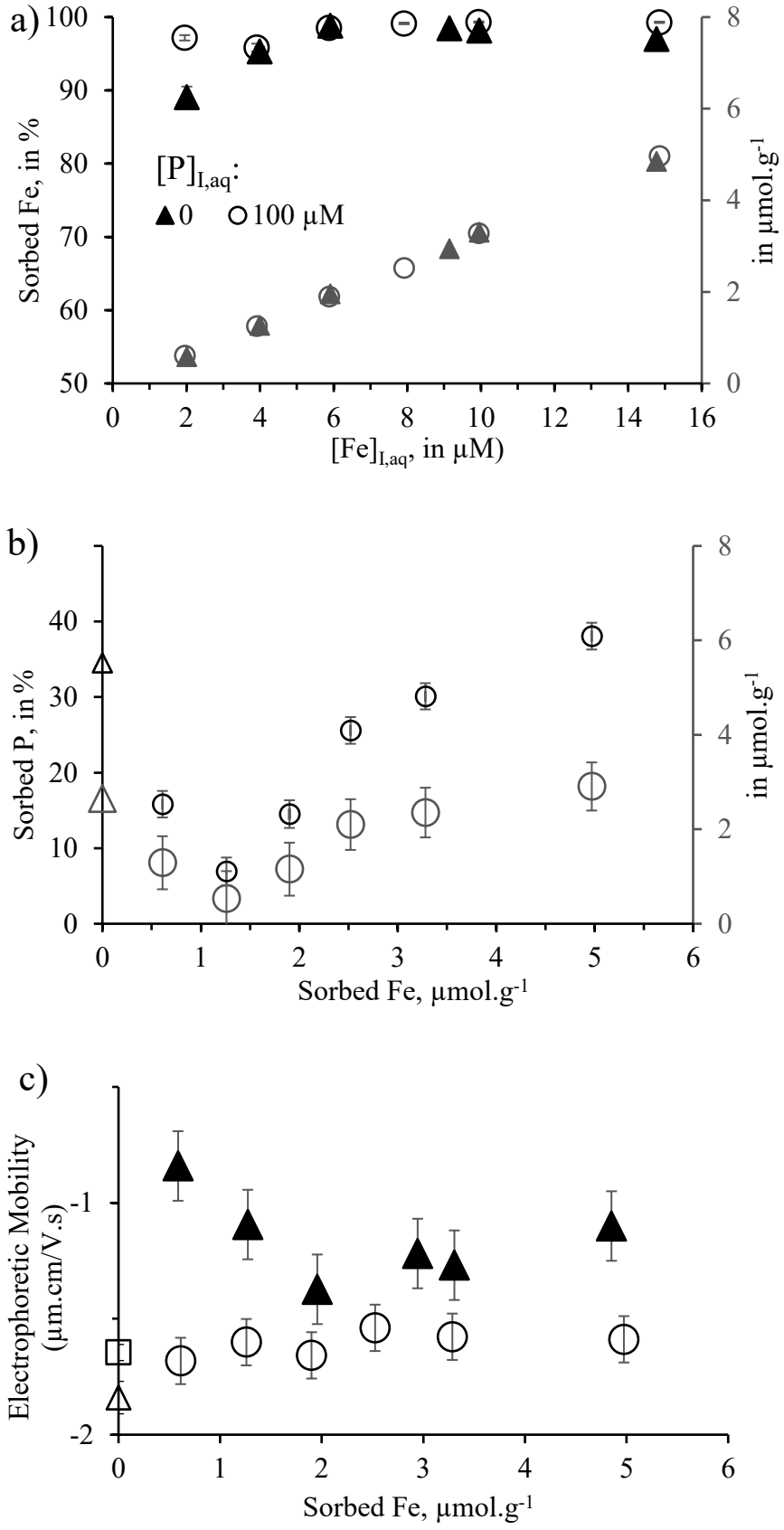

Fig.IV- 6. Results of experiments on effects of dissolved Fe concentration ($[Fe]_{I,aq}$: 2-15µM) and phosphate ligands ($[P]_{I,aq}$: 100 or 0µM) on the sorption of Fe^{3+} ions onto NaIdP at pH 4: (a)

Sorption precent (○▲) and amount (○▲) of Fe (▲▲: $[P]_{I,aq}$ = 0µM; ○○: $[P]_{I,aq}$ = 100µM), (b)Sorption precent (Δ○) and amount (Δ○) of phosphate ions, and (c) EM of NaIdP as a function of Fe surface coverage (Δ○:$[P]_{I,aq}$ = 100µM,; □: without sorbates; ▲:$[P]_{I,aq}$ = 0µM). Data of chapter 2 on P sorption in the absence of Fe(III) (Δ) and on EM of NaIdP without sorbates (□) are reported, too. Conditions: $R_{S/L}$: 3 $g.L^{-1}$ in 0.005M NaCl electrolyte solution, t_R: 4 days, t_{pre-eq}: 3 days.

3.2.3. ATR-FTIR spectroscopy of Fe(III) sorption in presence of phosphate ligands

Aqueous solutions. Although the ATR-FTIR spectral results of aqueous complexes of Fe(III) and phosphate ions have been briefly discussed in Chapter II, a more detailed discussion is given in this chapter. For this reason, the **Fig.II- 7** in Chapter II is re-shown in this chapter in order to make reading more convenient.

Before studying (co)sorption processes of dissolved Fe(III) and P(V) onto NaIdP by ATR-FTIR spectroscopy, FTIR measurements were conducted on aqueous solutions containing the Fe^{3+} ions and the phosphate ligands. The aim was to get IR reference spectra for iron-phosphate aqueous complexes and to identify a possible formation of Fe(III)-phosphate aqueous complexes and/or precipitates. Analysis of the iron-phosphate aqueous complexes was made for an 0.005 M NaCl electrolyte solution at pH 4 containing Fe ions and phosphate ligands in concentrations similar to those used in ATR-FTIR sorption experiments ($[Fe]_{I,aq}$=10 µM and $[P]_{I,aq}$=100 µM). Dominant aqueous species are expected to be $H_2PO_4^-$ and $FeHPO_4^-$, based on speciation calculations (**Fig.IV- 2**). **Fig.IV- 7**shows IR spectra recorded as a function of time (during ca. 6 hours) for the studied Fe-P solution. A broad IR band at 950-1200 cm^{-1} and a slight decrease in spectral absorbance with time was observed, while spectra shapes remain unchanged. Four IR bands at 1042, 1075, 1089 and 1147 cm^{-1} were identified after spectra decomposition (**Fig.IV- 7**), which can be attributed to antisymmetric P-O stretching (υ_3) in the

PO_4 unit. The band at 1075 cm^{-1} was assigned to the diprotonated aqueous phosphate species, i.e., $H_2PO_4^-$, on the basis of our previous identification by FTIR analysis of phosphate solutions containing no iron (cf. chapter 2). The other three υ_3 displayed no significant differences in band position and shape as a function of time, suggesting that these bands may be attributed to a single species. Tejedor-Tejedor and Anderson (1990) have studied the aqueous complexation of iron(III) by phosphate ligands, as a function of the Fe/P ratio at acidic pH by means of cylindrical optics (CIR)-FTIR. They identified two major bands at ~1150 and 1085-1050cm^{-1} on the spectrum obtained for a solution at pH 1 (at $[P]_{I,aq}=1.4\times10^{-2}M$ and $[Fe]_{I,aq}=8.0\times10^{-4}M$) and they assigned these bands to $FeHPO_4^{+}{}_{(aq)}$ and / or $FeH_2PO_4^{2+}{}_{(aq)}$, based on similarities with IR spectrum of $H_2PO_4^-$ (although latter complex could be excluded due to complementary UV-vis spectroscopy data, and thermodynamic and kinetic studies). In the present study, spectra decomposition (**Fig.IV- 7**) showed IR band positions consistent with those reported by Tejedor-Tejedor and Anderson (1990) for $FeHPO_4^{+}{}_{(aq)}$ and / or $FeH_2PO_4^{2+}{}_{(aq)}$ aqueous complexes. The bands at 1045, 1089 and 1147cm^{-1} were attributed to the $FeHPO_4^+$ aqueous complex, which has a C_1 molecular symmetry, because it was calculated to dominate the Fe(III) speciation in our solution (cf. speciation calculations performed with Visual MINTEQ code and database in **Fig.IV- 2**).

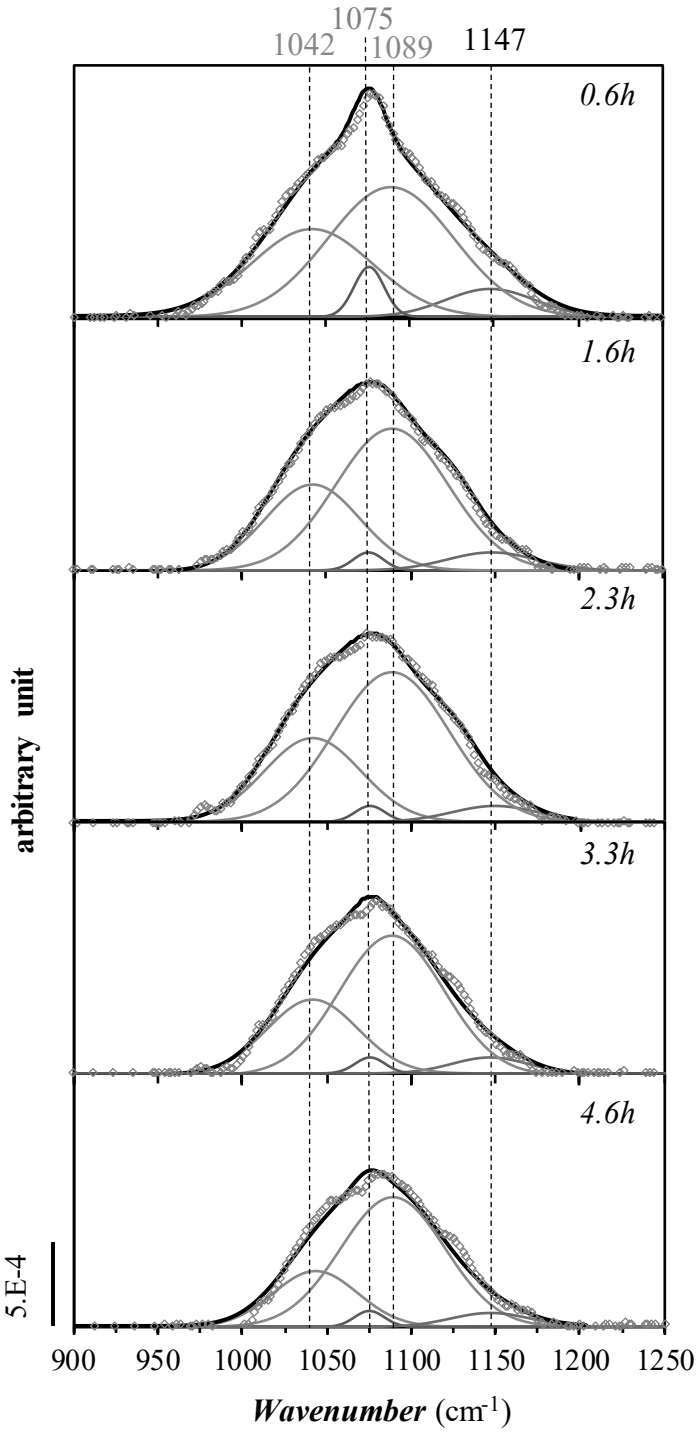

Fig.IV- 7. ATR FTIR spectra of a solution at $[P]_{I,aq}$ of 100 µM and $[Fe]_{I,aq}$ of 10 µM and pH 4. Background electrolyte: 0.005 M NaCl, t_R: up to 4.6 hours. Circles: experimental curve; lines: results of spectrum decomposition.

Co-sorption of iron and phosphate ions at the NaIdP-electrolyte solution interface. **Fig.IV- 8**a shows the IR spectra recorded in the region 900-1200cm^{-1} as a function of reaction time (t_R < 24 hours) during the (co)sorption at acidic pH (pH_F=4) of Fe^{3+} and phosphate ligands at the NaIdP-solution interface. The spectra are noisy and display a weak absorbance (at t_R=20 minutes) that decreases slightly with time. From 900cm^{-1} to higher wavenumbers, one can observe a band with a well-defined maximum at ~950cm^{-1}, which seems to remain stable as a function of time, and a broad band around 1000cm^{-1}. A main band is observable around 1070cm^{-1} at low t_R values and it shifts towards high wavenumbers after a few hours to enlarge as a broad band (at 1080 - 1110cm^{-1}) having a shoulder at ~1140cm^{-1} (t_R=5 hours). There was also observed a large band at 1120 and 1170cm^{-1} at low reaction time, whose absorbance decreased with t_R until disappearance. Weak absorbance of IR signals made it difficult to decompose the spectra. Nevertheless, eight bands could be identified (at ca. 946, 970, 1000, 1076, 1081, 1112, 1141 and 1162cm^{-1}, cf. **Fig.IV- 8**b), which can be attributed to υ_3 P-O stretching bands [15,23,220]. Those positioned at ~1076 and ~1162cm^{-1} were found to decrease in intensity with time, with the latter disappearing after a short reaction time. Former band overlaps with position of the band growing with time at ~1081 cm^{-1}, so that it is difficult to exclude its possible disappearance, too. These two bands (at 1076 and 1162 cm^{-1}) can be assigned to an outer-sphere surface complex (OSSC) of phosphate forming rapidly at NaIdP-solution interface. The positions are similar to those of aqueous phosphate species, i.e., $H_2PO_4^-{}_{(aq)}$, and of the OSSC of phosphate identified to form at NaIdP-phosphate-solution interface in the absence of Fe^{3+} ions (cf. "species A" in chapter 2 and Table C1). Moreover, their intensity at short t_R is higher than that observable for aqueous phosphate species formed at pH 4 and at similar concentrations of Fe^{3+} and phosphate ions, in the absence of clay (cf. **Fig.IV- 7**b). Time evolution of spectra observable in **Fig.IV- 8**a suggests that species A is rapidly formed at NaIdP –phosphate – Fe(III) - solution interface and transform subsequently into other surface species.

The other υ_3 bands reported for this experiment have maxima positions (at 946, 970, 1000, 1081, 1112, and 1141 cm^{-1}, **Fig.IV- 8**b) that are different from those of inner-sphere phosphate surface complexes identified to exist at NaIdP-phosphate-solution interface in the absence of metal ions (cf. chapters 2&3, Table C1). They thus likely relate to ferric phosphate surface species and / or to structural reorganizations at NaIdP surface along sorption. Borgnino et al. (2010) have investigated by ATR-FTIR spectroscopy the surface speciation of phosphate ions sorbed at the interface between a Fe(III)-modified montmorillonite and an aqueous solution. They found that phosphate ions were not adsorbed at surface of the clay itself but onto Fe(III)hydroxide coatings covering montmorillonite. These authors identified two sets of bands on IR spectra recorded at the interface between the Fe-modified clay and an aqueous phosphate solution at pH 4.5 (which exhibited maxima positions at 941, 1049 and 1088 cm^{-1}, 971, 1011 and 1128 cm^{-1}, and 962-957, 1062 and 1095 cm^{-1}, respectively). They concluded on the existence of several surface complexes -of C_{2v} symmetry or lower-, namely a nonprotonated bidentate surface complex ($(FeO)_2PO_2$), a monoprotonated bidentate surface complex ($(FeO)_2(OH)PO$), and a monodentate mononuclear complex ($(FeO)PO_3H$), respectively (cf. Table C1). The latter, which exhibited band positions at wavenumbers intermediate to those of $(FeO)_2PO_2$ and $H_2PO_4^-$ (as Fe is not as strongly bound than proton) was reported to be preferred at low coverage and to participating in H-bonding with an adjacent surface site. A set of bands (at 970, 1000, and 1112 cm^{-1}) amongst those observable in **Fig.IV- 8**b have positions close to those reported for $(FeO)_2(OH)PO$. However, we cannot rule out that they could also refer to structural reorganizations of the NaIdP–solution interface. Actually, the positions compare well with those of IR bands that were observed on the interface spectra recorded during ATR-FTIR experiments of NaIdP dissolution (cf. chapter 2). They were assigned to the OH bending vibrational mode of Al-Al-OH in the structure of clay minerals (for the bands at 970 cm^{-1}, cf. [193,194]) and to Si-O stretching band in the micas group, like illite [197] (for the bands at

1000 and 1112 cm^{-1}). The other υ_3 bands reported in **Fig.IV- 8**b (at 946, 1081, and 1141 cm^{-1}) are tentatively attributable to a Fe^{3+}-phosphate surface complex. Position of the two latter bands would suggest a limited formation of an outer-sphere ferric phosphate surface complex formed via electrostatic attraction or H-bonding between $FeHPO_4^{+}{}_{(aq)}$ ions and illite surface site i.e., $\equiv SO^{-}\cdots FeHPO_4^{+}$, and for which the P-O stretching bands would be slightly shifted compared to the aqueous complex (**Fig.IV- 7**). Although the hypothesis is not to be ruled out completely, it is not the preferred one, because the band at 1045 cm^{-1} observable for the aqueous complex is missing on the interface spectra reported in **Fig.IV- 8**b. We thus propose to attribute the set of bands peaking at 946, 1081, and 1141 cm^{-1} to a monodentate mononuclear surface complex formed either onto Fe-hydroxide coatings covering NaIdP (as $(FeO)PO_3$-H), as proposed in the work by Borgnino et al. (2010), and / or at edge sites of NaIdP surface (as $\equiv SO\text{-}FeHPO_4$). Finally, another hypothesis can be made as regards the attribution of the bands (other than those of P species A) observable in Fig 8b. Frost at al. (2002) [221] have collected the vibrational spectra of ferric phosphate minerals such as strunzite ($MnFe_2(PO_4)_2(OH)_2\cdot 6H_2O$) by using infrared and Raman spectroscopy. These authors have identified positions of P-O stretching bands for strunzite (at 963, 1006, 1080 and 1115cm^{-1}), which are close to those reported here. Therefore, it is highly possible that formation of a ferric phosphate surface precipitate may slightly contribute to IR signals recorded after several hours at the NaIdP-Fe-phosphate-solution interface (as the bands at 970 and 1112cm^{-1} appear lately on IR spectra, cf. **Fig.IV-8**b). Hypotheses of successive formation of ISSC and surface precipitates of ferric phosphate are supported by results of Fe sorption isotherm acquired in the presence of a high concentration of phosphate ions, which showed a non-linear increase in amounts of Fe and phosphate ions sorbed with $[Fe]_{I,aq}$ (**Fig.IV- 6**). Formation of a surface precipitate is consistent with EM results (**Fig.IV- 5**), too, that showed that EM (and hence surface charge) of illite remained constant at the highest $[Fe]_{I,aq}$ investigated (10-15µM).

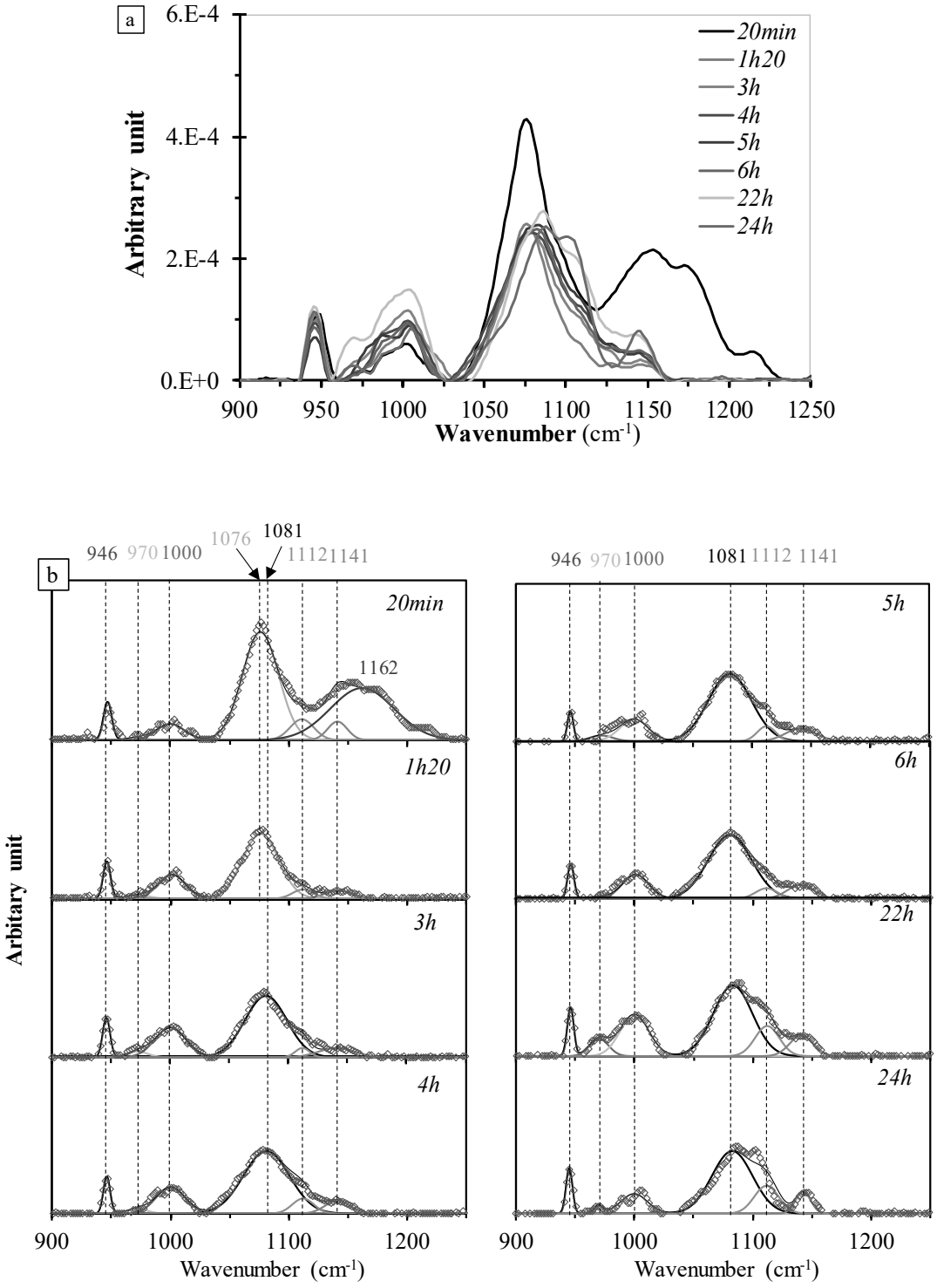

Fig.IV- 8. Results of ATR FTIR experiments of (co)sorption of iron(III) and phosphate ions at NaIdP – solution interface at pH 4: (a) in situ interface spectra as a function of reaction time (t_R) and (b) spectra decomposition. Conditions: $[Fe]_{I,aq}$=10µM, $[P]_{I,aq}$=100µM, 0.005M NaCl electrolyte solution.

3.3. Effect of Fe(III) ions on sorption of uranyl ions in the presence of phosphate ligands

3.3.1. Effect of Fe ions on U(VI) sorption edges

Batch experiments of (competitive) sorption of U(VI) and Fe(III) on NaIdP, in the presence of phopshate ligands, was carried out by adding simultaneously uranyl ions (~12µM), Fe^{3+} ions (10µM) and phosphate ligands (100µM) to clay – solution systems at different pH (3-7). U(VI) sorption edge is a S-shape curve showing a pH_{50} value at acidic pH (**Fig.IV- 9**a). The percentage of sorption increases with pH (in the range 3-5) and is almost complete at pH ~5. No significant effect of the presence of Fe ions was observable on the pH_{50} value of uranyl ions. Only a slight decrease in the percentage of sorption of uranyl ions was observed at pH 4 in the presence of Fe ions, which may suggest a very limited competitive effect of Fe ions on U(VI) sorption onto illite, in the presence of phosphate ligands. A very slight decrease in the percentage of Fe sorption at pH 4 is observable when comparing data obtained in the presence and in the absence of uranyl ions (for $[P]_{I,aq}$ = 100µM, **Fig.IV- 9**b). The percentage of phosphate ion sorbed increases slightly with pH (from 15% to 25%) in the pH range 3-5, and decreases with further increase in pH (**Fig.IV- 9**c). For a given pH, the percent sorption of P is slightly higher –and or equal within our analytical uncertainty-, than that recorded under similar conditions without U and Fe, and slightly lower than that recorded in the presence of U only (cf. chapters 2&3). Overall, batch sorption results suggest no important macroscopic signature of a potential competition between sorption onto NaIdP of uranyl ions and Fe ions, in the presence of phosphate ligands.

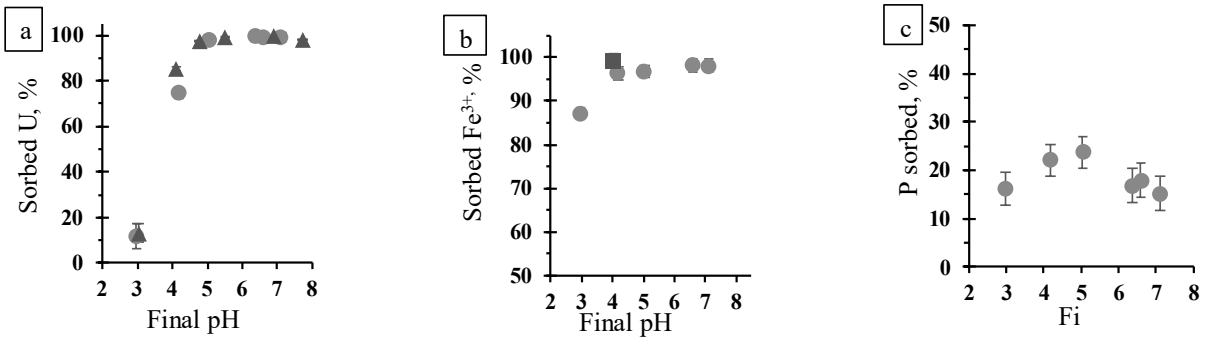

Fig.IV- 9. Results on the macroscopic (co)sorption of (a) UO_2^{2+} ions, (b) Fe^{3+} ions and (c) phosphate ligands added simultaneously to a NaIdP – solution suspension, as a function of final pH (pH_F). Conditions (●): $[U]_{I,aq}$=12µM, $[Fe]_{I,aq}$=10µM and $[P]_{I,aq}$=100µM, 0.005M NaCl electrolyte solution at a $R_{S/L}$ equal to 3g.L^{-1}, t_R=4 days and t_{pre-eq}=3 days. Data of chapter 3 on U sorption in the absence of Fe(III) (▲) and of this chapter on Fe sorption in the absence of U (■) are reported, too.

3.3.2. ATR-FTIR spectroscopy of Fe(III) and U(VI) sorption in the presence of phosphate ligands

Aqueous solutions. Aqueous species analysis was carried out by recording FTIR spectra of aqueous solutions at pH 4 in which uranyl ions, Fe^{3+} ions and phosphate ligands were added simultaneously ($[U]_{I,aq}$=12µM, $[Fe]_{I,aq}$ = 10 µM and $[P]_{I,aq}$ 100µM, 0.005M NaCl electrolyte). The aim was to collect reference spectra that are useful to identifying IR signals of aqueous species and/or precipitates of U(VI)/Fe(III)-phosphate, which can possibly contribute to IR signals collected at NaIdP – phosphate - solution interface during ATR FTIR sorption experiment of Fe and U, and to distinguish between OSSC and ISSC species formed at interface. IR spectra in the range 900-1200cm^{-1} are given in **Fig.IV- 10**a for the "reference" aqueous solution mentioned above. They display an intense band lying at ~1000 cm^{-1} and two weak bands visible at ~925 and ~1125 cm^{-1}. Spectra absorbance increased with increasing reaction time, and remained quite stable after a t_R values of 24 hours. Spectra **Fig.IV- 9**b) showed three well defined and sharp IR bands centered at 923, 997 and 1125 cm^{-1}, respectively. Such FTIR results are similar to those obtained for an aqueous solution containing no iron (with

all conditions being the same, cf. chapter 3), which evidenced the formation of a uranyl phosphate precipitate in solution, i.e., $(UO_2)_3(PO_4)_2 \cdot 4H_2O_{(s)}$, consistently with data of Comarmond et al. [134]. Regarding the molecular structure of the precipitate, monodentate coordination between phosphate and uranyl ions was proposed by Comarmond et al.[134] , and the bands at 997 and 1125 cm^{-1} were attributed to the P-O(H) υ_3 antisymmetric stretching band (which indicated that PO_4 unit has C_{3v} molecular symmetry). The weak band at 923 cm^{-1} was attributed to the υ_3 antisymmetric stretching band of U=O as suggested by Frost. [213], who studied uranyl micas minerals by using the vibrational spectroscopy, i.e., infrared and Raman spectroscopy. As the IR signal was dominated by the presence of the uranyl phosphate precipitate, IR signals attributable to aqueous uranyl-phosphate and/or iron-phosphate complexes species could not be directly observed from IR analysis of the unfiltered solution. Analysis of the solution obtained after ultrafiltration (at 1 kDa), showed a dramatic decrease in IR absorption compared to the unfiltered one (Fig 10a), suggesting that most of (colloidal-sized) uranyl-phosphate precipitate was removed by ultrafiltration procedure. Decomposition of the spectrum recorded for the filtered solution revealed two bands at 1045 and 1150 cm^{-1} (in addition to same bands as those observed at 923, 997 and 1125 cm^{-1} for the native solution). It is to be noted that the shape of the latter bands appeared larger than those observed for the U(VI)-phosphate precipitate, suggesting a possible contribution of aqueous uranyl species having similar band maxima. These results are in good agreement with those obtained by Comarmond et al. [134], who obtained same IR spectral features for a freshly prepared solution and for precipitates formed from an aged solution (under same solution conditions of pH=4, $[U]_{I,aq}$=20µM and $[P]_{I,aq}$=20µM). For the aqueous uranyl-phopshate complex, we already suggested $UO_2HPO_4 \cdot (H_2O)_4$ (or $UO_2H_2PO_4$ $(H_2O)_3OH$)) species having a monodentate coordination mode between uranyl and phosphate ions based on molecular symmetric considerations (cf. chapter 3). In contrast, the bands positioned at 1045 and 1150cm^{-1} that are

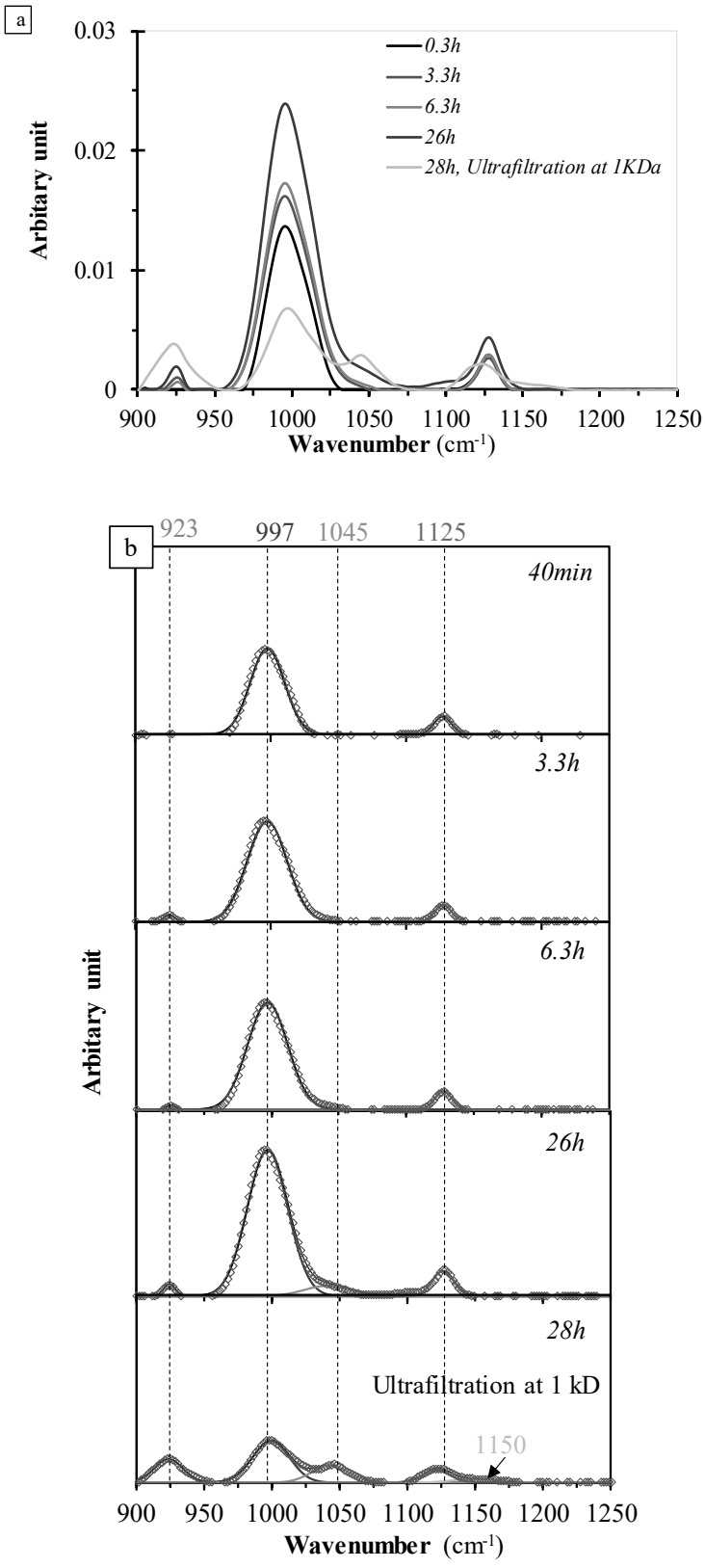

Fig.IV- 10. (a) In-situ ATR-FTIR spectra of aqueous species for the uranyl-iron-phosphate ions system and (b) the result of spectral decomposition. The experiment was carried out at $[U]_{I,aq}$

=10µm, $[Fe]_{I,aq}$=10µm and $[P]_{I,aq}$=100µm and pH 4 with an IS of 0.005M NaCl and a t_{eq} 24 hours.

visible after solution ultrafiltration, cannot be attributed to an aqueous uranyl-phosphate complex because they were not observed in the absence of Fe^{3+} ions (under similar conditions of pH=4, $[U]_{I,aq}$=8µM and $[P]_{I,aq}$=100µM, cf. Chapter 3). These bands may thus be attributed to an aqueous phosphate complex of iron(III). According to speciation calculations (**Fig.IV-3**a), the main iron-phosphate complex species is $FeHPO_4^+$ and $FeH_2PO_4^{2+}$ species is a minor one (l% and less than <0.5% of total concentration of phosphate ions, respectively). $FeHPO_4^+$ has three υ_3 P-O bands at 1042, 1089 and 1147 cm^{-1}, as shown in our spectra collected for a phosphated solution at pH 4 containing Fe(III) ($[Fe]_{I,aq}$=10µM and $[P]_{I,aq}$=100µM, cf. **Fig.IV-7**b in paragraph 3.2.3). However, only the bands at 1045 and 1150 cm^{-1} are visible in the spectrum recorded for the filtered aqueous solution containing both Fe and U ions (**Fig.IV-10**b).

Sorption of iron(III), uranyl ions and phosphate ions at the NaIdP-electrolyte solution interface. Unlike macroscopic results, the IR spectroscopy study described below shows some evidence of competitive sorption between U(VI) and Fe(III) in the presence of phosphate ligands at acidic pH (pH 4). **Fig.IV- 11**a shows in-situ ATR-FTIR spectra collected during 3 days after simultaneous addition of uranyl ions, Fe^{3+} ions and phosphate ligands ($[U]_{I,aq}$=10µM, $[Fe]_{I,aq}$=10µM and $[P]_{I,aq}$=100µM) in a 0.005M NaCl solution at pH 4 contacted with NaIdP. Spectra with low signal-to-noise ratios and low IR absorption were observed, making spectra decomposition and interpretation very difficult. Absorbance slightly increased with increasing reaction time. Based on comparing with IR spectra recorded during the (co)sorption of uranyl and phosphate ions (cf. chapter 3) and iron and phosphate ions (cf. paragraph 3.2.3), it seems that there were three broad bands located at wavenumbers comprised between 1025 and

1050cm^{-1}, 1050 and 1100cm^{-1}, 1050 and 1200cm^{-1}, respectively, at t_R lower than 24 hours. A change in shape of these spectra is observed at t_R values higher than 24 hours. A band at wavenumbers of 1025 - 1050cm^{-1} was found to slightly increase in intensity with time and to become more and more well defined (at t_R > 24 hours). Another band at ca. 1075cm^{-1}, which remained quite constant at t_R < 24 hours, was found to shift to higher wavenumber (at ca. 1082 cm^{-1}) and its intensity increased with time. A shoulder was moreover observable at 1110 - 1150 cm^{-1} at a t_R of 3 days. In contrast, the band at ~1150-1160 cm^{-1} decreased with increasing t_R and disappeared at t_R > 24 hours. At higher wavenumber, a band centered at ~1175 cm^{-1} is well visible at a t_R close to 3 days. Above-mentioned observations therefore suggest the formation of various surface species whose contributions vary as a function of reaction time. Decomposition of the spectra is given in **Fig.IV- 11**b, which shows six bands (at 1039, 1076, 1084, 1119, 1155 and 1175cm^{-1}). All these bands could be attributed to P-O stretching bands (υ_3). As previously described, the bands at 1076 and 1155 cm^{-1} are ascribed to the OSSC of $H_2PO_4^-$, i.e., ≡S··· $H_2PO_4^-$, formed via electrostatic forces and/or hydrogen bonding between the $H_2PO_4^-$ ions and the particle surface (P species A, cf. chapter 2). The species likely disappears with time to transform slowly into other surface species. Our previous study of uranyl sorption onto NaIdP in the presence of phosphate ions showed formation of three types of surface species, whose formation was dependent on reaction time and U concentration (cf. chapter 3 and Table C1). A rapidly-formed U-P species had a (weak) IR band at ~1125 cm^{-1}, which was independent of concentration of uranyl ions (2–10 µM), and was ascribed an ISSC of uranyl phosphate whose formation took place at high-affinity sites existing in limited amounts onto clay edges. The rapidly - formed U-P species B displayed an IR band at ~1050 cm^{-1} whose intensity increased with U concentration in the range 2-8 µM, and it was ascribed to a uranyl phosphato ISSC forming at low affinity sites onto clay edges, which predominated U speciation at low reaction times and appeared to be stable in the long term. Another uranyl-

phosphate surface species was formed at a long reaction time and / or at a high U concentration (U-P species C with three υ_3 P-O antisymmetric stretching band at 1114, 1080 and 992 cm^{-1}, which indicated a C_{2V} or lower molecular symmetry of PO_4 unit). Its bands position were found to be shifted significantly with respect to those reported for the group of autunite minerals in the literature but they compared well with them: 1118, 1074 and 985 cm^{-1} for autunite, and 1118, 1048 and 985 cm^{-1} for meta-autunite [213]. Hence, the U-P species C was hypothesized to be an autunite-like surface precipitate. Based on these previous results, there appears that no ISSC of uranyl phosphate were formed at NaIdP-phosphate-solution interface, in the presence of Fe ions. Only uranyl-phosphate surface precipitates were found to exist in low amounts and in the long term. Formation of Fe(III) phosphate surface precipitates is also possible (as these species have a main band peaking at ca. 1080cm^{-1} (cf. paragraph 3.2.3). The band observable at 1039cm^{-1} in **Fig.IV- 11**b accounts probably to formation of an inner-sphere phosphate surface complex (P species B having IR bands at 1035 cm^{-1} that predominates at high reaction time, cf. chapter 2) formed at edge sites of the clay platelets.

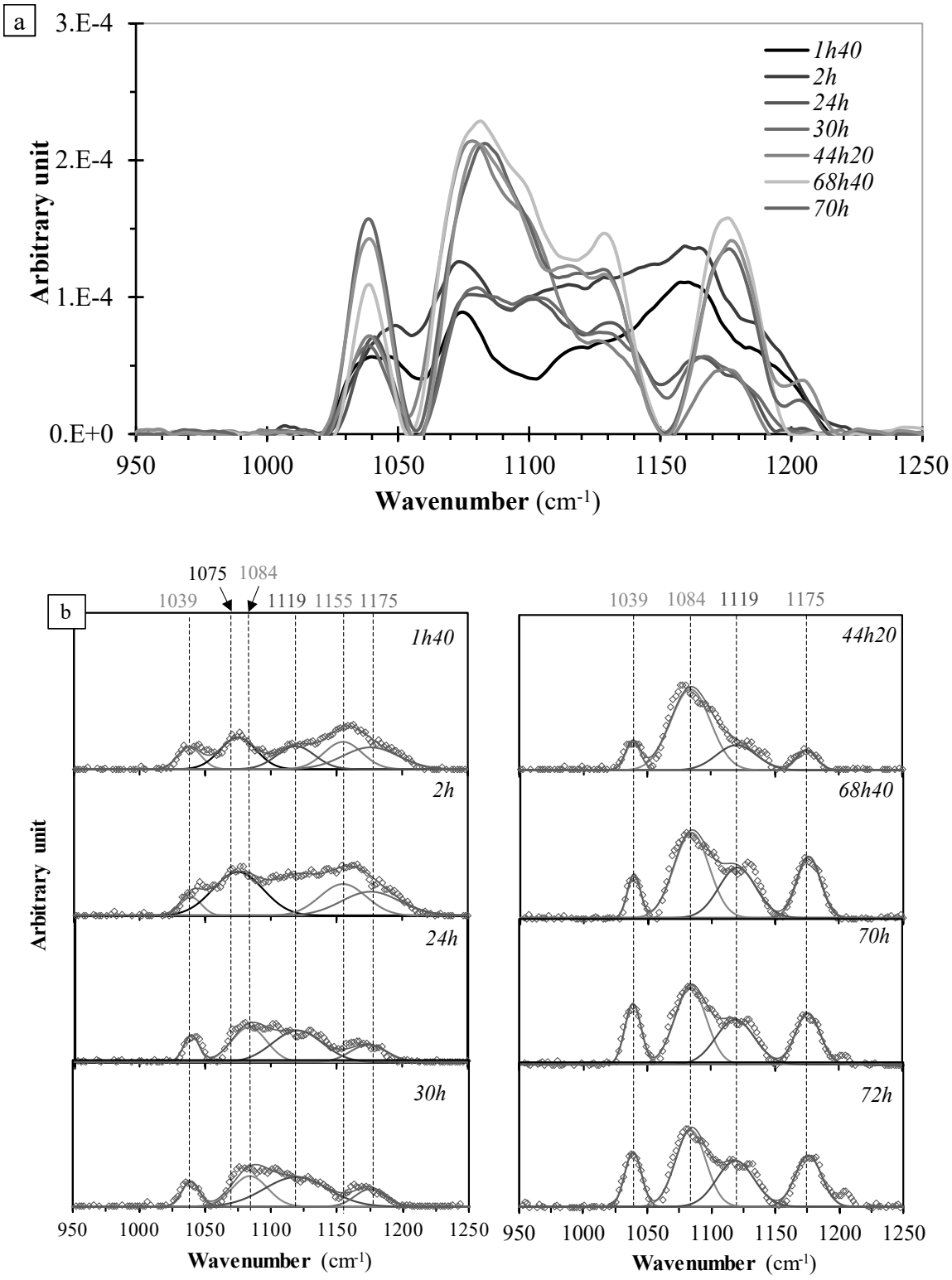

Fig.IV- 11. (a) In-situ ATR-FTIR spectra of simultaneous presence of uranyl, iron, and phosphate ligands at the NaIdP – solution interface and (b) the result of spectral decomposition. The experiment was carried out at pH 4, a t_R of 3 days and $[U]_{I,aq}$=10µm, $[Fe]_{I,aq}$=10µm and $[P]_{I,aq}$=100µm with an IS of 0.005M NaCl.

4. Summary and conclusions

First, reference spectra were obtained for the species formed in / from electrolyte solutions at pH 4 containing U(VI) and/or Fe(III) ions (10µM), in the presence of phosphate ligands (100µM). Speciation calculation showed that the main aqueous species expected to exist in these solutions at pH 4 are the ferric phosphate complex i.e., $FeHPO_4^+$, and the diprotonated phosphate ions i.e., $H_2PO_4^-$ (in the absence of U, at pH 4 and at ionic strength of 0.005M NaCl). IR bands presented here for these aqueous species are in good agreement with those reported in the literature. Aqueous speciation calculations and the in-situ ATR-FTIR analyses conducted for the ternary U(VI)-Fe(III)-phosphate system studied indicated the formation of three species: a U(VI)-phosphate precipitate ((UO2)3(PO4)2·4H2O(s)), an aqueous complex ($UO_2HPO_4 \cdot (H_2O)_4$) which has the same IR band position, and a Fe(III)-phosphate aqueous complex ($FeHPO_4^+$).

Second, the co-sorption of Fe and phosphate ions onto illite was investigated. The kinetics of Fe(III) ions sorption was studied experimentally and the macroscopic sorption results indicated two steps of Fe(III) sorption in the pH range 4-7, with the iron sorption being almost complete at a reaction time of 24 hours. Results of EM measurements (providing information on the surface charge of illite as a function of pH) suggested the formation of positively charged Fe-phosphato surface species at acidic pH (~4) and uncharged Fe-phosphato surface species and/or Fe-phosphate surface precipitates at higher pH, and / or the formation of Fe-colloids. Sorption isotherm of iron ions ($[Fe]_{I,aq}$=2-15µM) acquired in the presence of phosphate ions (100µM) at pH 4 showed a nearly complete Fe sorption. At low initial Fe concentration (2µM), a slight increase in percent of Fe sorption onto NaIdP was observed when adding phosphate ions, suggesting that formation of ternary complexes of iron-phosphate at illite surface promoted Fe sorption. In contrast, the amount of phosphate ions sorbed was found to decrease with increasing $[Fe]_{I,aq}$ (at $[Fe]_{I,aq}$ <4µM) suggesting a competitive sorption between iron and

phosphate ions for the high affinity sites (strong sites) at clay surface. At high $[Fe]_{I,aq}$ (4-10µM), the amount of iron sorbed increased with increasing the amount of phosphate sorbed. As surface charge of illite remained constant during co-sorption, formation of uncharged iron-phosphato surface complexes and/or Fe-phosphate surface precipitates was suggested. The in-situ ATR-FTIR analysis for the (co)sorption of iron and phosphate ions at the NaIdP-electrolyte solution interface at pH 4 suggested the formation of several Fe(III)-phosphate surface species: a monodentate mononuclear complex (e.g., ≡SO-$FeHPO_4$ and/or $(FeO)PO_3$-H), a monoprotonated bidentate complex (e.g., $(FeO)_2OHPO$)) and a surface precipitate (at high $[Fe]_{I,aq}$).

There was observed that Fe ions had a very slight effect on the macroscopic sorption of U(VI) ions onto illite, in the presence of phosphate ligands. In contrast, results of in-situ ATR-FTIR monitoring of simultaneous sorption of U(VI), Fe(III) and phosphate ions at the NaIdP-electrolyte solution interface at pH 4 evidenced an important effect of Fe(III) on the U(VI) surface speciation. Only Fe(III)-phosphate precipitates and/or a small amount of uranyl-phosphate precipitates could be formed at the illite surface, in the investigated conditions. It seems that no uranyl-phosphate surface complexes could be formed in the investigated system, highlighting a strong effect of iron ions on sorption of U(VI), in presence of phosphate ligands.

To our best knowledge, the present study is the first molecular-level study showing the strong effect of Fe(III) ions on the surface speciation of U(VI) ions onto a clay mineral, in the presence of phosphate ligands. As Fe(III) could be released substantially during the long-term degradation of the near-field multi-barriers system in HLW repositories, and phosphate ions are omnipresent in (ground)waters, results of the present study may serve to better understand the effect of the presence of Fe(III) ions on the migration / retention of U(VI) from repository to the (sub)surface environments.

General conclusion and perspectives

Our work was carried out under the context of the storage of radioactive waste in the deep geological repositories in argillaceous formation as host rock. A critical issue of the repository safety is the degradation of the near-field multi-barrier system in the long-term, as it could lead to the progressive migration of RNs from the disposal to human-assessable (sub)surface environments over a long period of time. A refined understanding of the immobilization of the RNs by their sorption onto host rock minerals is thus important to the safety assessment of such repositories. Our work contributes to the understanding at molecule level of the sorption mechanisms of uranium(VI) (as a main radionuclide in the spent nuclear fuel) onto Illite (as an important and even major clay mineral in the host rock formation in some radioactive waste repositories) under different model systems by combining the results of the traditional batch sorption experiments, the electrophoretic mobility analysis and the *in situ* ATR FTIR spectroscopy monitoring of the Illite-solution interface throughout the (co)-sorption process.

Phosphate ions sorption onto Illite

We first studied the sorption of phosphate ligands at the Illite – electrolyte solution interface as a preliminary study to investigating the co-sorption of uranyl and phosphate ions at the interface. We investigated the mechanisms of phosphate ion sorption on a homoionic Na-Illite, over a range of aqueous phosphate concentrations (20-250 µM) and clay-solution ratios leading to low to moderate coverage (2-6 $\mu mol.g^{-1}$) of the clay surface by phosphate. Macroscopic data indicated that the percentage of phosphate sorption is dependent on pH (for pH > 6), aqueous phosphate concentration, and the clay-to-solution ratio of the experiment, *i.e.*, the surface coverage of the clay by phosphate. The macroscopic and EM data further suggested a predominant mechanism of strong sorption of phosphate ions onto Illite, which confers negative charges on the mineral surface and involves several sorption species and/or surface sites present on the clay edges (limited amounts of high-affinity and low-affinity aluminol sites,

respectively). In situ IR data showed that, at acidic pH, three types of phosphate surface species form at the Illite-solution interface: an outer-sphere surface complex (OSSC) of phosphate ($\equiv SOH_2^+ \cdots H_2PO_4^-$), an inner-sphere surface complex (ISSC) of phosphate, probably a monodentate binuclear surface complex ($\equiv (SO)_2PO_2$), and, in very limited amounts, a monoprotonated monodentate binuclear surface complex ($\equiv (SO)_2(OH)PO$) or an Al-phosphate surface precipitate. Sorption of phosphate ions proceeds by the initial formation of the OSSC of phosphate, which dominates phosphate surface speciation only at short reaction times (< 1 day) and low aqueous phosphate concentrations, and which transforms with time into the ISSC of phosphate.

Co-sorption of uranyl and phosphate ions onto Illite

We then studied the mechanisms of sorption of trace levels of uranyl ions (1-10µM) and their co-sorption in the presence of phosphate ligands (50µM-250µM) on the surface of a homoionic Na-illite. Macroscopic data indicated that the percentage of uranyl sorption is dependent on pH, on aqueous U concentration and clay-to-solution ratio of the experiment, *i.e.*, the clay surface coverage by U, as well as on the presence and concentration of phosphate ligands. The macroscopic and EM data suggested mostly reversible mechanisms of P and U co-sorption that confer negative charges on the mineral surface and involve several types of uranyl phosphate surface species, depending on key parameters and/or surface sites present on the clay edges (limited amounts of high-affinity and low-affinity sites, respectively). In situ IR data provided evidence that, at acidic pH, three types of inner sphere uranyl phosphate surface complex form at the illite-solution interface, under the conditions studied. Two surface complexes formed rapidly at high and low affinity surface sites, respectively, with formation of the latter increasing with U surface coverage, and competed successfully against formation of outer-sphere and inner sphere surface complexes of phosphate. At high U concentration (10µM) and reaction

time (>1day), a third U-P surface complex having an autunite-like structure (likely as U-P polynuclear surface species) appears to additionally form on the NaIdP surface.

Co-sorption of iron(III) and phosphate ions onto Illite

In the third part, we investigated the Fe^{III} sorption at trace level (2-15µM) and their co-sorption in the presence of phosphate ligands (20 and 100µM) on the surface of a homoionic Na-Illite. The sorption edge of Fe ions indicates that the sorption of Fe is almost complete in the absence and presence of phosphate ions (20 and 100µM) over a wide pH range (4-8) at $R_{S/L}$: 3 g/L with a contact time of 24 hours. Sorption of small amounts of Fe ions decreases the negative surface charge of Illite, weakly in the presence of phosphate ligands and more weakly in the absence of phosphate ligands in the studied pH range. There is no change in the EM of Illite for surface coverage of iron in the $[Fe]_{I,aq}$ range of 2-10µM at pH 4 in the presence of phosphate (100µM). Phosphate sorption decreases at $[Fe]_{I,aq} \leq 2\mu M$ and then increases nonlinearly with sorbed Fe. According to the results of the sorption of Fe ions, phosphate ions and of the EM of Illite, , different sorption mechanisms in the phosphate-Fe-illite-solution system have been suggested: (i) sorption competition between Fe and phosphate ions for strong sites of the clay with low surface coverage of Fe, (ii) competition between the co-sorption of Fe-phosphate onto Illite and the formation of Fe-phosphate aqueous complexes for the $[Fe]_{I,aq} > 2\mu M$ and the increasing surface coverage of Fe ions, (iii) at high $[Fe]_{I,aq}$ and $[P]_{I,aq}$, a slight increase in phosphate sorption with Fe suggesting surface precipitation of iron-phosphate onto illite. In-situ infrared spectroscopy results for the (co)sorption of Fe (10 µM) and P (100µM) at pH 4 show that bands at 970, 1000 1084, and 1112 cm^{-1}, increasing with contact time up to 3 hours, suggest an ISC or surface precipitate of Fe-phosphate based on the comparison with the literature data. The band at 1140 cm^{-1} may suggest the formation of OSC of $FeHPO_4^+$ or hydrogen bonding between

$FeHPO_4^+$ and the illite surface because the band at 1140 cm^{-1} may be slightly shifted from the band at 1147 cm^{-1} of aqueous $FeHPO_4^+$ due to electrostatic forces or hydrogen bond(s).

Competitive effect of iron(III) on the sorption of uranyl ions onto Illite in the presence of phosphate ligands

In the last part, a more complex model system has been carried out in this work. We tried to study the competition effects between Fe^{III} and U^{VI} in the presence of phosphate ligands at the Illite – solution interface. The results of batch sorption experiments for the simultaneous addition of U (10µM) and Fe (10µM) in the presence of phosphate (100µM) at pH 4 and $R_{S/L}$ 3g/L show a slight decrease in the sorption of U and Fe ions, suggesting a competition effect between U and Fe ions for the surface sites of the clay. However, the sorption amount of phosphate ions remains quite constant, comparing to the co-sorption results of uranyl and phosphate ions at the interface. In-situ infrared spectroscopy results obtained under the same conditions show a decrease in overall absorbance, comparing to the co-sorption of U-phosphate and Fe-phosphate at the interface, respectively. The spectra exhibit absorbances at 1039 cm^{-1} and at the wavenumber range between 1055 and 1200 cm^{-1} after 20 hours. Spectral decomposition results show the absence of the band at 1050 cm^{-1}, which was attributed to the formation of the ISC of U-P at short reaction time or low $[U]_{I,aq}$. This may suggest a competition effect between U and Fe for the surface sites of the clay. The bands identified at 1083 and 1120 cm^{-1} may suggest the formation of an ISC or surface precipitate of Fe-P or an autunite-like precipitate of U-P at the clay surface. The band at 1083 cm^{-1} increases with reaction time, suggesting the formation of an ISC of U-P at the Illite surface. Comparing the band at 1114 cm^{-1} and 1112 cm^{-1} identified respectively in the co-sorption experiments of U-P and Fe-P to the band at 1120 cm^{-1} identified in the Fe-U-P-Illite-solution system, the latter band is broader, and its absorbance is higher, which may suggest a limited precipitate of U-P onto the clay. The band

at 1039 cm^{-1} corresponds to the ISC of phosphate formed at the illite surface. The band at 1175 cm^{-1} may suggest an ISC or surface precipitate of U-P. The decrease in overall absorbance in the wavenumber range of 900-1200 cm^{-1} may be explained by the competitive effects on surface sites of the clay.

Our work could be helpful for a refined understanding of the transport and retention process of uranyl ions in clay systems in the presence of phosphate and/or iron(III) ions, and for the transferability of experimental/mechanical data obtained on the behavior of uranyl to "real systems". This could be an essential aid in assessing the safety of radioactive waste disposal in deep clay rock formations.

Although some experiments of the effects of carbonate ligands and nickel ions on the U(VI) sorption at the Illite – electrolyte solution interface have been conducted during this work, some macroscopic and *in-situ* ATR FTIR data remain to be processed and interpreted. It should be noted that, according to our IR spectral results obtained for the sorption of U(VI) at trace level (1-10µM) in the presence of high concentration of carbonate ligands, the *in-situ* ATR FTIR measurements for the sorption of trace level of U(VI) at the Illite – electrolyte solution interface showed very little information that could be related to the U(VI)-carbonate surface species. Therefore, higher concentrations of U(VI) than those used in the previous experiments are in progress in order to gain significant IR signals linking to U(VI)-carbonate surface species. Another worthy work to be tried in future studies, it is the adsorption modeling for the U(VI) sorption in the presence of inorganic ligands (such as phosphate and carbonate ligands) and/or competitive cations (such as Fe(III) and Ni).

References

References

[1] B. Grambow, Geological Disposal of Radioactive Waste in Clay, ELEMENTS. 12 (2016) 239–245. https://doi.org/10.2113/gselements.12.4.239.

[2] G. Sposito, N.T. Skipper, R. Sutton, S. -h. Park, A.K. Soper, J.A. Greathouse, Surface geochemistry of the clay minerals, Proceedings of the National Academy of Sciences. 96 (1999) 3358–3364. https://doi.org/10.1073/pnas.96.7.3358.

[3] M. Marques Fernandes, B. Baeyens, R. Dähn, A.C. Scheinost, M.H. Bradbury, U(VI) sorption on montmorillonite in the absence and presence of carbonate: A macroscopic and microscopic study, Geochimica et Cosmochimica Acta. 93 (2012) 262–277. https://doi.org/10.1016/j.gca.2012.04.017.

[4] E.R. Sylwester, E.A. Hudson, P.G. Allen, The structure of uranium (VI) sorption complexes on silica, alumina, and montmorillonite, Geochimica et Cosmochimica Acta. 64 (2000) 2431–2438. https://doi.org/10.1016/S0016-7037(00)00376-8.

[5] L.D. Troyer, F. Maillot, Z. Wang, Z. Wang, V.S. Mehta, D.E. Giammar, J.G. Catalano, Effect of phosphate on U(VI) sorption to montmorillonite: Ternary complexation and precipitation barriers, Geochimica et Cosmochimica Acta. 175 (2016) 86–99. https://doi.org/10.1016/j.gca.2015.11.029.

[6] C. Tournassat, R.M. Tinnacher, S. Grangeon, J.A. Davis, Modeling uranium(VI) adsorption onto montmorillonite under varying carbonate concentrations: A surface complexation model accounting for the spillover effect on surface potential, Geochimica et Cosmochimica Acta. 220 (2018) 291–308. https://doi.org/10.1016/j.gca.2017.09.049.

[7] G. Montavon, S. Ribet, Y.H. Loni, F. Maia, C. Bailly, K. David, C. Lerouge, B. Madé, J.C. Robinet, B. Grambow, Uranium retention in a Callovo-Oxfordian clay rock formation: From laboratory-based models to in natura conditions, Chemosphere. 299 (2022) 134307. https://doi.org/10.1016/j.chemosphere.2022.134307.

[8] M. Del Nero, A. Froideval, C. Gaillard, G. Mignot, R. Barillon, I. Munier, A. Ozgümüs, Mechanisms of uranyl sorption, Geological Society, London, Special Publications. 236 (2004) 545–560. https://doi.org/10.1144/GSL.SP.2004.236.01.30.

[9] Y. Tang, R.J. Reeder, Uranyl and arsenate cosorption on aluminum oxide surface, Geochimica et Cosmochimica Acta. 73 (2009) 2727–2743. https://doi.org/10.1016/j.gca.2009.02.003.

[10] T. Hiemstra, W.H.V. Riemsdijk, A. Rossberg, K.-U. Ulrich, A surface structural model for ferrihydrite II: Adsorption of uranyl and carbonate, Geochimica et Cosmochimica Acta. 73 (2009) 4437–4451. https://doi.org/10.1016/j.gca.2009.04.035.

[11] C. Galindo, M.D. Nero, R. Barillon, E. Halter, B. Made, Mechanisms of uranyl and phosphate (co)sorption: Complexation and precipitation at α-Al2O3 surfaces, Journal of Colloid and Interface Science. 347 (2010) 282–289. https://doi.org/10.1016/j.jcis.2010.03.045.

[12] A. Singh, J.G. Catalano, K.-U. Ulrich, D.E. Giammar, Molecular-Scale Structure of Uranium(VI) Immobilized with Goethite and Phosphate, Environ. Sci. Technol. 46 (2012) 6594–6603. https://doi.org/10.1021/es300494x.

[13] Y. Jo, J.-Y. Lee, J.-I. Yun, Adsorption of uranyl tricarbonate and calcium uranyl carbonate onto γ-alumina, Applied Geochemistry. 94 (2018) 28–34. https://doi.org/10.1016/j.apgeochem.2018.05.004.

[14] M.A. Glaus, M. Aertsens, N. Maes, L. Van Laer, L.R. Van Loon, Treatment of boundary conditions in through-diffusion: A case study of 85Sr2+ diffusion in compacted illite, Journal of Contaminant Hydrology. 177–178 (2015) 239–248. https://doi.org/10.1016/j.jconhyd.2015.03.010.

[15] M.I. Tejedor-Tejedor, M.A. Anderson, The protonation of phosphate on the surface of goethite as studied by CIR-FTIR and electrophoretic mobility, Langmuir. 6 (1990) 602–611. https://doi.org/10.1021/la00093a015.
[16] Y. Arai, D.L. Sparks, ATR–FTIR Spectroscopic Investigation on Phosphate Adsorption Mechanisms at the Ferrihydrite–Water Interface, Journal of Colloid and Interface Science. 241 (2001) 317–326. https://doi.org/10.1006/jcis.2001.7773.
[17] J.R. Bargar, J.D. Kubicki, R. Reitmeyer, J.A. Davis, ATR-FTIR spectroscopic characterization of coexisting carbonate surface complexes on hematite, Geochimica et Cosmochimica Acta. 69 (2005) 1527–1542. https://doi.org/10.1016/j.gca.2004.08.002.
[18] G. Limousin, J.-P. Gaudet, L. Charlet, S. Szenknect, V. Barthès, M. Krimissa, Sorption isotherms: A review on physical bases, modeling and measurement, Applied Geochemistry. 22 (2007) 249–275. https://doi.org/10.1016/j.apgeochem.2006.09.010.
[19] S. Laura, B. Phiippe, S. Werner, Chimie des milieux aquatiques, 5e ed., Dunod, 2014. https://www.dunod.com/sciences-techniques/chimie-milieux-aquatiques (accessed April 8, 2023).
[20] A. Manceau, M.A. Marcus, N. Tamura, Quantitative Speciation of Heavy Metals in Soils and Sediments by Synchrotron X-ray Techniques, Rev Mineral Geochem. 49 (2002) 341–428.
[21] W. Stumm, L. Sigg, B. Sulzberger, Chemistry of the solid-water interface: processes at the mineral-water and particle-water interface in natural systems, Wiley, New York, 1992.
[22] C. Tournassat, I.C. Bourg, C.I. Steefel, F. Bergaya, Surface Properties of Clay Minerals, in: Developments in Clay Science, Elsevier, 2015: pp. 5–31. https://doi.org/10.1016/B978-0-08-100027-4.00001-2.
[23] E.J. Elzinga, D.L. Sparks, Phosphate adsorption onto hematite: An in situ ATR-FTIR investigation of the effects of pH and loading level on the mode of phosphate surface complexation, Journal of Colloid and Interface Science. 308 (2007) 53–70. https://doi.org/10.1016/j.jcis.2006.12.061.
[24] W. Stumm, Aquatic colloids as chemical reactants: surface structure and reactivity, (1993).
[25] P. Schindler, H.R. Kamber, Die Acidität von Silanolgruppen. Vorläufige Mitteillung, HCA. 51 (1968) 1781–1786. https://doi.org/10.1002/hlca.19680510738.
[26] Werner. Stumm, C.-B. Huang, S.R. Jenkins, Specific Chemical Interaction Affecting the Stability of Dispersed Systems, CROATICA CHEMICA ACTA. (1970).
[27] R.O. James, T.W. Healy, Adsorption of hydrolyzable metal ions at the oxide—water interface. II. Charge reversal of SiO2 and TiO2 colloids by adsorbed Co(II), La(III), and Th(IV) as model systems, Journal of Colloid and Interface Science. 40 (1972) 53–64. https://doi.org/10.1016/0021-9797(72)90173-7.
[28] J. Bowden, S. Nagarajah, N. Barrow, A. Posner, J. Quirk, Describing the adsorption of phosphate, citrate and selenite on a variable-charge mineral surface, Soil Res. 18 (1980) 49. https://doi.org/10.1071/SR9800049.
[29] N. Sahai, D.A. Sverjensky, Evaluation of internally consistent parameters for the triple-layer model by the systematic analysis of oxide surface titration data, Geochimica et Cosmochimica Acta. 61 (1997) 2801–2826. https://doi.org/10.1016/S0016-7037(97)00128-2.
[30] J.A. Davis, D.B. Kent, CHAPTER 5. SURFACE COMPLEXATION MODELING IN AQUEOUS GEOCHEMISTRY, in: M.F. Hochella, A.F. White (Eds.), Mineral-Water Interface Geochemistry, De Gruyter, 1990: pp. 177–260. https://doi.org/10.1515/9781501509131-009.

[31] G.E. Brown, How Minerals React with Water, Science. 294 (2001) 67–69. https://doi.org/10.1126/science.1063544.
[32] L. Pauling, THE STRUCTURE OF THE CHLORITES, Proc. Natl. Acad. Sci. U.S.A. 16 (1930) 578–582. https://doi.org/10.1073/pnas.16.9.578.
[33] G. Sposito, The surface chemistry of soils, Oxford University Press ; Clarendon Press, New York : Oxford [Oxfordshire], 1984.
[34] V.E. Jackson, K.E. Gutowski, D.A. Dixon, Density Functional Theory Study of the Complexation of the Uranyl Dication with Anionic Phosphate Ligands with and without Water Molecules, J. Phys. Chem. A. 117 (2013) 8939–8957. https://doi.org/10.1021/jp405470k.
[35] P.C. Burns, U6+ MINERALS AND INORGANIC COMPOUNDS: INSIGHTS INTO AN EXPANDED STRUCTURAL HIERARCHY OF CRYSTAL STRUCTURES, The Canadian Mineralogist. 43 (2005) 1839–1894. https://doi.org/10.2113/gscanmin.43.6.1839.
[36] I. Grenthe, J. Fuger, R.J.M. Konings, R.J. Lemire, A.B. Muller, C. Nguyen-Trung, H. Wanner, Chemical Thermodynamics of Uranium, (1992).
[37] W.M. Murphy, E.L. Shock, 5. Environmental Aqueous Geochemistry of Actinides, in: P.C. Burns, R.J. Finch (Eds.), Uranium, De Gruyter, 1999: pp. 221–254. https://doi.org/10.1515/9781501509193-010.
[38] K. Maher, J.R. Bargar, G.E. Brown, Environmental Speciation of Actinides, Inorg. Chem. 52 (2013) 3510–3532. https://doi.org/10.1021/ic301686d.
[39] G.R. Choppin, Soluble rare earth and actinide species in seawater, Marine Chemistry. 28 (1989) 19–26. https://doi.org/10.1016/0304-4203(89)90184-9.
[40] I. Grenthe, J. Fuger, R.J. Lemire, A.B. Muller, C. Nguyen-Trung Cregu, H. Wanner, Chemical thermodynamics of uranium, Elsevier Science Publishers, Netherlands, 1992.
[41] V. Eliet, G. Bidoglio, N. Omenetto, L. Parma, I. Grenthe, Characterisation of hydroxide complexes of uranium(VI) by time-resolved fluorescence spectroscopy, Faraday Trans. 91 (1995) 2275. https://doi.org/10.1039/ft9959102275.
[42] R.J. Silva, H. Nitsche, Actinide Environmental Chemistry:, Radiochimica Acta. 70–71 (1995) 377–396. https://doi.org/10.1524/ract.1995.7071.s1.377.
[43] S. Pompe, K. Schmeide, M. Bubner, G. Geipel, K.H. Heise, G. Bernhard, H. Nitsche, Investigation of humic acid complexation behavior with uranyl ions using modified synthetic and natural humic acids:, Radiochimica Acta. 88 (2000) 553–558. https://doi.org/10.1524/ract.2000.88.9-11.553.
[44] S.A. Cumberland, G. Douglas, K. Grice, J.W. Moreau, Uranium mobility in organic matter-rich sediments: A review of geological and geochemical processes, Earth-Science Reviews. 159 (2016) 160–185. https://doi.org/10.1016/j.earscirev.2016.05.010.
[45] A. Sandino, J. Bruno, The solubility of (UO2)3(PO4)2 4H20(s) and the formation of U(VI) phosphate complexes: Their influence in uranium speciation in natural waters, Geochimica et Cosmochimica Acta. 56 (1992) 4135–4145. https://doi.org/10.1016/0016-7037(92)90256-I.
[46] D. Gorman-Lewis, P.C. Burns, J.B. Fein, Review of uranyl mineral solubility measurements, The Journal of Chemical Thermodynamics. 40 (2008) 335–352. https://doi.org/10.1016/j.jct.2007.12.004.
[47] W. Um, Z. Wang, R.J. Serne, B.D. Williams, C.F. Brown, C.J. Dodge, A.J. Francis, Uranium Phases in Contaminated Sediments below Hanford's U Tank Farm, Environ. Sci. Technol. 43 (2009) 4280–4286. https://doi.org/10.1021/es900203r.
[48] D. Gorman-Lewis, T. Shvareva, K.-A. Kubatko, P.C. Burns, D.M. Wellman, B. McNamara, J.E.S. Szymanowski, A. Navrotsky, J.B. Fein, Thermodynamic Properties of Autunite, Uranyl Hydrogen Phosphate, and Uranyl Orthophosphate from Solubility and

Calorimetric Measurements, Environ. Sci. Technol. 43 (2009) 7416–7422. https://doi.org/10.1021/es9012933.
[49] M.F. Fanizza, H. Yoon, C. Zhang, M. Oostrom, T.W. Wietsma, N.J. Hess, M.E. Bowden, T.J. Strathmann, K.T. Finneran, C.J. Werth, Pore-scale evaluation of uranyl phosphate precipitation in a model groundwater system, Water Resources Research. 49 (2013) 874–890. https://doi.org/10.1002/wrcr.20088.
[50] V.S. Mehta, F. Maillot, Z. Wang, J.G. Catalano, D.E. Giammar, Effect of co-solutes on the products and solubility of uranium(VI) precipitated with phosphate, Chemical Geology. 364 (2014) 66–75. https://doi.org/10.1016/j.chemgeo.2013.12.002.
[51] M. Kanematsu, N. Perdrial, W. Um, J. Chorover, P.A. O'Day, Influence of Phosphate and Silica on U(VI) Precipitation from Acidic and Neutralized Wastewaters, Environ. Sci. Technol. 48 (2014) 6097–6106. https://doi.org/10.1021/es4056559.
[52] A. Sandino, J. Bruno, The solubility of (UO2)3(PO4)2 4H20(s) and the formation of U(VI) phosphate complexes: Their influence in uranium speciation in natural waters, Geochimica et Cosmochimica Acta. 56 (1992) 4135–4145. https://doi.org/10.1016/0016-7037(92)90256-I.
[53] J. Bruno, L. Duro, M. Grivé, The applicability and limitations of thermodynamic geochemical models to simulate trace element behaviour in natural waters. Lessons learned from natural analogue studies, Chemical Geology. 190 (2002) 371–393. https://doi.org/10.1016/S0009-2541(02)00126-2.
[54] K.H. Johannesson, W.B. Lyons, K.J. Stetzenbach, R.H. Byrne, The solubility control of rare earth elements in natural terrestrial waters and the significance of PO 4 3? and CO 3 2? in limiting dissolved rare earth concentrations: A review of recent information, Aquat Geochem. 1 (1995) 157–173. https://doi.org/10.1007/BF00702889.
[55] D. Gorman-Lewis, T. Shvareva, K.-A. Kubatko, P.C. Burns, D.M. Wellman, B. McNamara, J.E.S. Szymanowski, A. Navrotsky, J.B. Fein, Thermodynamic Properties of Autunite, Uranyl Hydrogen Phosphate, and Uranyl Orthophosphate from Solubility and Calorimetric Measurements, Environ. Sci. Technol. 43 (2009) 7416–7422. https://doi.org/10.1021/es9012933.
[56] M.F. Fanizza, H. Yoon, C. Zhang, M. Oostrom, T.W. Wietsma, N.J. Hess, M.E. Bowden, T.J. Strathmann, K.T. Finneran, C.J. Werth, Pore-scale evaluation of uranyl phosphate precipitation in a model groundwater system, Water Resources Research. 49 (2013) 874–890. https://doi.org/10.1002/wrcr.20088.
[57] M. Kanematsu, N. Perdrial, W. Um, J. Chorover, P.A. O'Day, Influence of Phosphate and Silica on U(VI) Precipitation from Acidic and Neutralized Wastewaters, Environ. Sci. Technol. 48 (2014) 6097–6106. https://doi.org/10.1021/es4056559.
[58] V.S. Mehta, F. Maillot, Z. Wang, J.G. Catalano, D.E. Giammar, Effect of co-solutes on the products and solubility of uranium(VI) precipitated with phosphate, Chemical Geology. 364 (2014) 66–75. https://doi.org/10.1016/j.chemgeo.2013.12.002.
[59] W. Um, Z. Wang, R.J. Serne, B.D. Williams, C.F. Brown, C.J. Dodge, A.J. Francis, Uranium Phases in Contaminated Sediments below Hanford's U Tank Farm, Environ. Sci. Technol. 43 (2009) 4280–4286. https://doi.org/10.1021/es900203r.
[60] D.E. Morris, P.G. Allen, J.M. Berg, C.J. Chisholm-Brause, S.D. Conradson, R.J. Donohoe, N.J. Hess, J.A. Musgrave, C.D. Tait, Speciation of Uranium in Fernald Soils by Molecular Spectroscopic Methods: Characterization of Untreated Soils, Environ. Sci. Technol. 30 (1996) 2322–2331. https://doi.org/10.1021/es950745i.
[61] T. Murakami, T. Ohnuki, H. Isobe, T. Sato, Mobility of uranium during weathering, American Mineralogist. 82 (1997) 888–899. https://doi.org/10.2138/am-1997-9-1006.

[62] R. Finch, T. Murakami, 3. Systematics and Paragenesis of Uranium Minerals, in: P.C. Burns, R.J. Finch (Eds.), Uranium, De Gruyter, 1999: pp. 91–180. https://doi.org/10.1515/9781501509193-008.
[63] J.L. Jerden, A.K. Sinha, L. Zelazny, Natural immobilization of uranium by phosphate mineralization in an oxidizing saprolite–soil profile: chemical weathering of the Coles Hill uranium deposit, Virginia, Chemical Geology. 199 (2003) 129–157. https://doi.org/10.1016/S0009-2541(03)00080-9.
[64] J.G. Catalano, J.P. McKinley, J.M. Zachara, S.M. Heald, S.C. Smith, G.E. Brown, Changes in Uranium Speciation through a Depth Sequence of Contaminated Hanford Sediments, Environ. Sci. Technol. 40 (2006) 2517–2524. https://doi.org/10.1021/es0520969.
[65] J.L. Jerden, A.K. Sinha, Geochemical coupling of uranium and phosphorous in soils overlying an unmined uranium deposit: Coles Hill, Virginia, Journal of Geochemical Exploration. 91 (2006) 56–70. https://doi.org/10.1016/j.gexplo.2005.12.003.
[66] Y. Arai, D.L. Sparks, Phosphate Reaction Dynamics in Soils and Soil Components: A Multiscale Approach, in: Advances in Agronomy, Elsevier, 2007: pp. 135–179. https://doi.org/10.1016/S0065-2113(06)94003-6.
[67] D.M. Singer, J.M. Zachara, G.E. Brown Jr, Uranium Speciation As a Function of Depth in Contaminated Hanford Sediments - A Micro-XRF, Micro-XRD, and Micro- And Bulk-XAFS Study, Environ. Sci. Technol. 43 (2009) 630–636. https://doi.org/10.1021/es8021045.
[68] J.E. Stubbs, L.A. Veblen, D.C. Elbert, J.M. Zachara, J.A. Davis, D.R. Veblen, Newly recognized hosts for uranium in the Hanford Site vadose zone, Geochimica et Cosmochimica Acta. 73 (2009) 1563–1576. https://doi.org/10.1016/j.gca.2008.12.004.
[69] A.J. Pinto, M.A. Gonçalves, C. Prazeres, J.M. Astilleros, M.J. Batista, Mineral replacement reactions in naturally occurring hydrated uranyl phosphates from the Tarabau deposit: Examples in the Cu–Ba uranyl phosphate system, Chemical Geology. 312–313 (2012) 18–26. https://doi.org/10.1016/j.chemgeo.2012.04.004.
[70] J. Bruno, J. De Pablo, L. Duro, E. Figuerola, Experimental study and modeling of the U(VI)-Fe(OH)3 surface precipitation/coprecipitation equilibria, Geochimica et Cosmochimica Acta. 59 (1995) 4113–4123. https://doi.org/10.1016/0016-7037(95)00243-S.
[71] M. Del Nero, S. Salah, T. Miura, A. Clément, F. Gauthier-Lafaye, Sorption/Desorption Processes of Uranium in Clayey Samples of the Bangombe Natural Reactor Zone, Gabon, Radiochimica Acta. 87 (1999) 135–150. https://doi.org/10.1524/ract.1999.87.34.135.
[72] M.M.S. Cabral Pinto, M.M.V.G. Silva, A.M.R. Neiva, Release, Migration, Sorption and (re)precipitation of U During a Granite Alteration under Oxidizing Conditions, Procedia Earth and Planetary Science. 8 (2014) 28–32. https://doi.org/10.1016/j.proeps.2014.05.007.
[73] M. Edahbi, B. Plante, M. Benzaazoua, M. Ward, M. Pelletier, Mobility of rare earth elements in mine drainage: Influence of iron oxides, carbonates, and phosphates, Chemosphere. 199 (2018) 647–654. https://doi.org/10.1016/j.chemosphere.2018.02.054.
[74] S. Salah, F. Gauthier-Lafaye, M. Del Nero, G. Le Bricon, G. Bracke, Behavior of REE in the Weathering Sequence of the Natural Fission Reactor at Bangombe (Oklo)., In: Abstr. of the Int. Conf. European Union of Geosciences EUG 10, Strasbourg, France,. (1999).
[75] M. Del Nero, A. Froideval, C. Gaillard, G. Mignot, R. Barillon, I. Munier, A. Ozgümüs, Mechanisms of uranyl sorption, Geological Society, London, Special Publications. 236 (2004) 545–560. https://doi.org/10.1144/GSL.SP.2004.236.01.30.

[76] Y. Wang, M. Frutschi, E. Suvorova, V. Phrommavanh, M. Descostes, A.A.A. Osman, G. Geipel, R. Bernier-Latmani, Mobile uranium(IV)-bearing colloids in a mining-impacted wetland, Nat Commun. 4 (2013) 2942. https://doi.org/10.1038/ncomms3942.
[77] L. Stetten, P. Blanchart, A. Mangeret, P. Lefebvre, P. Le Pape, J. Brest, P. Merrot, A. Julien, O. Proux, S.M. Webb, J.R. Bargar, C. Cazala, G. Morin, Redox Fluctuations and Organic Complexation Govern Uranium Redistribution from U(IV)-Phosphate Minerals in a Mining-Polluted Wetland Soil, Brittany, France, Environ. Sci. Technol. 52 (2018) 13099–13109. https://doi.org/10.1021/acs.est.8b03031.
[78] V.R. Vermeul, B.N. Bjornstad, B.G. Fritz, J.S. Fruchter, R.D. Mackley, D.R. Newcomer, D.P. Mendoza, M.L. Rockhold, D.M. Wellman, M.D. Williams, 300 Area Uranium Stabilization Through Polyphosphate Injection: Final Report, 2009. https://doi.org/10.2172/967237.
[79] Z. Pan, D.E. Giammar, V. Mehta, L.D. Troyer, J.G. Catalano, Z. Wang, Phosphate-Induced Immobilization of Uranium in Hanford Sediments, Environ. Sci. Technol. 50 (2016) 13486–13494. https://doi.org/10.1021/acs.est.6b02928.
[80] V. Montoya, B. Baeyens, M.A. Glaus, T. Kupcik, M. Marques Fernandes, L. Van Laer, C. Bruggeman, N. Maes, T. Schäfer, Sorption of Sr, Co and Zn on illite: Batch experiments and modelling including Co in-diffusion measurements on compacted samples, Geochimica et Cosmochimica Acta. 223 (2018) 1–20. https://doi.org/10.1016/j.gca.2017.11.027.
[81] S.J. Morrison, L.S. Cahn, Mineralogical residence of alpha-emitting contamination and implications for mobilization from uranium mill tailings, Journal of Contaminant Hydrology. 8 (1991) 1–21. https://doi.org/10.1016/0169-7722(91)90006-M.
[82] R.G. Riley, J.M. Zachara, F.J. Wobber, Chemical Contaminants on DOE Lands and Selection of Contaminant Mixtures for Subsurface Science Research, DOE/ER-0547T. U.S. Department of Energy. (1992).
[83] Y. Arai, M. McBeath, J.R. Bargar, J. Joye, J.A. Davis, Uranyl adsorption and surface speciation at the imogolite–water interface: Self-consistent spectroscopic and surface complexation models, Geochimica et Cosmochimica Acta. 70 (2006) 2492–2509. https://doi.org/10.1016/j.gca.2006.02.013.
[84] W.-M. Wu, J. Carley, M. Fienen, T. Mehlhorn, K. Lowe, J. Nyman, J. Luo, M.E. Gentile, R. Rajan, D. Wagner, R.F. Hickey, B. Gu, D. Watson, O.A. Cirpka, P.K. Kitanidis, P.M. Jardine, C.S. Criddle, Pilot-Scale in Situ Bioremediation of Uranium in a Highly Contaminated Aquifer. 1. Conditioning of a Treatment Zone, Environ. Sci. Technol. 40 (2006) 3978–3985. https://doi.org/10.1021/es051954y.
[85] R.C. Ewing, R.A. Whittleston, B.W.D. Yardley, Geological Disposal of Nuclear Waste: a Primer, ELEMENTS. 12 (2016) 233–237. https://doi.org/10.2113/gselements.12.4.233.
[86] S.V. Churakov, W. Hummel, M.M. Fernandes, Fundamental Research on Radiochemistry of Geological Nuclear Waste Disposal, Chimia (Aarau). 74 (2020) 1000–1009. https://doi.org/10.2533/chimia.2020.1000.
[87] T.A. Kurniawan, M.H.D. Othman, D. Singh, R. Avtar, G.H. Hwang, T. Setiadi, W. Lo, Technological solutions for long-term storage of partially used nuclear waste: A critical review, Annals of Nuclear Energy. 166 (2022) 108736. https://doi.org/10.1016/j.anucene.2021.108736.
[88] G. Montavon, S. Ribet, Y.H. Loni, F. Maia, C. Bailly, K. David, C. Lerouge, B. Madé, J.C. Robinet, B. Grambow, Uranium retention in a Callovo-Oxfordian clay rock formation: From laboratory-based models to in natura conditions, Chemosphere. 299 (2022) 134307. https://doi.org/10.1016/j.chemosphere.2022.134307.

[89] P. Krejci, T. Gimmi, L.R. Van Loon, On the concentration-dependent diffusion of sorbed cesium in Opalinus Clay, Geochimica et Cosmochimica Acta. 298 (2021) 149–166. https://doi.org/10.1016/j.gca.2021.01.012.
[90] M. Marques Fernandes, B. Baeyens, R. Dähn, A.C. Scheinost, M.H. Bradbury, U(VI) sorption on montmorillonite in the absence and presence of carbonate: A macroscopic and microscopic study, Geochimica et Cosmochimica Acta. 93 (2012) 262–277. https://doi.org/10.1016/j.gca.2012.04.017.
[91] B. Ma, L. Charlet, A. Fernandez-Martinez, M. Kang, B. Madé, A review of the retention mechanisms of redox-sensitive radionuclides in multi-barrier systems, Applied Geochemistry. 100 (2019) 414–431. https://doi.org/10.1016/j.apgeochem.2018.12.001.
[92] S. Goldberg, G. Sposito, A Chemical Model of Phosphate Adsorption by Soils: I. Reference Oxide Minerals, Soil Science Society of America Journal. 48 (1984) 772–778. https://doi.org/10.2136/sssaj1984.03615995004800040015x.
[93] Y. Arai, D.L. Sparks, Phosphate Reaction Dynamics in Soils and Soil Components: A Multiscale Approach, in: Advances in Agronomy, Elsevier, 2007: pp. 135–179. https://doi.org/10.1016/S0065-2113(06)94003-6.
[94] R.L. Parfitt, R.J. Atkinson, Phosphate adsorption on goethite (α-FeOOH), (1976).
[95] C. Luengo, M. Brigante, J. Antelo, M. Avena, Kinetics of phosphate adsorption on goethite: Comparing batch adsorption and ATR-IR measurements, Journal of Colloid and Interface Science. 300 (2006) 511–518. https://doi.org/10.1016/j.jcis.2006.04.015.
[96] D.B. Abdala, P.A. Northrup, Y. Arai, D.L. Sparks, Surface loading effects on orthophosphate surface complexation at the goethite/water interface as examined by extended X-ray Absorption Fine Structure (EXAFS) spectroscopy, Journal of Colloid and Interface Science. 437 (2015) 297–303. https://doi.org/10.1016/j.jcis.2014.09.057.
[97] M. Del Nero, C. Galindo, R. Barillon, E. Halter, B. Madé, Surface reactivity of α-Al2O3 and mechanisms of phosphate sorption: In situ ATR-FTIR spectroscopy and ζ potential studies, Journal of Colloid and Interface Science. 342 (2010) 437–444. https://doi.org/10.1016/j.jcis.2009.10.057.
[98] W. Li, A.-M. Pierre-Louis, K.D. Kwon, J.D. Kubicki, D.R. Strongin, B.L. Phillips, Molecular level investigations of phosphate sorption on corundum (α-Al2O3) by 31P solid state NMR, ATR-FTIR and quantum chemical calculation, Geochimica et Cosmochimica Acta. 107 (2013) 252–266. https://doi.org/10.1016/j.gca.2013.01.007.
[99] T. Roy, D. Wisser, M. Rivallan, M.C. Valero, T. Corre, O. Delpoux, G.D. Pirngruber, G. Lefèvre, Phosphate Adsorption on γ-Alumina: A Surface Complex Model Based on Surface Characterization and Zeta Potential Measurements, J. Phys. Chem. C. (2021) acs.jpcc.0c11553. https://doi.org/10.1021/acs.jpcc.0c11553.
[100] L. Borgnino, C.E. Giacomelli, M.J. Avena, C.P. De Pauli, Phosphate adsorbed on Fe(III) modified montmorillonite: Surface complexation studied by ATR-FTIR spectroscopy, Colloids and Surfaces A: Physicochemical and Engineering Aspects. 353 (2010) 238–244. https://doi.org/10.1016/j.colsurfa.2009.11.022.
[101] J.K. Edzwald, D.C. Toensing, M.C.-Yew. Leung, Phosphate adsorption reactions with clay minerals, Environ. Sci. Technol. 10 (1976) 485–490. https://doi.org/10.1021/es60116a001.
[102] F. Gérard, Clay minerals, iron/aluminum oxides, and their contribution to phosphate sorption in soils — A myth revisited, Geoderma. 262 (2016) 213–226. https://doi.org/10.1016/j.geoderma.2015.08.036.
[103] L. Dithmer, A.S. Lipton, K. Reitzel, T.E. Warner, D. Lundberg, U.G. Nielsen, Characterization of Phosphate Sequestration by a Lanthanum Modified Bentonite Clay: A Solid-State NMR, EXAFS, and PXRD Study, Environ. Sci. Technol. 49 (2015) 4559–4566. https://doi.org/10.1021/es506182s.

[104] T.J. Van Emmerik, D.E. Sandström, O.N. Antzutkin, M.J. Angove, B.B. Johnson, ^{31} P Solid-State Nuclear Magnetic Resonance Study of the Sorption of Phosphate onto Gibbsite and Kaolinite, Langmuir. 23 (2007) 3205–3213. https://doi.org/10.1021/la062765b.
[105] M. Dolui, S. Rakshit, M.E. Essington, G. Lefèvre, Probing Oxytetracycline Sorption Mechanism on Kaolinite in a Single Ion and Binary Mixtures with Phosphate using In Situ ATR-FTIR Spectroscopy, Soil Science Society of America Journal. 82 (2018) 826–838. https://doi.org/10.2136/sssaj2018.01.0020.
[106] Y. Arai, Effects of Dissolved Calcium on Arsenate Sorption at the Kaolinite-Water Interface, Soil Science. 175 (2010) 207–213. https://doi.org/10.1097/SS.0b013e3181dd799d.
[107] Y. Arai, D.L. Sparks, J.A. Davis, Arsenate Adsorption Mechanisms at the Allophane−Water Interface, Environ. Sci. Technol. 39 (2005) 2537–2544. https://doi.org/10.1021/es0486770.
[108] Y.S.R. Chen, J.N. Butler, Werner. Stumm, Kinetic study of phosphate reaction with aluminum oxide and kaolinite, Environ. Sci. Technol. 7 (1973) 327–332. https://doi.org/10.1021/es60076a007.
[109] Y.-S.R. Chen, J.N. Butler, W. Stumm, Adsorption of phosphate on alumina and kaolinite from dilute aqueous solutions, Journal of Colloid and Interface Science. 43 (1973) 421–436. https://doi.org/10.1016/0021-9797(73)90388-3.
[110] K.O. Adebowale, I.E. Unuabonah, B.I. Olu-Owolabi, Adsorption of some heavy metal ions on sulfate- and phosphate-modified kaolin, Applied Clay Science. 29 (2005) 145–148. https://doi.org/10.1016/j.clay.2004.10.003.
[111] T.E. Payne, G.R. Lumpkin, T.D. Waite, Uranium (VI) Adsorption on Model Minerals: Controlling factors and surface complexation modelling, (1998).
[112] Z. Guo, C. Yan, J. Xu, W. Wu, Sorption of U(VI) and phosphate on γ-alumina: Binary and ternary sorption systems, Colloids and Surfaces A: Physicochemical and Engineering Aspects. 336 (2009) 123–129. https://doi.org/10.1016/j.colsurfa.2008.11.032.
[113] Z. Guo, Y. Li, W. Wu, Sorption of U(VI) on goethite: Effects of pH, ionic strength, phosphate, carbonate and fulvic acid, Applied Radiation and Isotopes. 67 (2009) 996–1000. https://doi.org/10.1016/j.apradiso.2009.02.001.
[114] T. Hiemstra, W.H.V. Riemsdijk, A. Rossberg, K.-U. Ulrich, A surface structural model for ferrihydrite II: Adsorption of uranyl and carbonate, Geochimica et Cosmochimica Acta. 73 (2009) 4437–4451. https://doi.org/10.1016/j.gca.2009.04.035.
[115] G.D. Turner, J.M. Zachara, J.P. Mckinley, S.C. Smith, Surface-charge properties and UO z' adsorption of a subsurface smectite, (1996). https://doi.org/10.1016/0016-7037(96)00169-X.
[116] M.H. Bradbury, B. Baeyens, Sorption modelling on illite Part I: Titration measurements and the sorption of Ni, Co, Eu and Sn, Geochimica et Cosmochimica Acta. 73 (2009) 990–1003. https://doi.org/10.1016/j.gca.2008.11.017.
[117] M. Marques Fernandes, A.C. Scheinost, B. Baeyens, Sorption of trivalent lanthanides and actinides onto montmorillonite: Macroscopic, thermodynamic and structural evidence for ternary hydroxo and carbonato surface complexes on multiple sorption sites, Water Research. 99 (2016) 74–82. https://doi.org/10.1016/j.watres.2016.04.046.
[118] C. Joseph, M. Stockmann, K. Schmeide, S. Sachs, V. Brendler, G. Bernhard, Sorption of U(VI) onto Opalinus Clay: Effects of pH and humic acid, Applied Geochemistry. 36 (2013) 104–117. https://doi.org/10.1016/j.apgeochem.2013.06.016.

[119] J.R. Bargar, R. Reitmeyer, J.A. Davis, Spectroscopic Confirmation of Uranium(VI)−Carbonato Adsorption Complexes on Hematite, Environ. Sci. Technol. 33 (1999) 2481–2484. https://doi.org/10.1021/es990048g.
[120] J.R. Bargar, R. Reitmeyer, J.J. Lenhart, J.A. Davis, Characterization of U(VI)-carbonato ternary complexes on hematite: EXAFS and electrophoretic mobility measurements, Geochimica et Cosmochimica Acta. 64 (2000) 2737–2749. https://doi.org/10.1016/S0016-7037(00)00398-7.
[121] A. Froideval, M. Del Nero, R. Barillon, J. Hommet, G. Mignot, pH dependence of uranyl retention in a quartz/solution system: an XPS study, Journal of Colloid and Interface Science. 266 (2003) 221–235. https://doi.org/10.1016/S0021-9797(03)00528-9.
[122] A. Froideval, M. Del Nero, C. Gaillard, R. Barillon, I. Rossini, J.L. Hazemann, Uranyl sorption species at low coverage on Al-hydroxide: TRLFS and XAFS studies, Geochimica et Cosmochimica Acta. 70 (2006) 5270–5284. https://doi.org/10.1016/j.gca.2006.08.027.
[123] K. Müller, H. Foerstendorf, V. Brendler, A. Rossberg, K. Stolze, A. Gröschel, The surface reactions of U(VI) on γ-Al2O3 — In situ spectroscopic evaluation of the transition from sorption complexation to surface precipitation, Chemical Geology. 357 (2013) 75–84. https://doi.org/10.1016/j.chemgeo.2013.08.033.
[124] Y. Jo, J.-Y. Lee, J.-I. Yun, Adsorption of uranyl tricarbonate and calcium uranyl carbonate onto γ-alumina, Applied Geochemistry. 94 (2018) 28–34. https://doi.org/10.1016/j.apgeochem.2018.05.004.
[125] E.R. Sylwester, E.A. Hudson, P.G. Allen, The structure of uranium (VI) sorption complexes on silica, alumina, and montmorillonite, Geochimica et Cosmochimica Acta. 64 (2000) 2431–2438. https://doi.org/10.1016/S0016-7037(00)00376-8.
[126] C.J. Chisholm-Brause, J.M. Berg, R.A. Matzner, D.E. Morris, Uranium(VI) Sorption Complexes on Montmorillonite as a Function of Solution Chemistry, Journal of Colloid and Interface Science. 233 (2001) 38–49. https://doi.org/10.1006/jcis.2000.7227.
[127] C. Hennig, T. Reich, R. Dähn, A.M. Scheidegger, Structure of uranium sorption complexes at montmorillonite edge sites, Radiochimica Acta. 90 (2002) 653–657. https://doi.org/10.1524/ract.2002.90.9-11_2002.653.
[128] J.G. Catalano, G.E. Brown, Uranyl adsorption onto montmorillonite: Evaluation of binding sites and carbonate complexation, Geochimica et Cosmochimica Acta. 69 (2005) 2995–3005. https://doi.org/10.1016/j.gca.2005.01.025.
[129] M. Stockmann, K. Fritsch, F. Bok, M.M. Fernandes, B. Baeyens, R. Steudtner, K. Müller, C. Nebelung, V. Brendler, T. Stumpf, K. Schmeide, New insights into U(VI) sorption onto montmorillonite from batch sorption and spectroscopic studies at increased ionic strength, Science of The Total Environment. 806 (2022) 150653. https://doi.org/10.1016/j.scitotenv.2021.150653.
[130] T.E. Payne, G.R. Lumpkin, T.D. Waite, Uranium (VI) Adsorption on Model Minerals: Controlling factors and surface complexation modelling, (1996).
[131] M. Del Nero, C. Galindo, R. Barillon, B. Madé, TRLFS Evidence for Precipitation of Uranyl Phosphate on the Surface of Alumina: Environmental Implications, Environ. Sci. Technol. 45 (2011) 3982–3988. https://doi.org/10.1021/es2000479.
[132] D.L. Sparks, Environmental soil chemistry, Academic Press, Inc., San Diego, 1995.
[133] A. Gładysz-Płaska, E. Grabias, M. Majdan, Simultaneous adsorption of uranium(VI) and phosphate on red clay, Progress in Nuclear Energy. 104 (2018) 150–159. https://doi.org/10.1016/j.pnucene.2017.09.010.
[134] M.J. Comarmond, R. Steudtner, M. Stockmann, K. Heim, K. Müller, V. Brendler, T.E. Payne, H. Foerstendorf, The Sorption Processes of U(VI) onto SiO_2 in the Presence of

Phosphate: from Binary Surface Species to Precipitation, Environ. Sci. Technol. 50 (2016) 11610–11618. https://doi.org/10.1021/acs.est.6b02075.
[135] A. Singh, K.-U. Ulrich, D.E. Giammar, Impact of phosphate on U(VI) immobilization in the presence of goethite, Geochimica et Cosmochimica Acta. 74 (2010) 6324–6343. https://doi.org/10.1016/j.gca.2010.08.031.
[136] L.D. Troyer, F. Maillot, Z. Wang, Z. Wang, V.S. Mehta, D.E. Giammar, J.G. Catalano, Effect of phosphate on U(VI) sorption to montmorillonite: Ternary complexation and precipitation barriers, Geochimica et Cosmochimica Acta. 175 (2016) 86–99. https://doi.org/10.1016/j.gca.2015.11.029.
[137] A. Gładysz-Płaska, E. Grabias, M. Majdan, Simultaneous adsorption of uranium(VI) and phosphate on red clay, Progress in Nuclear Energy. 104 (2018) 150–159. https://doi.org/10.1016/j.pnucene.2017.09.010.
[138] F.M. Mirabella, Internal reflection spectroscopy: theory and applications, Marcel Dekker, New York, 1993. http://www.gbv.de/dms/bowker/toc/9780824787301.pdf (accessed May 16, 2023).
[139] G. Lefèvre, In situ Fourier-transform infrared spectroscopy studies of inorganic ions adsorption on metal oxides and hydroxides, Advances in Colloid and Interface Science. 107 (2004) 109–123. https://doi.org/10.1016/j.cis.2003.11.002.
[140] S.J. Hug, B. Sulzberger, In situ Fourier Transform Infrared Spectroscopic Evidence for the Formation of Several Different Surface Complexes of Oxalate on TiO2 in the Aqueous Phase, Langmuir. 10 (1994) 3587–3597. https://doi.org/10.1021/la00022a036.
[141] M. Del Nero, C. Galindo, G. Bucher, S. Georg, V. Mazan, R. Barillon, Speciation of oxalate at corundum colloid–solution interfaces and its effect on colloid aggregation under conditions relevant to freshwaters, Colloids and Surfaces A: Physicochemical and Engineering Aspects. 418 (2013) 165–173. https://doi.org/10.1016/j.colsurfa.2012.11.011.
[142] K. Nakamoto, Infrared and Raman spectra of inorganic and coordination compounds. A: Theory and applications in inorganic chemistry, 6. ed, Wiley, Hoboken, NJ, 2009.
[143] G. Lu, A.J. Haes, T.Z. Forbes, Detection and identification of solids, surfaces, and solutions of uranium using vibrational spectroscopy, Coordination Chemistry Reviews. 374 (2018) 314–344. https://doi.org/10.1016/j.ccr.2018.07.010.
[144] F. Quiles, A. Burneau, Infrared and Raman spectra of uranylžVI/ oxo-hydroxo complexes in acid aqueous solutions: a chemometric study, (2000) 11.
[145] K. Nakamoto, Infrared and Raman Spectra of Inorganic and Coordination Compounds, Handbook of Vibrational Spectroscopy. (2006) 21.
[146] P. Persson, N. Nilsson, S. Sjöberg, Structure and Bonding of Orthophosphate Ions at the Iron Oxide–Aqueous Interface, Journal of Colloid and Interface Science. 177 (1996) 263–275. https://doi.org/10.1006/jcis.1996.0030.
[147] F. Zaera, Probing Liquid/Solid Interfaces at the Molecular Level, Chem. Rev. 112 (2012) 2920–2986. https://doi.org/10.1021/cr2002068.
[148] M.I. Tejedor-Tejedor, M.A. Anderson, “In situ” ATR-Fourier transform infrared studies of the goethite (α-FeOOH)-aqueous solution interface, Langmuir. 2 (1986) 203–210. https://doi.org/10.1021/la00068a016.
[149] S.J. Hug, In SituFourier Transform Infrared Measurements of Sulfate Adsorption on Hematite in Aqueous Solutions, Journal of Colloid and Interface Science. 188 (1997) 415–422. https://doi.org/10.1006/jcis.1996.4755.
[150] H. Wijnja, C.P. Schulthess, ATR –FTIR and DRIFT spectroscopy of carbonate species at the aged k-Al2O3/water interface, (1999) 12.

[151] H. Wijnja, C.P. Schulthess, Vibrational Spectroscopy Study of Selenate and Sulfate Adsorption Mechanisms on Fe and Al (Hydr)oxide Surfaces, Journal of Colloid and Interface Science. 229 (2000) 286–297. https://doi.org/10.1006/jcis.2000.6960.
[152] P.A. Connor, A.J. McQuillan, Phosphate Adsorption onto TiO_2 from Aqueous Solutions: An in Situ Internal Reflection Infrared Spectroscopic Study, Langmuir. 15 (1999) 2916–2921. https://doi.org/10.1021/la980894p.
[153] C. Su, D.L. Suarez, Selenate and Selenite Sorption on Iron Oxides An Infrared and Electrophoretic Study, Soil Sci. Soc. Am. J. 64 (2000) 101–111. https://doi.org/10.2136/sssaj2000.641101x.
[154] D. Rivera, P.E. Poston, R.H. Uibel, J.M. Harris, In Situ Adsorption Studies at Silica/Solution Interfaces by Attenuated Total Internal Reflection Fourier Transform Infrared Spectroscopy: Examination of Adsorption Models in Normal-Phase Liquid Chromatography, Anal. Chem. 72 (2000) 1543–1554. https://doi.org/10.1021/ac990968h.
[155] S.B. Johnson, T.H. Yoon, A.J. Slowey, G.E. Brown, Adsorption of Organic Matter at Mineral/Water Interfaces: 3. Implications of Surface Dissolution for Adsorption of Oxalate, Langmuir. 20 (2004) 11480–11492. https://doi.org/10.1021/la048559q.
[156] H. Gulley-Stahl, P.A. Hogan, W.L. Schmidt, S.J. Wall, A. Buhrlage, H.A. Bullen, Surface Complexation of Catechol to Metal Oxides: An ATR-FTIR, Adsorption, and Dissolution Study, Environ. Sci. Technol. 44 (2010) 4116–4121. https://doi.org/10.1021/es902040u.
[157] T.K. Ronson, A.J. McQuillan, Infrared Spectroscopic Study of Calcium and Phosphate Ion Coadsorption and of Brushite Crystallization on TiO2, Langmuir. 18 (2002) 5019–5022. https://doi.org/10.1021/la011676q.
[158] E.J. Elzinga, R. Kretzschmar, In situ ATR-FTIR spectroscopic analysis of the co-adsorption of orthophosphate and Cd(II) onto hematite, Geochimica et Cosmochimica Acta. 117 (2013) 53–64. https://doi.org/10.1016/j.gca.2013.04.003.
[159] M.A.G. Hinkle, Z. Wang, D.E. Giammar, J.G. Catalano, Interaction of Fe(II) with phosphate and sulfate on iron oxide surfaces, Geochimica et Cosmochimica Acta. 158 (2015) 130–146. https://doi.org/10.1016/j.gca.2015.02.030.
[160] J. Liu, R. Zhu, T. Xu, Y. Xu, F. Ge, Y. Xi, J. Zhu, H. He, Co-adsorption of phosphate and zinc(II) on the surface of ferrihydrite, Chemosphere. 144 (2016) 1148–1155. https://doi.org/10.1016/j.chemosphere.2015.09.083.
[161] J. Liu, R. Zhu, X. Liang, L. Ma, X. Lin, J. Zhu, H. He, S.C. Parker, M. Molinari, Synergistic adsorption of Cd(II) with sulfate/phosphate on ferrihydrite: An in situ ATR-FTIR/2D-COS study, Chemical Geology. 477 (2018) 12–21. https://doi.org/10.1016/j.chemgeo.2017.12.004.
[162] M.J. Comarmond, R. Steudtner, M. Stockmann, K. Heim, K. Müller, V. Brendler, T.E. Payne, H. Foerstendorf, The Sorption Processes of U(VI) onto SiO_2 in the Presence of Phosphate: from Binary Surface Species to Precipitation, Environ. Sci. Technol. 50 (2016) 11610–11618. https://doi.org/10.1021/acs.est.6b02075.
[163] M. Stockmann, K. Fritsch, F. Bok, M.M. Fernandes, B. Baeyens, R. Steudtner, K. Müller, C. Nebelung, V. Brendler, T. Stumpf, K. Schmeide, New insights into U(VI) sorption onto montmorillonite from batch sorption and spectroscopic studies at increased ionic strength, Science of The Total Environment. (2021) 150653. https://doi.org/10.1016/j.scitotenv.2021.150653.
[164] R.H. Byrne, J.H. Lee, L.S. Bingler, Rare earth element complexation by PO43− ions in aqueous solution, Geochimica et Cosmochimica Acta. 55 (1991) 2729–2735. https://doi.org/10.1016/0016-7037(91)90439-C.

[165] R. Guillaumont, T. Fanghänel, J. Fuger, I. Grenthe, V. Neck, D.A. Palmer, M.H. Rand, UPDATE ON THE CHEMICAL THERMODYNAMICS OF URANIUM, NEPTUNIUM, PLUTONIUM, AMERICIUM AND TECHNETIUM, OECD Nuclear Energy Agency; Elsevier: Amsterdam. (2003).
[166] K. Maher, J.R. Bargar, G.E. Brown, Environmental Speciation of Actinides, Inorg. Chem. 52 (2013) 3510–3532. https://doi.org/10.1021/ic301686d.
[167] S.A. Cumberland, G. Douglas, K. Grice, J.W. Moreau, Uranium mobility in organic matter-rich sediments: A review of geological and geochemical processes, Earth-Science Reviews. 159 (2016) 160–185. https://doi.org/10.1016/j.earscirev.2016.05.010.
[168] W.F. Bleam, P.E. Pfeffer, S. Goldberg, R.W. Taylor, R. Dudley, A phosphorus-31 solid-state nuclear magnetic resonance study of phosphate adsorption at the boehmite/aqueous solution interface, Langmuir. 7 (1991) 1702–1712. https://doi.org/10.1021/la00056a023.
[169] C. Shang, J.W.B. Stewart, P.M. Huang, pH effect on kinetics of adsorption of organic and inorganic phosphates by short-range ordered aluminum and iron precipitates, Geoderma. 53 (1992) 1–14. https://doi.org/10.1016/0016-7061(92)90017-2.
[170] R. Finch, T. Murakami, 3. Systematics and Paragenesis of Uranium Minerals, in: P.C. Burns, R.J. Finch (Eds.), Uranium, De Gruyter, 1999: pp. 91–180. https://doi.org/10.1515/9781501509193-008.
[171] D.E. Morris, P.G. Allen, J.M. Berg, C.J. Chisholm-Brause, S.D. Conradson, R.J. Donohoe, N.J. Hess, J.A. Musgrave, C.D. Tait, Speciation of Uranium in Fernald Soils by Molecular Spectroscopic Methods: Characterization of Untreated Soils, Environ. Sci. Technol. 30 (1996) 2322–2331. https://doi.org/10.1021/es950745i.
[172] J.L. Jerden, A.K. Sinha, Phosphate based immobilization of uranium in an oxidizing bedrock aquifer, Applied Geochemistry. 18 (2003) 823–843. https://doi.org/10.1016/S0883-2927(02)00179-8.
[173] J.L. Jerden, A.K. Sinha, Geochemical coupling of uranium and phosphorous in soils overlying an unmined uranium deposit: Coles Hill, Virginia, Journal of Geochemical Exploration. 91 (2006) 56–70. https://doi.org/10.1016/j.gexplo.2005.12.003.
[174] J.L. Jerden, A.K. Sinha, L. Zelazny, Natural immobilization of uranium by phosphate mineralization in an oxidizing saprolite–soil profile: chemical weathering of the Coles Hill uranium deposit, Virginia, Chemical Geology. 199 (2003) 129–157. https://doi.org/10.1016/S0009-2541(03)00080-9.
[175] J.G. Catalano, J.P. McKinley, J.M. Zachara, S.M. Heald, S.C. Smith, G.E. Brown, Changes in Uranium Speciation through a Depth Sequence of Contaminated Hanford Sediments, Environ. Sci. Technol. 40 (2006) 2517–2524. https://doi.org/10.1021/es0520969.
[176] D.M. Singer, J.M. Zachara, G.E. Brown Jr, Uranium Speciation As a Function of Depth in Contaminated Hanford Sediments - A Micro-XRF, Micro-XRD, and Micro- And Bulk-XAFS Study, Environ. Sci. Technol. 43 (2009) 630–636. https://doi.org/10.1021/es8021045.
[177] J.E. Stubbs, L.A. Veblen, D.C. Elbert, J.M. Zachara, J.A. Davis, D.R. Veblen, Newly recognized hosts for uranium in the Hanford Site vadose zone, Geochimica et Cosmochimica Acta. 73 (2009) 1563–1576. https://doi.org/10.1016/j.gca.2008.12.004.
[178] A.J. Pinto, M.A. Gonçalves, C. Prazeres, J.M. Astilleros, M.J. Batista, Mineral replacement reactions in naturally occurring hydrated uranyl phosphates from the Tarabau deposit: Examples in the Cu–Ba uranyl phosphate system, Chemical Geology. 312–313 (2012) 18–26. https://doi.org/10.1016/j.chemgeo.2012.04.004.

[179] Y. Arai, M.A. Marcus, N. Tamura, J.A. Davis, J.M. Zachara, Spectroscopic Evidence for Uranium Bearing Precipitates in Vadose Zone Sediments at the Hanford 300-Area Site, Environ. Sci. Technol. 41 (2007) 4633–4639. https://doi.org/10.1021/es062196u.
[180] J. Bruno, J. De Pablo, L. Duro, E. Figuerola, Experimental study and modeling of the U(VI)-Fe(OH)3 surface precipitation/coprecipitation equilibria, Geochimica et Cosmochimica Acta. 59 (1995) 4113–4123. https://doi.org/10.1016/0016-7037(95)00243-S.
[181] M. Del Nero, S. Salah, T. Miura, A. Clément, F. Gauthier-Lafaye, Sorption/Desorption Processes of Uranium in Clayey Samples of the Bangombe Natural Reactor Zone, Gabon, Radiochimica Acta. 87 (1999) 135–150. https://doi.org/10.1524/ract.1999.87.34.135.
[182] M.M.S. Cabral Pinto, M.M.V.G. Silva, A.M.R. Neiva, Release, Migration, Sorption and (re)precipitation of U During a Granite Alteration under Oxidizing Conditions, Procedia Earth and Planetary Science. 8 (2014) 28–32. https://doi.org/10.1016/j.proeps.2014.05.007.
[183] M. Edahbi, B. Plante, M. Benzaazoua, M. Ward, M. Pelletier, Mobility of rare earth elements in mine drainage: Influence of iron oxides, carbonates, and phosphates, Chemosphere. 199 (2018) 647–654. https://doi.org/10.1016/j.chemosphere.2018.02.054.
[184] Md.S. Alam, T. Cheng, Uranium release from sediment to groundwater: Influence of water chemistry and insights into release mechanisms, Journal of Contaminant Hydrology. 164 (2014) 72–87. https://doi.org/10.1016/j.jconhyd.2014.06.001.
[185] S. Salah, F. Gauthier-Lafaye, M. Del Nero, G. Le Bricon, G. Bracke, Behavior of REE in the Weathering Sequence of the Natural Fission Reactor at Bangombe (Oklo)., In: Abstr. of the Int. Conf. European Union of Geosciences EUG 10, Strasbourg, France,. (1999).
[186] V. Bout-Roumazeilles, E. Cortijo, L. Labeyrie, P. Debrabant, Clay mineral evidence of nepheloid layer contributions to the Heinrich layers in the northwest Atlantic, Palaeogeography, Palaeoclimatology, Palaeoecology. 146 (1999) 211–228.
[187] G.W. Brindley, G. Brown, Crystal Structures of Clay Minerals and Their X-ray Identification., Mineralogical Society, 1980.
[188] M.H. Bradbury, B. Baeyens, Sorption modelling on illite Part I: Titration measurements and the sorption of Ni, Co, Eu and Sn, Geochimica et Cosmochimica Acta. 73 (2009) 990–1003. https://doi.org/10.1016/j.gca.2008.11.017.
[189] R.J. Atkinson, R.L. Parfitt, R.St.C. Smart, Infra-red study of phosphate adsorption on goethite, J. Chem. Soc., Faraday Trans. 1. 70 (1974) 1472. https://doi.org/10.1039/f19747001472.
[190] C. Poinssot, B. Baeyens, M.H. Bradbury, Experimental and modelling studies of caesium sorption on illite, Geochimica et Cosmochimica Acta. 63 (1999) 3217–3227. https://doi.org/10.1016/S0016-7037(99)00246-X.
[191] G.M. Beene, R. Bryant, D.J.A. Williams, Electrochemical properties of illites, Journal of Colloid and Interface Science. 147 (1991) 358–369. https://doi.org/10.1016/0021-9797(91)90168-8.
[192] Q. Du, Z. Sun, W. Forsling, H. Tang, Acid-Base Properties of Aqueous Illite Surfaces, (n.d.) 11.
[193] D. Vantelon, M. Pelletier, L.J. Michot, O. Barres, F. Thomas, Fe, Mg and Al distribution in the octahedral sheet of montmorillonites. An infrared study in the OH-bending region, Clay Miner. 36 (2001) 369–379. https://doi.org/10.1180/000985501750539463.

[194] J. Madejová, Baseline Studies of the Clay Minerals Society Source Clays: Infrared Methods, Clays and Clay Minerals. 49 (2001) 410–432. https://doi.org/10.1346/CCMN.2001.0490508.
[195] C.T. Johnston, G.S. Premachandra, Polarized ATR-FTIR Study of Smectite in Aqueous Suspension, Langmuir. 17 (2001) 3712–3718. https://doi.org/10.1021/la010184a.
[196] R. Ellerbrock, M. Stein, J. Schaller, Comparing amorphous silica, short-range-ordered silicates and silicic acid species by FTIR, In Review, 2022. https://doi.org/10.21203/rs.3.rs-1623376/v1.
[197] M. Ritz, L. Vaculíková, E. Plevová, APPLICATION OF INFRARED SPECTROSCOPY AND CHEMOMETRIC METHODS TO IDENTIFICATION OF SELECTED MINERALS, Acta Geodynamica et Geromaterialia. 8 (2011) 47–58.
[198] R.J. Hunter, Electroviscous and Viscoelectric Effects, in: Zeta Potential in Colloid Science, Elsevier, 1981: pp. 179–218. https://doi.org/10.1016/B978-0-12-361961-7.50009-2.
[199] R.J. Hunter, A.E. Alexander, Surface properties and flow behavior of kaolinite. Part I: Electrophoretic mobility and stability of kaolinite sols, Journal of Colloid Science. 18 (1963) 820–832. https://doi.org/10.1016/0095-8522(63)90076-X.
[200] S.Y. Guo, M. Del Nero, O. Courson, S. Meyer-Georg, R. Barillon, Speciation studies at the Illite - solution interface: Part 1 - Sorption of phosphate ions, Colloids and Surfaces A: Physicochemical and Engineering Aspects. (Submitted).
[201] E.J. Elzinga, D.L. Sparks, Phosphate adsorption onto hematite: An in situ ATR-FTIR investigation of the effects of pH and loading level on the mode of phosphate surface complexation, Journal of Colloid and Interface Science. 308 (2007) 53–70. https://doi.org/10.1016/j.jcis.2006.12.061.
[202] W. Li, A.-M. Pierre-Louis, K.D. Kwon, J.D. Kubicki, D.R. Strongin, B.L. Phillips, Molecular level investigations of phosphate sorption on corundum (α-Al2O3) by 31P solid state NMR, ATR-FTIR and quantum chemical calculation, Geochimica et Cosmochimica Acta. 107 (2013) 252–266. https://doi.org/10.1016/j.gca.2013.01.007.
[203] C. Nguyen Trung, G.M. Begun, D.A. Palmer, Aqueous uranium complexes. 2. Raman spectroscopic study of the complex formation of the dioxouranium(VI) ion with a variety of inorganic and organic ligands, Inorg. Chem. 31 (1992) 5280–5287. https://doi.org/10.1021/ic00051a021.
[204] F. Quilès, A. Burneau, Infrared and Raman spectroscopic study of uranyl complexes: hydroxide and acetate derivatives in aqueous solution, Vibrational Spectroscopy. 18 (1998) 61–75. https://doi.org/10.1016/S0924-2031(98)00040-X.
[205] F. Quilès, C. Nguyen-Trung, C. Carteret, B. Humbert, Hydrolysis of Uranyl(VI) in Acidic and Basic Aqueous Solutions Using a Noncomplexing Organic Base: A Multivariate Spectroscopic and Statistical Study, Inorg. Chem. 50 (2011) 2811–2823. https://doi.org/10.1021/ic101953q.
[206] L. Borgnino, C.E. Giacomelli, M.J. Avena, C.P.D. Pauli, Phosphate adsorbed on Fe(III) modified montmorillonite: Surface complexation studied by ATR-FTIR spectroscopy, (2010) 7.
[207] J. Čejka, A. Muck, To the infrared spectroscopy of natural uranyl phosphates, Phys Chem Minerals. 11 (1984) 172–177. https://doi.org/10.1007/BF00387848.
[208] M.H. Bradbury, B. Baeyens, Sorption modelling on illite. Part II: Actinide sorption and linear free energy relationships, Geochimica et Cosmochimica Acta. 73 (2009) 1004–1013. https://doi.org/10.1016/j.gca.2008.11.016.

[209] I. Jeon, K. Nam, Change in the site density and surface acidity of clay minerals by acid or alkali spills and its effect on pH buffering capacity, Sci Rep. 9 (2019) 9878. https://doi.org/10.1038/s41598-019-46175-y.
[210] V. Pekárek, V. Veselý, A study on uranyl phosphates—II sorption properties of some 1- to 4-valent cations on uranyl hydrogen phosphate heated to various temperatures, Journal of Inorganic and Nuclear Chemistry. 27 (1965) 1151–1158. https://doi.org/10.1016/0022-1902(65)80427-4.
[211] C. Tournassat, E. Ferrage, C. Poinsignon, L. Charlet, The titration of clay minerals, Journal of Colloid and Interface Science. 273 (2004) 234–246. https://doi.org/10.1016/j.jcis.2003.11.022.
[212] R. Dahn, B. Baeyens, M.H. Bradbury, Uptake mechanisms of U(6) by illite as determined by X-ray absorption spectroscopy, Organisation for Economic Co-Operation and Development - Nuclear Energy Agency, Nuclear Energy Agency of the OECD (NEA), 2007.
[213] R.L. Frost, An infrared and Raman spectroscopic study of the uranyl micas, Spectrochimica Acta Part A: Molecular and Biomolecular Spectroscopy. 60 (2004) 1469–1480. https://doi.org/10.1016/j.saa.2003.08.013.
[214] G.D. Turner, J.M. Zachara, J.P. Mckinley, S.C. Smith, Surface-charge properties and UO z' adsorption of a subsurface smectite, (1996).
[215] M.M. Fernandes, A.C. Scheinost, B. Baeyens, Sorption of trivalent lanthanides and actinides onto montmorillonite: Macroscopic, thermodynamic and structural evidence for ternary hydroxo and carbonato surface complexes on multiple sorption sites, Water Research. 99 (2016) 74–82. https://doi.org/10.1016/j.watres.2016.04.046.
[216] D. Féron, D. Crusset, J.-M. Gras, Corrosion issues in nuclear waste disposal, Journal of Nuclear Materials. 379 (2008) 16–23. https://doi.org/10.1016/j.jnucmat.2008.06.023.
[217] G. De Combarieu, M.L. Schlegel, D. Neff, E. Foy, D. Vantelon, P. Barboux, S. Gin, Glass–iron–clay interactions in a radioactive waste geological disposal: An integrated laboratory-scale experiment, Applied Geochemistry. 26 (2011) 65–79. https://doi.org/10.1016/j.apgeochem.2010.11.004.
[218] E. Gaucher, C. Robelin, J.M. Matray, G. Négrel, Y. Gros, J.F. Heitz, A. Vinsot, H. Rebours, A. Cassagnabère, A. Bouchet, ANDRA underground research laboratory: interpretation of the mineralogical and geochemical data acquired in the Callovian–Oxfordian formation by investigative drilling, Physics and Chemistry of the Earth, Parts A/B/C. 29 (2004) 55–77. https://doi.org/10.1016/j.pce.2003.11.006.
[219] L. Fralova, Transport diffusif de l'uranium dans la roche argileuse du Callovo-Oxfordien, mécanismes et sensibilité aux perturbations chimiques, Thèse.fr. (2020) 147.
[220] Y. Arai, D.L. Sparks, ATR–FTIR Spectroscopic Investigation on Phosphate Adsorption Mechanisms at the Ferrihydrite–Water Interface, Journal of Colloid and Interface Science. 241 (2001) 317–326. https://doi.org/10.1006/jcis.2001.7773.
[221] R.L. Frost, W.N. Martens, T. Kloprogge, P.A. Williams, Vibrational spectroscopy of the basic manganese and ferric phosphate minerals: strunzite, ferrostrunzite and ferristrunzite, Njmm. 2002 (2002) 481–496. https://doi.org/10.1127/0028-3649/2002/2002-0481.

Appendices

Appendix A : Supporting information of chapter II

Fig. A1. Calculated distribution of aqueous phosphate species (in %) as a function of pH at $[P]_{I,aq}$: 100µM. Solution electrolyte: 0.005 M NaCl. Reactions and equilibrium constants used in calculation are given in Table A1. Visual MINTEQ (Ver 3.1) code and the database are used for the calculation.

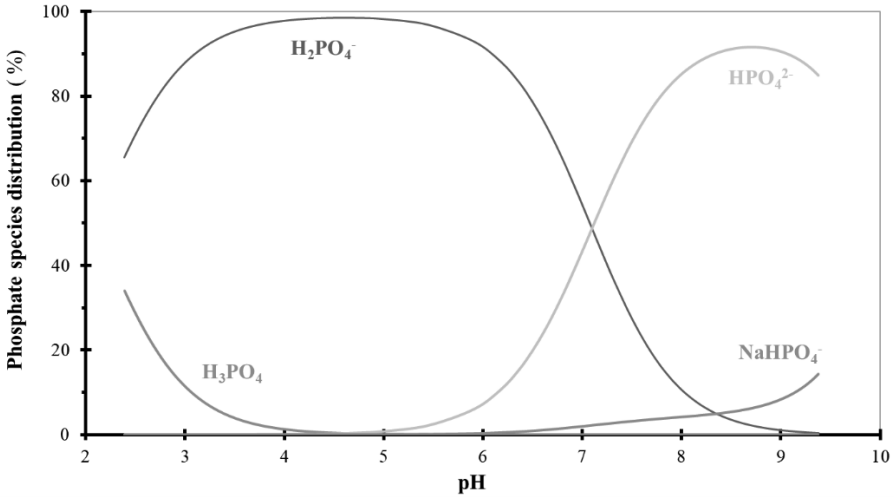

Table A1 Equilibrium constants used in the calculation of aqueous species distribution of phosphate ions. The MINTEQA2 database is used for the calculation in Visual MINTEQ (Ver 3.1).

Equilibrium Reactions	Log K
$PO_4^{3-} + H^+ \leftrightharpoons HPO_4^{2-}$	12.375
$PO_4^{3-} + 2\ H^+ \leftrightharpoons H_2PO_4^{2-}$	19.573
$PO_4^{3-} + 3H^+ \leftrightharpoons H_3PO_4^{2-}$	21.721
$2\ Na^+ + PO_4^{3-} \leftrightharpoons Na_2PO_4^-$	2.59
$Na^+ + PO_4^{3-} \leftrightharpoons NaPO_4^{2-}$	1.43
$Na^+ + H_2O \leftrightharpoons NaOH_{(aq)} + H^+$	-13.897
$Na^+ + Cl^- \leftrightharpoons NaCl_{(aq)}$	-0.3
$Na^+ + CO_3^{2-} \leftrightharpoons NaCO_3^-$	1.27
$H^+ + CO_3^{2-} \leftrightharpoons HCO_3^-$	10.329
$2H^+ + CO_3^{2-} \leftrightharpoons H_2CO_{3(aq)}$	16.681
$H_2O \leftrightharpoons H^+ + OH^-$	-13.997
$2\ Na^+ + H^+ + PO_4^{3-} \leftrightharpoons Na_2HPO_{4\ (aq)}$	13.32
$Na^+ + H^+ + PO_4^{3-} \leftrightharpoons NaHPO_4^-$	13.445
$Na^+ + 2\ H^+ + PO_4^{3-} \leftrightharpoons NaH_2PO_{4\ (aq)}$	19.873

$Na^+ + H^+ + CO_3^{2-} \leftrightharpoons NaHCO_{3\,(aq)}$ 10.029

Table A2 Trace element composition ($\mu g.g^{-1}$) of IdP and NaIdP samples. The analytical uncertainties, which depend on the concentration of element, are in the range of 5-20%.

	As	Ba	Be	Bi	Cd	Co	Cr	Cs	Cu	Ga	Ge
IdP	31.6	316	6.72	1.05	0.17	12.9	80.5	99.4	32.3	33.8	2.12
NaIdP	22.3	207	7.35	1.09	0.07	13.7	90.7	74.2	32.4	36.7	2.06

	Hf	In	Mo	Nb	Ni	Pb	Rb	Sb	Sc	Sn	Sr
IdP	1.38	0.11	< D.L.	14.8	34.3	33.5	551	1.16	14.28	8.77	180
NaIdP	1.42	0.11	< D.L.	15.9	39.3	30.8	473	0.97	16.00	9.00	72.2

	Ta	Th	U	V	W	Y	Zn	Zr	La	Ce	Pr
IdP	1.77	8.87	3.38	89.4	3.54	14.6	150	45.7	22.0	43.8	5.17
NaIdP	1.83	9.39	2.84	96.1	3.46	4.85	163	42.5	15.4	26.7	3.12

	Nd	Sm	Eu	Gd	Tb	Dy	Ho	Er	Tm	Yb	Lu
IdP	19.5	4.05	0.91	3.26	0.52	2.98	0.57	1.43	0.20	1.23	0.17
NaIdP	10.9	1.94	0.34	1.30	0.19	1.04	0.20	0.53	0.08	0.59	0.09

Table A3 Final concentrations of cations (μM) in experimental 0.005M NaCl solutions brought in contact with IdP and NaIdP at various values of clay-to-solution ratios – $R_{S/L}$ (1-6$g.L^{-1}$and 0.5-3$g.L^{-1}$, respectively). Experimental conditions for IdP (initial pH2.3, reaction time t_R of 5 days), for NaIdP (initial pH2.6-7.4, t_R: 3- or 7-days). The chemical analysis of solution was carried out after phase separation by centrifugation at 9000rpm for 3h (cutoff 16nm).

IdP - electrolyte solution system - 5 days						
$R_{S/L}$	*1.0*	*2.0*	*3.0*	*3.9*	*5.0*	*6.0*
pH_{Final}	*2.6*	*3.2*	*6.0*	*6.6*	*7.0*	*7.2*
[Al]	90.6 ± 0.8	111 ± 1	10.17 ± 0.30	9.21 ± 0.24	7.36 ± 0.16	9.80 ± 0.03
[Mg]	54.1 ± 0.5	86.6 ± 0.8	84.3 ± 0.8	97.3 ± 0.90	111 ± 1	126 ± 1
[K]	236 ± 2	273 ± 2	276 ± 3	267 ± 3	242 ± 2	305 ± 1
[Si]	138 ± 2	196 ± 2	182 ± 1	200 ± 4	219 ± 1	242 ± 4
[Fe]	2.59 ± 0.05	1.90 ± 0.02	3.14 ± 0.51	2.73 ± 0.08	2.30 ± 0.04	2.98 ± 0.02
[Mn]	2.44 ± 0.06	4.05 ± 0.07	2.40 ± 0.03	2.12 ± 0.05	1.79 ± 0.01	1.51± 0.03

[Ti]	0.033 ± 0.020	0.018 ± 0.004	0.110 ± 0.004	0.100 ± 0.004	0.090 ± 0.010	0.130± 0.004
[Li]	1.48 ± 0.06	2.90 ± 0.03	2.64 ± 0.21	3.13 ± 0.15	3.68 ± 0.12	4.22 ± 0.04
[Ca]	0.87 ± 0.01	1.49 ± 0.02	1.96 ± 0.01	2.26 ± 0.02	2.43 ± 0.02	2.51 ± 0.03

NaIdP - electrolyte solution system - 3 days									
$R_{S/L}$	*0.5*	*1.5*	*3.0*	*3.0*	*3.0*	*3.0*	*3.0*	*3.0*	*3.0*
pH_{Final}	*3.4*	*3.0*	*2.9*	*3.5*	*4.2*	*5.2*	*7.0*	*7.1*	*7.6*
[Al]	25.6 ± 0.7	45.3 ± 0.3	92.7 ± 2.1	52.9 ± 0.4	28.2 ± 0.4	5.00 ± 0.32	3.99 ± 0.21	25.92 ± 0.39	37.0 ± 0.31
[Mg]	13.1 ± 0.2	30.74 ± 0.14	62.1 ± 1.1	14.6 ± 0.1	46.3 ± 0.3	21.1 ± 0.2	5.26 ± 0.03	8.15 ± 0.03	10.8 ± 0.1
[K]	50.3 ± 1.0	267 ± 1	105 ± 2	108 ± 1	153 ± 1	171 ± 2	111 ± 1	62.0 ± 0.2	93.2 ± 0.5
[Si]	73.5 ± 1.86	121 ± 1	245 ± 4	214 ± 6	201 ± 6	144 ± 1	114 ± 1	146 ± 2	172 ± 1
[Fe]	4.15 ± 0.1	2.63 ± 0.03	3.61 ± 0.07	14.2 ± 0.3	2.99 ± 0.12	0.68 ± 0.02	0.71 ± 0.04	7.19 ± 0.11	10.1 ± 0.1
[Fe] *(3nm)*	<D.L.	0.89 ± 0.01	1.32 ± 0.01	-	-	-	-	-	-
[Mn]	<D.L.	<D.L.	<D.L.	<D.L.	0.67 ± 0.01	0.18 ± 0.01	<D.L.	<D.L.	<D.L.
[Ti]	<D.L.	<D.L.	<D.L.	0.100 ± 0.003	0.060 ± 0.007	<D.L.	<D.L.	0.040 ± 0.003	0.050 ± 0.001
[Li]	<D.L.	<D.L.	<D.L.	2.10 ± 0.01	2.67 ± 0.02	2.14 ± 0.02	1.79 ± 0.01	1.74 ± 0.01	1.86 ± 0.01
[Ca]	2.90 ± 0.16	9.26 ± 0.18	14.8 ± 0.4	15.0 ± 0.1	79.4 ± 0.1	45.3 ± 0.1	14.6 ± 0.1	11.8 ± 0.1	8.27 ± 0.02

	NaIdP - electrolyte solution system - 7 days		
$R_{S/L}$	*0.5*	*0.5*	*0.5*
pH_{Final}	*6.8*	*6.8*	*4.8*
[Al]	3.41 ± 0.14	3.11 ± 0.34	<D.L.
[Mg]	2.76 ± 0.03	2.67 ± 0.09	5.51 ± 0.07
[K]	145 ± 1	127 ± 1	32.9 ± 0.6
[Si]	35.8 ± 0.5	36.2 ± 1.2	35.8 ± 0.7
[Fe]	1.030 ± 0.025	0.960 ± 0.106	0.010 ± 0.011
[Mn]	<D.L.	<D.L.	<D.L.
[Ti]	<D.L.	<D.L.	<D.L.
[Li]	<D.L.	<D.L.	<D.L.
[Ca]	1.79 ± 0.12	2.79 ± 0.07	0.86 ± 0.18

Table A4 Final concentrations of anions in experimental 0.005M NaCl solutions brought in contact with IdP and NaIdP at various values of clay-to-solution ratios -$R_{S/L}$ (1-6g.$L^{-1}$and 0.5-3g.L^{-1}, respectively). Experimental conditions for IdP (initial pH2.3, reaction time t_R of 5 days), for NaIdP (initial pH2.6-7.4, t_R:3- or 7-days). Solid-liquid separation was carried out by centrifugation at 9000rpm for 3h (cutoff: 16nm).

	$R_{S/L}$ ($g.L^{-1}$)	pH_{Final}	$[PO_4^{3-}]$ (µM)	$[F^-]$ (µM)	$[NO_3^-]$ (µM)	$[SO_4^{2-}]$ (µM)	t_R (days)
IdP	1.0	2.6	22.2±1.3	16.4±0.8	7.2±0.4	2.0±0.1	5
	2.0	3.2	40.1±1.3	31.1±1.6	6.9±0.3	3.9±0.2	
	3.0	6.0	43.9±1.3	24.5±1.2	6.0±0.3	5.4±0.3	
	3.9	6.6	45.2±1.3	32.4±1.6	6.1±0.3	6.3±0.3	
	5.0	7.0	48.4±1.3	38±1.9	7.0±0.3	6.7±0.3	
	6.0	7.2	45.3±1.3	38.8±1.9	6.7±0.3	7.3±0.4	
NaIdP	0.5	3.4	1.14±0.06	5.46±0.27	1.22±0.06	< D.L.	3
	1.0	3.5	1.38±0.07	6.93±0.35	2.02±0.1	< D.L.	
	1.5	3.0	1.54±0.08	8.4±0.42	2.8±0.14	< D.L.	
	2.0	2.9	1.87±0.09	10.5±0.5	2.46±0.12	< D.L.	
	2.5	2.9	1.81±0.09	8.8±0.44	3.1±0.15	< D.L.	
	3.0	2.9	1.94±0.1	12.8±0.6	2.41±0.12	< D.L.	
	0.5	6.8	< D.L.	5.08±0.25	1.43±0.07	< D.L.	7
	0.5	6.8	< D.L.	5.7±0.28	2.05±0.1	< D.L.	
	0.5	4.8	< D.L.	< D.L.	0.97±0.05	< D.L.	
	0.5	4.7	< D.L.	< D.L.	10.8±0.5	< D.L.	
	3.0	4.3	< D.L.	6.44±0.32	2.83±0.14	< D.L.	
	3.0	3.0	< D.L.	10.3±0.5	2.32±0.12	< D.L.	
	3.0	5.6	< D.L.	5.34±0.27	0.68±0.03	< D.L.	
	3.0	6.8	< D.L.	8.36±0.42	< D.L.	< D.L.	

Fig. A2. Concentrations of Fe ions vs. pH of final experimental 0.005M NaCl solutions brought in contact with NaIdP at various clay-to–solution ratios -$R_{S/L}$ (1-3g.L^{-1}) (data in Table A3). Experimental conditions: initial pH2.65-7.4: (a) $R_{S/L}$:1-3g.L^{-1}, t_R=3-7 days, *plain-circle*: 16nm cutoff, *open-circle:* 3ka cutoff (<3nm); (b) $R_{S/L}$:3g.L^{-1}, t_R=3 days, cutoff: 16nm. $R_{S/L}$ =●○: 0.5g.L^{-1}, ●■: 1.5g.L^{-1}, ●○: 3.0g.L^{-1}.

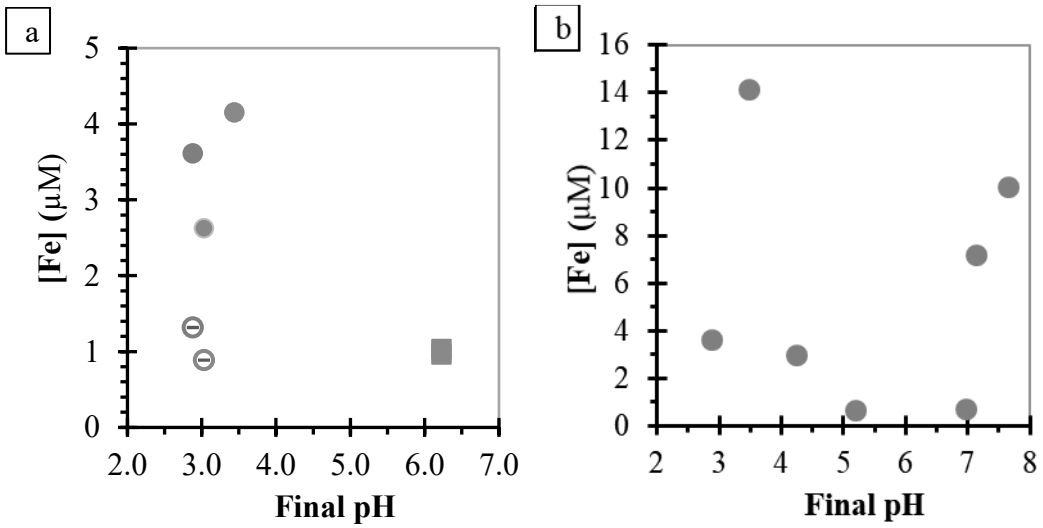

Fig. A3. Concentrations of (a) phosphate ions (Data in Table A4) and (b) phosphorus vs. pH of final experimental 0.005M NaCl solutions brought in contact with NaIdP at various clay-to-solution ratios -$R_{S/L}$ (0.5-3g.L^{-1}). Experimental conditions: initial pH: 2.65-7.4, t_R: 3 days. $R_{S/L}$ =●: 0.5g.L^{-1}, ▲: 1.0g.L^{-1}, △: 1.5g.L^{-1}, ♦: 2.0g.L^{-1}, ●: 2.5g.L^{-1}, ■: 3.0g.L^{-1}.

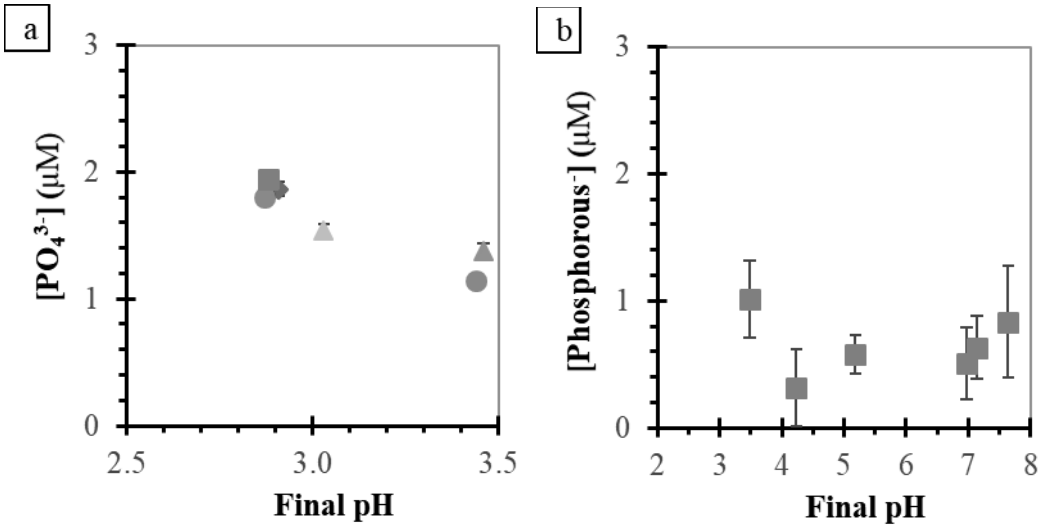

Table A5 Calculated aqueous species in experimental solutions contacted with IdP at various $R_{S/L}$: 3-6g.L^{-1}, during a reaction time of 5 days. The input data can be found in Tables A3-4.

	Calculated concentration (mol. L^{-1})			
$R_{S/L}$	*3*	*4*	*5*	*6*
pH_{final}	*6.0*	*6.6*	*7.0*	*7.2*
$Al(OH)_2^+$	1.0E-06	7.5E-07	4.7E-07	7.5E-07
$Al(OH)_3$ (aq)	1.9E-06	1.6E-06	1.2E-06	1.6E-06
$Al(OH)_4^-$	5.4E-06	5.1E-06	4.5E-06	5.0E-06
AlF_2^+	1.1E-06	1.2E-06	7.7E-07	1.6E-06
Ca^{2+}	1.9E-03	2.2E-03	2.4E-03	2.5E-03
$CaCl^+$	3.1E-05	3.6E-05	3.8E-05	3.9E-05
$CaHPO_4$ (aq)	4.3E-06	5.3E-06	6.6E-06	5.7E-06
$CaSO_4$ (aq)	8.1E-07	1.0E-06	1.2E-06	1.3E-06
Cl^-	1.0E-02	1.0E-02	1.0E-02	1.0E-02
F^-	2.1E-05	2.8E-05	3.5E-05	3.3E-05
$Fe(OH)_2^+$	3.1E-06	2.7E-06	2.3E-06	3.0E-06
$H_2CO_3^*$ (aq)	1.3E-05	1.3E-05	1.3E-05	1.3E-05
$H_2PO_4^-$	2.6E-05	2.5E-05	2.4E-05	2.5E-05
H_4SiO_4	1.8E-04	2.0E-04	2.2E-04	2.4E-04
HCO_3^-	3.3E-05	3.8E-05	4.5E-05	3.8E-05
HPO_4^{2-}	1.2E-05	1.3E-05	1.5E-05	1.3E-05
K^+	2.7E-04	2.7E-04	2.4E-04	3.0E-04
KCl (aq)	1.1E-06	1.1E-06	9.6E-07	1.2E-06
Li^+	2.6E-06	3.1E-06	3.7E-06	4.2E-06
Mg^{2+}	8.2E-05	9.4E-05	1.1E-04	1.2E-04
$MgCl^+$	2.1E-06	2.4E-06	2.7E-06	3.1E-06
Mn^{2+}	2.4E-06	2.2E-06	1.7E-06	1.5E-06
Na^+	5.0E-03	5.0E-03	5.0E-03	5.0E-03
NaCl (aq)	2.0E-05	2.0E-05	2.0E-05	2.0E-05
NO_3^-	6.0E-06	6.1E-06	6.9E-06	6.6E-06
SO_4^{2-}	4.5E-06	5.1E-06	5.4E-06	5.8E-06

Table A6 Calculated saturation index of minerals for the experimental 0.005M NaCl solutions contacted with IdP at various $R_{S/L}$: 3-6g.L^{-1}, during a reaction time of 5 days. The input data can be found in Tables A3-4.

	Calculated saturation index			
$R_{S/L}$	*3*	*4*	*5*	*6*
pH_{Final}	*6.0*	*6.6*	*7.0*	*7.2*
$Al(OH)_3$ (amorphous)	0.2	0.1	-0.04	0.1
$Al(OH)_3$	2.7	2.6	2.5	2.6
Al_2O_3	2.3	2.1	1.9	2.1
$Al_4(OH)_{10}SO_4$	2.2	1.8	1.2	1.9
$AlPO_4$ 1.5H_2O	0.5	0.4	0.1	0.3
Boehmite	2.4	2.3	2.2	2.3
Diaspore	4.1	4.0	3.9	4.0
FCO_3-Apatite	12.6	14.0	15.4	14.5
$Fe(OH)_{2.7}Cl_{0.3}$	7.3	7.3	7.3	7.3
Ferrihydrite	6.9	3.7	3.7	3.7
Ferrihydrite (aged)	4.2	4.2	4.2	4.2
Gibbsite	3.2	3.1	3.0	3.1
Goethite	6.4	6.4	6.4	6.4
Halloysite	4.9	4.8	4.6	5.0
Hematite	15.2	15.2	15.2	15.3
Hydroxyapatite	4.2	4.8	5.4	4.9
Imogolite	5.2	5.1	4.9	5.2
Kaolinite	7.0	6.9	6.8	7.1
Lepidocrocite	5.5	5.5	5.5	5.6
Maghemite	7.4	7.4	7.4	7.5
Magnesioferrite	6.1	6.3	6.5	6.4
$MnHPO_4$	2.1	2.1	2.1	1.9
Quartz	0.3	0.3	0.3	0.4
Rutile	0.7	-1.4	-1.4	0.7
Strengite	2.4	2.3	2.2	2.3
Variscite	2.1	2.0	1.7	2.0

Table A7 Protonation (pK^+) and deprotonation constant (pK^-)of hydroxyl functional groups at clay, Al- and Fe-oxide surface.

	Model*	pK^- $\equiv SOH \leftrightharpoons \equiv SO^- + H^+$	Surface group	pK^+ $\equiv SOH + H^+ \leftrightharpoons \equiv SOH_2^+$	
Montmorillonite	TLM	6.65	$\equiv SiOH_{edge}$	0.95	[1]
		11.5	$\equiv AlOH_{edge}$	-5.78	
	DLM	8.5	$\equiv AlOH_{edge}$	-5.1	[2]
	MUSIC	7.9	$\equiv SiOH_{edge}$	N.A.	[3]
		8.2	$\equiv SiOH_{edge}$	2.8	
		22.4	$\equiv AlOH_{edge}$	-10.5	
		17	$\equiv Al_2OH_{edge}$	-4.8	
		7.2	$\equiv AlSiOH_{edge}$	4.2	
Illite	CCM *(1 pKa model)*	4.12-4.23	Surface sites	N.A.	[4]
	CCM *(2 pKa model)*	4.17-4.44	Surface sites	N.A.	
		6.35-7.74	Surface sites	N.A.	
	TLM	8.1	$\equiv SiOH_{edge}$	-1.1	[5]
		11.7	$\equiv AlOH_{edge}$	-5.3	
	2SPNE	6.2	$\equiv S^sOH$ & $\equiv S^{w1}OH$	-4.0	[6]
		10.5	$\equiv S^{w2}OH$	-8.5	
	NEM	8.91 ± 0.18	Surface sites	-6.43 ± 0.41	[7]
	CCM	7.71 ± 0.15	Surface sites	-5.17 ± 0.42	
kaolinite	CCM	8.3–9.4	Surface sitesedge	-0.8 – -2.0	[8]
	DLM	8.1	Surface sites	-2.1	
	TLM	8.2	Surface sites	-1.1	
	DLM	7.7	$\equiv SiOH_{edge}$	N.A.	[2]
		6.1	$\equiv AlOH_{edge}$	-4.8	
	CCM	8.23	$\equiv SiOH_{edge}$	N.A.	[9]
		5.28	$\equiv AlOH_{edge}$	-2.33	
γ-Al_2O_3	CCM	9.9–10.8	Aluminol	-5.3 – -6.2	[8]
	DLM	9.8	Aluminol	-6.3	
	TLM	11.5	Aluminol	-5.5	
Amorphous silica	CCM	8.0–9.8	Silanol	0.8 – 2.0	
	DLM	8.1	Silanol	1.1	
	TLM	8.0	Silanol	0.3	
Hematite	CCM	9.8 – 10.5	Ferrinol	-6.0 – -6.8	
	DLM	9.7	Ferrinol	-7.0	
	TLM	11.3	Ferrinol	-5.7	

* CCM: Constant Capacitance Model, DLM: Double Layer Model, TLM: Triple Layer Model, 2SPNE: Two Site Protolysis Non-Electrostatic.

Table A8 Wavenumber (cm^{-1}) of Si-O stretching and OH deformation of clay minerals.

	Band position (cm^{-1})	Vibration mode	
Kaolinite	1005, 1027, 1115	Si-O stretching	[10]
Montmorillonite	992, 1002, 1003, 1006, 1113, 1116	Si-O stretching	[10]
Hectorite	989	Si-O stretching	[10]
Mica-montmorillonite	989	Si-O stretching	[10]
Palygorskite	978, 1019, 1194	Si-O stretching	[10]
Montmorillonite	1021, 1046, 1075-1084, 1117	Si-O stretching	[11]
Illite	1030	Si-O stretching	[13]
Montmorillonite	850, 885, 890	AlFeOH	[10,12]
Montmorillonite	837-846	AlMgOH	[12]
Montmorillonite	913-916	AlAlOH	[12]
Mica-montmorillonite	928-929	AlAlOH	[12]
Illite	916	AlAlOH	[13]
Illite	831	Al-O and / or AlMgOH	[13]
Montmorillonite	840, 875, 920	OH-	[11]

References

[1] J.M. Zachara, S.C. Smith, Edge Complexation Reactions of Cadmium on Specimen and Soil-Derived Smectite, Soil Science Society of America Journal. 58 (1994) 762–769. https://doi.org/10.2136/sssaj1994.03615995005800030018x.

[2] E. Tertre, S. Castet, G. Berger, M. Loubet, E. Giffaut, Surface chemistry of kaolinite and Na-montmorillonite in aqueous electrolyte solutions at 25 and 60°C: Experimental and modeling study, Geochimica et Cosmochimica Acta. 70 (2006) 4579–4599. https://doi.org/10.1016/j.gca.2006.07.017.

[3] C. Tournassat, J.-M. Greneche, D. Tisserand, L. Charlet, The titration of clay minerals, Journal of Colloid and Interface Science. 273 (2004) 224–233. https://doi.org/10.1016/j.jcis.2003.11.021.

[4] Q. Du, Z. Sun, W. Forsling, H. Tang, Acid-Base Properties of Aqueous Illite Surfaces, (n.d.) 11.

[5] D.A. Kulik, S.U. Aja, V.A. Sinitsyn, S.A. Wood, Acid–base surface chemistry and sorption of some lanthanides on K+-saturated Marblehead illite: II. a multisite–surface complexation modeling, Geochimica et Cosmochimica Acta. 64 (2000) 195–213. https://doi.org/10.1016/S0016-7037(99)00174-X.

[6] M.H. Bradbury, B. Baeyens, Sorption modelling on illite Part I: Titration measurements and the sorption of Ni, Co, Eu and Sn, Geochimica et Cosmochimica Acta. 73 (2009) 990–1003. https://doi.org/10.1016/j.gca.2008.11.017.

[7] Y. Liu, D.S. Alessi, S.L. Flynn, Md.S. Alam, W. Hao, M. Gingras, H. Zhao, K.O. Konhauser, Acid-base properties of kaolinite, montmorillonite and illite at marine ionic strength, Chemical Geology. 483 (2018) 191–200. https://doi.org/10.1016/j.chemgeo.2018.01.018.

[8] D.A. Sverjensky, N. Sahai, Theoretical prediction of single-site surface-protonation equilibrium constants for oxides and silicates in water, Geochimica et Cosmochimica Acta. 60 (1996) 3773–3797. https://doi.org/10.1016/0016-7037(96)00207-4.

[9] P.V. Brady, R.T. Cygan, K.L. Nagy, Molecular Controls on Kaolinite Surface Charge, Journal of Colloid and Interface Science. 183 (1996) 356–364. https://doi.org/10.1006/jcis.1996.0557.

[10] J. Madejová, Baseline Studies of the Clay Minerals Society Source Clays: Infrared Methods, Clays and Clay Minerals. 49 (2001) 410–432. https://doi.org/10.1346/CCMN.2001.0490508.

[11] C.T. Johnston, G.S. Premachandra, Polarized ATR-FTIR Study of Smectite in Aqueous Suspension, Langmuir. 17 (2001) 3712–3718. https://doi.org/10.1021/la010184a.
[12] D. Vantelon, M. Pelletier, L.J. Michot, O. Barres, F. Thomas, Fe, Mg and Al distribution in the octahedral sheet of montmorillonites. An infrared study in the OH- bending region, Clay Miner. 36 (2001) 369–379. https://doi.org/10.1180/000985501750539463.
[13] J. Madejová, W.P. Gates, S. Petit, IR Spectra of Clay Minerals, in: Developments in Clay Science, Elsevier, 2017: pp. 107–149. https://doi.org/10.1016/B978-0-08-100355-8.00005-9.

Appendix B : Supporting information of chapter III

Fig. B1 Sorption isotherms of uranyl ions (% of total U sorbed) onto NaIdP, in the absence and in the presence of phosphate ligands (●: 0µM, ●: 100µM), for experiments conducted at pH: (a) 3.0, (b) 3.5 and (c) 4.1. Experimental conditions: reaction time, t_R, of 4 days; clay-to-solution ratio, $R_{S/L}$, of 3g/L, electrolyte solution: 0.005M NaCl electrolyte. Suspensions were pre-equilibrated with electrolyte for a duration ($t_{pre\text{-}equil}$) of 3 days prior to addition of the sorbates.

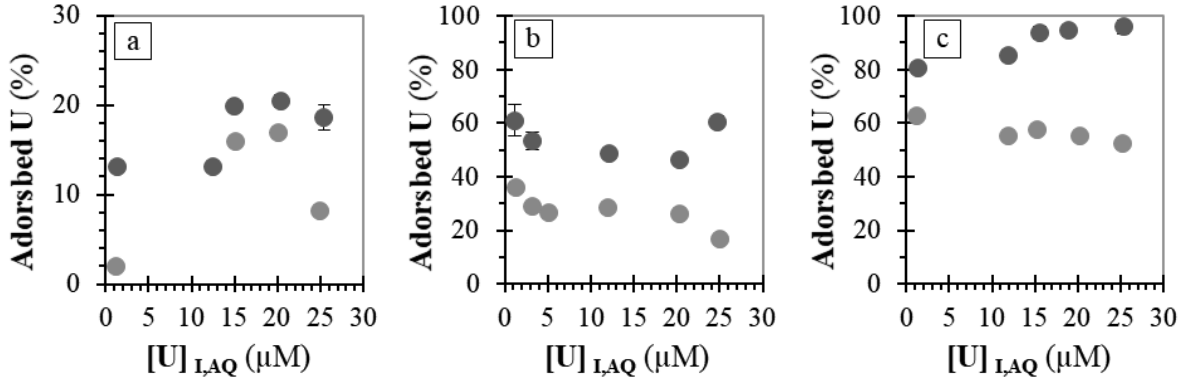

Fig. B2 Sorption isotherms of uranyl ions (in µmol.g^{-1}) on NaIdP, in the absence and in the presence of phosphate ligands (●: 0µM, ●: 100µM), for experiments conducted at pH: (a) 3.0, (b) 3.5 and (c) 4.1. Experimental conditions given in caption of Fig. A1.

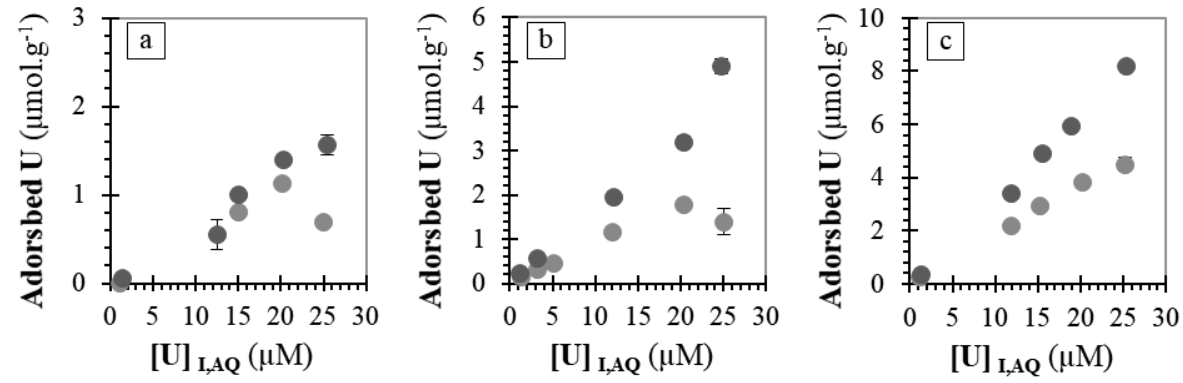

Fig. B3. Percentage of sorption of uranyl ions onto NaIdP as a function of pH (sorption edge) obtained from batch experiments conducted at different clay-to-solution ratios, $R_{S/L}$ (■: 1 g.L^{1}, ▲: 2 g.L^{-1} et ●: 3g.L^{-1}) and at total U(VI) concentrations of: (a) 1 µM and (b) 12µM. Experimental conditions: reaction time, t_R, of 4 days; electrolyte solution: 0.005M NaCl electrolyte. Suspensions were pre-equilibrated with the electrolyte solution for a duration ($t_{pre\text{-}equil}$) of 3 days prior to addition of U.

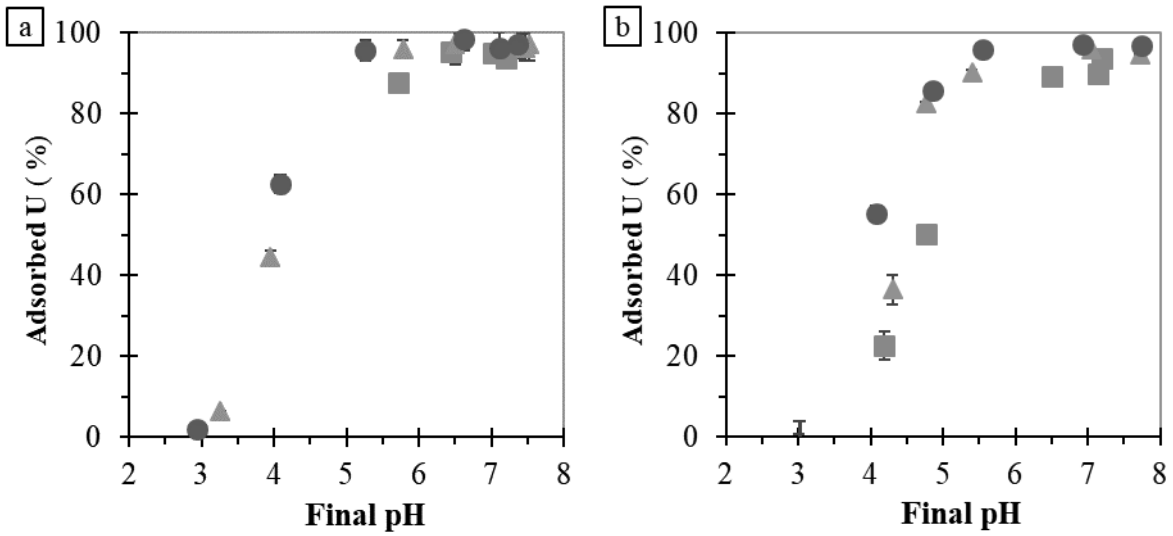

Fig. B4. Surface coverage of NaIdP by uranyl ions (in µmol.g^{-1}) as a function of pH for batch experiments conducted at different clay-to-solution ratios $R_{S/L}$ (■: 1 g.L^{1}, ▲: 2 g.L^{-1} et ●: 3g.L^{-1}) and at total U(VI) concentrations of: (a) 1 µM and (b) 12µM. Experimental conditions are given in caption of Fig. A3.

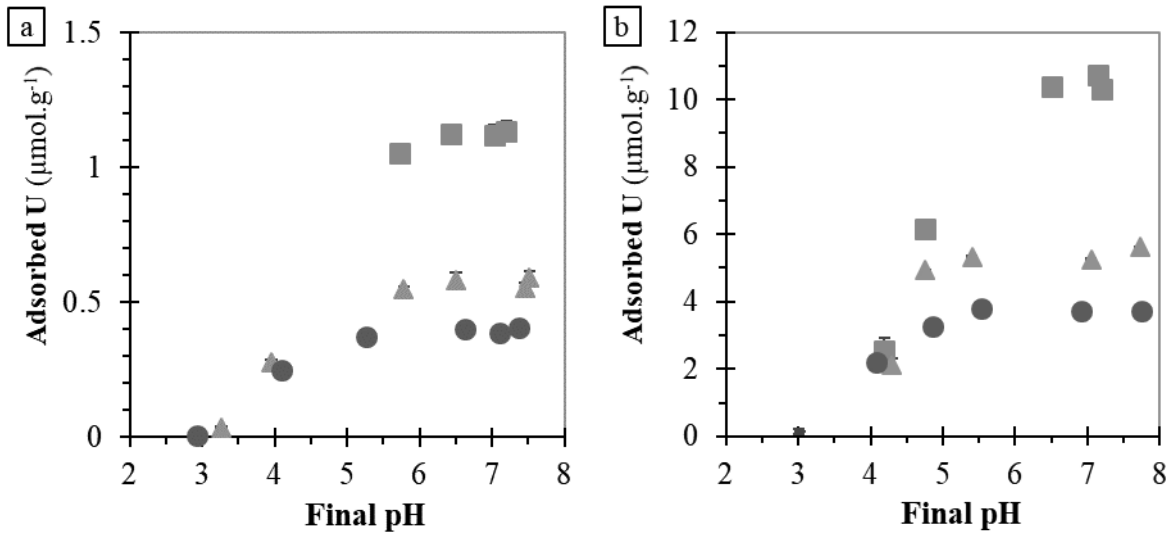

Fig. B5. Percentage of sorption of phosphate ions onto NaIdP as a function of total concentration of uranyl ions ($[U]_{I,aq}$) for U-P co-sorption experiments conducted at two total concentrations of P ($[P]_{I,aq}$ = 20µM (●) and 100µM (●)). Experimental conditions: $R_{S/L}$ = 3g.L^{1}, pH 3.5-4.0, reaction time, t_R = 4 days; electrolyte solution: 0.005M NaCl; $t_{pre\text{-}equil}$ = 3 days).

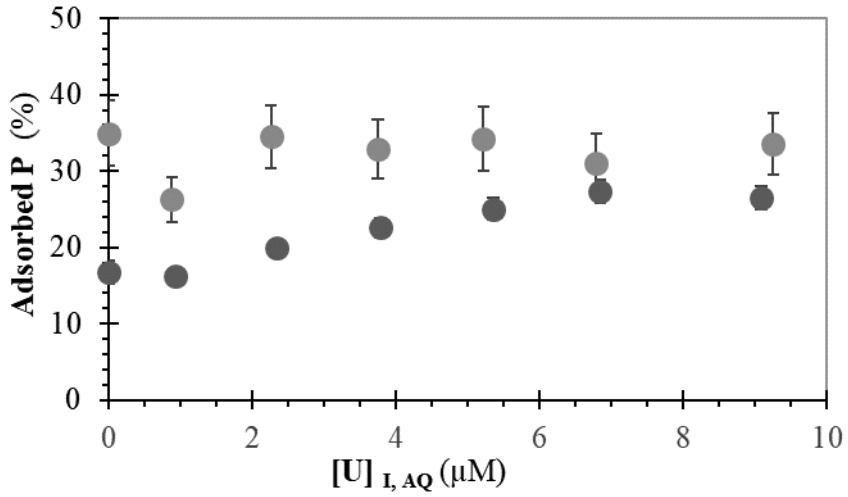

Fig. B6. Surface coverage of NaIdP by phosphate ions (in µmol.g^{-1}) as a function of total concentration of uranyl ions ($[U]_{I,aq}$) for U-P co-sorption experiments conducted at two total concentrations of P ($[P]_{I,aq}$ = 20µM (●) and 100µM (●)). Experimental conditions given in caption of Fig. A5.

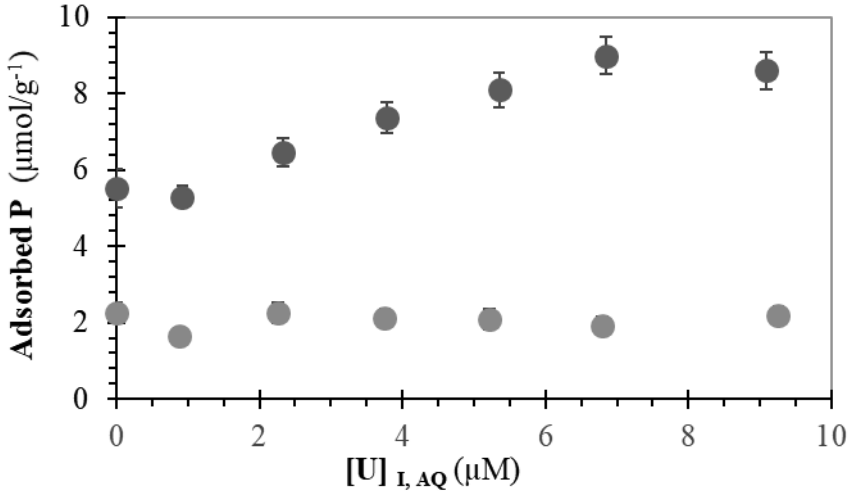

Fig. B7. Results of blank experiments (without NaIdP) on the formation of colloidal phases in solutions aged during 4 days at various total concentrations of U ($[U]_{I,aq}$), in the presence of 20 µM (●) and 100µM (○) of phosphate ions, at acidic pH (3.3-4.1). Electrolyte solution: 0.005M NaCl.

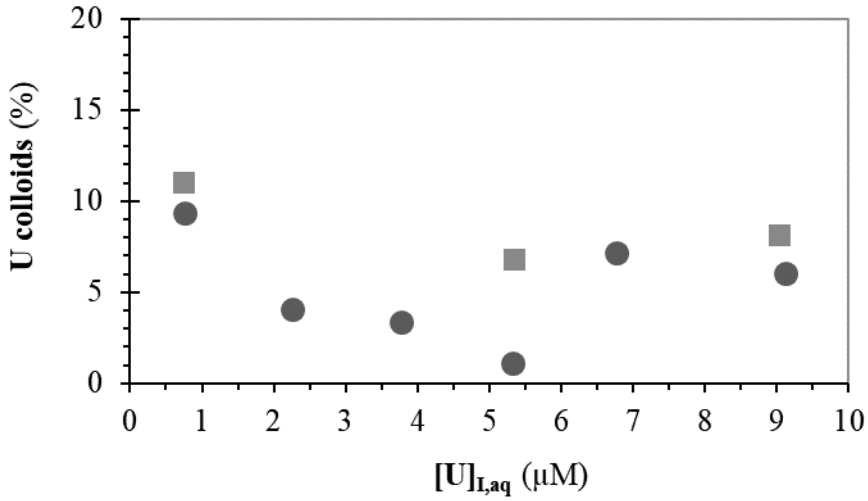
U colloids (%)
20
15
10
5
0
0
1
2
3
4
5
6
7
8
9
10
[U]I,aq (µM)

Fig. B8. Aqueous speciation of U(VI) (in %) as a function of pH, as calculated by using the Visual MINTEQ (Ver: 3.1) code and data base, for a total concentration of U(VI) of: (a) 2μM and (b) 10μM, in the presence of 100μM of phosphate ions. Electrolyte solution: 0.005M NaCl.

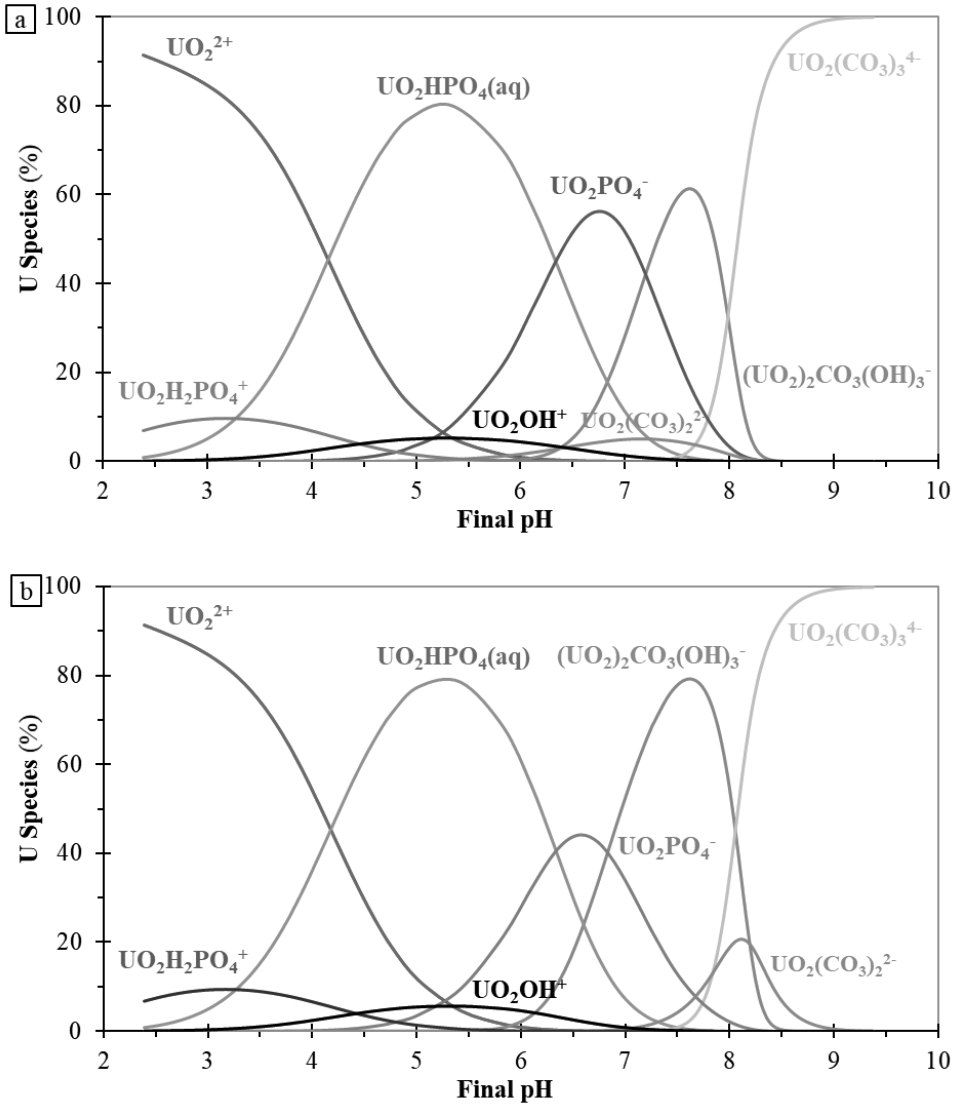

Table B1. Equilibrium constants of aqueous species used in the speciation calculations (*Database: Visual MINTEQ (Ver:3.1) code*).

Equilibrium Reactions	Log K)
$UO_2^{2+} + H_2O \leftrightharpoons UO_2OH^+ + H^+$	-5.25
$UO_2^{2+} + 2H_2O \leftrightharpoons UO_2(OH)_{2\,(aq)} + 2H^+$	-12.15
$UO_2^{2+} + 3H_2O \leftrightharpoons UO_2(OH)_3^- + 3H^+$	-20.25
$UO_2^{2+} + 4H_2O \leftrightharpoons UO_2(OH)_4^- + 4H^+$	-32.4
$2UO_2^{2+} + H_2O \leftrightharpoons (UO_2)_2OH^{3+} + H^+$	-2.7
$2UO_2^{2+} + 2H_2O \leftrightharpoons (UO_2)_2(OH)_2^{2+} + 2H^+$	-5.62
$3UO_2^{2+} + 4H_2O \leftrightharpoons (UO_2)_3(OH)_4^{2+} + 4H^+$	-11.9
$3UO_2^{2+} + 5H_2O \leftrightharpoons (UO_2)_3(OH)_5^+ + 5H^+$	-15.55
$3UO_2^{2+} + 7H_2O \leftrightharpoons (UO_2)_3(OH)_7^- + 7H^+$	-32.2
$4UO_2^{2+} + 7H_2O \leftrightharpoons (UO_2)_3(OH)_7^+ + 7H^+$	-21.9
$UO_2^{2+} + CO_3^{2-} \leftrightharpoons UO_2CO_3$ (aq)	9.94
$UO_2^{2+} + 2CO_3^{2-} \leftrightharpoons UO_2(CO_3)_2^{2-}$	16.61
$UO_2^{2+} + 3CO_3^{2-} \leftrightharpoons UO_2(CO_3)_3^{4-}$	21.84
$3UO_2^{2+} + 6CO_3^{2-} \leftrightharpoons (UO_2)_3(CO_3)_6^{6-}$	54
$2UO_2^{2+} + CO_3^{2-} + 3H_2O \leftrightharpoons (UO_2)_2CO_3(OH)_3^- + 3H^+$	-0.86
$3UO_2^{2+} + CO_3^{2-} + 3H_2O \leftrightharpoons (UO_2)_3CO_3(OH)_3^+ + 3H^+$	0.66
$UO_2^{2+} + Cl^- \leftrightharpoons UO_2Cl^+$	0.17
$UO_2^{2+} + 2Cl^- \leftrightharpoons UO_2Cl_{2\,(aq)}$	-1.1
$UO_2^{2+} + PO_4^{3-} \leftrightharpoons UO_2PO_4^-$	13.23
$UO_2^{2+} + PO_4^{3-} + H^+ \leftrightharpoons UO_2HPO_{4\,(aq)}$	19.6
$UO_2^{2+} + PO_4^{3-} + 2H^+ \leftrightharpoons UO_2H_2PO_4^+$	22.83
$UO_2^{2+} + PO_4^{3-} + 3H^+ \leftrightharpoons UO_2H_3PO_4^{2+}$	22.47
$PO_4^{3-} + H^+ \leftrightharpoons HPO_4^{2-}$	12.375
$PO_4^{3-} + 2H^+ \leftrightharpoons H_2PO_4^{2-}$	19.573
$PO_4^{3-} + 3H^+ \leftrightharpoons H_3PO_4^{2-}$	21.721
$2Na^+ + PO_4^{3-} \leftrightharpoons Na_2PO_4^-$	2.59
$Na^+ + PO_4^{3-} \leftrightharpoons NaPO_4^{2-}$	1.43
$Na^+ + H_2O \leftrightharpoons NaOH_{\,(aq)} + H^+$	-13.897
$Na^+ + Cl^- \leftrightharpoons NaCl_{\,(aq)}$	-0.3
$Na^+ + CO_3^{2-} \leftrightharpoons NaCO_3^-$	1.27
$H^+ + CO_3^{2-} \leftrightharpoons HCO_3^-$	10.329
$2H^+ + CO_3^{2-} \leftrightharpoons H_2CO_{3(aq)}$	16.681
$H_2O \leftrightharpoons H^+ + OH^-$	-13.997
$2Na^+ + H^+ + PO_4^{3-} \leftrightharpoons Na_2HPO_{4\,(aq)}$	13.32

$Na^+ + H^+ + PO_4^{3-} \leftrightharpoons NaHPO_4^-$	13.445
$Na^+ + 2H^+ + PO_4^{3-} \leftrightharpoons NaH_2PO_{4\ (aq)}$	19.873
$Na^+ + H^+ + CO_3^{2-} \leftrightharpoons NaHCO_{3\ (aq)}$	10.029

Table B2. Calculated saturation index *(SI)* of a solution at total concentrations of U(VI) and phosphate ions of 10µM and 100µM, respectively, at pH4. Solubility constants of uranium-phosphate minerals used in calculations are reported, too (*Database: Visual MINTEQ (Ver:3.1) code*).

Solid phases	Equilibrium Reactions	Log K	SI *(pH4)*
Schoepite	$UO_3 \cdot 2H_2O_{(s)} + 2H^+ \leftrightharpoons UO_2^{2+} + 3H_2O$	4.869	-2.759
$UO_2(OH)_{2\ (beta)}$	$UO_2(OH)_{2\ (beta)} + 2H^+ \leftrightharpoons UO_2^{2+} + 2H_2O$	4.869	-2.98
$UO_{3\ (s)}$	$UO_{3\ (s)} + 2H^+ \leftrightharpoons UO_2^{2+} + H_2O$	4.869	-5.068
$(UO_2)_3(PO_4)_{2\ (s)}$	$(UO_2)_3(PO_4)_{2\ (s)} \leftrightharpoons 3UO_2^{2+} + 2PO_4^{3-}$	-49.974	1.975
H-Autunite	$(UO_2)_2(H_2PO_4)_{2\ (s)} \leftrightharpoons 2UO_2^{2+} + 2PO_4^{3-} + 2H^+$	-52.843	-2.126
Na-Autunite	$(UO_2)_2(H_2PO_4)_{2\ (s)} \leftrightharpoons 2UO_2^{2+} + 2PO_4^{3-} + 2Na^+$	-42.928	0.773
Rutherfordine	$UO_2CO_{3(S)} \leftrightharpoons UO_2^{2+} + CO_3^{2-}$	-16.700	-4.178

Appendix C : Supporting information for chapter IV

Table C1. Surface species suggested by this work.

Studied system pH4, 0.005M NaCl, 3g.L^{-1}	IR active band position (cm^{-1}) P-O(υ_3)				Surface species Molecular symmetry of PO_4 unit	Surface complex models
P-NaIdP						
$[P]_{I,aq}$: 50-300µM (t_R: ~20h) and 100µM (t_R: ~3 days)	1075	1160	1215		≡S···$H_2PO_4^-$ (C_{2v})	OSSC
	1005	1037	1095		≡$(SO)_2PO_2$ (C2v or lower)	Bidentate binuclear
	1132				≡$(SO)_2(OH)PO$ (C_1)	Monodentate mononuclear
Fe(III)-P-NaIdP						
$[Fe]_{I,aq}$: 10µM, $[P]_{I,aq}$: 100µM (t_R: ~3 days)	1075	1162			≡S···$H_2PO_4^-$ (C_{2v})	OSSC
	970	1000	1084	1112		ISSC and/or surface precipitate (Fe-P-NaIdP)
	1140				≡S···$FeHPO_4^+$	OSSC
	940					ISSC (Fe-P-NaIdP)
U(VI)-P-NaIdP						
$[U]_{I,aq}$: 2-10µM and $[P]_{I,aq}$: 100µM (t_R ~7h)	1075	1155			≡S···$H_2PO_4^-$ (C_{2v})	OSSC
	1050					ISSC (U-P-NaIdP) at weak sites
	1125					ISSC (U-P-NaIdP) at strong sites
$[U]_{I,aq}$: 8µM and $[P]_{I,aq}$: 100µM (t_R: ~3 days)	992	1081	1114			"Autunite-like" surface complex
	1052					ISSC (U-P-NaIdP) at strong sites
U(VI)&Fe(III)&phosphate ions-NaIdP						

$[U]_{I,aq}$: 10µM, $[Fe]_{I,aq}$: 10µM, $[P]_{I,aq}$: 100µM (t_R ~3 days)	1084	1120	1175		ISSC and/or surface precipitate (Fe-P-NaIdP) at short t_R
	1075	1155		$\equiv S\cdots H_2PO_4^-$ (C_{2v})	OSSC
	1039			$\equiv(SO)_2PO_2$ (C_{2v} or lower)	Bidentate binuclear

Table C2. Aqueous species suggested by this work.

Studied ions and their concentration	pH	IR active band position (cm^{-1}) P-O(υ_3)			U-O(υ_3)	Aqueous species and molecular symmetry of PO_4 unit
Phosphate ions						
45-225µM	4.0	1075	1157			$H_2PO_4^-$ (C_{2v})
50-150µM	4.9	1074	1159			$H_2PO_4^-$ (C_{2v})
30-225µM	6.2	1076	1156			$H_2PO_4^-$ (C_{2v})
30-150µM	7.0	1077	1158			$H_2PO_4^-$ (C_{2v}) and HPO_4^{2-} (C_{3v})
Fe(III) and phosphate ions						
$[Fe]_{I,aq}$: 10µM, $[P]_{I,aq}$: 100µM	4.0	1042	1089	1147		$FeHPO_4^+$ (C_1)
		1075				$H_2PO_4^-$ (C_{2v})
U(VI) and phosphate ions						
$[U]_{I,aq}$: 2µM, $[P]_{I,aq}$: 100µM	4.0	996	1122		924	$(UO_2)_3(PO_4)_{2(s)}$ (C_{3v}) and $UO_2HPO_4(H_2O)_4$ (C_{3v})
$[U]_{I,aq}$: 8µM, $[P]_{I,aq}$: 100µM	4.0	997	1122		927	$(UO_2)_3(PO_4)_{2(s)}$ (C_{3v}) and $UO_2HPO_4(H_2O)_4$ (C_{3v})
		1052	1170			U-P complex (C_{2v} or lower)
U(VI), Fe(III) and phosphate ions $[U]_{I,aq}$: 10µM, $[Fe]_{I,aq}$: 10µM, $[P]_{I,aq}$: 100µM	4.0	997	1125		923	$(UO_2)_3(PO_4)_{2(s)}$ (C_{3v}) and $UO_2HPO_4(H_2O)_4$ (C_{3v})
		1045	1150			$FeHPO_4^+$ (C_{2v} or lower)

Table C3. Literature data of surface species of phosphate at oxi-hydroxydes and clay minerals.

Phosphate–Mineral	P-O υ_3&υ_1 and position (cm^{-1})					Surface specie assignment	Ref.
P-Aluminum (hydr)oxides							
Alumina gel	1130-1140		1040-1050			surface precipitate (Al-phosphate gel)	Nanzyo. 1984
Aged Al_2O_3		1115			900	surface precipitate ($AlPO_4$(s))	Laiti et al., 1996
Al_2O_3	1126	1080	1017	959	901	Monodentate and/or bidentate, surface precipitate of $AlPO_4$	Roy et al., 2021
Al_2O_3	1130-1131	1092-1096	1053-1060	1020-1025	1005-1010	$\equiv(AlO)_2PO_2$ and $\equiv(AlO)_2(OH)PO$	Li et al., 2013
Aged Al_2O_3	1130-1137					Surface precipitate	Del Nero et al., 2010
		1084	1033			ISSC	
P-Iron (hydr)oxides							
Goethite	1120-1128		1004-1010	975-982		$\equiv(FeO)_2(OH)PO$, C_1	Tejedor-Tejedor and Anderson. 1990
		1088-1106	1038-1048			$\equiv(FeO)_2PO_2$, C_{2v}	
			1023-1026	1002-996		$\equiv FeOPO_3$, C_{3v}	
	1178		1001		876	$\equiv FeOPO(OH)_2$, C_{3v}	Persson et al., 1996
	1122		1049	939	820	$\equiv FeOPO_2(OH)$, C1	
			1057	970	830	$\equiv FeOPO_3$, C_{3v}	
Ferrihydrite		1102	1020	920		$\equiv$(FeO)2(OH)PO, C1	Arai and Sparks., 2001
		1088	1021	952		$\equiv(FeO)_2PO_2$, C_{2v} or lower	
Hematite	1117		1007	964		$\equiv(FeO)_2(OH)PO$, C_1 or $\equiv FeO(OH)PO_2\cdots H$, C1	Elzinga et al., 2006
		1086	1035	960		$\equiv FeOPO_3$, C_{3v} or low	
P-Clay							

Iron(III) modified-montmorillonite		1088	1049	941		≡$(FeO)_2PO_2$, C_{2v} or lower	Bognino et al., 2010
	1128		1011	978		≡$(FeO)_2(OH)PO$, C_1	
		1095-1096	1062	962-957		≡$(FeO)_2PO_2$, C_{2v} or lower and / or ≡$FeOPO_3\cdots H$	
			1020-1023	988-983	935-931	≡$FeOPO_3$, C_{3v}	
Kaolinite	1138					ISSC and /or surface precipitate	Dolui et al., 2018
		1108	1076			Multi-surface complexes	
Na-Illite du Puy	1003	1037	1095			≡$(SO)_2PO_2$ (C_{2v} or lower)	This study
	1160	1075				≡$S\cdots H_2PO_4^-$ (C_{2v})	
	1132					≡$SO(OH)PO_2$ (C_1)	

Shangyao GUO

Study of the mechanisms and species involved in the retention of uranium(VI) at trace concentration at the clay-solution interface

Résumé:
Le stockage dans des formations argileuses profondes comme une barrière géologique est une option envisagée pour la gestion à long terme des déchets radioactifs. Ces formations ont des capacités fortes à retarder la migration des radionucléides (RN) grâce à leur propriété physicochimique pertinente. Or la dégradation à long terme du système multi-barrières en champ proche est un problématique crucial pour la sûreté de stockage des sites, car elle pourrait entraîner la migration progressive des RN vers des environnements accessibles à l'humain sur une longue période. Dans le cadre des études de sûreté, une compréhension affinée des mécanismes de la sorption des RN sur les roches argileuses est indispensable afin de développer des modèles prédictifs fiables du transport réactif des RN dans ces roches, en conditions de champ proche ou lointain des stockages, et notamment en cas de perturbations chimiques des milieux. L'objectif principal de cette étude est d'acquérir des connaissances mécanistes sur la sorption des ions uranyle en présence de ligands phosphate et des ions Fe^{3+} sur une roche argileuse (illite du puy, noté IdP).
Pour pouvoir attendre à cet objectif, des expériences de sorption des ions uranyle en lots, des analyses de la mobilité électrophorétique des particules argileuses et des mesures de la spectroscopie IRTF RTA in-situ de l'interface illite-solution tout au long des processus de (co)sorption des ions uranyle ont été réalisés.
Les résultats obtenus sur la (co)sorption d'ions uranyle et phosphate suggèrent la coexistence de plusieurs espèces de l'ion phosphate et espèces phosphatées de l'ion uranyle à l'interface argile-solution, dont la contribution varie en fonction de concentrations en phosphate, en ions uranyle et temps de réaction, avec une transition observée au cours de la sorption entre formation de complexes de sphère externes en complexes de sphère interne. Les résultats des effets des ions Fe^{3+}sur la sorption des ions uranyle en présence de ligands phosphate suggèrent spectroscopiquement un effet compétitif fort entre ces métaux pour la surface de l'illite.
Cette étude a mis en évidence la formation des différentes espèces, impliquant ligands phosphate, ions uranyle, et ions Fe^{3+} compétiteurs, qui coexistent à l'interface illite-solution, pour des concentrations traces en métaux. Ces données mécanistes, et l'approche utilisée, contribuent à une compréhension plus fine du processus du transport d'ions uranyle et de leur rétention dans des systèmes argileux, et à la transférabilité des données expérimentales / mécanistes obtenues sur le comportement de l'uranium (VI) à des « systèmes réels ».

Abstract:
Deep clay rock formation as a geological barrier in a repository is a suitable option for the long-term management of radioactive waste, as these formations have a remarkable capacity to retard radionuclides (RN) due to their outstanding physicochemical properties. However, the long-term degradation of the near-field multi-barrier system is a crucial issue of repository safety, as it could lead to the gradual migration of RN to human-accessible environments over a long period.
In this context, a refined understanding of RN sorption mechanisms on clay rocks is mandatory to develop reliable predictive models of reactive transport in these rocks under near-field or far-field storage conditions, especially in the cases of chemical perturbation of mediums. The main aim of this study is to gain mechanistic knowledge of the sorption of uranyl ions in the presence of phosphate ligands and Fe^{3+} ions on a clay rock (illite du puy, noted IdP).
To achieve this objective, the traditional batch sorption experiments of uranyl ions at trace level onto illite, electrophoretic mobility analyses of clay particles, and in-situ ATR FTIR measurements of the illite–solution interface along the (co)sorption process have been carried out.
The results obtained on the (co)sorption of uranyl and phosphate ions suggested the coexistence of several species of phosphate and uranyl-phosphate at the clay-solution interface, whose contribution varied as a function of concentrations of phosphate and uranyl ions and reaction time, with a transition observed during sorption between the formation of outer-sphere complexes and inner-sphere complexes. The results of the effects of Fe^{3+} ions on the sorption of uranyl ions in the presence of phosphate ligands spectroscopically suggested a significant competitive effect between these metals for the surface sites of illite.
The contribution of this study is to highlight the formation of different species involving the phosphate ligands, uranyl ions, and competing Fe^{3+} ions, coexisting at the illite–water interface for trace concentrations of metals. These mechanistic data, and the method used, contribute to a better understanding of the process of transport and retention of uranyl ions in clay systems and to the transferability of experimental/mechanical data obtained on the behavior of uranium (VI) to "real systems".